Temperature-induced phase transition of grafted hydrogels : from primary structure to mechanical properties

Cécile Mussault

SORBONNE UNIVERSITÉ
CRÉATEURS DE FUTURS
DEPUIS 1257

Sorbonne Université

ED 397 : Physique et Chimie des Matériaux

Laboratoire Sciences et Ingénierie de la Matière Molle (SIMM)

Temperature-induced phase transition of grafted hydrogels: from primary structure to mechanical properties

Par Cécile MUSSAULT

Thèse de doctorat de Chimie et Physico-chimie des Polymères

Dirigée par Dominique HOURDET, Alba MARCELLAN et Nicolas SANSON

Présentée et soutenue publiquement le 06/11/2018

Devant un jury composé de :

Costas PATRICKIOS	Professor at the University of Cyprus	Rapporteur
Catherine AMIEL	Professeur à l'Université Paris-Est Créteil	Rapporteur
Odile FICHET	Professeur à l'Université de Cergy-Pontoise	Examinateur
Philippe GUEGAN	Professeur à Sorbonne Université	Examinateur
Dominique HOURDET	Professeur à Sorbonne Université	Co-encadrant
Alba MARCELLAN	Maître de Conférences à Sorbonne Université	Co-encadrant
Nicolas SANSON	Maître de Conférences à Sorbonne Université	Co-encadrant

Acknowledgments

I first would like to thank the Doctoral School of Sorbonne University (ED 397, Sorbonne University, Paris, France) for funding my researches and Christian Fretigny for giving me the opportunity to carry out my PhD at the SIMM laboratory at the ESPCI.

I express my gratitude to all my jury members: Catherine Amiel, Odile Fichet, Philippe Guégan and Costas Patrickios. I sincerely appreciate their interest for my work and the interesting scientific conversations we had about it.

I also thank my supervisors Dominique Hourdet, Alba Marcellan and Nicolas Sanson for their scientific knowledge, engagement and advices. I especially thank you for the support you gave me on both personal and professional aspects. I would have never managed to learn so much without the three of you.

I thank Guylaine Ducouret for her help on rheological experiments, Mohammed Hanafi who helped me with the SEC characterization of my polymers, Nadège Pantoustier for her advices on polymer synthesis and Alexandre and Ludovic for helping me designing some laboratory devices.

I would like to thank Annie Brûlet from the Léon Brillouin Laboratory (CEA Saclay) for her help on my small angle neutron scattering experiments and Christophe Tribet for his help on capillary electrophoresis experiments.

I am grateful to Hui Guo for the time he spent working with me during my internship at the laboratory before to begin my PhD on a very similar subject. Thank you for your energy, kindness, engagement and the scientific knowledge you were always happy to share with me. It helped me a lot for the experiments I performed during my PhD.

I thank Kamélia Hamdidi, Héloïse Rispaud and Alexandre Tribalet who I appreciated working with.

I especially would like to thank all the SIMM members and especially Anne-Charlotte, Antoine, Cyprien, Francisco, Gabo, Mélanie and Miléna who have become real friends to me but also Ana, Armand, Bruno, Cécile, Charles, Charline, Christophe, Freddy, Gilles, Guillaume, Heiva, Helen, Irvin, Julien, Justine, Mehdi, Paul, Romain, Valentine, Xavier, Yinjun etc. for tea breaks, swimming and climbing sessions, intense conversations, writing week-ends, lunches, holidays etc. In a word, I thank you all for the numerous moments that made me enjoy these three years at the laboratory.

I am very grateful to my friends from elementary school, prépa, engineering school and university: Anthony, Batoul, Caroline, Emilie, Guillaume, Jamila, Julie, Mario, Mathilde, Meltem, Nassima and Thomas.

I express all my gratitude to my family. You have always been by my side, whatever were the difficulties to face. I can’t thank you enough for your advices, trust, support and endless love which are priceless to me.

THANK YOU !

Abbreviations

CE	Capillary Electrophoresis
DLS	Dynamic Light Scattering
DN	Double network
DSC	Differential Scanning Calorimetry
GPD-Nx(y-z)	Grafted hydrogel with PDMA backbone and PNIPAm grafts with x their average molar and y and z the weight percentage of PDMA covalent network and PNIPAm side-chains, respectively
GPA-N36	Grafted hydrogel with PNAGA backbone and PNIPAm grafts with an average molar mass M_n=36 kg/mol
NMR	Nuclear Magnetic Resonance
SANS	Small Angle Neutron Scattering
SEC	Size Exclusion Chromatography
LCST	Lower Critical Solution Temperature
UCST	Upper Critical Solution Temperature
NC	Nano-composite

AA	Acrylic acid
AET.HCl	Cysteamine hydrochloride
AM	Acrylamide
D_2O	Deuterated water
DCCI	Dicyclohexylcarbodiimide
DMA	*N*,*N*-dimethylacrylamide
DMSO	Dimethyl sulfoxide
Et_2O	Diethyl ether
Et_3N	Triethylamine
H_2O	Water
KPS	Potassium Persulfate
MBA	*N*,*N'*-methylene-bis(acrylamide)
MeOH	Methanol
NAGA	*N*-acryloyl glycinamide
NaOH	Sodium hydroxide
NHS	*N*-Hydroxysuccinimide
NIPAm	*N*-isopropylacrylamide
NMP	*N*-methyl-2-pyrrolidone
PNIPAm	Poly(N-isopropylacrylamide)
PDMA	Poly(N,N-dimethylacrylamide)
PNAGA	Poly(N-acryloyl glycinamide)
TEMED	*N*,*N*,*N'*,*N*'-Tetramethylethylenediamine
THF	Tetrahydrofuran

Symbols

°C	Celsius degree
T	Temperature
w/w	Weight ratio
v/v	Volume ratio
r	Molar ratio
$r_{\%}$	Percentage molar ratio
Đ	Dispersity
M_n	Number average molar mass
M_w	Weight average molar mass
M_{sc}	Average molar mass of PNIPAm side-chains
M_g	Average molar between two consecutive grafts
M_c	Number average molar mass between the two adjacent nearest cross-linking points
$[M]_0$	Initial monomer M concentration
$[polymer]_0$	Initial polymer concentration
$[X]_0$	Initial cross-linker concentration
C^*	Overlap concentration
C_T	Transfer constant
k_p	Propagation rate constant
k_{trX}	Transfer rate constant
DPn	Degree of polymerization
DP_{ncum}	Cumulative degree of polymerization
α_M	Monomer conversion
m_{dry}	Gel weight in the dry state
m_{sw}	Gel weight in the swollen state

m_{th}	Theoretical gel weight
ΔH	Transition enthalpy
T_c	Critical solution temperature
T_{in}	T at the very beginning of the phase transition
T_{max}	T at the maximum of the endotherm
Q_0	Swelling ratio in “weight” at preparation state
Q_{eq}	Swelling ratio in “weight” at equilibrium
Q_V	Swelling ratio in “volume”
Q_{Veq}	Swelling ratio in “volume” at equilibrium
ϕ_{eq}	Volume fraction of polymer in the swollen state
ϕ_0	Volume fraction of polymer in the preparation state
ϕ_1	Volume fraction of solvent in gel
ϕ_2	Volume fraction of polymer in gel
ϕ_{cyl}	Volume fraction of cylinders
ϕ_{PNIPAm}	Volume fraction of PNIPAm
X_{12}	Flory interaction parameter
b	Kuhn length
Å	Angstrom
G_c	Fracture energy in elastomers
G_0	Fracture energy in unfilled rubbers
J_r	Energy required to rupture one covalent bond
ξ	Correlation length
ξ_b	Blob size
ξ_n	Mesh size
t	Time
V	Volume
V_2	Volume of rich-PNIPAm microdomains

V_1	Molar volume of the solvent
V_2	Molar volume of the monomer unit
S_{spe}	Specific syrface of rich-PNIPAm microdomains
S_2	Surface area of rich-PNIPAm microdomains
v_{pol}^{spe}	Specific volume of the dry polymer
ΔF	Free energy
ΔF_m	Free energy mixing term
ΔF_{el}	Free energy elastic term
f	Functionality of the junction points
R_0	Radius
R_g	Radius of gyration of the polymer chain
$R_{g,l}$	Radius of gyration of a linear polymer chain
$R_{g,b}$	Radius of gyration of a branched polymer chain
R^2	Mean square end to end distance of network strands in their final state
R_0^2	Mean square end to end distance of network strands at preparation state
R_θ^2	Mean square end to end distance of network strands in unperturbed conditions
R_{ref}^2	Mean square end to end distance of a free chain with the same number of monomers as a network strand in the same solution
Π_{gel}	Osmotic pressure inside the gel
Π_m	Mixing contribution to the osmotic pressure inside the gel
Π_{el}	Elastic contribution to the osmotic pressure inside the gel
Π_{out}	Osmotic pressure of the surrounding medium
N_A	Avogadro's number
l	Monomer length
l_c	Length of the insoluble block

a_0	Equilibrium area per molecule at the aggregate interface
v	Volume of insoluble block
v_m	Monomer volume
n_e	Number of elastically active chains
n_{sc}	Degree of polymerization of the side-chains
n_g	Number of monomers between two consecutive side-chains
n_g^{-1}	Grafting density
j	Number of junctions points per strand
g	Branching index
N_{ag}	Average aggregation number
N_c	Number of monomer units between cross-links
N_x	Mean number of “equivalent” units between junctions
N	True average degree of polymerization of strands
a_T	Time-temperature superposition shift factor
$I(q)$	Scattering intensity
$I_{//}(q)$	Scattering intensityalong the parallel axis
$I_{\perp}(q)$	Scattering intensity along the perpendicular axis
$I_{sol}(q)$	Thermodynamic fluctuations
$I_{ex}(q)$	Excess scattering
λ_θ	Wavelength of the incident neutron beam
θ	Scattering angle
q	Scattering vector
q_{peak}	Value of the scattering vector at the maximum of the peak
Inv_{exp}	Experimental invariant
Inv_{th}	Theroretical invariant
Ξ	Lengthscale characterizing the static inhomogeneities
d_c	Characteristic distance between PNIPAm domains

ρ_i	Scattering length density
ρ_{cyl}	Scattering length density of the phase-separated phase
ρ_{sol}	Scattering length density of the surrounding medium
f_{PNIPAm}	Fraction of PNIPAm side-chains
L_{cyl}	Length of the cylinders
p	Packing parameter
R	Ideal gas constant
L	Length of the sample
L_0	Initial length of the sample
L_i	Initial length of the sample before mechanical test
w	Width
h	Thickness
l_{over}	Overlap length
ΔL	Displacement
λ	Deformation ratio
λ_c	Deformation ratio at break
ε_c	Deformation at break
c	length of the notch
E	Elastic modulus
F	Force
F_{max}	Failure force
l_g	Average length of PNIPAm grafts
G	Shear modulus
G'	Shear storage modulus
G''	Shear loss modulus
$tan\ \delta$	loss tangent
ω	Radial frequency (rad/s)

f_1	Frequency (Hz)
ε	Strain
σ_{nom}	Nominal stress
σ_R	Reduced stress
W	Strain energy density
G_0	Fracture energy in unfilled rubbers
G_c	Fracture energy in elastomers
v_c	Crack velocity
G_{adh}	Adhesion energy
$E_{20°C}/E_{60°C}$	Stiffening ratio

Contents

General Introduction

General introduction

Hydrogels have been sparking an increasing interest for the last four decades but have always been everywhere around us. They are present in nature for millennia in the human body as tendons for example but also in flora as algae or sea anemones. As polymer networks, that can be expanded throughout their whole volume by aqueous fluid (IUPAC definition), they have attracted interest in fields such as food science or agriculture. They are also promising candidates especially in the biomedical domain, for applications such as tissue engineering or targeted drug delivery systems.

Synthetic hydrogels have thus been extensively explored but they often do not meet the mechanical properties that are crucial to respond to specific and complex physiological functionalities. Indeed, they are most of the time fragile in terms of toughness, extensibility and stiffness due to their high water content. Thus, in order to extend their applicability, numerous ways of reinforcement have been investigated to elaborate gels with targeted mechanical properties. For example, some strategies have focused on improving extensibility of hydrogels by preparing “ideal” networks, i.e. 3D macromolecular architectures with isomolecular elastic strands free from cross-linking inhomogeneities.

Another way to improve the mechanical properties of the gels is to prepare interpenetrating networks by introducing a first one into a loosely cross-linked polymer network. In these systems, also called "double network gels," the first network is a sacrificial one that breaks under stress and prevents the second one from being damaged. The gel thus retains its macroscopic integrity even if its mechanical properties progressively irreversibly weaken with loading. However, all the strategies mentioned above show some limitations in terms of toughness and/or extensibility but especially in terms of self-healing. To solve this issue, alternative strategies involving sacrificial physical bonds have been developed. The idea is to introduce, into a chemically cross-linked polymer network, reversible physical bonds (i.e. sacrificial ones) able to dissipate energy by breaking under mechanical loading. As a matter of fact, it retards the propagation of a crack into the gel but it also allows self-healing as the physical interactions are reversible and can reform. Nonetheless, the reversibility of these interactions can be difficult to control in a complex medium such as water.

With the idea of controlling the physical interactions more finely and/or “on demand”, *stimuli*-responsive polymers are natural candidates as many different environmental parameters can dramatically and reversibly modulate their solubility such as pH, temperature,

light, magnetic field etc... Among these *stimuli*, the temperature is probably the most studied as it is easy to control and it is a critical parameter in many technological fields, particularly in biomedical applications. In addition, there is a large number of thermo-responsive polymers in aqueous media which offers a wide choice in the design of thermo-responsive hydrogels.

However, when crossing the critical temperature, thermo-responsive polymers undergo a phase-transition with a conformation change from coil to globule at the nanoscale which macroscopically generates a large volume change of the hydrogel. This volume transition is interesting for specific applications such as responsive soft actuators but it implies a significant reduction in the water content which therefore could limit their applications, especially in the biomedical field. Moreover, when studying the impact of the phase transition on the mechanical properties of the gel, it is really difficult to separate the contribution associated with the volume variation, i.e. overall polymer concentration, from the one related to the formation of a biphasic or segregated morphology.

By combining into the same polymer network both water-soluble and thermo-responsive polymers, Hui Guo as recently developed in his PhD work (2015), an efficient strategy to maintain a relatively high swelling level while avoiding the change of volume at the transition temperature. In this case, it was shown that the process of polymer phase-separation induces the reversible formation of polymer-rich domains embedded in a highly swollen phase. Under mechanical loading, the physical bonds formed within these domains can break reversibly and dissipate energy that strongly enhances the mechanical properties of the gel (elastic modulus and elongation at break).

Although this concept of thermo-reinforced networks has been clearly demonstrated with graft polymer architectures, the relationships between the primary structure of the network, its segregated morphology above the transition temperature and the final mechanical properties of the network are yet to be specified. In order to investigate these relations in a more systematic way, we have extended the initial work of Hui Guo by preparing a homologous series of grafted hydrogels based on a lightly cross-linked hydrophilic network decorated with thermo-responsive side-chains.

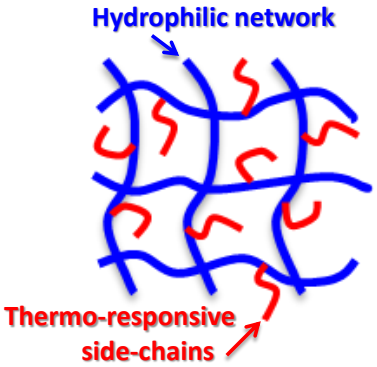

Figure. Primary structure of thermo-responsive grafted hydrogels

In the present study, special attention has been paid to the influence of the macromolecular architecture of the network (hydrophilic/thermo-responsive ratio and average molar mass of responsive side chains) over the self-assembling process and the resulting mechanical properties. Subsequently, the concept of hydrogels thermo-responsive toughening induced by the universal process of polymer phase-separation was extended to Upper Critical Solution Temperature (UCST) polymers. Indeed, by replacing the hydrophilic macromolecular network with a UCST-type polymer, we have studied the possibility of designing double temperature responsive hydrogels, capable of inducing reinforcing biphasic morphologies not only during heating but also during cooling.

The following manuscript is divided into 5 chapters, the broad outline of which follows:

1. **Chapter 1** first presents the literature background on the numerous strategies developed during the last three decades in order to achieve mechanical toughening of gels as well as their limitations. Then, it will mainly focus on thermo-responsive polymers and a particular attention will be paid to the concept of mechanical reinforcement of hydrogels induced by the process of polymer phase-separation.
2. **Chapter 2** introduces the design of two series of grafted hydrogels with: (i) the variation of the average molar mass of thermo-responsive side-chains grafted in a similar hydrophilic network and (ii) the variation of the hydrophilic/thermo-responsive polymers ratio using the same thermo-responsive side-chains. The synthesis and the characterization of thermo-responsive macromonomers as well as the elaboration of grafted hydrogels will be described in this chapter.
3. **Chapter 3** aims bridging the gap between the primary structure of the hydrogels, described in chapter 2, with thermodynamic behaviour as well as the biphasic morphology developed above the transition temperature.

4. **Chapter 4** focuses on the mechanical properties of hydrogels and their thermo-responsiveness with the goal of identifying how the structural parameters and their self-assembling behaviour influence the mechanical properties in terms of strength, extensibility and toughness.
5. **Chapter 5** finally expands the concept of mechanical reinforcement induced by the polymer phase separation by combining into the same hydrogel both LSCT and UCST polymers. This chapter has been published in **Macromolecular Rapid Communications**, *2017*, 38, 1700287.

Chapter 1

State of the art

Chapter 1: State of the art

I. Hydrogels: basic concepts, applications and research focuses

I.1. Hydrogels history and definitions

The word "hydrogel" exists since 1894[1,2] and was first used to describe a colloidal gel made with inorganic salts. Even if the behaviour of tridimensional polymer networks in solvent and especially in water is known since Staudinger, it is only in the 60's that a cross-linked network material was first reported in literature as "hydrogel" as we described it nowadays i.e. defined as two- or multi-component systems consisting of a three-dimensional network of polymer chains and water that fills the space between macromolecules.2 This hydrogel was a polyhydroxyethylmethacrylate (pHEMA) network developed with the ambitious goal of using it in permanent contact applications with human tissues. Attention for hydrogels due to their exceptional promise in wide range of applications has exponentially increased since that time, especially from the last fourty years.2,[3]

Polymer hydrogels possess high swelling (up to more than 99 % of their total weight) due to the thermodynamical affinity between the polymer network and the solvent itself. The macromolecules which constitute the polymer network can be either physically or covalently cross-linked. Physical cross-linking (respectively chemical one) results in a material called "physical hydrogel" (respectively "chemical hydrogel") (see **Figure 1.1**).[4]

Physical hydrogels are made of polymer chains interacting with each other through physical interactions with a longer life-time than the observation timescale, thus leading to a 3D polymer network architecture. Those interactions can be associative ones, entanglements or even due to phase-separation. As a result, the reversible liquid-solid state called sol-gel transition depends on the environment as the physical cross-links are reconfigurable. On the contrary, chemical hydrogels cannot go back to the liquid state once the polymer chains are covalently and permanently bonded.

[1] J. M. Bemmelen, **Zeitschrift für Chemie und Industrie der Kolloide**, *1907*, 1, 213-214
[2] N. Chirani, L'H. Yahia, L. Gritsch, F. L. Motta, S. Chirani and S. Fare, **J Biomedical Sci.**, *2015*, 4, 1-23
[3] N. A. Peppas and R. S. Stauffer, **Journal of Controlled Release**, *1991*, 16, 305-310
[4] D. Lombardo M. A. Kiselev, S. Magazù, and P. Calandra, **Advances in Condensed Matter Physics Volume 2015**, *2015*, Article ID 151683

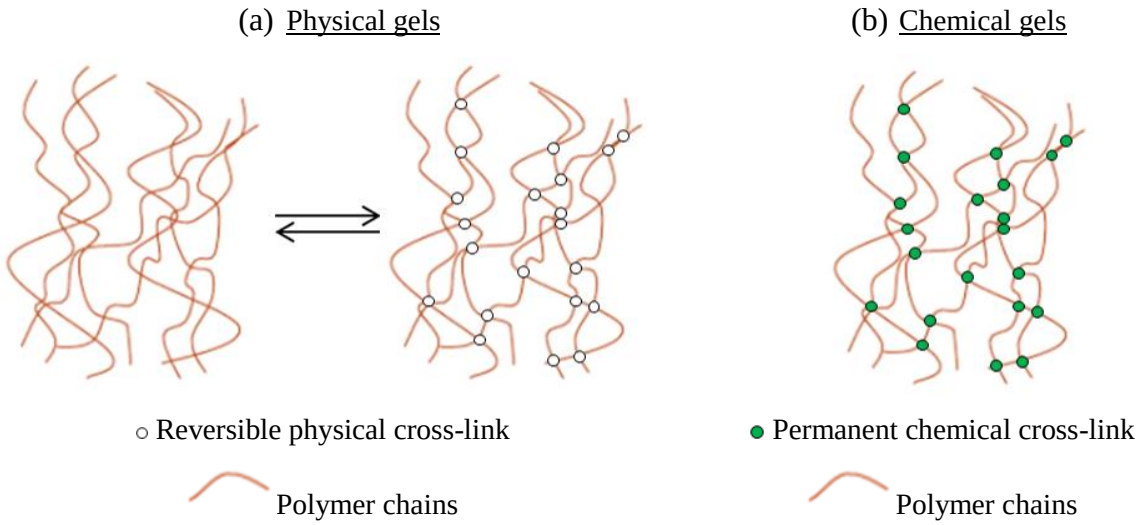

Figure 1.1. Schematic representation of **(a)** physical and **(b)** chemical hydrogels

Hydrogels can be found everywhere in our daily life, being either natural or synthetic. Our body is a good example as it is made of tendons, vitreous parts of the eye and other biological components which are hydrogels. It makes these ones especially interesting for the biomedical field. They are also the first synthetic materials employed for permanent use in the human body.2 From now on, they have already been used in biomedical applications such as contact lenses,[5] drug delivery[6,7] or even tissue engineering.[8] Many other industrial fields are also interested in and/or prospecting for these elastic materials: agriculture,[9] coal dewatering, sensors[10] etc.

I.2. Hydrogels as smart materials: applications and perspectives

Industrial needs, especially in biomedical fields, request to both enhance the mechanical properties of hydrogels and to modulate together their shape and properties. In fact, they need to be flexible, extensible and mechanically resistant against stress and fracture in order to be easily manipulated so then industrialised.

Thus, to be suitable for different applications or perspectives, hydrogels have to meet some specific mechanical, macroscopic and nano-/micro-scopic properties. As these aspects are dependent on hydrogels bulk network structure, it is important to be able to tune it to

[5] A. Childs, H. Li, D.M. Lewittes, B. Dong, W. Liu, X. Shu, C. Sun and H.F. Zhang, **Scientific Reports**, *2016*, 6, article 34905
[6] L. Xinming C. Yingde, A.W. Lloyd, S.V. Mikhalovsky, S.R. Sandeman, C.A. Howel and L. Liewen, **Cont. Lens Anterior Eye**, *2008*, 31, 57-64
[7] T. R. Hoare and D. S. Kohane, **Polymer**, *2008*, 49, 1993-2007
[8] I. M. El-Sherbiny and M. H. Yacoub, **Glob. Cardiol. Sci. Pract.**, *2013*, 38, 316–342
[9] R. Vundavalli, S. Vundavalli, M. Nakka and D.S. Rao, **Procedia Materials Science**, *2015*, 10, 548-554
[10] A. Richter, G. Paschew, S. Klatt, J. Lienig, K-F. Arndt and H-J.P. Adler, **Sensors**, *2008*, 8, 561-581

fulfill most of the requirements needed for a wide range of applications. Some crucial parameters which characterize the network structure are the volume fraction of polymer in the swollen state (ϕ_{eq}), the number average molar mass between two adjacent cross-linking points (M_c) and the network mesh (or pore) size.[11,12,13] All these parameters are related to the characteristics of the cross-links connecting the polymer chains together. Indeed, at low cross-linking agent concentration, the polymer chains will not percolate through a three dimensional network whereas when this concentration is increased, effective cross-links are created and a macroscopic hydrogel is obtained. Moreover, increasing the cross-linking density implies a reduction in swelling capacity.[14] Indeed, the mobility of polymer chains is reduced by the presence of cross-links which immobilize them on certain portions. As a result, these polymer chains are less able to extend so the mesh size is reduced while the global polymer volume fraction at the swollen state is increased and the absorption capacity of gels is reduced.

As all these network parameters can be measured through a range of experimental techniques or calculated by application of network deformation theories, it is possible to link them to the hydrogels properties. For example, a correlation between the mesh size of a swollen cross-linked network and its equilibrium polymer volume fraction has been established by T. Canal and N. Peppas.[15] Then, both the initial monomer and/or polymer concentration in solution and the one of cross-linkers also impact the network parameters as they control M_c so the polymer chains possibility to extend to get a higher swollen state and a lower ϕ_{eq}.

Chemically cross-linked hydrogels can be obtained by different types of synthesis:[14,15,16] cross-linking by complementary groups chemical reaction, high energy radiation, conventional or controlled free radical polymerization or even by using enzymes. The resulting cross-linking is impacted by the synthesis pathway.

To conclude, the way of synthesizing gels and especially the initial concentrations in monomers/polymers, the cross-linking density, the distribution of cross-linking points, the concentration of elastically active polymer chains and their length between two cross-linking

[11] T. R. R. Singh, G. Laverty and R. Donnelly, **Hydrogels: Design, Synthesis and Application in Drug Delivery and Regenerative Medicine**, **CRC Press/Tailor & Francis Group**, *2018*, Boca Raton
[12] S. Kahn, A. Ullah, K. Ullah and N-u. Rehman, **Designed monomers and polymers**, *2016*, 19, 456-478
[13] N. A. Peppas, Y. Huang, M. Torres-Lugo, J. H. Ward and J. Zhang, **Annu. Rev. Biomed. Eng.**, *2000*, 2, 9-29
[14] L. C. Dong, A. S. Hoffman and Q. Yan, **J. Biomater. Sci. Polym. Ed.**, *1994*, 5, 473–484
[15] T. Canal and N. A. Peppas, **J. Biomed. Mater. Res.**, *1989*, 23, 1183–1193
[16] M. F. Akhtar, M. Hanif and N. M. Ranjha, **Saudi Pharmaceutical Journal**, *2016*, 24, 554–559

points are thus crucial parameters to control the structure of the polymer network and consequently the hydrogels properties. As a matter of fact, they are decisive to meet some expectations as they will influence both the swelling and the mechanical properties of hydrogels. The nature of polymer chains and the topology of the network also have an important impact on these properties especially in terms of responsiveness towards environmental parameters such as pH, temperature etc. This part will be discussed further.

I.3. Mechanical properties of hydrogels

Hydrogels mechanical properties are driven by many parameters such as the chemical nature of the polymer network, architecture and concentration, the presence of heterogeneities etc. that can all lead to drastic changes in their behaviour. As a matter of fact, both of them influence a lot the swelling/deswelling degree of hydrogels, their rheological behaviour but also their mechanical properties at high deformation: resistance to stress, torsion and fracture. The hydrogels properties are thus strongly correlated to their network structure.

Hydrogels are often represented as a fish net but in reality, as previously explained, depending on many parameters, they can also have different types of defects making them improper for some applications. The presence of cross-linking heterogeneities appearing during the gelation process is thus preventing the polymer chains to extend to their maximum, like a perfect homogeneous network, resulting in reduced limit extensibility and ability to swell.

These non-relaxing frozen domains called inhomogeneities can be of three types: spatial inhomogeneities, topological inhomogeneities or connectivity ones (see **Figure 1.2**).[17]

- During hydrogel formation, the cross-linking points are formed in a non-homogeneous spatial distribution leading to the presence of spatial inhomogeneities (see **Figure 1.2.a**).[18]
- Loops, trapped entanglements and dangling chains are also created in the polymer network depending on its topology and resulting in the existence of topological inhomogeneities (see **Figure 1.2.b**).

[17] F. Ikkai and M. Shibayama, **Journal of Polymer Science Part B: Polymer Physics**, *2005*, 43, 617-628
[18] M. Shibayama, **Macromol. Chem. Phys**, *1998*, 199, 1-30

- The sizes and spatial distribution of the clusters are linked to a percolation problem with the presence of connectivity inhomogeneities (see **Figure 1.2.c**).

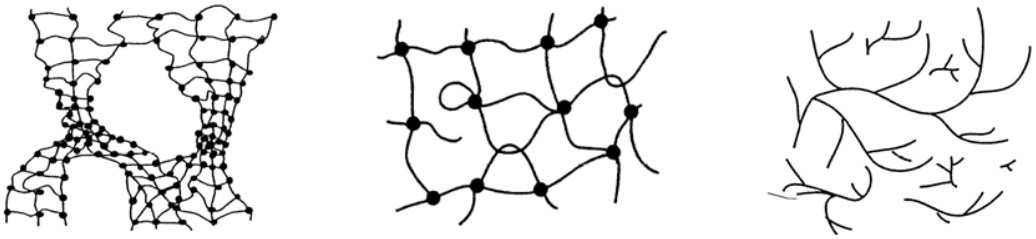

(a) Spatial inhomogeneities | **(b)** Topological inhomogeneities | **(c)** Connectivity inhomogeneities

Figure 1.2. Shibayama's classification of inhomogeneities in gels (from F. Ikkai and M. Shibayama)[17]

Many parameters influence the polymer network heterogeneities such as the nature of monomers and/or polymers engaged, pressure, temperature, polymer network fraction and type or degree of ionisation but also the reactivity between monomers and cross-linker agents. Hydrogels mechanical properties are often addressed to be poor due to the presence of inhomogeneities which reduce the extensibility of polymer chains and because the lack of dissipation process at high water content, the loss modulus *G''* being negligible compared to the storage modulus *G'*. Thus, they usually are soft fragile materials with little extensibility. These poor mechanical properties reduce drastically the possibilities of applications especially in the biomaterials field where high standards have to be met as outlined above.

Different models have been studied to predict the mechanical behaviour of hydrogels. These models are based on the elastic behaviour of rubbers. Rubbers are lightly cross-linked networks responding to external stresses with a rapid rearrangement of the polymer segments due to their fast dynamics. Chemical hydrogels are often compared to cross-linked elastomers and reported to have lower stiffness (~10 kPa), strength (~100 kPa) and fracture toughness (~10 J/m^2).[19] According to this definition, the model for rubber elasticity can be extended to hydrogels as swollen rubbery materials.[20]

Actually, hydrogels are mostly hydrophilic by definition which makes them able to swell but decreases their mechanical properties compared to rubbers. Moreover, by increasing the

[19] P. Calvert, **Adv. Mater.**, *2009*, 21, 743-756
[20] K. S. Anseth, C. N. Bowman and L. Brannon-Peppas, **Biomaterials**, *1996*, 17, 1647-1657

amount of solvent used during the synthesis, the structure and nature of the polymer network formed are really different from the one prepared in bulk polymerization. As a matter of fact, with increasing the amount of solvent, the cross-linking agent tends to form cycles rather than cross-links which creates heterogeneities not contributing to the mechanical strength of the elastic material.[19] Increasing the amount of cross-linking agent also leads to the formation of similar heterogeneities. Thus, the fraction of cross-links effectively participating in the formation of elastic strands is reduced even though their absolute number is increased due to the globally higher cross-linking density.[19] In this manner, both the amounts of cross-linking agent and solvent impact on the hydrogels swelling degree and, consequently, on their mechanical properties.

In addition to the other mechanical parameters (modulus, extensibility, etc.), fracture resistance is a determining parameter for the use of hydrogels in diverse application fields. Based on the schematic picture of a network formed by a collection of long and flexible chains as shown in **Figure 1.3**, the fracture resistance properties of hydrogels can be estimated using the Lake and Thomas[21] model initially proposed to calculate the threshold fracture energy G_0 needed to propagate a crack in unfilled rubbers (**Eq. 1.1**):

Eq. 1.1: $$G_0 = \Sigma J_r N_c$$

where Σ is the surface density of chains crossing the fracture plane, N_c is the number of monomer units between cross-links, and J_r is the energy required to rupture one covalent bond.

Such argument is based on the assumption that the transmitted load throughout the network brings each bond in a polymer strand crossing the interface close to its maximal free energy (i.e. the dissociation energy of the weakest bond in the monomer unit).

[21] G. Lake and A. Thomas, **Proceedings of the Royal Society of London A: Mathematical, Physical and Engineering Sciences**, *1967*, 300, 108-119

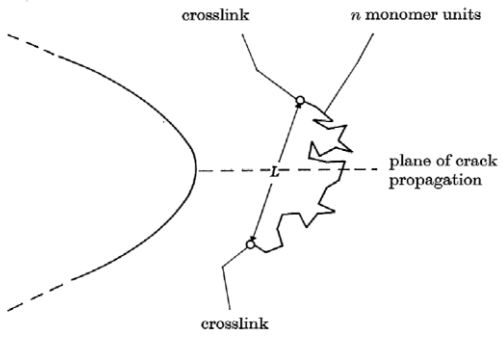

Figure 1.3. Schematic view showing a polymer chain lying across the plane of crack propagation (from G. Lake and A. Thomas)[21]

Fracture energy in elastomers can be written as the combination of two contributions: an interfacial term and a second contribution related to viscoelastic losses due to monomer friction in a volume near the crack tip. Thus, A. N. Gent proposed the following expression for the fracture energy, G_c **(Eq. 1.2)** [22]:

Eq. 1.2: $G_c = G_0\left(1 + f(a_T v_c)\right)$

where G_0 is mostly related to the chemistry of the interface and the second contribution ($1+f(a_T v)$), depending on the mechanical dissipation in the volume, is related to the crack velocity v_c and the time-temperature superposition and shift factor a_T.

As mentioned above, in rubbers this second term can typically enhance the mechanical energy required to propagate a crack by two or three orders of magnitude. In contrast, chemically cross-linked hydrogels do not exhibit such dissipative processes and typical G_c values are quite in line with the Lake and Thomas' elastic prediction. As a result, besides gels softness, highly swollen gels demonstrate high fragility and particular sensitivity to defects or heterogeneities. Indeed, in the case of highly swollen networks, the theoretical value of threshold fracture energy G_0 decreases with polymer volume fraction and G_0 values obtained for gels are typically ~1 J/m^2 while they are 10 times higher for unfilled rubbers due to viscoelastic dissipation.

To conclude, the swelling degree is often predetermined by the gels targeted applications but high water content weakens hydrogels, inevitably leading to poor mechanical properties. Therefore, to tackle this problem which precludes their use, it is important to develop alternative ways to reinforce hydrogels and make them as strong and extensible as rubbers while keeping their high swelling degree.

[22] A. N. Gent, **Langmuir,** *1996*, 12, 4492-4496

II. Macromolecular strategies to reinforce hydrogels

Research carried out these last decades has highlighted many different ways for improving hydrogel mechanical properties. These numerous methods can be separated into two major groups:

- Modification of the covalent architecture of hydrogels
- Introduction of secondary physical interactions into polymer networks

II.1. Architectural modification of polymer networks

As explained above, hydrogel mechanical properties are strongly linked to the presence of heterogeneities in the polymer network. To solve this problem, research was focused during these last decades on synthesizing polymer networks with a minimum of heterogeneities.[20] Here, we present the literature background on the existing syntheses ways allowing to obtain hydrogels with a more homogeneous structure either at the preparation state or during mechanical loading. To this extent, slide-ring gels, tetra-PEG star hydrogels and other click-chemistry based gels were studied. Then, the case of double networks (DN) presenting the concept of sacrificial bonds will be studied.

II.1.1. Looking towards a homogeneous polymer network

An interesting way to reinforce hydrogels is to synthesize ideal homogeneous networks. Indeed, a homogeneous network is more resistant to stress and strain as the applied load is distributed over a larger fraction of chains with a uniform strain distribution. Thus, the number of sites available for micro crack formation (i.e., nucleation of defects) is decreased and the gel is less prompt to be damaged. This homogeneity principle is used in slide-ring gels, tetra-PEG star hydrogels and other click-chemistry based networks.

II.1.1.1. Slide ring gels

Slide ring gels are based on a simple concept: topologically interlocking of the polymeric chains instead of covalent or physical cross-linking.[23] The nanoscale "inhomogeneities" in this type of polymer network do not decrease the mechanical strength of the gel as they are not "fixed" (i.e., cyclic molecules are able to slide along the polymer chains) (see **Figure 1.4.a-c**). As a matter of fact, the extensibility of the gel is highly

[23] Y. Okumura and K. Ito, **Adv. Mater.**, *2001*, 13, 485-487

improved thanks to the *pulley effect*: cyclic molecules sliding and equalizing the applied tension.[24]

Y. Okumura and K. Ito were the first to introduce the concept of slide-ring gels in 2001.[23] They synthesized a polyrotaxane in which α-cyclodextrin groups were sparsely distributed on a poly(ethylene glycol) (PEG) chain of high molar mass and then they chemically paired the α-cyclodextrins. The resulting gels made of 10 wt % polymer concentration were transparent, flexible and considered as superabsorbents: they could absorb water up to 1600 times the weight of their dry PEG content.

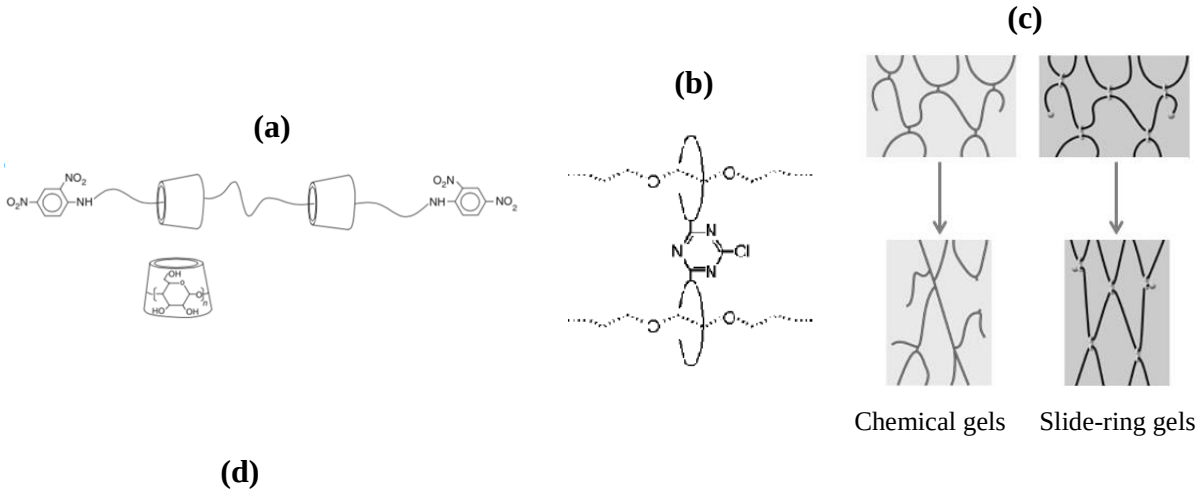

Figure 1.4. **(a)** The polyxoratane consisting of poly(ethylene glycol) around which α-cyclodextrin groups revolve. **(b)** The "figure-of-eight cross-link": covalently cross-linked cyclodextrins. **(c)** Schematic comparison between chemical gels (nanoscale heterogeneities) and slide-ring gels (*pulley effect* of cyclic molecules and polymer chains (from Y. Okumura and K. Ito)[23] **(d)** Stress-strain curves of slide-ring gels at 10 wt % polymer concentration with different concentrations of cyanuric chloride as α-cyclodextrin cross-linker (from K. Ito)[24]

Despite their high extensibility conferred by the *pulley effect*, slide-ring hydrogels are still weak elastic materials. Their elastic modulus (E) and fracture energy ($\mathcal{G}_c$) are around 10 kPa and 4 J/m^2 respectively at 10 wt % polymer concentration and the cyclic molecules can easily aggregate depending on the hydrogel environment.[25] This aggregation results in a tremendously lower extensibility due to the reduction of the cyclic molecules mobility.

[24] K. Ito, **Polymer Journal**, *2007*, 39, 489-499
[25] C. Liu, H. Kadono, K. Mayumi, K. Kato, H. Yokoyama and K. Ito, **ACS Macro Lett.**, *2017*, 6, 1409−1413

II.1.1.2. Tetra-PEG hydrogels

Ten years ago, another type of gels with a highly homogeneous 3D architecture was synthesized by T. Sakai's group: tetra-PEG hydrogels. They are made of two well-defined symmetrical tetrahedron like macromonomers of similar size.[26,27,28] The first macro-monomer is a tetra-amine-terminated PEG (TNPEG) and the second one is tetra-NHS-glutarate terminated PEG (TAPEG) with respectively propylamine and succinimide glutarate terminal groups. When mixing these two macromonomers in water, the gelation takes place in few minutes while self-reaction is avoided leading to a well-controlled network as shown in **Figure 1.5.a**. Indeed, the network formation occurs by the creation of amide bonds due to spontaneous chain stretching and coupling of succinimidyl ester and amine groups at chain ends. This gelation process can be followed by Flory's classical theory.[29]

Thanks to the unique impenetrable sphere-like behaviour of the tetra-arm star polymers in semi-dilute solution, the existence of topological defects in the micro-network structure is highly decreased (see **Figure 1.5.a-b**).[27] As a matter of fact, it prevents the formation of loops and defects during the gelation which are known to weaken the network properties.

The compressive mechanical properties of such gels are highly enhanced compared to conventional ones (see **Figure 1.5.c**): their maximum stress at break is up to 27 MPa at 14 wt % polymer concentration using TAPEG and TNPEG (M_n = 20 kg/mol) in stœchiometric quantities whereas the one of conventional hydrogels is around 10-100 kPa.[30] Varying the polymer concentration, tetra-PEG gels exhibit fracture energy $\mathcal{G}_c \sim$ 10-100 J/m^2.[31]

[26] T. Sakai, T. Matsunaga, Y. Yamamoto, C. Ito, R. Yoshida, S. Suzuki, N. Sasaki, M. Shibayama and U-i. Chung, **Macromolecules**, *2008*, 41, 5379-5384
[27] Y. Akagi, T. Matsunaga, M. Shibayama, U-i. Chung and T. Sakai, **Macromolecules**, *2010*, 43, 488-493
[28] A. Costa and J. Mano, **European Polymer Journal**, *2015*, 72, 344-364
[29] P.J. Flory, **J. Am. Chem. Soc.**, *1941*, 63, 3083-3090
[30] T. Sakai, Y. Akagi, T. Matsunaga, M. Kurakazu, U-i. Chung and M. Shibayama, **Macromol. Rapid Commun.**, *2010*, 31, 1954–1959
[31] Y. Akagi, H. Sakurai, J.P. Gong, U-i. Chung and T. Sakai, **J. Chem. Phys.**, *2013*, 139, 144905

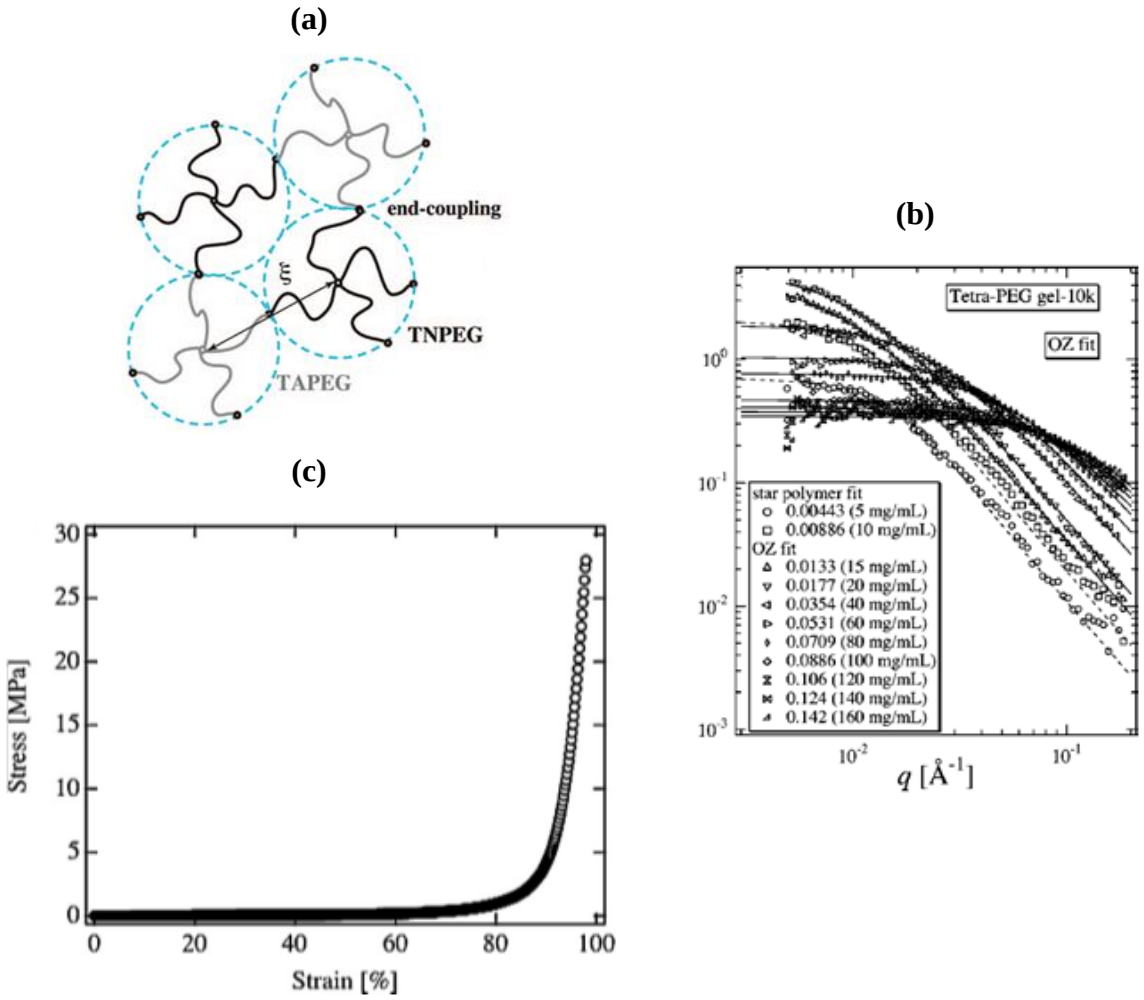

Figure 1.5. **(a)** Schematic representation showing a Tetra-PEG gel network with ξ the mesh size (from Y. Akagi et al.)[27] **(b)** Evolution of the SANS profiles of Tetra-PEG gels towards the polymer concentration. The Tetra-PEG gels are made of 10 kg/mol molar mass TAPEG and TNPEG. The dashed lines are fitted functions for imperfect gels at low macromonomer concentrations and the solid ones are fitted with the Ornstein-Zernike function (OZ)[27] **(c)** Compression stress-strain curve of Tetra-PEG networks at 14 wt % polymer concentration and made of 20 kg/mol molar mass TAPEG and TNPEG (from T. Sakai et al.)[30]

The correlation between mechanical properties and the structure of tetra-PEG hydrogels have been deeply studied by Small Angle Neutron Scattering (SANS), Dynamic Light Scattering (DLS) and mechanical experiments (see **Figure 1.5.b**). It brings to light the following results.[27,32] As the control of inhomogeneities in these gels is dependent on the concentration of TAPEG and TNPEG,[27] these macromonomers need to be introduced in stœchiometric quantities to prevent the formation of heterogeneities in the polymer network. In these conditions, their mechanical elastic and shear moduli, are proportional to the initial polymer concentration. The importance of cross-end-coupling of A- and B- type tetra-PEG to

[32] M. Shibayama, **Macromolecules**, *2009*, *42*, 1344–1351

get hydrogels with extremely low defects is also highlighted. Tetra-PEG macromonomers behaving as impenetrable space-filled blobs in the semi-dilute regime, the resulting polymer network at C (polymer concentration) = C* (overlap concentration) has an optical transmittance of ~100 %. It proves the strong correlation between the mechanical properties enhancement and the existence of a highly homogeneous polymer network.

II.1.1.3. Other hydrogel architectures based on click-chemistry

An efficient way to reduce the level of inhomogeneities in hydrogels is to use well-controlled chemical reactions such as click-chemistry.[33,34,35] D.A. Ossipov and J. Hilborn[35] were the firsts to elaborate hydrogels with click-chemistry principle based on the researches of V.V. Rostovtsev.[36] Indeed, V.V. Rostovtsev et al. developped a new method to get a thermally and hydrolytically stable triazole connection. This synthesis not only induces high yielding and almost perfect regioselectivity but also offers an unprecedented level of selectivity, reliability and a broad scope for organic syntheses purposes depending on the creation of covalent links between various building blocks. By using this click-chemistry approach, D.A. Ossipov and J. Hilborn have shown that the synthesis of poly(vinyl alcohol) (PVA) networks was more effective in gel formation, giving higher values of the gel fractions and well-defined networks compared to the use of tetra-functional cross-linkers.[35]

At the same time, M. Malkoch et al. developed PEG-based hydrogels exhibiting both higher elastic modulus and extensibility proving that their mechanical properties are enhanced (elastic modulus up to ~680 MPa with strain at break of ~400 %) while keeping a water content up to 89 wt %.[34] This mechanical enhancement has been confirmed for other types of polymer networks such as HA- (Hyaluronic acid sodium salt).[33] Independently of the polymer network nature, the mechanical properties of hydrogels can be controlled by the cross-linking macromolecules type: the weight fraction (concentration) and the functionality (number of functional groups) play a role on the structure of the polymer network, and consequently on the mechanical improvement.[33,35] Another way to improve mechanical properties is to modulate the average molar mass of the polymer chains which constitute the network.[34]

On the other hand, click-chemistry based hydrogels are good candidates for biomedical applications, especially as drug released agents and scaffold engineering, thanks to

[33] V. Crescenzi, L. Cornelio, C. Di Meo, S. Nardecchia and R. Lamanna, **Biomacromolecules**, *2007*, 8, 1844-1850
[34] M. Malkoch, R. Vestberg, N. Gupta, L. Mespouille, P. Dubois, A.F. Mason, J.L. Hedrick, Q. Liao, C.W. Frank, K. Kingsburye and C.J. Hawker, **Chem. Commun.**, *2006*, 26, 2774–2776
[35] D.A. Ossipov and J. Hilborn, **Macromolecules**, *2006*, 39, 1709-1718
[36] V.V. Rostovtsev, L.G. Green, V.V. Fokin and K.B. Sharpless, **Angew. Chem. Int. Ed.**, *2002*, 41, 2596-2599

their well-defined network and the high degree of reproducibility in terms of gel fraction and reaction time. Their stability in different environmental conditions and their high tolerance to various additives are also crucial advantages for biomedical applications. Nonetheless, this click-chemistry reaction type requires to use Cu(I) which induces problems of toxicity, limiting its use to some biomedical needs only.

Slide-ring gels, tetra-PEG hydrogels and other click-chemistry based gels strategies have been developed to delay crack initiation by decreasing the polymer network inhomogeneities. Thus, the stretch ability of the gel is efficiently improved as crack initiation is delayed. Though, when it comes to gel toughness improvement, the fracture energy is still low as decreasing the network heterogeneities does not help to increase the energy dissipation and to slow down the crack propagation. Another concept is thus needed to also enhance fracture resistance.

II.1.2. Sacrificial bond concept

Tough chemical gels are obtained by introducing dissipation mechanism at the molecular level through the interpenetration of "strong" and "weak" polymer networks. It makes it an interesting strategy to enhance hydrogels fracture energy and lower their weakness against defects like double networks (DN) gels synthesized first by J.P. Gong et al.[37] DN gels synthesis usually consists in a two-step process: (1) synthesizing first a tightly cross-linked network; (2) swelling it in a monomer solution with a low cross-linking agent ratio to polymerize a second loosely cross-linked network into the first one. As a matter of fact, the second network in the final gel is in large excess compared to the first one (~7-20 wt %). The first network is often made of a polyelectrolyte polymer to ensure both high swelling to the gel and inter-locked entanglements to the second network. Thus, as shown in **Figure 1.6.a**, the highly extended and so rigid first network acts as a sacrificial network by breaking upon mechanical loading while the second network confers macroscopic integrity and good extensibility to the gel.[37] As shown in **Figure 1.6.b**, the breaking of sacrificial bonds during mechanical loading leads to an irreversible gel softening.[38]

[37] J.P. Gong, Y. Katsuyama, T. Kurokawa and Y. Osada, **Adv. Mater.**, *2003*, 15, 1155-1158

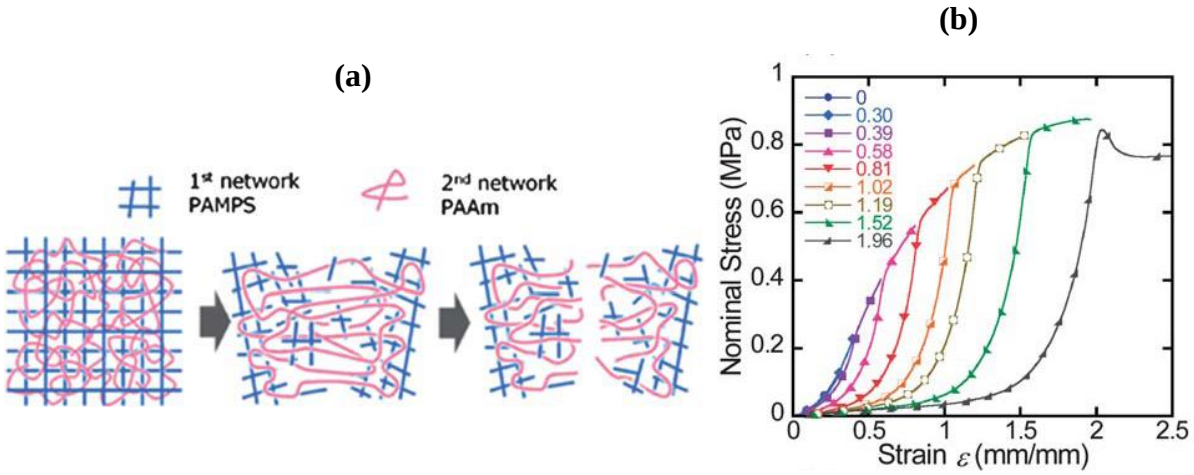

Figure 1.6. **(a)** Schematic structure and behaviour under mechanical loading of poly(2-acrylamido-2-methylpropanesulfonate/poly(acrylamide) (PAMPS/PAAm) DN gels (from T. Nakajima et al.)[38] **(b)** Tensile hysteresis loops of DN gels in the pre-necking region. DN gels are made of PAMPS and PAAm respectively cross-linked at 4.4 mol % and 0.1 mol % with a molar ratio of 2:1. Their total polymer weight concentration is about 10 wt %. The symbol numbers denote the pre-experienced strain, ε_{max}, before measurement of each stress–strain curve. The tensile velocity was fixed at 100 mm/min (from T. Nakajima et al.)[38]

The structure of DN gels with poly(2-acrylamido-2-methylpropanesulfonate (PAMPS) and polyacrylamide (PAAm) networks was optimized by J.P. Gong while keeping the water content at about 70-90 wt %.[39] The resulting gels exhibit high Young modulus (~0.1-1.0 MPa), improved failure tensile stress (~1-10 MPa) with maximal strain up to 1000-2000 %, good failure compressive stress (~20-60 MPa) with strain up to 90-95 % and higher tearing fracture energy (~100-1000 J/m^2). In other words, such hydrogels possess hardness, strength and toughness at low polymer weight concentration (about 10-30 wt %).[39]

Their high fracture energy is due to their ability to slow down the fracture propagation by dissipating energy in a large zone around the crack tip. It is assumed that on the strongly stretched region in front of the crack tip, necking occurs and the gel transforms into a very soft one. Indeed, upon deformation, the rigid network breaks into small clusters. These ones efficiently disperse the stress around the crack tip into the surrounding damage zone and thus increase gels toughness (see **Figure 1.7**).[39] Moreover, as DN usually possess some covalent bonds between the first and the second network, due to residual double bonds on the first network before cross-linking the second one, these additional bonds also participate to the increase of the gel toughness.[40]

[38] T. Nakajima, T. Kurokawa, S. Ahmed, W-l. Wu and J.P. Gong, **Soft Matter**, *2013*, 9, 1955-1966
[39] J. P. Gong, **Soft Matter**, *2010*, 6, 2583-2590
[40] T. Nakajima, H. Furukawa, Y. Tanaka, T. Kurokawa, Y. Osada, and J.P. Gong, **Macromolecules**, *2009*, 42, 2184-2189

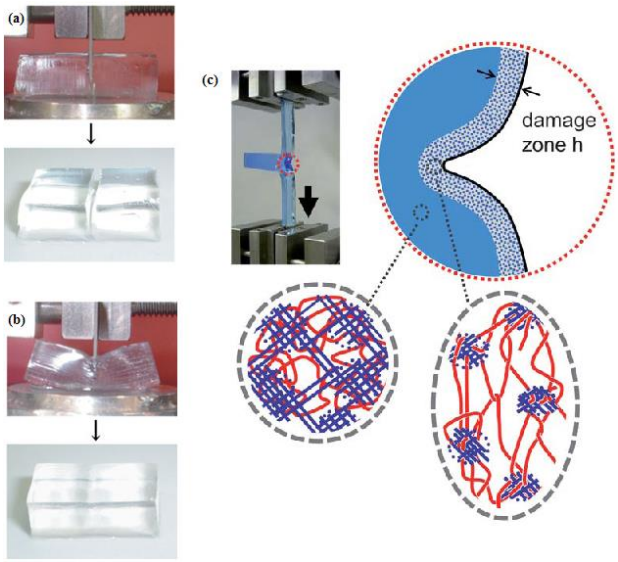

Figure 1.7. (a) and **(b)** Pictures demonstrating the strength of a DN hydrogel resisting slicing with a cutter contrary to a single network gel. Both gels are at ~10 wt % polymer concentration (a) Single network of PAMPS at 4 mol % of cross-linker respect to AMPS monomers and (b) Double network PAMPS/PAAm with the molar ratio between PAMPS and PAAm kept at 1:2 (i.e. same first network as for (a) with a second network made by polymerizing AAm monomer with 0.1 mol % of cross-linker) (from J.P. Gong et al.)[37] (c) Illustration of local damage zone at the crack front of DN gels (from J.P. Gong)[39]

Double networks gels are tough and with improved mechanical properties compared to slide-ring gels, click-chemistry based hydrogels and tetra-PEG ones. However, once the stress induces the break of the first network, the damage is irreversible. Clusters are formed and they slide, acting like cross-linkers and leading to an irreversible gel softening.

To conclude, architectural modification can induce higher extensibility and/or higher fracture resistance and strength. However, the energy dissipated during mechanical loading comes from covalent bonds breaking. The damages are thus irreversible and the hydrogels do not recover their initial properties after resting time. Synthesizing a network with reversible bonds, i.e. bonds able to break and reform is then interesting to bring dynamics to it and confer self-healing properties allowing getting reinforced hydrogels even after cyclic mechanical loading.

II.2. Playing with reversible sacrificial bonds into polymer networks

To this aim, another interesting strategy to reinforce hydrogels is to add physical cross-linking to a chemically cross-linked network. It thus combines both the high stability of covalent bonds (energy of 347 kJ/mol to break a C-C covalent bond) to secondary physical interactions (London dispersion type hydrophobic interactions is 4-8 kJ/mol;[41] bond dissociation energy for hydrogen bonding is 8-35 kJ/mol) allowing a transient cross-linking. Indeed, contrary to covalent bonds, physical interactions are reversible, allowing rearrangements of the polymer network. Therefore, they contribute to self-healing, higher

[41] T.L. Sun, T. Kurokawa, S. Kuroda, A.B. Ihsan, T. Akasaki, K. Sato, M.A. Haque, T. Nakajima and J.P. Gong, **Nature materials**, *2013*, 12, 932-937

toughness, good extensibility and also to fracture energy enhancement as the energy dissipation involved during physical interactions breaking and reformation processes retards fracture propagation.

Besides, physical cross-linking is of first importance to develop *stimuli*-responsive materials as most of them are sensitive to environmental conditions such as pH, temperature, ionic strength etc.

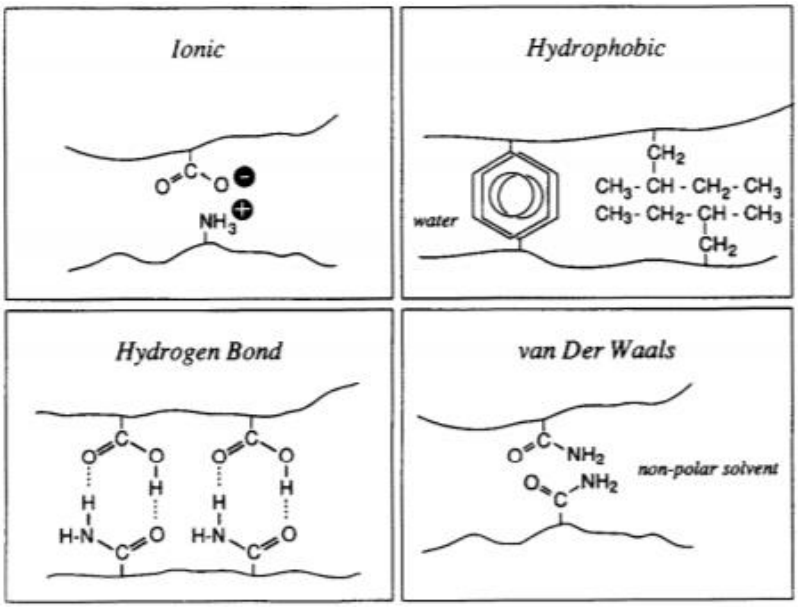

Figure 1.8. Schematic representation showing fundamental physical interactions (from M. Shibayama and T. Tanaka)[42]

As shown in **Figure 1.8**, a wide panel of physical interactions can be used to design tough gels.[42] To this purpose, many different strategies based on physical cross-linking have been investigated such as nanocomposites gels, hydrogen bonding that can also be coupled with microgels or dipole-dipole interactions, ionic interactions, crystallites and hydrophobic interactions. Some representative works will be presenting in the following.

II.2.1. Nanocomposites hydrogels (NC)

NC hydrogels are made of an organic polymer network containing inorganic particles. The interactions between the organic polymer network and the inorganic fillers are then physical ones such as Van der Waals forces, electrostatic interactions, surface complexes or hydrogen bonds. They are synthesized by cross-linking water-soluble polymer in the presence

[42] M. Shibayama and T. Tanaka, **Adv. Polym. Sci.**, *1993*, 109, 1-62

of already built inorganic particles. The presence of inorganic filler (usually with size of the same order of magnitude than the mesh size) into the polymer network impacts the mechanical properties. As a matter of fact, the presence of rigid, high density inorganic particles provides mechanical strength to the gel, enhancing its elastic modulus.

II.2.1.1. Clay platelets nanocomposites

K. Haragushi and T. Takehisa[43] first developped nanocomposites hydrogels with water-swellable clay nanosheets (NC) (Laponite XLG $[Mg_{5.34}Li_{0.66}Si_8O_{20}(OH)_4]Na_{0.66}$ clays of 30 nm diameter and 1 nm thickness with an ion-exchange capacity of 10^4 meq/100g). The inorganic clays are exfoliated and homogeneously dispersed in an aqueous media before to initiate the polymerization of the *N*-isopropylacrylamide (NIPAm) (without chemical cross-linker) from their surface. As a result, the clay platelets act as multifunctional cross-linking agents but contrary to "conventional" hydrogels, the polymer chains are not restricted by a large number of cross-links. These gels possess a high transparency due to the homogeneity of the network, whatever is the clay platelet content. Moreover, compared to "conventional" hydrogels, their mechanical properties are tremendously enhanced against stresses such as bending, compression, torsion and elongation (**Figure 1.9.c-d**). They break at elongations up to ~1000 % with a monotonic increase in stress up to ~100 kPa (see **Figure 1.9.e**) (compared to ~30 kPa for "conventional" hydrogels) with increasing strain and reversibility and recovery up to 98 % after large deformation. These exceptional mechanical properties while keeping water content around 90 wt % are due to the possibility for the polymer chains to extend reversibly without breaking of the polymer network short chains (see **Figure 1.9.a-b**).

[43] K. Haraguchi and T. Takehisa. **Adv. Mater.,** *2002*, 14, 1120-1124

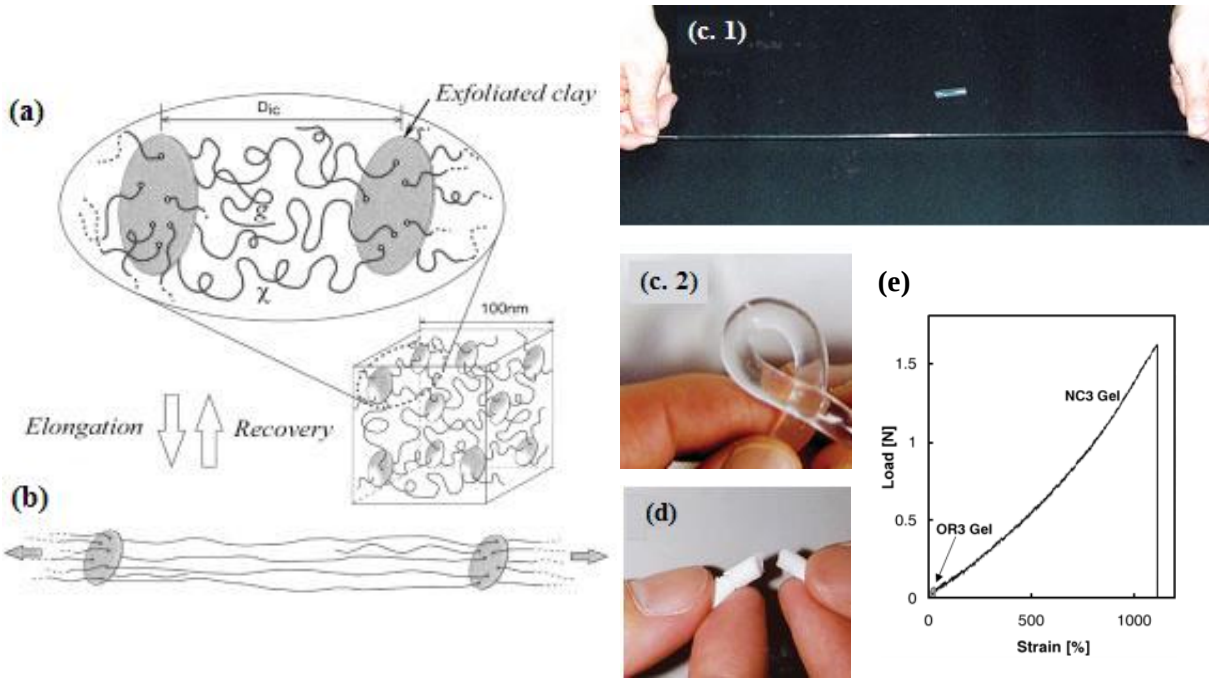

Figure 1.9. Schematic illustrations of network structure and mechanical properties of NC and conventional hydrogels at 10 wt % PNIPAm concentration. **(a)** Schematic representation of a 100 nm cube of a NC gel consisting of uniformly dispersed (exfoliated) inorganic clay and two primarily types of flexible polymer chains, χ and g, grafted onto two neighbouring clay sheets and one clay sheet respectively. In the model, only a small number of polymer chains are depicted for simplicity. **(b)** Elongated structure model for a NC gel. **(c)** All NC gels are transparent, very tough, and can withstand high levels of deformations at 23 °C, such as elongation (1) and torsion (2) independently of the preparation conditions. **(d)** All conventional PNIPAm hydrogels are weak and brittle at 23 °C, irrespective of their composition and the preparation conditions **(e)** Stress-strain curves of a NC3 hydrogel (NC gel at 0.03 mol/l Laponite clay content and 10 wt % PNIPAm). The approximate data for an OR3 gel (conventional 10 wt % PNIPAm hydrogels chemically cross-linked at 3 mol % towards the monomer content) are also depicted for comparison. The mechanical tests are performed at 23 °C. (from K. Haraguchi and T. Takehisa)[43]

First, NC hydrogels mechanical properties depend on the initial conditions of polymerization.[44,45] Indeed, the mechanical properties can be modified via (i) the average molar mass of the network chains and corresponding formation of cross-linking (ii) the efficiency of the initiation, particularly at high content of clay and low initiators amount, (iii) the formation of highly cross-linked microgel-like heterogeneities at high content of initiators (for certain initiators such as ammonium persulfate). Then, the increase of the clay content, from 4 to 8 wt %, improves the fracture toughness from 2400 to 6800 J/m^2, respectively. This phenomenon is explained by viscoelastic energy dissipation occurring in the gel. It is thus time-dependent on clay-clay and polymer-clay interactions. As a matter of fact, during NC

[44] B. Strachota, J. Hoda and L. Matejka, **Eur Pol J.**, *2016*, 77, 1-15
[45] A. Klein, P.G. Whitten, K. Resch and G. Pinter, **J. Polym. Sci, part B : Polym. Phys.**, *2015*, 53, 1763-1773

gels deformation, orientation of clay platelets is induced,[45] leading to strain-hardening thus to strain delocalization and higher fracture energy.

Based on this strategy, layered nanocomposites (L-NC) were designed by mimicking the nacre micro- and nano- structure. The nanoplatelets of clay (Laponite XLG) were assembled in a lamellar structure into a PNIPAm polymer network.[46] Thanks to this well-defined lamellar structure, L-NC gels possess mechanical properties even better than the standard NC gels.

The polymer/clay nanocomposite system has also been combined with other strategies to get homogeneous polymer network structures. One of the most successful examples of this combination is dendritic nanocomposites (D-NC). A combination of clay nanoparticles with the ideal structure of tetra-PEG hydrogels confers both recovery after structure damage (i.e. self-healing) and high hydrogel strength compared to pure tetra-PEG networks.[47]

It is also worth mentioning that NC gels are self-healable.[47,48] However, for all NC gels some drawbacks and limitations subsist: clay platelets gel content cannot exceed ~12 wt % as they tend to aggregate which implies weaker mechanical properties.

II.2.1.2. Self-healing hybrid hydrogels with silica nanoparticles

Within this strategy of organic/inorganic networks, D. Hourdet and A. Marcellan developped silica nanocomposite hydrogels with enhanced mechanical properties.[49,50] These systems possess some advantages over polymer-clay nanocomposites as they are not only mechanically reinforced in terms of extensibility, strength, stiffness and toughness but they are also easily prepared from commercially silica nanoparticles that are stable, well-dispersed, isotropic and can be readily functionalized. Moreover, as for clay-platelets gels, the mechanical properties can be enhanced with the total amount of silica nanoparticles in the polymer network.[49] This improvement is remarkable especially with poly(*N*-alkylacrylamide) matrix. Adsorb polymer segments onto the nanoparticles can play the role of exchangeable sacrificial bonds. Indeed, the nanoparticles adsorb onto the gel interface and act as connectors between polymer chains (see **Figure 1.10**). Thus, under stress, the polymer chains can reorganize and dissipate energy by relaxation (see **Figure 1.11.a**). A striking reinforcement effect coupled with time-dependence of dissipative and recovery processes has been

[46] J. Wang, L. Lin, Q. Chen and L. Jiang, **Angew. Chem. Int. Ed.**, *2012*, 51, 4676-4680
[47] Q. Wang, J.L. Mynar, M. Yoshida, E. Lee, M. Lee, K. Okuro, K. Kinbara and T. Aida, **Nature**, *2010*, 463, 339-343
[48] K. Haraguchi, K. Uyama and H. Tanimoto, **Macromol. Rapid Commun.**, *2011*, 32, 1253-1258
[49] L. Carlsson, S. Rose, D. Hourdet and A. Marcellan, **Soft Matter**, *2010*, 6, 3619-3631
[50] S. Rose, A. Dizeux, T. Narita, D. Hourdet and A. Marcellan, **Macromolecules**, *2013*, 46, 4095-4104

established for poly(*N*,*N*-dimethylacrylamide) (PDMA) chemically cross-linked network by embedding silica nanoparticles (see **Figure 1.11**). In fact, the self-healing is fast as the recovery process is about 10 s.[50]

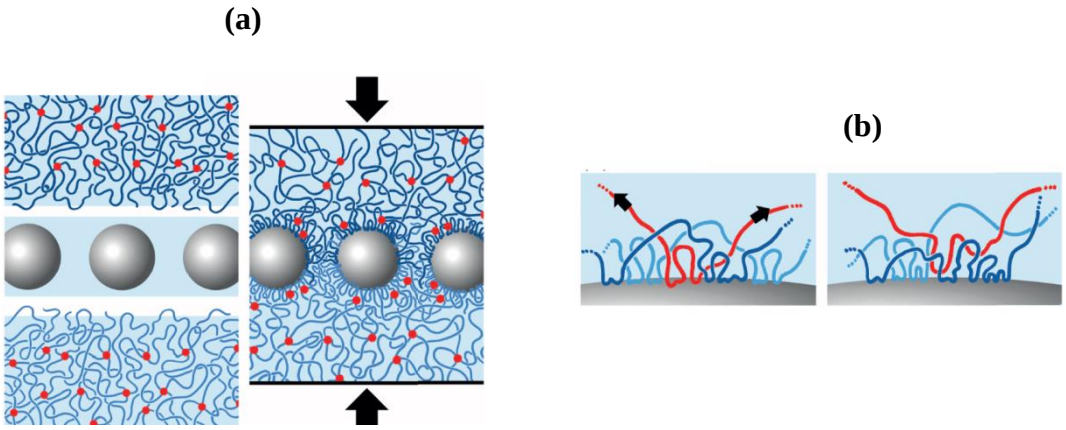

Figure 1.10. Gluing gels by nanoparticles solutions. **(a)** Schematic illustration of the concept of gluing swollen polymer networks together using particles. The nanoparticule diameter is comparable with the gel network mesh size. Network chains are absorbed on nanoparticules and anchor particles to gel pieces. Particles act as connectors between gel surfaces. Adsorbed chains also form bridges between particles. The black arrows indicate the pressure applied to squeeze the gel layers together. **(b)** Particle adsorption is irreversible because particles are anchored to the gel networks by numerous attechments (red, light- and dark-blue strands). At equilibrium or under tension (indicated by black arrows) a monomer that detaches from a particle surface (red strand) can be replaced by a monomer belonging to the same or a different network strand (shown here as a dark-blue strand). Such exchange processes and rearrangements allow large deformations and energy dissipation under stress (from S. Rose et al.)[51]

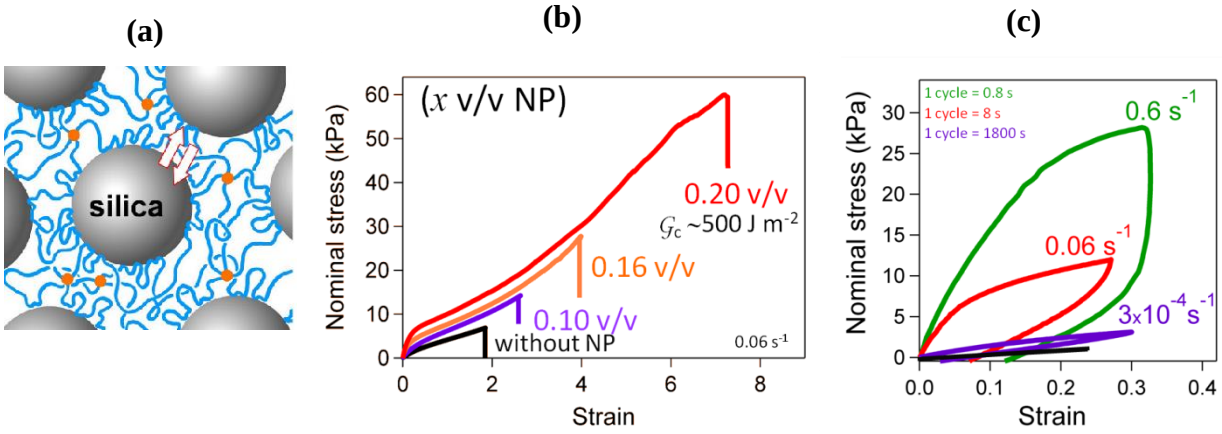

Figure 1.11. **(a)** Schematic representation of hybrid hydrogels combining permanent covalent cross-links (orange dots) and exchangeable bonds (symbolized by arrows). Here polymer adsorption on silica nanoparticles act as exchangeable cross-links. **(b)** Stress-strain curves of PDMA/Silica nanocomposite hydrogels depending on their silica nanoparticles content (from no nanoparticles to 20 % nanoparticles volume ratio) **(c)** Strain rate effect of hybrid hydrogel at 20 % nanoparticles volume ratio: loading-unloading cycles for varied strain rates. The chemical gels (i.e. without nanoparticules) results are also represented as a reference (in black). The gels for (b) and (c) are made of ~88 wt % water content with a 1.0 mol % cross-linking molar ratio towards initial DMA monomers content (from S. Rose et al.)[50]

The possibility of developing efficient and reversible interactions between silica nanoparticles and polymers was then developped by S. Rose et al[51] as an original method for gluing not only synthetic hydrogels but also human tissues with important applications in vivo organ repair.[52]

Nanocomposites, as promising for hydrogels mechanical reinforcement, were developed with a large panel of nanoparticles: surfactants,[53] graphene oxide[54] or even cellulose nanocrystals.[55] All of them possess mechanical reinforcement that have been investigated and explained by different mechanisms such as particle-induced monomer reinforcement[56] or silica/hydrogen bonding as already seen above.[50]

II.2.2. Crystallites

B. Kurt et al. synthesized semi-crystalline hydrogels by copolymerizing either dimethylacrylamide (DMA) or acrylic acid (AAc) monomers with n-octadecyl acrylate (C18A) hydrophobic monomers. The resulting polymer network is then immersed in water for few days and the obtained hydrogels are respectively named DMA/C18A and AAc/C18A. By changing the temperature, these hydrogels go through a reversible order-disorder transition. As a matter of fact, at temperature above the transition one (~50 °C), the hydrogel is soft and extensible but when cooled under 50 °C, crystalline aggregates between the n-stearyl acrylate units of the alkyl side chains are formed (**Figure 1.12.a**).[59] With its very low amount of water (less than 30 wt %), the gel is then mechanically robust with good resistance to fracture (~20 kJ/m^2), Young modulus higher than 300 MPa and even exhibit shape memory properties.[59,60,57] Moreover, thanks to the physical nature of cross-links, the Young modulus, fracture stress and yield stress can be enhanced by increasing the strain rate (see **Figure 1.12.b**). When heated again, the polymer network can recover to its initial shape thanks to its entropic elasticity. As demonstrated in **Figure 1.12.c** this faculty gives rise to fatigue resistance by immersing gels in water at 70 °C between two compressive cycles (at a constant

[51] S. Rose, A. Prevoteau, P. Elzière, D. Hourdet, A. Marcellan and L. Leibler, **Nature**, *2014*, 382-385
[52] A. Meddahi-Pellé, A. Legrand, A. Marcellan, L. Louedec, D. Letourneur, L. Leibler, **Angew. Chem. Int. Ed.**, *2014*, 53, 6369-6373
[53] J. Liu, C. Chen, C. He, J. Zhao, X. Yang, H. Wang, **ACS Nano**, *2012*, 6, 8194-8202
[54] C. He, K. Jiao, X. Zhang, M. Xiang, Z. Li, H. Wang, **Soft Matter**, *2011*, 7, 2943-2942
[55] J. Yang, C.R. Han, F. Xu, R.C. Sun, **Nanoscale**, *2014*, 6, 5934-5943
[56] S. Abdurrahmanoglu and O. Okay, **J Appl Polym Sci**, *2010*, 116, 2328-2335
[57] B. Kurt, U.Gulyuz, D.D. Demir and O. Okay, **Eur Pol J**, *2016*, 81, 12-23

strain rate and up to 90 % compression) where they fully recover their mechanical properties.[60] This is due to the dynamic of intermolecular bonds into alkyl chains which can be broken then reformed by heating then cooling back the samples. Self-healing is another interesting property of these gels which is correlated to the presence of dynamic physical bonds.

Some other semi-crystalline gels with improved mechanical behaviour have been studied such as hydrogels made of poly(vinyl alcohol) crystallites or polypeptides.[58,59] Despite their interesting shape memory properties and stiffness, this type of gel is not very extensible at low temperatures where the structure is totally "frozen". Moreover, as seen above, its water content is lower than the one of conventional hydrogels (~90 wt %).

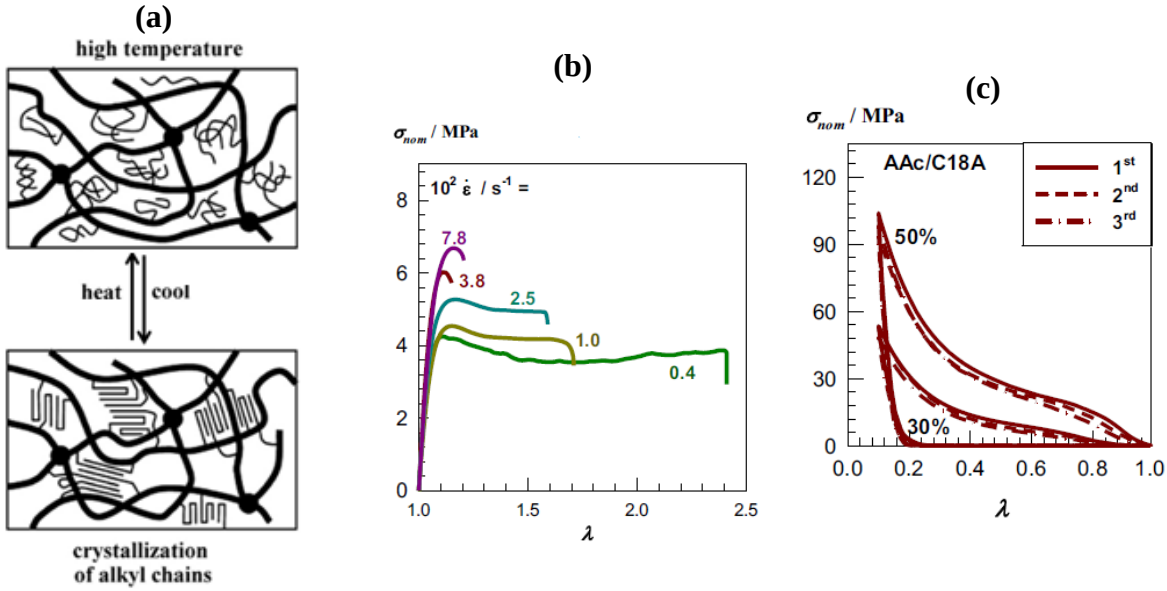

Figure 1.12. **(a)** Schematic representation of the dynamic of intermolecular bonds into alkyl chains by heating/cooling process. Alkyl chains are in melt state at high temperature and in crystalline state after cooling (from K. Inomata et al.)[59] **(b)** Nominal stress σ_{nom} vs deformation ratio λ curves of DMA/C18A hydrogels at 29 wt % water content with 30 mol % hydrophobic C18A at various strain rates.[57] **(c)** Three successive loading/unloading cycles up to 90 % compression for the AAc/C18A hydrogels at 27 wt % (respectively 11 wt %) water content with 30 mol % (respectively 50 mol %) hydrophobic C18A. Note that between each cycle, the gel samples were immersed in a water bath at 70 °C (from B. Kurt et al.)[57]

[58] L Zhang, J. Zhao, J. Zhu, C. He and H. Wang, **Soft Matter**, *2012*, 8, 10439-10447
[59] K. Inomata, T. Terahama, R. Sekoguchi, T. Ito, H. Sugomito and E. Nakanishi, **Polymer**, *2012*, 53, 3281-3286

II.2.3. Ionically cross-linked hydrogels

Introducing either cations or anions on the polymer chains by copolymerization or partial ionisation causes strong repulsive interactions but combining these polymer chains with opposite multi-functional ions can lead to strong intra-/inter- polymer chains attractive electrostatic interactions. Indeed, strong hydrogels exhibiting interesting self-healing properties and bearing both high stress and fracture energy have been synthesized by introducing ionic cross-linkers into a polymer network.[60,61] Many different cations can be used (Zn^{2+}, Ca^{2+}, Ni^{2+}, Co^{2+}, Cu^{2+}, Fe^{3+}, etc.), especially divalent ones, to form ionic cross-linking with polymers such as alginate or triblock copolymers, poly(methyl methacrylate)-*b*-poly(methacrylic acid)-*b*-poly(methyl methacrylate) (PMMA-PMAA-PMMA).[60,61] Indeed, in this case, the PMMA parts connected between them by PMAA form frozen aggregates within the network while the PMAA parts can interact with cations thus adding physically cross-linking to the network. These hydrogels are sensitive to the pH, the nature of the cation and the concentration of the cation. Consequently, these parameters impact their mechanical properties.

An example of this type of gel is a combination between a covalently cross-linked poly(acrylamide) (PAAm) network with a ionically cross-linked Ca^{2+}/poly(alginate) (PAlg) one, made by J-Y. Sun et al.[62] These two polymer networks are entangled and some covalent cross-links are created between the amine functions of PAAm and the carboxylic groups of PAlg. Thanks to the combination of these two networks, the gels synthesized are both extensible like the weak PAAm network and rigid like the pure PAlg gels cross-linked with Ca^{2+}. They form strong gels at polymer concentration of 14 wt % with strain at break ~23 (and ~17 if notched), Young modulus ~156 kPa (see **Figure 1.13.f**) and fracture energy ~9 kJ/m^2. In fact, the Ca^{2+}/PAlg ionic cross-linking forms a "zip" between alginate polymer chains (see **Figure 1.13.a-c and e**) that dissipates energy during stretching by "unzipping" (background hysteresis reinforcement), lowering the stress concentration of the PAAm network while this one bridges the crack and stabilizes deformation (crack bridging reinforcement). Thus, it leads to a hybrid hydrogel with small permanent deformation and self-healing properties as the "unzipped" cross-linking points can reform after unloading and dissipate energy again when submitted to another stretch. However, as shown in **Figure**

[60] K.J. Henderson, T.C. Zhou, K.J. Otim and K.R. Shull, **Macromolecules**, *2010*, 43, 6193–6201
[61] P. Lin, T. Zhang, X. Wang, B. Yu and F. Zhou, **Small Journal**, *2016*, 12, 4386-4392
[62] J-Y. Sun, X. Zhao, W.R.K. Illeperuma, O. Chaudhuri, K. Hwan Oh, D. J. Mooney, J.J. Vlassak and Z. Suo, **Nature**, *2012*, 489, 133-136

1.13.d, this recovery process is quite slow (~1 day) and needs to be done at ~80 °C to get 80 % recovery.

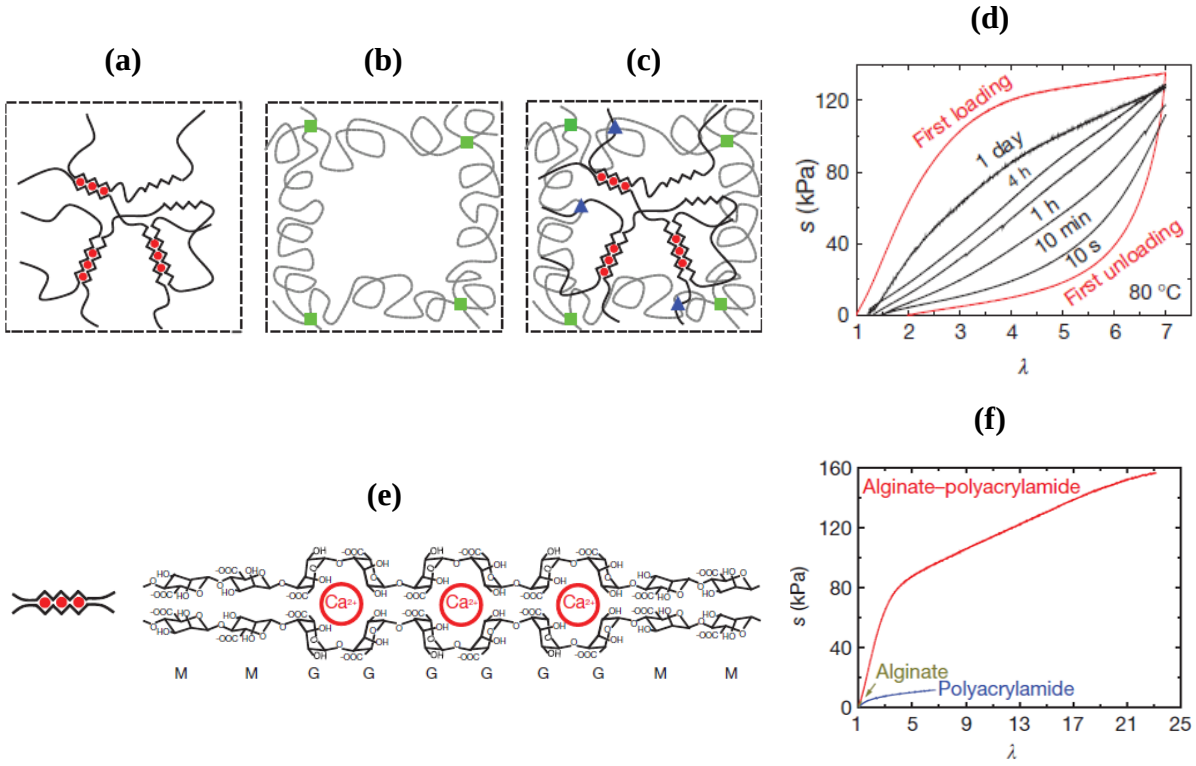

Figure 1.13. Schematic representation of three types of hydrogels: **(a)** Alginate gel where the G blocks on different polymer chains form ionic cross-links through Ca2+ (red circles). **(b)** Polyacrylamide gel chemically cross-linked with *N*,*N*-methylenebisacrylamide (MBA) (green square). **(c)** Alginate-polyacrylamide hybrid gel in which the polymer networks are intertwined and joined by covalent links (blue triangles). The alginate/acrylamide weight ratio is 1:8. The weight of the covalent cross-linker, MBA, was fixed at 6 10^{-4} the one of acrylamide; the weight of the ionic cross-linker, calcium sulfate ($CaSO_4$), was fixed at 1.3 10^{-1} the one of alginate. The total polymer weight content is 14 wt %. **(d)** Recovery of gels (same gels as in **(c)**) stored at 80 °C after loading for different durations as labeled. s represents the stress and λ the strain. **(e)** Schematic representation of alginate polymer chains ionic cross-linking through Ca2+ **(f)** Stress–stretch curves of the three types of gel, each stretched to rupture. The nominal stress, s, is defined as the force applied on the deformed gel, divided by the cross-sectional area of the un-deformed gel. (from J-Y. Sun et al.)[62]

By using the same concept and pre-stretching a covalently cross-linked copolymer network of acrylic acid and acrylamide and ionically cross-linking it in this state with Fe^{3+} cations, P. Lin et al. managed to synthesize a gel with an elastic modulus of about 40 MPa which is stretchable to even more than 200 %.[61] Nevertheless, this mechanical reinforcement which comes from the freezing of molecular orientation in the pre-stretched stress is only effective in the direction parallel to it.

II.2.4. Hydrogen bonds

Hydrogen bonds are attractive interactions between an electronegative atom and a hydrogen atom bonded to another electronegative atom. The resulting bonding energy is relatively low (~8-35 kJ/mol) compared to covalent bonds. This kind of interactions has been widely applied in the field of supramolecular chemistry[63,64] and biomedical science.[65] In the hydrogel field, the introduction of hydrogen bonds is another important strategy for hydrogel reinforcement.

Hydrogen bonds were first introduced in hydrogels by J. Zhang et al. by simply copolymerizing vinyl-4,6-diamino-1,3,5-triazine with a chain-length modulable polyethylene glycol diacrylates (PEGDA).[66] The resulting H-bonds between diaminotriazine groups increase both tensile and compressive strengths up to ~0.1-2 MPa for gels at ~90 wt % polymer concentration. By increasing the PEG chain length the gel elongation is increased to 700 %. They also exhibit striking fatigue resistance thanks to hydrogen bonding reinforcing effect and effective energy dissipation of flexible PEG chains. However, the fracture energy is not improved and the association strength of H-bonds is relatively low due to competition of water for binding sites.[67,68] H-bonds formation and strength can also easily be influenced by pH, so are their macroscopically behaviours. Some examples of gels reinforced by H-bonding are presented in the following.

II.4.2.1. Macromolecular microspheres composite (MMC)

As already discussed, the presence of high density particles into the soft polymer network can reinforce hydrogels especially with inorganic particles such as silica.[49] Nonetheless, mechanical reinforcement can also be obtained using dense organic nano- or micro-particles (MMSs) made of chemically cross-linked poly(acrylamide)[69], poly(styrene)[70] or other polymers, first peroxidized in order to act as both initiator and cross-linker to graft polymer chains at their surface. The polymer chains grafted at the surface of MMSs are numerous and supposed to be long enough to entangle and consequently form a well-defined polymeric

[63] Y. Hua, A.H. Flood, **Chemical Society Reviews**, *2010*, 39, 1262-1271
[64] P. Cordier, F. Tournilhac, C. Soulié-Ziakovic, L. Leibler, **Nature**, *2008*, 451, 977-980
[65] B. Kuhn, P. Mohr, M. Stahl, **Journal Of Medicinal Chemistry**, *2010*, 53, 2601-2611
[66] J. Zhang, N. Wang, W. Liu, X. Zhao and W. Lu, **Soft Matter**, *2013*, 9, 6331-6337
[67] F. Cavillon PhD : **Caractérisation de la liaison hydrogène dans des systèmes moléculaires d'intérêt biologique par diffusion de neutrons**, *2004*
[68] E.A. Appel, J. del Barrio, X.J. Loh, O.A. Scherman, **Chemical Society Reviews**, *2012*, 41, 6195-6214
[69] S. Kara and Ö. Peckan, **Polymer**, *2000*, 41, 3093-3097

network with MMSs acting as cross-linkers. This type of hydrogels is called macromolecular microspheres composite (MMC) (see **Figure 1.14**)[70].

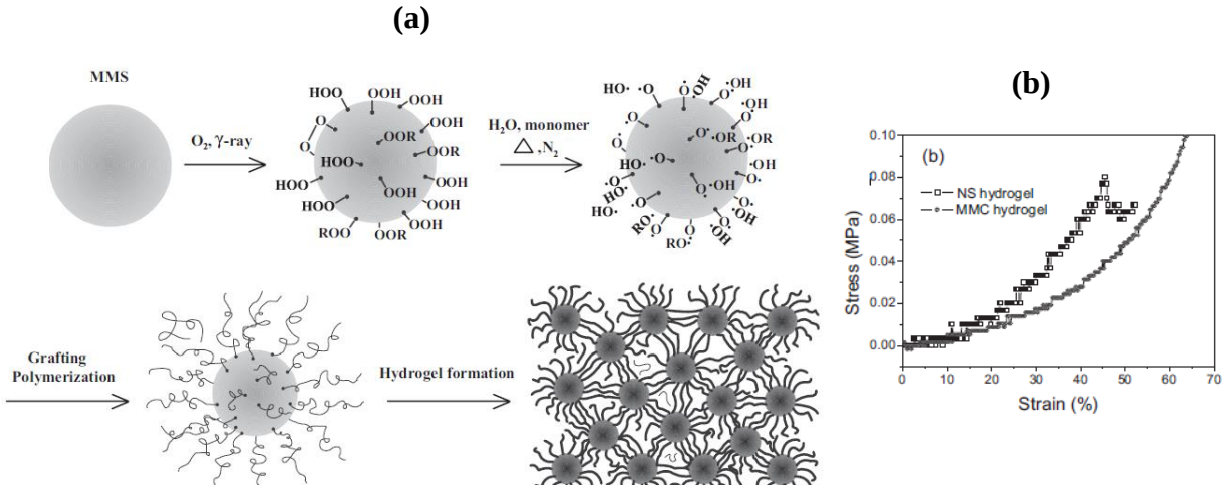

Figure 1.14. **(a)** Proposed mechanism for the formation of a macromolecular microsphere composite hydrogel and a macromolecular microsphere composite hydrogel microstructure. In this case the MMSs are mainly composed of styrene and the grafted polymer chains are polyacrylic acid **(b)** The stress–strain curves for a NS gel (pure polyacrylic acid network (PAA) at 12.5 wt % polymer concentration) and a MMC one (made of PAA and polystyrene MMSs with 1:23 the weight ratio between PAA and MMSs; the MMC gel is at 11 wt % polymer content) (from T. Huang et al.)[70]

To improve mechanical reinforcement, it is important that the entangled polymer chains possess physical interactions between them. To this effect, grafted poly(acrylic acid) (PAA) chains forming intra- and inter- H-bonds are used as they provide energy dissipation mechanism. Indeed, when intra- or inter-chain hydrogen bonds form, on the local sequence of a polymer chain, a certain configuration appears and helps stabilizing this specific chain conformation.

Thanks to these physical interactions, MMC hydrogels possess impressive mechanical properties at 89 wt % water content: they have both a high resistance to strain during compressive tests (do not break even at 10.2 MPa and 97.9 % strain) and good recovery process as they quickly recover their original shape after being squeezed.[70] If they are ionized they can swell up to 900 times their dry weight but become fragile.

The concentration of MMSs, the irradiation time, the monomer concentration and the reaction temperature affect a lot MMSs mechanical properties because they influence the number of "cross-linking" points and the length of polymer chains between them.[70,71] Their mechanical

[70] T. Huang, H.G. Xu, K.X. Jiao, L.P. Zhu, H.R. Brown, H.L. Wang, **Adv. Mater.**, *2007*, 19, 1622-1626
[71] N. Tanaka, H. Kitano and N. Ise, **J. Phys. Chem.**, *1990*, 94, 6290-6299

properties are reduced with increasing water content or when gels are swollen in urea or high pH solution, proving the importance of H-bonds in the enhancement of mechanical properties.[70] Moreover, depending on the chemical nature of the MMSs particles, they can be responsive to different environmental parameters such as temperature, light, pH etc.

Besides, MMC hydrogels are very interesting compared to nanocomposite gels, as they are made only of organic components. However, their incredibly high swelling needs to be restricted for some biomedical applications and the numbers of grafting chains to the MMSs surface is dependent on the chemical nature of the polymer chains used to build the microsphere. Although, in spite of achieving high tensile and compressive strengths, the fracture energy is still low as H-bonds alone do not provide high energy dissipative mechanism.

II.4.2.2. Dipole-dipole and H-bonding interactions cooperativeness

To synthesize hydrogels with good resistance to fracture, the idea of combining H-bonding interactions with dipole-dipole ones have been explored.[72] These hydrogels are synthesized in dimethylsulfoxide (DMSO) by one-step copolymerization of acrylonitrile (AN), acrylamide (AAm) and 2-acrylamido-2-methyl-1-propanesulfonic acid (AMPS) in the presence of a hydrophilic cross-linker (see **Figure 1.15.a**) and are then immersed in water to exchange the solvent. These three monomers are respectively the dipole, H-bonding and anionic monomers. The resulting gels are named DHIR-*a*-*b*-*c*-*x* with *a*, *b*, *c* respectively the weight percentage of AN, AMPS and AAm in the total monomer content, and *x* is the mass ratio of cross-linker to total monomers. While the anionic PAMPS polymer chains allow the gel to swell, the dipole-dipole and H-bondings interactions of the PAN and PAAm counterparts improve their resistance: At 22 wt % polymer content, the resulting elastic modulus is up to 8.3 MPa and 4.8 MPa for tensile and compressive stress respectively with an elongation at break ~700 % and a fracture energy reaching 5500 J/m^2 as the breaking and reformation of both H-bonds and dipole-dipole interactions highly dissipates energy (see **Figure 1.15.c**). Reversible mechanical properties after undergoing cyclic loading-unloading cycles have also been reported (see **Figure 1.15.b**).

Despite their good mechanical reinforcement, these gels have a real inconvenient linked to their synthesis: a solvent exchange is needed after in-situ preparation.

[72] Y. Zhang, Y. Li and W. Liu, **Adv. Funct. Mater.**, *2015*, 25, 471-480

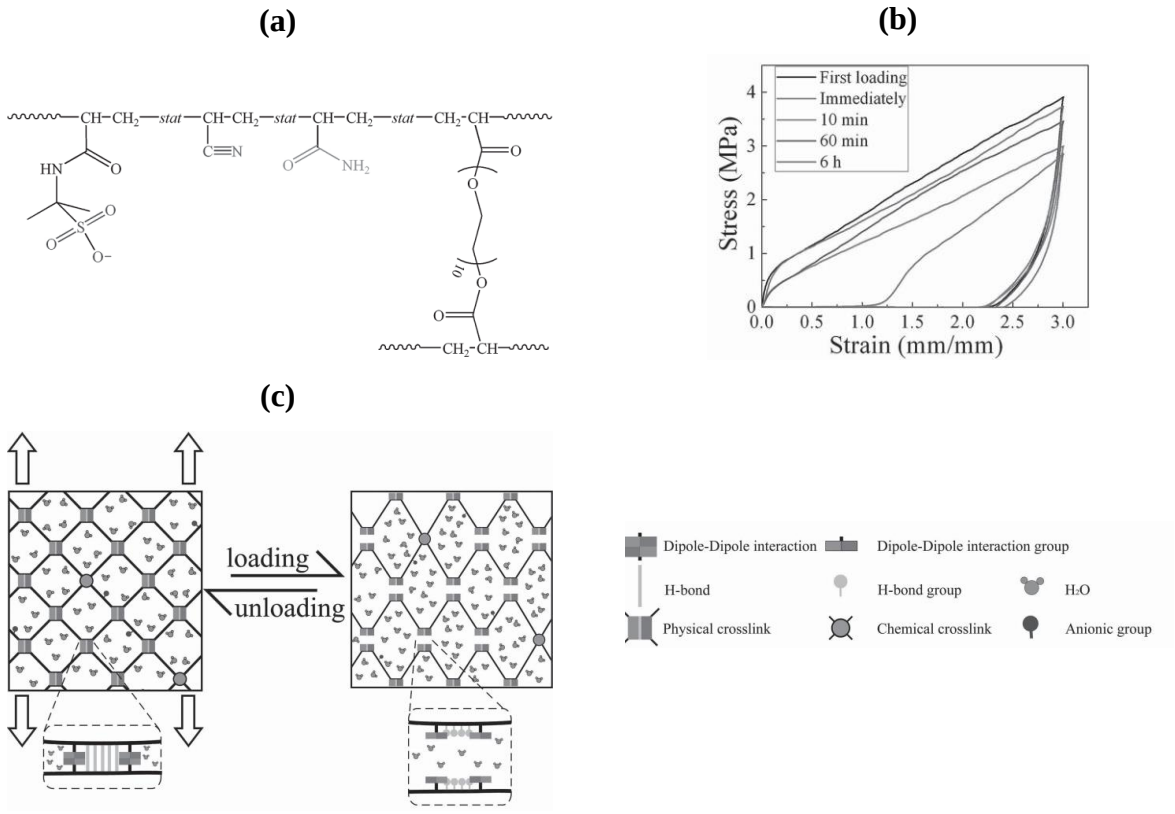

Figure 1.15. **(a)** Molecular structure of a DHIR gel **(b)** Mechanical recovery of DHIR60–5–35–0.0625 hydrogel at ~78 wt % water content for different waiting times under cyclic tensile tests **(c)** Mechanism underlying the energy dissipation of DHIR hydrogel network during the cycling test at different resting times (from Y. Zhang et al.)[72]

II.2.5. Hydrophobic interactions

Hydrophobic interactions can also participate to hydrogels reinforcement. They consist in the formation of highly hydrogen bonded water molecules that form ordered structures in the local area of hydrophobic polymer chains. These hydrophobic interactions can be controlled by changing the chemical nature and the molar mass of the hydrophobic group.

An example of gels reinforced by hydrophobic interactions is self-healing hydrophobically modified poly(acrylic acid) (PAA) hydrogels with cetyltrimethylammonium (CTA) at the end of C18 alkyl chains.[73,74] Mixed micelles are formed by association between C18 alkyl chains beared by the PAA backbone and CTA molecules. Besides these reversible hydrophobic interactions, electrostatic interactions occur between positively charged CTA molecules and PAA (see **Figure 1.16.a-c**). At ~45 wt % water content they are extensible up

[73] D. C. Tuncaboylu, M. Sari, W. Oppermann and O. Okay, **Macromolecules**, *2011*, 44, 4997–5005
[74] U. Gulyuz and O. Okay, **Macromolecules**, *2014*, 47, 6889−6899

to 600 % with a stress at break ~1.5 MPa and possess shape memory properties with full recovery depending on the pH, they cannot recover their initial length after deformation due to the lack of permanent cross-links (see **Figure 1.16.d**).[74] Although they exhibit mechanical reinforcement, these gels are at low water content and a solvent exchange is needed for their preparation.

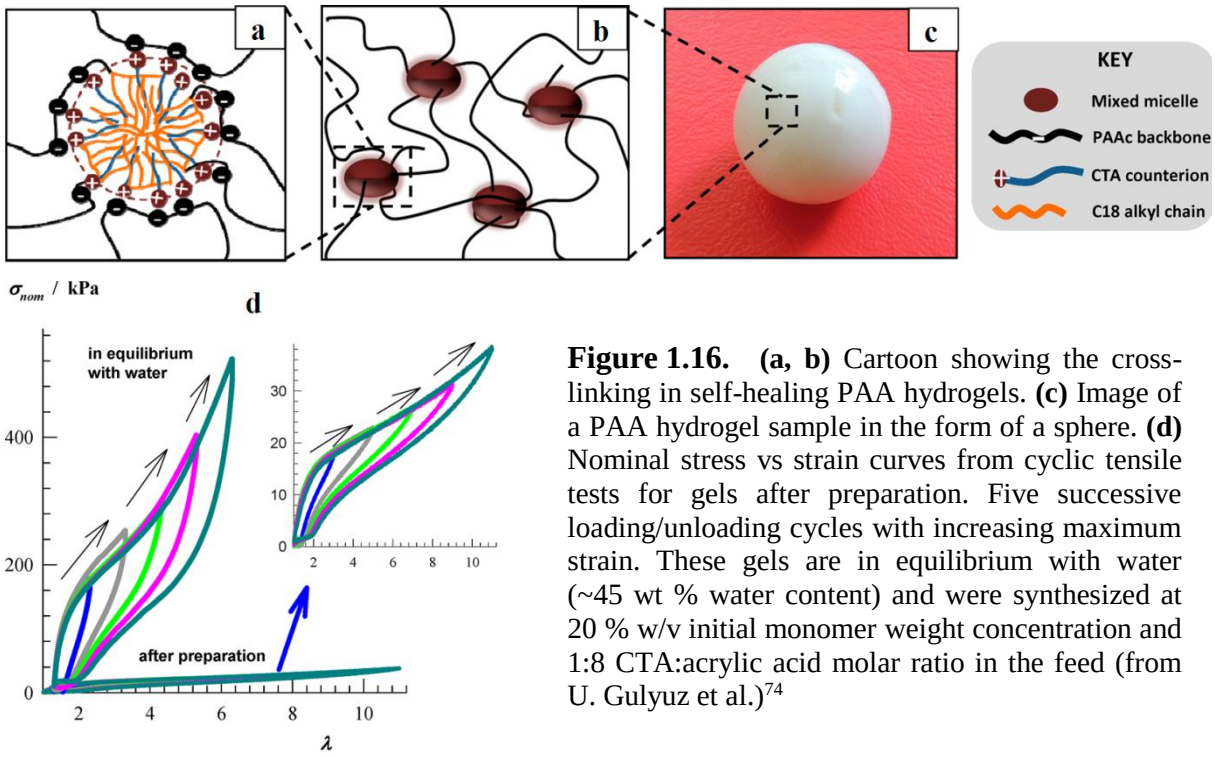

Figure 1.16. **(a, b)** Cartoon showing the cross-linking in self-healing PAA hydrogels. **(c)** Image of a PAA hydrogel sample in the form of a sphere. **(d)** Nominal stress vs strain curves from cyclic tensile tests for gels after preparation. Five successive loading/unloading cycles with increasing maximum strain. These gels are in equilibrium with water (~45 wt % water content) and were synthesized at 20 % w/v initial monomer weight concentration and 1:8 CTA:acrylic acid molar ratio in the feed (from U. Gulyuz et al.)[74]

Moreover, M.A. Haque et al. demonstrated in 2010 that introducing surfactant hydrophobic bilayers into chemical hydrogels lead to anisotropic properties as a uni-directional swelling of gels together with color change by stretching the gel.[75] Actually, these properties are obtained by polymerizing a surfactant (dodecyl glyceryl itaconate; DGI) (PDGI) into a chemically cross-linked network of poly(acrylamide) (PAAm) (concept initially developed by T. Tanaka et al.[76]). This lamellar structure consists in periodical stacking of several thousands of rigid hydrophobic bilayers with uni-directional alignment in the ductile and hydrophilic PAAm network (see **Figure 1.17.a**).

Thus, the one-dimensional swelling occurs in the direction perpendicular to the lamellar bilayers while it is completely constrained in the direction of the bilayers. Tensile

[75] M.A. Haque, G. Kamita, T. Kurokawa, K. Tsujii and J.P. Gong, **Adv. Mater**., *2010*, 22, 5110-5114
[76] K. Tsujii, M. Hayakawa, T. Onda and T. Tanaka, **Macromolecules**, *1997*, 30, 7397-7402

elongation (parallel to the bilayers elongation) gives rise to structural change of the bilayers structure leading to a color change.

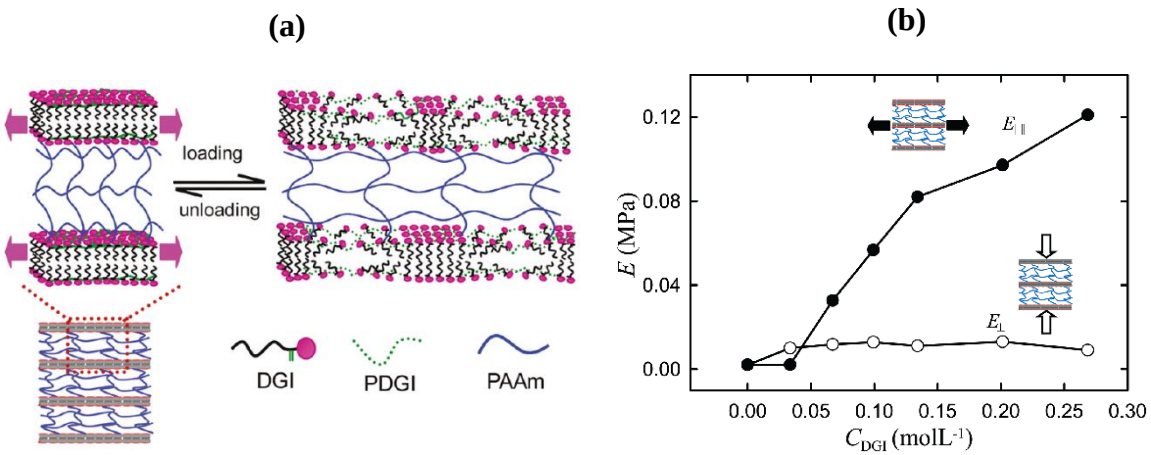

Figure 1.17. **(a)** Illustration of the stratified structure of PDGI/PAAm hydrogel consisting in PDGI lamellar bilayers as hard segments and PAAm ductile matrix. The fracture process of the bilayers on uniaxial elongation in the direction parallel to the bilayers is also represented. **(b)** Nominal stress as a function of strain at a stretching velocity of 200 mm/min for PAAm gel and PDGI/PAAm gel with and without lamellar bilayer structure. The tensile deformation was performed along the lamellar bilayers direction as indicated by the illustration (from M.A. Haque et al.)[75]

Moreover, by developing this bilayer structure until centimetre scale, the hydrogel can sustain large stress and dramatically enhance the bulk mechanical properties parallel to the bilayers direction (see **Figure 1.17.b**).[77] As a matter of fact, the bilayer structure change observed during tensile tests, dissipates energy whatever is the applied strain. The hydrogels possess time and temperature self-recovery as at 25 °C, full recovery of shape and properties is reached after 15 min but happens only after few seconds at 50 °C. After several successive loading-unloading cycles at 25 °C (waiting 15 min between every cycle), the gel properties are still the same, traducing a high fatigue resistance.

Furthermore, the balance between the rigid-like nature of the bilayers (enabling recovery) and the lipid-like one (allowing extraordinary blunting by reducing the maximum stress at crack tip) makes the gel self-recoverable and tremendously tough especially against fracture (work of extension ~5 MJ/m^3).

Indeed, based on the principle to introduce sacrificial bonds into a chemically cross-linked network to dissipate energy and prevent damaging as for double networks hydrogels (DN), PDGI-PAAm gels with unidirectional aligned macromolecular bilayers are as tough as them in terms of fracture energy. Though, in DN hydrogels, once the sacrificial bonds have

[77] M.A. Haque, T. Kurokawa, G. Kamita and J.P. Gong, **Macromolecules**, *2011*, 44, 8916-8924

been broken they cannot reform whereas in these hydrophobically reinforced hydrogels, the physical sacrificial bonds breaking is reversible and confers full self-recovery properties. Although these gels are reinforced, their mechanical properties are only attained for deformation parallel to the bilayer structure and these ones form with specific conditions only (water content 93.5-96.5 wt % with PDGI/PAAm mass ratio between 1:2 and 1:4 and the need to shear the solution to get bigger domains).

II.2.6. Polymer phase separation

Playing with polymer phase-separation, phenomenon common to all polymers, is another interesting and universal way of both reinforcing hydrogels and getting on-demand properties whatever is the direction of the mechanical loading. Polymer phase-separation traduces a conformational change of polymer chains from coil (swollen state) to globule (collapsed state) (see **Figure 1.18.a**).[78] Phase-separation was first observed with polymer in solutions and then extended to gels.[79,80] As a matter of fact, gels can be seen as a "single polymer molecule" as all the monomer units are connected to the others forming one unique giant macromolecule on a macroscopic scale. In this manner, it is not surprising that gels also exhibit phase-transition phenomenon (see **Figure 1.18.b**). This phase separation can be driven by different forces such as hydrophobic interactions, Van der Waals forces, ionic ones or even hydrogen bonding.[81] Polymer phase-separation is thus another promising way of reinforcing hydrogels by introducing physical interactions into the polymer network.

Figure 1.18. Schematic representation of polymer phase-separation induced by a stimulus for **(a)** a polymer chain exhibiting a coil-globule transition and **(b)** a hydrogel

[78] A. Dabbagh, B.J.J. Abdullah, H. Abdullah, M. Hamdi and N.H.A. Kasim, **Journal of Pharmaceutical Sciences**, *2015*, 104, 2414-2428
[79] H.G. Schild and D.A. Tirrell, **J. Phys. Chem.**, *1990*, 94, 4352-4356
[80] T. Tanaka**, Phys. Rev. Lett.**, *1978*, 40, 820-823
[81] V. Aseyev, H. Tenhu and F.W. Winnik, **Adv. Polym. Sci.**, *2011*, 242, 29-89

II.2.6.1. Polymer phase separation driven by electrostatic forces

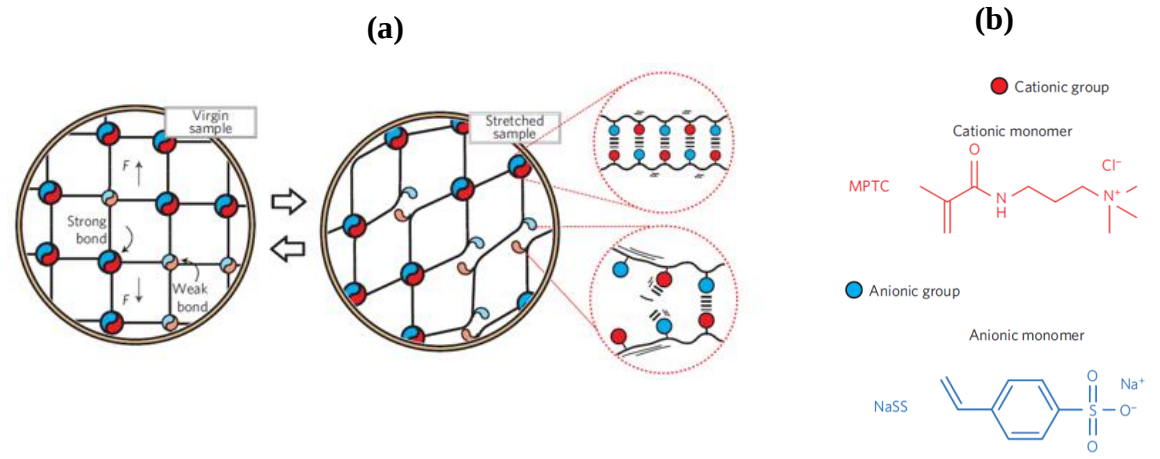

Figure 1.19. Schematic representations of physical hydrogels composed of polyampholytes. **(a)** Illustration of polyampholyte networks with ionic bonds of different strength. The strong bonds serve as permanent cross-linking points, and the weak ones act as reversible sacrifical bonds that rupture under deformation. **(b)** Chemical structures of both the cationic monomer (MPTC) and the anionic one (NaSS) used in this work. **(c)** The effect of polymer concentration (C_m in mol/l) dependence on the swelling volume ratio Q_v and Young's modulus E of the polyampholyte hydrogels. The NaSS and MPTC monomers are introduced in quantities such as the anionic molar fraction of the system is kept at 0.52 (from T.L. Sun et al.)[83]

Hydrogels made with polyampholytes chains which are polymer chains possessing both anionic and cationic repeat units on their backbone can undergo polymer phase-separation through strong electrostatic complexes.[82] In this context, T.L. Sun et al. developed a tough viscoelastic physical hydrogel by randomly copolymerizing 3-(methacryloylamino)propyl-trimethylammonium chloride (MPTC) as cationic monomers with sodium p-styrenesulphonate (NaSS) as anionic ones.[83,84] The complex formation between cationic and anionic monomer units gives rise to ionic interactions of different strength (strong or weak) depending on how they are distributed on the polymer backbone. The strong

[82] P. G. Higgs and J-F. Joanny, **The journal of chemical physics**, *1991*, 94, 1543-1554
[83] T. L. Sun, T. Kurokawa, S. Kuroda, A. B. Ihsan, T. Akasaki, K. Sato, M. A. Haque, T. Nakajima and J.P. Gong, **Nature Materials**, *2013*, 12, 932-937
[84] A. B. Ihsan, T. L. Sun, T. Kurokawa, S. N. Karobi, T. Nakajima, T. Nonoyama, C. K. Roy, F. Luo and J. P. Gong, **Macromolecules**, *2016*, 49, 4245-4252

bonds keep the gel in shape acting as permanent cross-linkers while the weak ones, which are reversible, confer good mechanical properties thanks to energy dissipation (see **Figure 1.19.a-b**).[83] Gels with polymer concentration of 34 wt % (=1.6 mol/l) or more exhibit a stress up to 1.8 MPa (see **Figure 1.19.c**) with strain ~750 %, tearing energy measuring the resistance of crack propagation ~4 kJ/m^2 and fast self-healing with 100 % self-recovery i.e. very high fatigue resistance.

Nonetheless, these hydrogels are in a highly collapsed state and not very swollen, with only 50-70 wt % of water content compared to ~90 wt % for « conventional ones ». Moreover, even if polyampholyte gels lead to improved mechanical properties, they are really vulnerable to mobile ions, prompt to destabilize the gel as they screen electrostatic interactions.

Consequently, the applications of polyampholyte gels are limited to some extent especially under physiological and engineering conditions.

II.2.6.2. Polymer phase separation driven by Van der Waals forces

For binary systems, involving Van der Waals interactions, both the temperature and the polymer-solvent affinity can influence the phase diagram. For instance, the introduction of a bad solvent for the polymer chains into the gel environment will reinforce the polymer-polymer attractive interactions. Thus, the polymer chains will tend to collapse in a globule conformation and to aggregate between them in polymer-rich domains.

This polymer phase-separation induced by changing the quality of the solvent has been used by K. Sato et al. as reinforcing mechanism.[85] For this purpose, they have synthesized poly(acrylamide) (PAAm) hydrogels cross-linked at 0.1 mol % with regard to acrylamide (AAm) monomer. The gel swelling was decreased by adding *N*,*N*-dimethylformamide (DMF, poor solvent for PAAm gels) to the water environment, i.e., by increasing the ratio of poor/good solvent. By comparison, the same PAAm gels can be simply deswelled by increasing the osmotic pressure in the external medium using PEG chains with moderate average molar mass (*Mw* = 20 kg/mol). The first method reveals a drastic decrease of the swelling behaviour (at ~60 wt % of DMF/water concentration) with a macroscopic aspect going from transparent to white opaque whereas the second method gives rise to a linear deswelling of the gel without optical change (see **Figure 1.20.a-d**). Therefore, it is

obvious that varying the solvent content induces polymer phase-separation depending on its affinity with the polymer chains.

Moreover, this gel highlights the crucial role of polymer phase-separation towards mechanical reinforcement. Indeed, at DMF concentration ≤ 70 wt % the PAAm gel is in a rubbery state but then an abrupt change in both elastic modulus (up to ~210 MPa) and fracture energy (up to ~10^4 J/m^2) occurs at ~75 wt % of DMF (i.e., close to the critical DMF concentration for visible phase-separation) while the gel deswells and the polymer concentration goes from ~4-5 to ~60 wt % (see **Figure 1.20.e**). The mechanical enhancement, leading to high Young modulus coupled with fracture energy among the highest ever observed, is due to the formation of dense phase-separated domains dissipating viscous energy by breaking polymer-polymer interactions thus acting as sacrificial physical bonds. In addition, the breaking of these bonds is reversible and confers self-healing properties to the gel which are both time- and temperature- dependent (recover fully after 24h at ambient temperature but in 5 min at 75 °C) (see **Figure 1.20.f**). However, at DMF concentration ≥ 90 wt %, the PAAm network becomes rigid and very brittle due to too strong polymer-polymer interactions preventing possible internal structural change. This highlights the importance of the phase-separation on the mechanical reinforcement as for the gels gently deswollen to the same polymer content (~60 wt %) by dialysis in PEG solution, the Young modulus and fracture energy are much lower, respectively ~50 kPa and ~10^3 J/m^2.

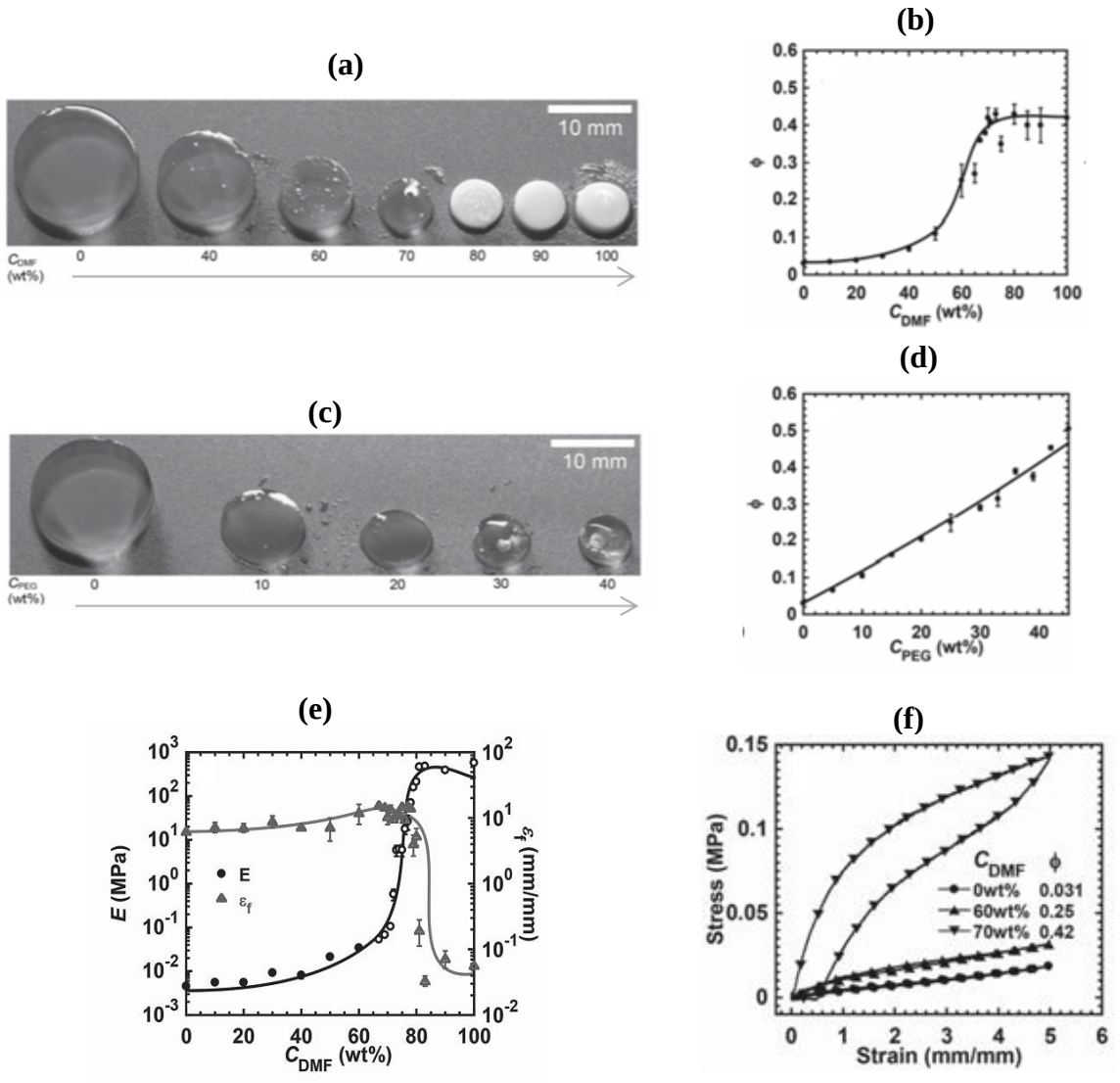

Figure 1.20. Pictures, polymer volume change and mechanical behaviour of PAAm hydrogels in DMF/water solvent (p-PAAm) and PEG aqueous solution (o-PAAm). **(a)** The p-PAAm gels in high DMF concentration C_{DMF} became turbid while **(c)** o-PAAm gels kept transparent even at the same volume fraction in 40 wt % of PEG solution **(b)** Polymer volume fraction of p-PAAm gels increased abruptly at C_{DMF} = 60 wt %, while **(d)** that of o-PAAm gels monotonously increases with increasing PEG concentration C_{PEG} to the same level of volume fraction with p-PAAm. Each measurement was performed for 3-8 times, and the errors of some measurements were so small that the error bars were hidden behind the plots **(e)** Influence of the DMF concentration on the p-PAAm gels modulus E and fracture strain ε_f **(f)** Stress vs strain curves of loading and unloading uniaxial tests of p-PAAm gels at 0–70 wt % DMF weight concentration. The stretching velocity is 100 mm/min. (from K. Sato et al.)[85]

As seen previously, polymer phase-separation phenomenon is thus an interesting way for mechanical reinforcement, self-healing and recovery process as it allows introducing dissipative domains into a polymer network. Moreover, contrary to all the above mentioned strategies applied to improve gels in terms of mechanical properties, hydrogels reinforcement

[85] K. Sato, T. Nakajima, T. Hisamatsu, T. Nonoyama, T. Kurokawa and J.P. Gong, Adv. Mater., 2015, 27, 6990-6998

by phase-separation is capitalizing on the *stimuli*-responsive feature of gels. Indeed, polymer phase-separation is very sensitive to many different environmental parameters depending on the nature of the polymers; pH, salt concentration, temperature,[86] solvent composition, light,[87,88,89] electric field,[90] stress,[91] radiation force[87,92] etc. Thus, as their mechanical properties can be tuned, switched on/off, by a wide range of either internal or external stimuli, *stimuli*-sensitive hydrogels pave the way to numerous efficient industrial applications especially in the biomedical field with the example of injectable hydrogels or drug delivery systems releasing their content at only specific targeted places of the human body.

Nonetheless, as the whole network is connected, the formation of a rich-polymer phase induced by phase-separation usually goes with a drastic change in volume (see **Figure 1.18.b**). This gel shrinking, giving rise to networks with a high polymer concentration makes the *stimuli*-responsive hydrogels less interesting for some applications such as in biomedical field where their major advantage is to be soft materials with very high water content. Moreover, the reversibility of the phase-separation induced by *stimuli* like solvent quality, pH or ionic strength can be obtained only by changing the composition of the aqueous environment involving the addition of molecules and/or diffusion process.

In this context, our overall strategy has been to use a reversible phase separation process, which can be managed under isochoric conditions, in order to strongly and easily modify the properties of hydrogels having a high swelling ratio (over 80% by weight). In this aim, the temperature was chosen as *stimulus* as it is easy to control and to apply to many different fields.

III. Thermo-responsive toughening of hydrogels

III.1. Critical solution temperature: UCST and LCST behaviours

According to the chemical nature of the repeat units constituting the polymer chain, their length between cross-linking points and also their concentration, a gel shrinking during

[86] A. S. Hargreaves and M. A. Foster, **Journal of dentistry**, *1976*, 4, 33-41
[87] A. Suzuki and T. Tanaka, **Nature**, *1990*, 346, 345-347
[88] S. Juodkazis, N. Mukai, R. Wakaki, A. Yamaguchi, S. Matsuo and H. Misawa, **Nature**, 2000, 408, 178-181
[89] M. Irie, **Advances in Polymer Science**, *2005*, 110, 49-65
[90] G. Giannetti, Y. Hirose, Y. Hirokawa and T. Tanaka, **in Molecular Electronic Devices (F.L. Carter et al Editors), Elsevier Appl. Sci.**, *1988*, London
[91] S. Hirotsu and A. Onuki, *1989*, 58, 1508-1511
[92] S. Juodkazis, N. Mukai, R. Wakaki, A. Yamaguchi, S. Matsuo and H. Misawa, Nature, **2000**, 408, 178-181

phase-transition can be observed either by increasing or decreasing the temperature. Indeed, this phenomenon depends on the type of phase diagram of the polymer, i.e., LCST (Lower Critical Solution Temperature) or UCST (Upper Critical Solution temperature (see **Figure 1.21.a-b**). In some case, polymers can exhibit both LCST and UCST behaviours (see **Figure 1.21.c**).[93,94]

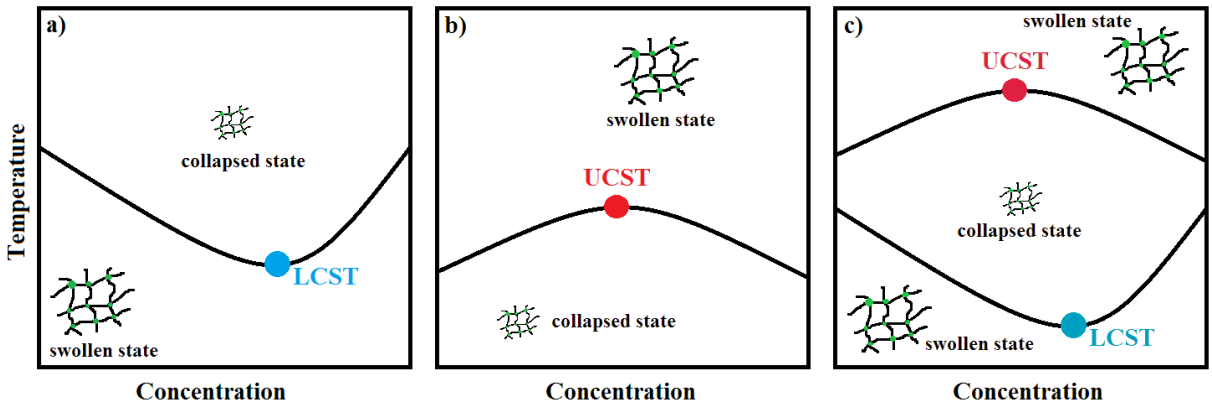

Figure 1.21. Schematic representations of swollen/collapsed hydrogels exhibiting **(a)** LCST (lower point of the curve), **(b)** UCST (upper point of the curve) or **(c)** both LCST and UCST behaviours (respectively lower and upper points of the curves)

While the UCST behaviour in binary system is the standard phenomenon described by the Flory-Huggins theory,[93] the LCST behaviour is often observed in water which is a very complex solvent. Transition temperatures in both UCST and LCST binary systems can be shifted by changing various parameters like the average molar mass of the polymer,[95] the polymer concentration or by adding a ternary component like salt, co-solvent, surfactant etc. Examples of polymers exhibiting temperature induced phase transition in water[81] are PNIPAm (LCST)[96], poly(N-acryloylglycinamide) (PNAGA) (UCST)[97] and poly(ethylene oxide) (PEO) (both LCST and UCST).[98] Of course, there are many other homopolymers exhibiting a phase separation phenomenon in water and infinity of copolymers that can be developed to precisely adjust the transition temperature. The possibility to use these thermo-responsive polymers as chemical tools to induce phase-separation either by increasing or

[93] S.L. Shenoy, P.C. Painter and M.M. Coleman, **Polymer**, *1999*, 40, 4853-4863
[94] S. Y. Oh and Y. C. Bae, **Polymer**, *2012*, 53, 3772-3779
[95] W.J. MacKnight and F.E. Karasz, **Polymer blends in Comprehensive polymer science and supplements ed. Elsevier, Pergamon Press**, *1989*, 7, 111-130
[96] A. Halperin, M. Kröger and F. M. Winnik, **Angew. Chem. Int. Ed.**, *2015*, 54, 15342-15367
[97] F. Meeussen, E. Nies, H. Berghmans, S. Verbrugghe, E. Goethals and F. Du Prez, **Polymer**, *2000*, *41*, 8597-8602
[98] H. Schäfer-Soenen, R. Moerkerke, H. Berghmans, R. Koningsveld, K. Dušek and K. Šolc, **Macromolecules**, *1997*, 30, 410-416

decreasing the temperature is thus really interesting for further applications as discussed above.

III.2. Thermo-responsive toughening of hydrogels based on PNIPAm phase separation

III.2.1. Homo-PNIPAm hydrogels

As PNIPAm exhibits many advantages (**Table 2**) compared to other LCST polymers, it is up to now the most widely studied LCST one. The PNIPAm thermo-responsive behaviour was discovered in 1967 by J.S. Scarpa et al.[99] and was later called LCST, in 1968.[101] However, despite its numerous advantages, it is not really considered as biocompatible in the case of residual monomers. Indeed, the monomers (see **Figure 1.22**) even if not classified as carcinogenic, mutagenic or reprotoxic substance, have an unpleasant and strong smell.

Table 2: PNIPAm advantages

Biomedical field	LCST close to body temperature (~31-32°C)[100,101]
	Not very sensitive to physiological conditions as it is a non-ionic polymer[102]
LCST stable on time in large panel of media	Chemically stable without suffering from hydrolysis under specific conditions[103]
	LCST almost similar, on a large range of pH, polymer concentration, polymer chains average molar mass[104,96] and almost totally independent of architecture
Mechanical reinforcement	Polymer dynamics slowed down in phase-separated domains above LCST[102]
Marketing	Can be used in large quantities as the NIPAm monomer is commercially produced

[99] J. S. Scarpa, D. D. Mueller, I. M. Klotz, **Journal of the American Chemical Society**, *1967*, *89*, 6024-6030
[100] M. P. Algi and O. Okay, **Eur. Polym. J**, *2014*, *59*, 113-121
[101] M. Heskins and J. E. Guillet, **J Macromol Sci A**, *1968*, 2, 1441-1455
[102] V. Aseyev, H. Tenhu, F. Winnik, **Adv. Polym. Sci.**, *2011*, 242, 29-89
[103] J. Ramos, A. Imaz and J. Forcada, **Polymer Chemistry**, *2012*, 3, 852-856
[104] F. Afroze, E. Nies and H. Berghmans, **Journal Of Molecular Structure**, *2000*, *554*, 55-68

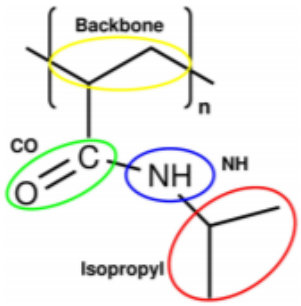

Figure 1.22. Schematic representation of poly(*N*-isopropylacrylamide) (from N. van der Vegt et al.)[105]

PNIPAm phase separation in water is driven by coupling hydrophobic interactions and H-bonds.[106] At low temperature (T<32 °C), hydrogen bonds are formed between the amide groups (C=O or NH) of each repeat unit and water molecules, leading to exothermic dissolution in water. Moreover, water molecules also self-organize with entropic penalty by forming clathrates around the hydrophobic isopropyl groups. However, a temperature increase above 32 °C destabilizes the hydration shell around the isopropyl groups that self-associate through hydrophobic interactions. Meanwhile, more binding sites are free to form H-bonds between the CONH groups of PNIPAm as the water molecules initially bound to PNIPAm chains are released. These two phenomena cause a conformational change of PNIPAm chains from coil to globule. Nonetheless, even when collapsed, the PNIPAm chains are still partially hydrated.[107] The LCST can be shifted to either higher or lower temperatures by manipulating various parameters such as copolymerizing with more or less hydrophobic comonomers,[108] changing solvent composition[109,110] and adding salt[111,112] or surfactant molecules.[113,114]

Using the PNIPAm thermo-responsiveness, M. Shibayama et al. performed experiments under isochoric conditions and demonstrated that PNIPAm phase-separation can reinforce the gel properties.[115] For this purpose, homo-PNIPAm hydrogels were synthesized at an initial polymer concentration of 30 wt % using 10 mol % of cross-linker relative to the

[105] F. Rodriguez-Ropero and N.F.A. van der Vegt, **J. Phys. Chem. B**, *2014*, 118, 7327-7334
[106] X. Wang, X. Qu and C. Wu, **Macromolecules**, *1998*, 31, 2972-2976
[107] M. Philipp, U. Müller, R.J. Jimenez Rioboo, R. Sanctuary, P. Müller-Buschbaum and J. Krüger, **Soft Matter**, *2013*, 9, 9887-9896
[108] C. K. Han and Y. H. Bae, **Polymer**, *1998*, 39, 2809-2812
[109] Y. Suzuki, K. Tomonaga, M. Kumazaki, and I. Nishio, **Polymer Gels and Networks**, *1996*, 4, 129-142
[110] E. Kutnyanszky, A. Embrechts, M.A. Hempenius and G.J. Vancso, **Chemical Physics Letters**, *2012*, 535, 126-130
[111] N. Ishida and S. Biggs, **Macromolecules**, *2007*, 40, 9045-9052
[112] H. Du, R. Wickramasinghe and X. Qian, **The Journal of Physical Chemistry B**, *2010*, 114, 16594-16604
[113] E. Tiktopulo, V. Bychkova, J. Ricka and O. Ptitsyn, **Macromolecules**, *1994*, 27, 2879-2882
[114] D. Dhara and P.R. Chatterji, **Journal of Macromolecular Science, Part C: Polymer Reviews**, *2000*, 40, 51-68
[115] M. Shibayama, M. Morimoto and S. Nomura, **Macromolecules**, *1994*, 27, 5060-5066

monomer concentration. The resulting gel named NB10 remains isochoric (i.e., no volume change is visible) in the range of studied temperature (from 20 to 70 °C). This specific condition allows separating the intricate contributions of the phase-separation and the change of the polymer concentration induced by the gel volume transition. It is then possible to reveal the role of phase-separation only and to highlight the mechanisms involved in the mechanical toughening.

Indeed, the dynamic mechanical measurements performed on NB10 gels reveal a jump in both storage and loss moduli around 40 °C (see **Figure 1.23.a**). This clearly highlights the gel reinforcement induced by the PNIPAm phase-separation itself as there is no volume change (i.e., no variation of polymer concentration). During the PNIPAm phase-transition, as the gel keeps its volume constant and the polymer chains are connected to each other by chemical cross-links, the polymer gel self-assembles into a continuous PNIPAm-rich phase alternating with solvent-rich domains (see **Figure 1.23.b**).[115]

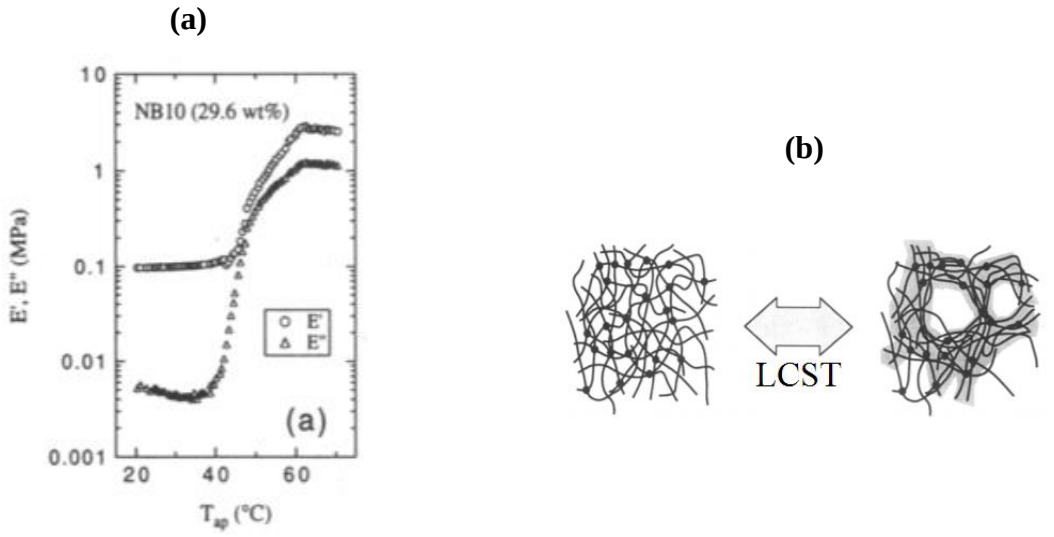

Figure 1.23. **(a)** Apparent temperature (T_{ap}, °C) dependencies of the dynamic storage modulus, *E'*, and loss modulus, *E''* as a function of temperature for NB10 (29.6 wt % of PNIPAm). **(b)** Schematic illustration of NB10 macro-network at T<LCST and T>LCST

This pioneering work of M. Shibayama et al. proved that the reversible PNIPAm phase-separation can lead to mechanical reinforcement in gels by polymer reorganisation.[115] However, the gels are still at high polymer concentration which limits their possibility of applications.

III.2.2. Role of the macromolecular architecture in thermo-responsive hydrogels

Using the principle of mechanical reinforcement by phase-separation, H. Guo et al. synthesized thermo-responsive hydrogels resistant to fracture propagation at high temperature despite their high water content (83 wt %).[116] For this purpose, a well-controlled network topology was designed on the basis of a chemically cross-linked thermo-responsive PNIPAm network randomly grafted with hydrophilic poly(*N*,*N*-dimethylacrylamide) (PDMA) pendant chains (see **Figure 1.24**). By optimizing both thermo-responsive and hydrophilic polymer components, it was possible to prepare a gel, named GPN-D, with a heterogeneous PNIPAm structure at high temperature (T>T_c with T_c the phase transition temperature of the PNIPAm network) able to keep its volume constant with a high level of water (83 wt %) when studied in its preparation state thanks to the hydrophilic PDMA balancing the collapsing effect of PNIPAm phase-separation (see **Figure 1.24, GPN-D gel**).

The study of GPN-D gels by differential scanning calorimetry experiments and small angle neutron scattering experiments brings to light that during phase-separation of PNIPAm (at T>T_c with T_c≈30 °C), the polymer networks reorganize into rich and poor PNIPAm-phase domains (see **Figure 1.25.a**).

This reorganization induces a remarkable mechanical reinforcement at 60 °C: the striking increase of Young modulus coupled to a doubled strain at break is observed in **Figure 1.25.b** and the ~1000 J/m^2 fracture energy required to propagate the crack across the entire gel is 30 times higher than at 20 °C for a gel at 83 wt % water content due to the appearance of crack bifurcation (see **Figure 1.25.c**).

[116] H. Guo, N. Sanson, D. Hourdet and A. Marcellan, **Adv. Mater.**, *2016*, 28, 5857-5864

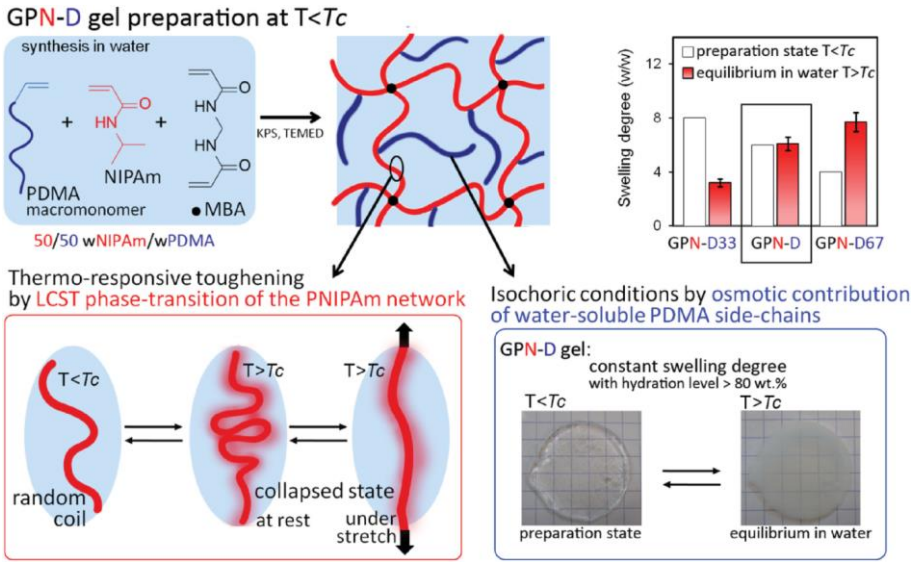

Figure 1.24. Gel topology: synthesis and design. Thermo-associative PNIPAm chains are shown as red chains and hydrophilic non-responsive PDMA chains are in blue. The condition of network formation, i.e., at preparation state, was defined as the gel reference state. The GPN-D network is prepared at 20 °C, below the phase-transition temperature of PNIPAm domains T_c, with an equal weight fraction of PDMA macromonomer and PNIPAm network 50/50 w/w. Cross-linking density was fixed at 0.1 mol % (corresponding to a molar mass between cross-links ≈ 80 kg/mol) with an initial NIPAm concentration of 8.33 wt % and PDMA macromonomers (M_n ≈ 80 kg/mol). The weight fraction of PDMA grafted chains strongly impacts the swelling behavior. Inset: the swelling degree, Q, defined as the weight ratio of the hydrated gel to the dried gel, is given at preparation state Q_0 (white bars) and at equilibrium in water at $T >> T_c$ (at 60 °C: red bars) for GPN-D (50/50 PNIPAm/PDMA), GPN-D33 (67/33 PNIPAm/PDMA), and GPN-D67 (33/67 PNIPAm/PDMA). (from H. Guo et al.)[116]

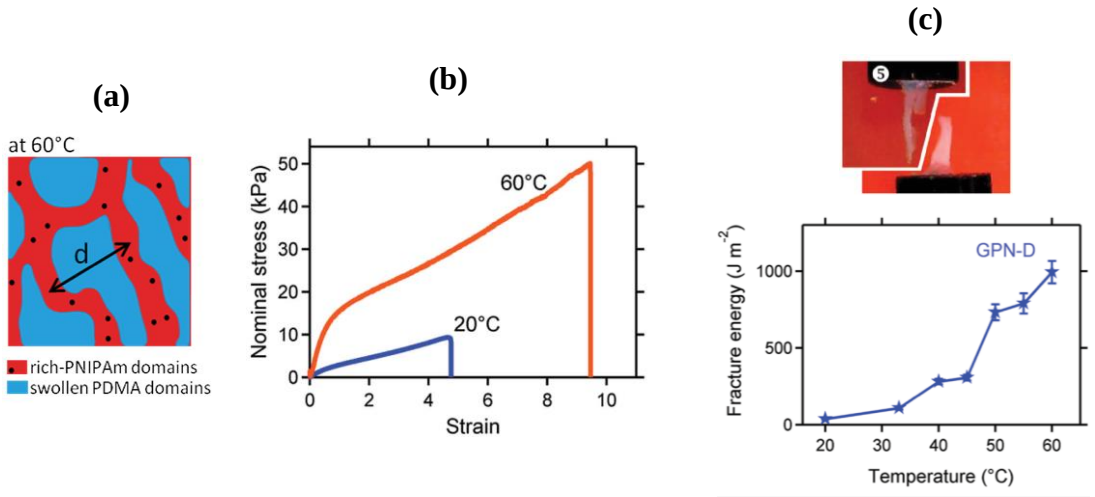

Figure 1.25. **(a)** Structure is depicted as bi-continuous domains: the percolating PNIPAm-rich domains that are topologically defined as the network containing the chemical cross-links (•), embedded into a PDMA hydrated matrix. The PNIPAm volume fraction in collapsed domains is estimated to be around 0.70–0.75 as calculated according to the scattering invariant. **(b)** Tensile stress–strain force curves of GPN-D at 20 °C and 60 °C **(c)** Photo of the crack bifurcation at macroscopic scale in GPN-D gels and the fracture energies of crack propagation related to it. (from H. Guo et al.)[116]

It is noteworthy to precise that this reinforcement is due to dissipative mechanisms originating from the rearrangements induced by the phase-separated micro-domains, involving intra- and inter-chains disruptions of interacting NIPAm/NIPAm segments upon stretching. Indeed, stretching the collapsed polymer chains (obtained by phase-transition) leads to configurationally interesting chain transitions with a predicted abrupt unravelling of a weakly deformed globule forming a stretched chain of blobs (see **Figure 1.26**).[117,118,119,120] Actually, the deformation of the globular dense domains involves two processes (see **Figure 1.26**)[117]: (1) At low deformations, the blobs of size ξ_c retained their original volume; they are only spatially rearranged while being deformed from a sphere to an ellipsoid. For further deformation, the globule shape changed and can be represented by a cylinder assuming that the globule volume is constant. This process takes place until a linear string of blobs is obtained. (2) Stretching the sample even further will result in blob structural changes leading to the formation of smaller blobs of size ξ_p.

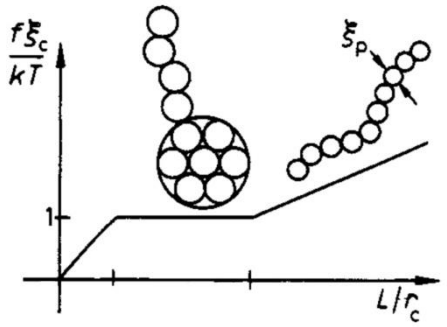

Figure 1.26. A schematic representation, ignoring finite-size effects, of the different configurations assumed by a collapsed flexible chain under deformation. $f\xi_c/kT$ and L/r_c respectively correspond to the normalized force and the normalized stretch. ξ_c and ξ_p correspond to the size of the blobs (adapted from A. Halperin and B. Zhulina)[117]

For GPN-D gels, this unravelling phenomenon goes along with the breaking of hydrophobic interactions and H-bonds inducing stress release and energy dissipation. As a matter of fact, contrary to covalent bond breaking, the breaking of hydrophobic interactions and H-bonds is reversible and the energetic component of the free energy favours the association of PNIPAm segments and the replacement of lost links.

[117] A. Halperin and B. Zhulina, **Europhys. Lett.**, *1991*, 15, 417-421
[118] A. Craig and E. M. Terentjev, **J. Chem. Phys.**, *2005*, 122, 194901
[119] A. Craig and E. M. Terentjev, **J. Chem. Phys.**, *2005*, 122, 194902
[120] A. A. Polotsky, M. Daoud, O. V. Borisov and T. M. Birshtein, **Macromolecules**, *2010*, 43, 1629-1643

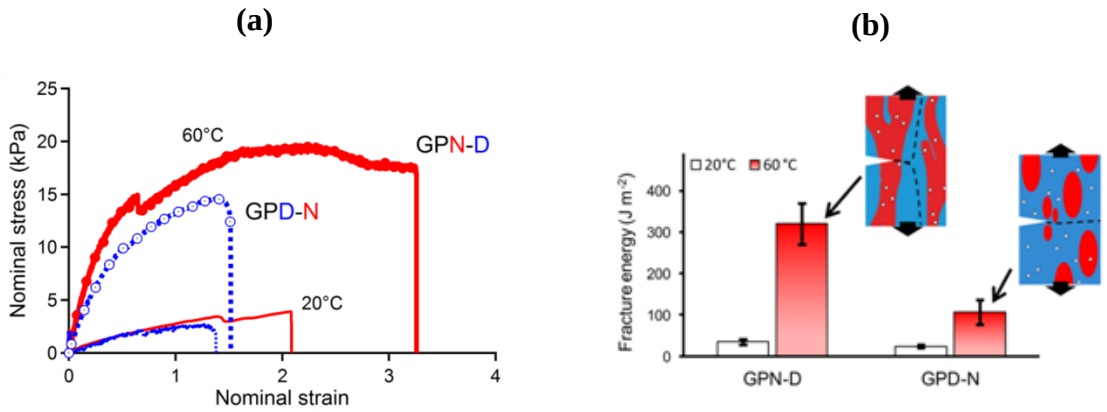

Figure 1.27. **(a)** Fracture behaviour of GPN-D (red continuous line) and GPD-N (blue dashed line) notched specimens at 20 and 60 °C and **(b)** Fracture energies obtained at 20 and 60 °C. The scheme is a view of the reinforcing mechanisms at microscale. Dotted lines refer to damage mechanisms and define weak interfaces (from H. Guo, C. Mussault et al.)[121]

A gel with the reverse topology (GPD-N), i.e., PDMA network with grafted PNIPAm chains as thermo-responsive polymers has also been investigated by H. Guo, C. Mussault et al.[121]. It reveals the importance of the gel topology that has been probed by keeping constant the total polymer content, the cross-linking molar ratio towards monomers, the weight ratio between PDMA and PNIPAm and a similar molar mass for PDMA and PNIPAm grafts. At these conditions, both GPD-N and GPN-D, studied under isochoric conditions, clearly display different mechanical properties[122] under large deformation but are both mechanically reinforced at high temperature in terms of strength, toughness and extensibility as shown in **Figure 1.27**.

Then, by combining hydrophilic polymers with thermo-responsive ones, H. Guo has demonstrated during his Thesis the possibility to drive reversibly and easily the mechanical reinforcement of highly swollen gels in isochoric conditions. In the present work, using the same strategy, the impact of the composition of the gel is studied to demonstrate its crucial role for structuring the rich PNIPAm phase at high temperature and the relative mechanical properties.

[121] H. Guo, C. Mussault, A. Marcellan, D. Hourdet and N. Sanson, **Macromolecules**, *2017*, 49, 4295-4306
[122] H. Guo, N. Sanson, D. Hourdet and A. Marcellan, **Adv. Mater.**, *2016*, 28, 5857–5864

IV. Objective of the dissertation

As described in this chapter, many different strategies have been investigated to reinforce hydrogels especially during the last two decades. Among them, the ones implying reversible physical interactions seem to be the most promising in terms of mechanical reinforcement. Indeed, these physical interactions play the role of a highly dissipative network by breaking under mechanical loading. They are also sensitive to *stimuli* as a small change in the gel medium can lead to switching on/off these physical interactions thus controlling the reinforcement. Consequently, the introduction of responsive polymers into a chemically cross-linked network is a very interesting way to reinforce the mechanical properties under controlled environment. Thermo-responsive polymers are then good candidates for this purpose as temperature is a parameter easy to control and there is a large number of thermo-responsive polymers exhibiting phase-separation in water (LCST or UCST).

In this framework, Hui Guo et al. have recently succeeded in developing a series of responsive hydrogels by combining hydrophilic and LCST polymers in order to control and to drive the temperature induced phase transition in isochoric conditions keeping a high level of swelling. This original and versatile strategy has clearly highlighted that the topology of grafted hydrogels was controlling the phase separated morphology beyond the critical temperature and finally the resulting macroscopic properties. While this pioneering work has mainly focused on the comparison between hydrogels of opposite topologies, the role of the parameters involved in the primary structure of the network remain to be studied. This was the starting point of my Doctoral work devoted to the study of the properties of hydrophilic networks grafted with temperature-responsive side-chains. In this context, our objective was to address more specifically the following questions:

1) What is the influence of the **average molar mass of thermo-responsive side-chains** (LCST) on the thermodynamic properties of hydrogels as well as their relation with the self-assembling behaviour above the critical temperature, the resulting segregated morphology and the mechanical properties?

2) For a given molar mass (size) of the thermo-responsive side-chains, how does **the average composition between hydrophilic and thermo-responsive** components affect the previously mentioned characteristics and properties?

3) Finally, by **substituting the hydrophilic network by a thermo-responsive one** having an UCST-type behaviour, is it possible to extend the universal concept of polymer

phase-separation to obtain a swollen network having a schizophrenic mechanical reinforcement at both high and low temperatures?

To achieve this goal, two series of grafted hydrogels, designed with a hydrophilic PDMA network carrying thermo-responsive PNIPAm side-chains, were prepared with the following characteristics:

- **GPD-Nx**: In this series, hydrogels were synthesized with the same total polymer weight concentration ($[polymer]_0$=16.7 wt %; i.e., a swelling at the preparation state Q_0=6), using equal amounts of hydrophilic PDMA and thermo-responsive PNIPAm (50/50 in weight) and a constant molar ratio between the cross-linker (MBA) and the monomer (DMA) (r_{MBA}=0.1 mol % with MBA being *N*,*N*′-methylenebis(acrylamide)). For this series, prepared with a similar PDMA network (same concentration of DMA and same cross-linking ratio), the variable is the average molar mass of PNIPAm side-chains ranging between 20 to 120 kg/mol. It results in six different hydrogels named GPD-Nx with x being the average molar mass of PNIPAm grafts in kg/mol (see **Figure 1.28**).

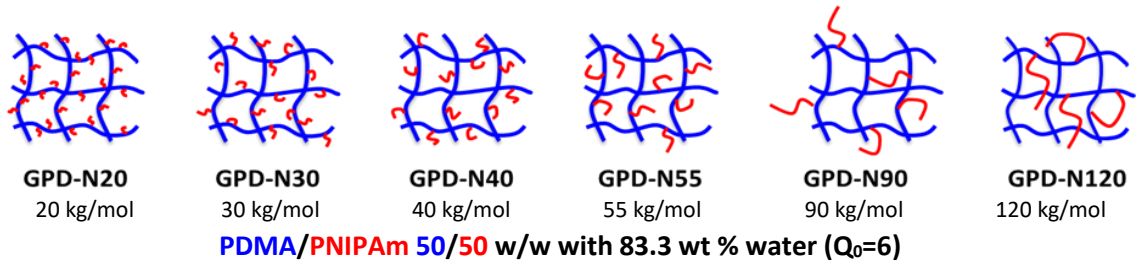

Figure 1.28. Schematic representation of the theoretical structure of grafted hydrogels GPD-Nx where x is the average molar mass of the thermo-responsive grafts. In this series, both the "PDMA/PNIPAm" weight ratio (50/50) and the cross-linking molar ratio (0.1 mol %) are kept constant. The chemically cross-linked PDMA network is the same for the whole series while the average molar mass of PNIPAm grafts varies from 20 to 120 kg/mol. The PDMA covalent network and the PNIPAm macromonomers are drawn in blue and red, respectively.

- **GPD-N55(y-z)**: In this series, hydrogels were synthesized with the same total polymer weight concentration as in the previous series ($[polymer]_0$=16.7 wt %; i.e., a swelling at the preparation state Q_0=6), the same cross-linking ratio between MBA and DMA (r_{MBA}=0.1 mol %) and using the same PNIPAm macromonomer (M_n=55 kg/mol). For this series, the variable is the initial weight ratio between DMA monomer and

PNIPAm macromonomer which was varied from 82/18 to 69/31 (weight ratio) in order to probe the hydrophilic/hydrophobic behaviour at high temperature.

Four GPD-N55(y-z) gels were synthesized with y and z the weight percentage of PDMA covalent network and PNIPAm side-chains, respectively (see **Figure 1.29**).

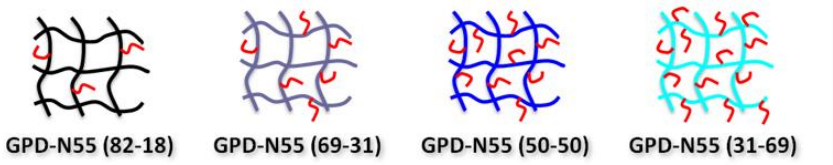

83.3 wt % water (Q_0=6)

PDMA/PNIPAm w/w	82/18	69/31	50/50	31/69
PDMA in gel (wt %)	13.7	11.5	8.35	5.2
PNIPAm in gel (wt %)	3.0	5.2	8.35	11.5

Figure 1.29. Schematic representation of GPD-Nx(y-z) networks prepared with various weight ratio between PDMA network (y) and PNIPAm grafts (z). In this series, the weight ratio (y-z) between the PDMA covalent network and the PNIPAm macromonomers varies from 69/31 to 31/69 (weight ratio). The PNIPAm macromonomers are drawn in red and the PDMA networks in dark blue, blue and light blue respectively for 69, 50 and 31 wt % of the total polymer weigth.

The synthesis of PNIPAm macromonomers, grafted hydrogels and homo-PDMA and homo-PNIPAm networks used as references are reported and discussed in Chapter 2.

Then, the characterization of the thermodynamic and self-assembling properties of grafted hydrogels, as a function of temperature, are discussed in Chapter 3. For that purpose, a comprehensive set of techniques combining swelling experiments, Differential Scanning Calorimetry (DSC), turbidimetry and Small Angle Neutron Scattering (SANS) analysis are carried out.

Afterwards, Chapter 4 will focus on the mechanical behaviour of GPD-Nx and GPD-N55 (y-z) hydrogels obtained at low and high deformations using uniaxial tensile tests, fracture tests, shape memory experiments, and adhesion tests as a function of temperature.

Finally, Chapter 5 expands the concept of mechanical reinforcement induced by the polymer phase separation by combining into the same hydrogel both LSCT and UCST polymers. This chapter has been published in **Macromolecular Rapid Communications**, *2017*, 38, 1700287.

Chapter 2

Synthesis of PNIPAm precursors and grafted hydrogels

Chapter 2: Synthesis of PNIPAm precursors and grafted hydrogels

Chapter 2: Synthesis of PNIPAm precursors and grafted hydrogels

I. Introduction

Grafted hydrogels were synthesized by conventional free radical cross-linking copolymerization of DMA monomers and PNIPAm macromonomers in the presence of MBA as chemical cross-linker. First, the synthesis of the PNIPAm macromonomers with average molar masses ranging from 20 to 120 kg/mol will be described along with their characterisation by Size Exclusion Chromatography (SEC) and Nuclear Magnetic Resonance (NMR). Then, the syntheses of GPD-Nx and GPD-N55(y-z) grafted hydrogels and those of homo-PDMA and homo-PNIPAm networks, used as references, will be detailed. The polymerization efficiency will be analyzed for all hydrogels by quantifying the extractables, i.e., the residual DMA monomers, PNIPAm macromonomers and free polymer chains embedded in the network.

II. Experimental section

II.1. Materials

The following chemicals were used for PNIPAm macromonomer and hydrogel syntheses: *N*-isopropylacrylamide (NIPAm, ≥ 97 %, Aldrich), *N*,*N*-dimethylacrylamide (DMA, ≥ 99 %, Aldrich), cysteamine hydrochloride (AET.HCl, ≥ 97 %, Aldrich), potassium peroxodisulfate (KPS, ≥ 99 %, Aldrich), acrylic acid (AA, anhydrous > 99 %, Fluka), dicyclohexylcarbodiimide (DCCI, 99 %, Aldrich), *N*,*N*′-methylenebis(acrylamide) (MBA, ≥ 98 %, Aldrich), tetramethylethylenediamine (TEMED, ≥ 99.5 % Aldrich), triethylamine (Et_3N, ≥ 99 %, Aldrich) and sodium hydroxide (NaOH, ≥ 97 %, Aldrich) were used as received. All organic solvents were of analytical grade and water was purified with a Millipore system combining a reverse osmosis membrane (Milli RO) and ion exchange resins (Milli Q) for synthesis and purification.

II.2. Characterization

Nuclear magnetic resonance (NMR) spectroscopy. The characterization of the PNIPAm precursors was performed in D_2O on a Bruker Avance III HD spectrometer operating at 400 MHz for ^1H, using a standard 5 mm broadband Smart probe at 25 °C.

Size Exclusion Chromatography (SEC). The characterization of the absolute molecular weights of the polymer samples was carried out by SEC with a Viscotek triple detector (TDA 302) equipped with three columns (OH-pak). During the analysis carried out at 40 °C, the flow rate was controlled at 1.0 mL/min using 2 wt % Et_3N in tetrahydrofuran (THF) as mobile phase. The molar masses were derived from a universal calibration curve based on Pullulan standards from Sopares (OmniSEC software).

Measurements of gels weight loss. The samples at their preparation state were initially cut, weighted and placed in a large excess of water at 20 °C which was exchanged once a day for two weeks. Then, the gels were weighted and dried at 60 °C for 48 hours. The gel weight loss was calculated as follows: $gel\ weight\ loss = \left(1 - \frac{m_{dry}}{m_{th}}\right) * 100$ where m_{dry} is the gel dried weight and m_{th} is the theoretical weight of polymer contained in the gel sample at the preparation state, calculated as the mass of the masses of monomer(s) and cross-linker (assuming 100 % conversion to polymer).

III. PNIPAm macromonomers

III.1. Synthesis

The synthesis of the PNIPAm macronomers was performed with a two-step reaction, as already described in a previous work,[1] using a telomerization process with cysteamine hydrochloride (AET.HCl) followed by modification of the amino end-group with acrylic acid in order to introduce the vinyl function. The synthesis procedure is presented in **Figure 2.1** and the characteristics of the synthesized PNIPAm macromonomers are summarized in **Table 2**.1.

The first step consisted of synthesizing PNIPAm telomers functionalized with an amine group at one end. It was achieved by free radical polymerization using 2-aminoethanethiol hydrochloride ($HS\text{-}C_2H_4\text{-}NH_3^+,Cl^-$; AET.HCl) as chain transfer agent. The

[1] H. Guo, A. Brulet, P. Rajamohanan, A. Marcellan, N. Sanson and D. Hourdet, **Polymer**, *2015*, 60, 164-175.

reaction was carried out in an aqueous solution in a three necked flask immersed in an ice bath (T ≈ 0 °C). Typically, 100 mmol of NIPAm monomer was dissolved in water with 2.0 mmol of AET.HCl for 2 hours and then left under nitrogen flow for 1 hour. In the meantime, a 10 ml solution of 1.0 mmol potassium persulfate ($K_2S_2O_8$; KPS), the initiator, was left under nitrogen flow for 30 minutes in an ice bath (T ≈ 0 °C). Then, the KPS solution was quickly added to the monomer/chain transfer agent solution. The reaction was allowed to proceed overnight under a nitrogen flow still in an ice bath to avoid the phase separation of PNIPAm telomers during polymerization. Thereafter, a slight excess of NaOH was added to deprotonate the amino groups and the resulting PNIPAm-NH_2 telomers were purified by dialysis against pure water for one week and freeze dried. After dialysis and freeze drying, the yield of the PNIPAm amino-terminated telomers varied between 20 and 75 wt % depending on the size of the polymer and the relative membrane cut-off.

The telomerization process allows controlling both the end-group functionality of the polymer and its average molar mass thanks to the chain transfer reaction. Six PNIPAm amino-terminated telomers with average molar masses from 20 to 120 kg/mol were synthesized by varying the molar ratio between NIPAm monomer and the AET.HCl chain transfer agent. The molar ratio between the KPS initiator and the chain transfer agent was kept constant at 1:2. The quantities used for each synthesis and the PNIPAm telomer/macromonomer characteristics are listed in **Table 2**.1.

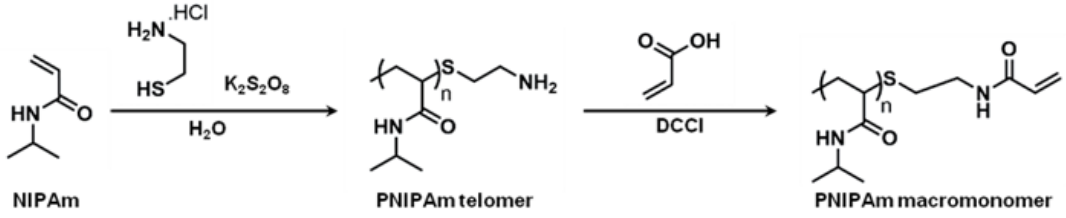

Figure 2.1 Two-step synthesis of the PNIPAm macromonomer

Ideally, the chain growth starts with the addition of the telogen radical to the first monomer rather than with a radical stemming from the initiator. The propagation proceeds by addition of a certain number of monomers, while termination occurs by transfer to the telogen. Under these assumptions, considering that 1) telogen controls initiation and transfer reactions, 2) other transfer mechanisms are negligible (solvent, monomer etc.) and 3) bimolecular termination involving two propagating radicals is also negligible, oligomers can be readily prepared under control of telogen concentration (SH). In that case, the

instantaneous number-average degree of polymerization $(DP_n)_i$ is given by the following relation:

$$\frac{1}{(DP_n)_i} = C_T \frac{(SH)}{(M)} \qquad \textbf{Eq. 2.1}$$

while the cumulative DP_n follows:

$$(DP_n)_{cum} = \frac{\alpha_M}{R_0\left(1-\left(1-\alpha_M\right)^{Ct}\right)} \qquad \textbf{Eq. 2.2}$$

with α_M the monomer conversion, C_T the transfer constant ($C_T = k_{trX} / k_p$ with k_{trX} and k_p being the transfer and propagation rate constants, respectively) and R_0 the initial telogen/monomer concentration ratio ($R_0=(SH)_0/(M)_0$).

By plotting the number-average degree of polymerization of telomers (except for the PNIPAm-120) versus the molar ratio between the monomer and the telogen in **Figure 2.2**, we obtain C_T = 0.15 for the transfer constant by forcing the linear regression through the origin. This rough determination, which relies on the assumption that the conversion yield is not too high to avoid a broadening of the molar mass distribution as described by **Equation 2.2** is in good agreement with the literature data which reports a weak transfer constant for aminoethanethiol compared with that of other thiols.[2]

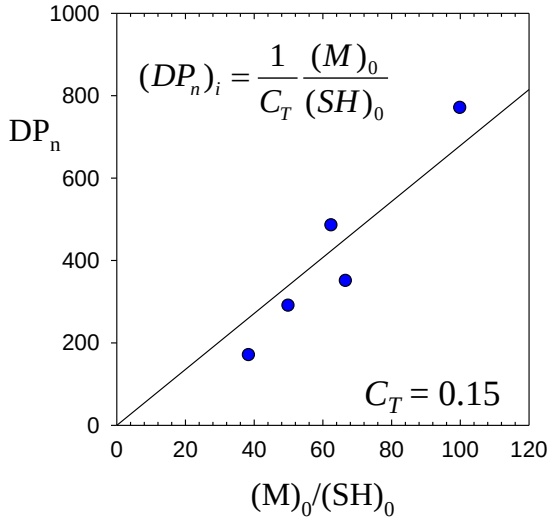

Figure 2.2 Variation of the DPn of telomers versus the initial molar ratio between the NIPAm monomer and the telogen

[2] C. Boyer, C. Loubat, J. J. Robin and B. Boutevin, **J Polym Sci A Polym Chem**, *2004*, 42, 5146-5160

In the peculiar case of PNIPAm-120, we obtain a value far too high (DP_n=1070) compared to what we could expect from the initial ratio $(M)_0/(SH)_0$=50. At this point we do not really have any explanation other than some problems related to a slow transfer reaction at low temperature and/or higher pH or the occurrence of side reactions.

The second step of the PNIPAm macromonomer synthesis consisted of functionalizing the PNIPAm telomers with acrylic acid in order to get the vinyl function (see **Figure 2.1**). For this purpose, 0.26 mmol of PNIPAm telomers were typically dissolved in approximately 50 ml of *N*-methyl-2-pyrrolidone (NMP) with a 15-fold excess of acrylic acid (4.0 mmol) for 2 hours before rapidly adding dicyclohexylcarbodiimide (DCCI) in stœchiometric quantity relative to acrylic acid. The reaction was left overnight at ambient temperature. After the reaction, 100 ml of water was added in order to precipitate the resulting dicyclohexylurea. The solution was then filtered and purified by dialysis against pure water for one week. Finally, the solution was freeze-dried. The resulting PNIPAm macromonomers were obtained with 80-90 wt % yield towards this second step except for the highest average molar mass telomers (120 kg/mol) which led to only a 60 wt % yield. Indeed, for these PNIPAm macromonomers, their surprisingly high average molar mass compared to the amount of initiator employed may be due to possible recombination reactions and/or less reactive KPS molecules. Moreover, the solution obtained after both steps of their synthesis is very viscous.

Table 2.1. PNIPAm macromonomers formulations and characteristics

Sample	NIPAm[a] (mol)	KPS[b] (mol %)	AET.HCl[b] (mol %)	M_n[c] (kg/mol)	M_w[c] (kg/mol)	DPn	$Đ$
PNIPAm-20	0.1	1.3	2.6	18.9	22.4	≈170	1.2
PNIPAm-30	0.1	1.0	2.0	32.9	48.2	≈290	1.5
PNIPAm-40	0.1	0.75	1.5	39.3	52.8	≈350	1.3
PNIPAm-55	0.1	0.8	1.6	54.9	73.9	≈485	1.4
PNIPAm-90	0.1	0.5	1.0	87.2	123.3	≈770	2.4
PNIPAm-120	0.1	0.9	1.8	121.0	177.2	≈1070	1.5

[a] The initial monomer concentration was fixed at 94.2 g/l

[b] KPS/NIPAm monomer (respectively AET.HCl/NIPAm monomer) molar ratio

[c] Average molar masses and dispersities were determined by Size Exclusion Chromatography using triple detection

III.2. Characterization

All PNIPAm macromonomers were characterized using ^{1}H NMR spectroscopy in deuterated water (D_2O) and Size Exclusion Chromatography (SEC) in THF solvent. The results are shown in **Figure 2.3** and **Figure 2.4** and the characteristics of the macromonomers have already been given in **Table 2.1**.

A typical ^{1}H NMR spectrum of PNIPAm macromonomer is given in **Figure 2.3**. The ^{1}H NMR signal assignment is the following: ^{1}H NMR (400 MHz, D_2O): δ= 6.42 ppm (dd, 1H, J_1=10.3Hz, J_2=16.7Hz), δ =6.29 ppm (dd, 1H, J_1=1.3Hz, J_2=16.8Hz), δ=5.84 ppm (dd, 1H, J_1=1.3Hz, J_2=10.3Hz), δ= 3.91 ppm (1H), δ=2.07 (2H, J=46.1Hz), δ=1.58 (1H, J=55.4Hz), δ=1.15 (6H). Due to the average molar mass of the synthesized macromonomers, the peak area assigned to the protons of the vinyl end-group exhibits a very low intensity compared to the peak areas assigned to protons of the PNIPAm chain (see **Figure 2.3**). Consequently, the quantification of the functionalization (second step of the macromonomer synthesis) is difficult to determine. However, as a 15-fold excess of vinyl groups has been added in the second step of the PNIPAm synthesis, we will assume that most of the PNIPAm chains possess a terminal carbon-carbon double bond.

The average molar masses of the synthesized PNIPAm macromonomers were determined by Size Exclusion Chromatography in THF solution with 2 wt % triethylamine (Et_3N) as mobile phase. The normalized signals obtained with refractive index measurements and the results are presented in **Figure 2.4** and **Table 2.1** respectively.

(a)

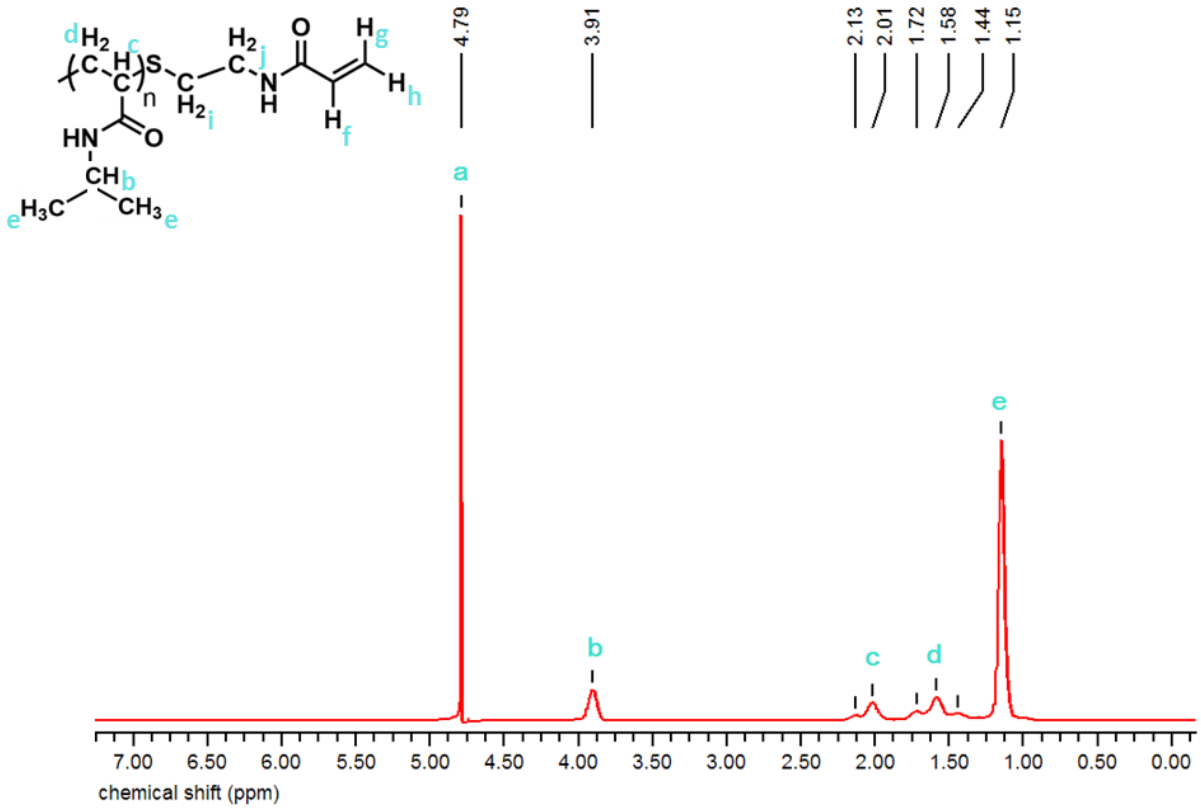

(b)

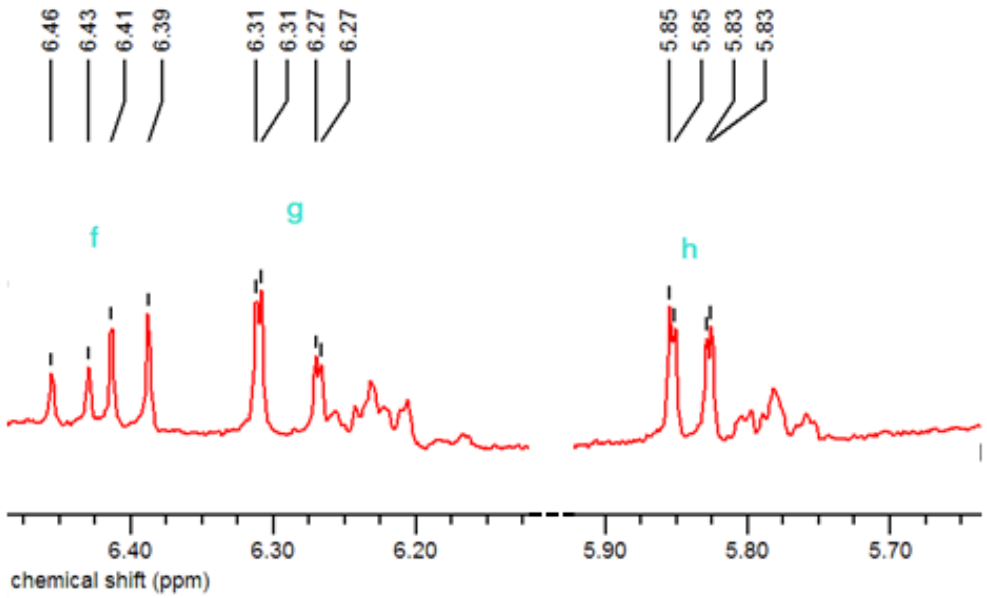

Figure 2.3 ^{1}H NMR spectrum of PNIPAm-20 macromonomer in D_2O. The ^{1}H NMR signal located at 4.79 ppm corresponds to D_2O. **(a)** PNIPAm-20 ^{1}H NMR spectrum; **(b)** zoom x1000 of PNIPAm-20 ^{1}H NMR spectrum from 5.7 to 6.5 ppm

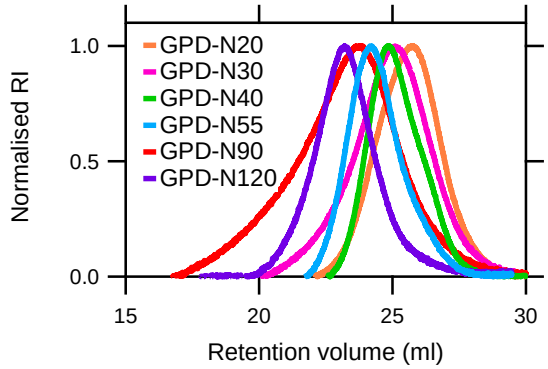

Figure 2.4 Normalised Refractive index vs retention volume curves of PNIPAm macromonomers from 20 to 120 kg/mol. These chromatograms were obtained by SEC in THF solution with 2 wt % of Et_3N as mobile phase

In conclusion, six PNIPAm macromonomers of different average molar masses were successfully synthesized by the two-step process described above. Subsequently, these PNIPAm macromonomers were used to synthesize GPD-Nx and GPD-N55(y-z) hydrogels.

IV. Hydrogel synthesis

IV.1. Introduction

The influence of both hydrogel chemical composition and topology on their nano/microscopic structure and mechanical properties has been demonstrated.1[3,4,5] It is, therefore, important to carefully control the topology of the hydrogels and the chemical composition to be studied. To this purpose, two different series of grafted hydrogels tailored with a cross-linked PDMA network bearing PNIPAm pendant chains were synthesized. The first series, GPD-Nx, was prepared with an equal weight fraction of cross-linked PDMA and PNIPAm macromonomer. Only the average molar mass of incorporated PNIPAm macromonomers was varied (x=M_n in kg/mol). For the second series of grafted hydrogels, GPD-N55(y-z), the average molar mass of the PNIPAm macromonomer was kept constant (x=M_n=55 kg/mol), whereas the weight percentage between the PDMA covalent network (y) and the PNIPAm macromonomers (z) was varied.

The schematic structures of the two series of grafted hydrogels, GPD-Nx and GPD-N55(y-z), are presented in **Figure 1.28** and **Figure 1.29** in Chapter 1.

[3] J. Zhang, R. Xie, S.-B. Zhang, C.-J. Cheng, X.-J. Ju and L.-Y. Chu, **Polymer**, *2009*, 50, 2516-2525
[4] R. Yoshida, K. Uchida, Y. Kaneko, K. Sakai, A. Kikuchi, Y. Sakurai, and T. Okano, **Nature**, *1995*, 374, 240-242
[5] M. M. Soledad Lencina, Z. Iatridi, M. A.Villar and C. Tsitsilianis, **European Polymer Journal**, *2014*, 61, 33-44

IV.2. Synthesis of Grafted hydrogels

The synthesis of the GPD-Nx hydrogels (see **Figure 2.5**) (also named GPD-Nx(50-50) was carried out in aqueous solution in a 20 ml sealed glass vessel immersed in an ice bath. Typically, to synthesize 10 g of GPD-Nx, 833 mg of PNIPAm macromonomer, 833 mg of DMA, 22.7 mg of potassium persulfate (KPS, initiator) and 1.3 mg of *N*,*N*'-methylenebis(acrylamide) (MBA, cross-linker) were dissolved at ambient temperature in 8.3 ml of water and then left for 30 min under nitrogen atmosphere in an ice bath. Then, 0.1 ml of an aqueous solution containing 12.6 µl of *N*,*N*,*N'*,*N'*-Tetramethylethylenediamine (TEMED) was transferred under nitrogen atmosphere into the reaction medium. The reaction was then either rapidly injected through a septum into glass moulds locked into a sealed reactor under nitrogen atmosphere to get hydrogel plates of 2 mm width or left into a sealed syringe to get cylinders of 8 mm diameter. In both cases, the reaction was allowed to proceed 24 hours at ambient temperature.

For all the GPD-Nx syntheses, the KPS/DMA (r_{KPS}) and MBA/DMA (r_{MBA}) molar ratios were fixed at 1.0 mol % and 0.1 mol %, respectively. KPS and TEMED were added in stœchiometric molar quantities, i.e., TEMED/DMA=1.0 mol %. The theoretical total polymer weight concentration was kept at 16.7 wt % and the weight ratio between DMA monomers and PNIPAm macromonomers is always 50/50.

GPD-Nx formulations (presented in **Table 2.2**) were chosen in order to get a large range of topology for probing the mechanical properties. In fact, as only the PNIPAm macromonomers average molar masses varied, while both the DMA monomer concentration and the chemical cross-linker molar ratio were fixed at 8.3 wt % and 0.1 mol %, respectively, all GPD-Nx hydrogels were theoretically formulated with the same density of elastic strands between cross-links.

The same procedure was followed to synthesize the GPD-N55(y-z) hydrogels, again keeping the theoretical total polymer weight concentration constant at 16.7 wt % and r_{KPS} and r_{MBA} constant at 1.0 mol % and 0.1 mol %, respectively. However, in order to study the influence of the weight ratio between the water-soluble/LCST components of the hydrogels, the average molar mass of PNIPAm macromonomers was kept constant at 55 kg/mol, while the weight ratio between the DMA monomer and the PNIPAm macromonomer was varied. The corresponding GPD-N55(y-z) formulations are presented in **Table 2.2**.

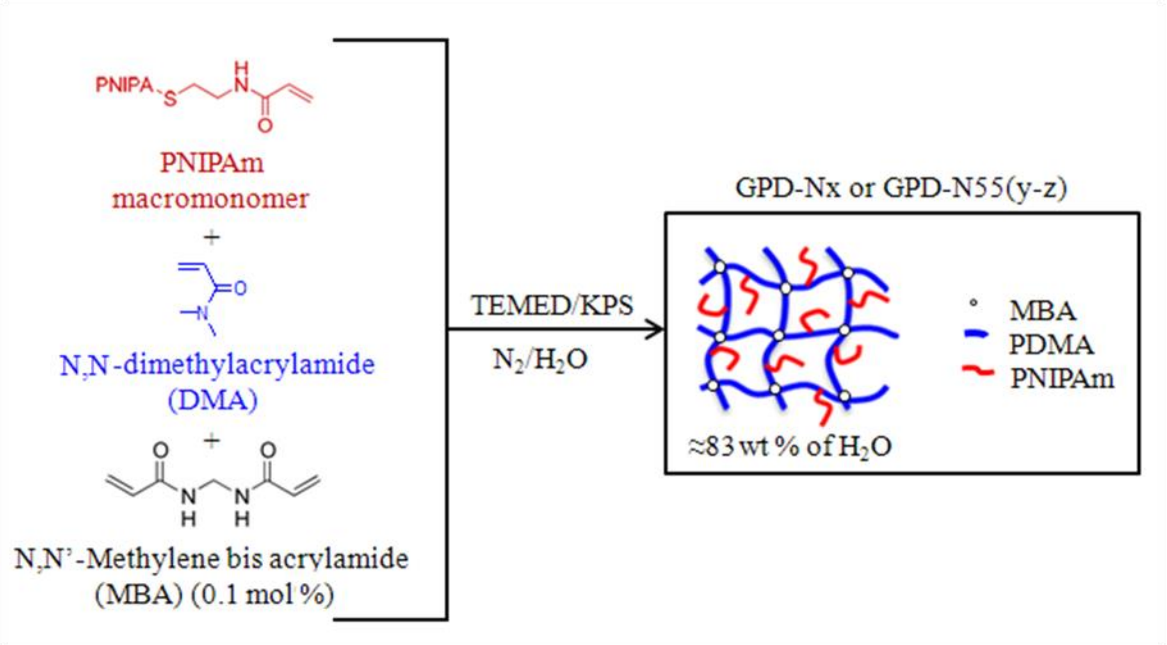

Figure 2.5 Schematic representation of the GPD-Nx and GPD-N55(y-z) hydrogel syntheses

Note that for both GPD-Nx and GPD-N55(y-z) hydrogel series, the key-point in the design of these formulations was to prevent the gel collapse from its preparation state when heated above the transition temperature of PNIPAm. This means that the equilibrium swelling (Q_{eq}) at T=60 °C should be at least equal to or higher than the initial swelling in the preparation state (Q_0). As shown in **Table 2.2** and discussed in the next chapter, this necessary condition is fulfilled for all the hydrogels which are able to maintain a high level of hydration, typically more than 80 wt % of water over the whole temperature range.

It is noteworthy that for all formulations, the resulting hydrogels were transparent at room temperature as shown in **Figure 2.6** which reveals their macroscopic homogeneity on length scales at and above the visible wavelengths.[6,7]

Figure 2.6 Image of a freshly synthesized GPD-N30 hydrogel at room temperature. The other GPD-Nx and GPD-N55(y-z) hydrogels synthesized present a similar aspect

[6] J. Chen, M. Liua, N. Zhang, P. Dai, C. Gao, L. Ma and H. Liu, **Sensors and actuators B**, *2010*, 149, 34-43
[7] K. Okeyoshi, T. Abe, Y. Noguchi, H. Furukawa and R. Yoshida, **Macromol. Rapid Commun.**, *2008*, 29, 897-903

Table 2.2. Formulations of the GPD-Nx and GPD-N55(y-z) hydrogels[a]

Sample	Water (g)	DMA monomer weight (g)	PNIPAM macromonomer (g)	M_n macro-monomer ($kg \cdot mol^{-1}$)	$Đ$	Q_0	Polymer weigth loss (wt %)	T_c (°C)	Q_{eq} T=20°C	Q_{eq} T=60°C
GPD-N20	8.31	0.83	0.83	18.9	1.2	6	10.3± 0.1	36.4	37.7± 0.6	17.1± 0.6
GPD-N30	8.31	0.83	0.83	32.6	1.5	6	11.4± 0.16	31.7	36.7± 0.6	13.8± 0.6
GPD-N40	8.31	0.83	0.83	39.3	1.3	6	11.2± 1.5	34.0	49.1± 0.6	9.9± 0.6
GPD-N55	8.31	0.83	0.83	54.9	1.4	6	9.4± 2.0	34.7	38.7± 2.4	10.4± 0.6
GPD-N90	8.31	0.83	0.83	87.2	2.4	6	6.2± 1.0	32.8	44.1± 1.2	9.9± 1.2
GPD-N120	8.31	0.83	0.83	121.0	1.5	6	5.5± 0.6	33.5	41.2± 0.6	9.4± 0.6
GPD-N55 (82-18)	8.29	1.37	0.30	54.9	1.4	6	1.6± 1.6	32.4	32.5± 1.8	18.2± 0.3
GPD-N55 (69-31)	8.30	1.15	0.52	54.9	1.4	6	4.8± 1.6	31.8	35.3± 1.8	16.6± 0.2
GPD-N55 (50-50)	8.31	0.83	0.83	54.9	1.4	6	9.4± 3.0	34.7	38.7± 1.8	10.4± 0.6
GPD-N55 (31-69)	8.32	0.52	1.15	54.9	1.4	6	17.1± 3.0	35.0	68.0± 1.8	6.9± 1.3

[a] Q_0 and Q_{eq} are the swelling ratios at the preparation state and at thermodynamic equilibrium in water, respectively. T_c is the phase transition temperature corresponding to the maximum of the endothermic peak obtained by Differential Scanning Calorimetry. Polymer weight loss corresponds to the weight ratio between dried gels (dried at 60 °C for 2 days after swelling them for 2 weeks) and the initial amount of monomer plus macromonomer.

IV.3. Synthesis of homo-PDMA and homo-PNIPAm hydrogels

In order to study the impact of PNIPAm grafts on the properties of grafted hydrogels, homo-PDMA networks were synthesized without PNIPAm macromonomers following the same procedure (see **Figure 2.7**) and the same formulation as with the GPD-Nx and GPD-N55(y-z) presented in **Table 2.3**. In these conditions, the initial weight of PNIPAm macromonomers engaged into GPD-Nx and GPD-N55(y-z) formulations was substituted by the same weight of water.

Homo-PNIPAm hydrogels were also prepared according to the same protocol as the one used for the homo-PDMA gels (see **Figure 2.7**), while retaining the same synthesis parameters, namely the molar ratios KPS, TEMED and MBA of 1.0 mol %, 1.0 mol % and 0.1 mol % relative to the NIPAm monomer, respectively.

The macroscopic homogeneity of both the PDMA and PNIPAm covalent networks is highlighted by their transparency at room temperature.

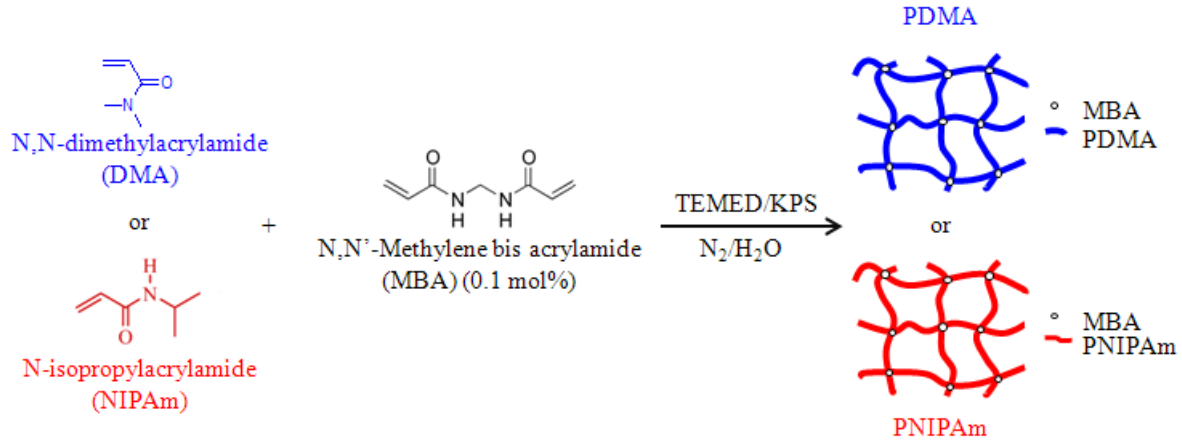

Figure 2.7 Synthesis procedure for both the pure PDMA and PNIPAm covalent networks

Table 2.3. Formulations of the homo-PDMA and homo-PNIPAm hydrogels[a]

Hydrogel	Water (g)	DMA Monomer (g)	NIPAm Monomer (g)	Initial monomer concentration $[DMA]_0$[b] or $[PNIPAm]_0$[c] (wt %)	Q_0	Polymer weigth loss (wt %)	Q_{eq} T=20°C	Q_{eq} T=60°C
PDMAref (82-18)	8.59	1.37	0	13.7[b]	7.3	4.4 ± 0.5	39.6 ± 0.4	28.9 ± 2.9
PDMAref (69-31)	8.82	1.15	0	11.5[b]	8.7	7.0 ± 0.3	47.7 ± 2.0	36.9 ± 0.8
PDMAref (50-50)	9.14	0.83	0	8.3[b]	12.0	12.8 ± 0.5	69.4 ± 0.4	52.3 ± 8.5
PDMAref (31-69)	9.47	0.52	0	5.2[b]	19.3	19.5 ± 0.3	113.3 ± 1.8	88.5 ± 0.4
PNIPAm 8.3 wt %	9.14	0	0.83	8.3[c]	12.0	17.7 ± 1.9	81.5 ± 6.2	2.3 ± 0.1
PNIPAm 16.0 wt %	8.36	0	1.60	16.0[c]	6.2	15.8 ± 1.7	80.8 ± 5.3	2.3 ± 0.1

[a] Q_0 and Q_{eq} are the swelling ratios at the preparation state and at thermodynamic equilibrium in water, respectively. Polymer weight loss corresponds to the weight ratio between dried gels (dried at 60 °C for 2 days after swelling them for 2 weeks) and the initial amount of monomer plus macromonomer.

V. Extractable material

During the synthesis of the grafted hydrogels, the PNIPAm macromonomers are expected to copolymerize with DMA and MBA to form a chemically cross-linked PDMA network with PNIPAm side-chains grafted onto it. However, the monomer conversion may be not quantitative, as the grafting of the PNIPAm macromonomer. It is crucial to verify the efficiency of the network copolymerization. Indeed, free LCST polymer chains embedded in the hydrogel network can influence its properties.[8] Note that it was not possible to quantitatively determine the yield of the macromonomer functionalisation.

V.1. Homo-PDMA hydrogels

As the two series of grafted hydrogels, GPD-Nx and GPD-N55 (y-z), are constituted of a PDMA cross-linked network, the conversion of DMA monomer was first studied in the case of the homo-PDMA hydrogel. For that purpose, PDMA hydrogels, prepared with different initial concentrations of DMA $[DMA]_0$=5.2 to 3.7 wt %: see **Table 2.3**), were swollen to equilibrium in pure water for several days, then dried and weighed to obtain the amount of extractable material that left the network (unreacted monomers or free polymer chains).

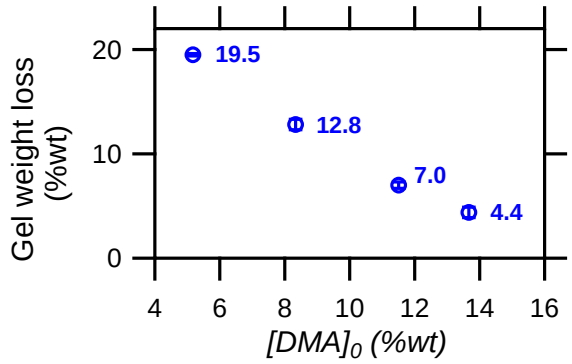

Figure 2.8 Gel weight loss (i.e. extractables) from the homo-PDMA hydrogels as a function of the initial DMA weight concentration

Although we have not characterized the nature of extractable material, monomer or polymer, we will assume as shown in preliminary studies on DMA polymerization[9] that the conversion of DMA monomer is almost complete and that consequently extractables are mainly polymeric material. The results presented in **Figure 2.8** reveal that the weight loss for

[8] H. Guo, N. Sanson, A. Marcellan and D. Hourdet, **Macromolecules**, *2016*, 49, 9568−9577
[9] L. Carlson, S. Rose, D. Hourdet and A. Marcellan, **Soft Matter**, *2010*, 6, 3619-3631

homo-PDMA hydrogels is strongly dependent on the initial DMA monomer concentration ($[DMA]_0$). At low DMA concentration (5.2 wt %), the weight loss is very high (19.5 wt %) whereas it decreases with increasing monomer concentration reaching 4.4 wt % for $[DMA]_0$=13.7 wt %. The high fraction of extractable material observed at $[DMA]_0$=5.2 wt %, can be attributed to the low efficiency of the cross-linking reaction as this concentration is just a little above the critical concentration for gelation. In these conditions one can expect that a significant fraction of uncross-linked PDMA chains can be released outside the gel during the swelling experiment. This result is in good agreement with those of L. Carlsson et al.9 who highlighted that at the same molar ratio between cross-linker and DMA monomer (r_{MBA}=0.1 %mol), a minimum DMA concentration of 4.5 wt % was required to get a macroscopic gel. Below 4.5 wt %, the cross-linking polymerization only gives rise to a suspension of unconnected polymer chains and microgels. Of course, by increasing the monomer concentration above the gelation threshold, it is expected that the fraction of uncross-linked polymer chains, and then extractable material, will decrease (see **Figure 2.8**) if we assume a constant and quantitative monomer conversion for all the hydrogels.

It is now interesting to compare these results to the ones obtained for both the GPD-Nx and GPD-N55(y-z) in order to study the efficiency of the PNIPAm macromonomer polymerization.

V.2. GPD-Nx and GPD-N55(y-z) hydrogels

As the PNIPAm macromonomer chains are end-functionalized with a double bond, they are expected to copolymerize with the DMA monomer. However, we observed that the external aqueous medium used during the first “washing” step of the gels became slightly cloudy when heating above 32 °C, regardless of the average molar mass of PNIPAm macromonomer used in the hydrogel synthesis. This indicated that a fraction of PNIPAm macromonomer was not incorporated into the covalent PDMA network and can diffuse within the gel and in the external medium.

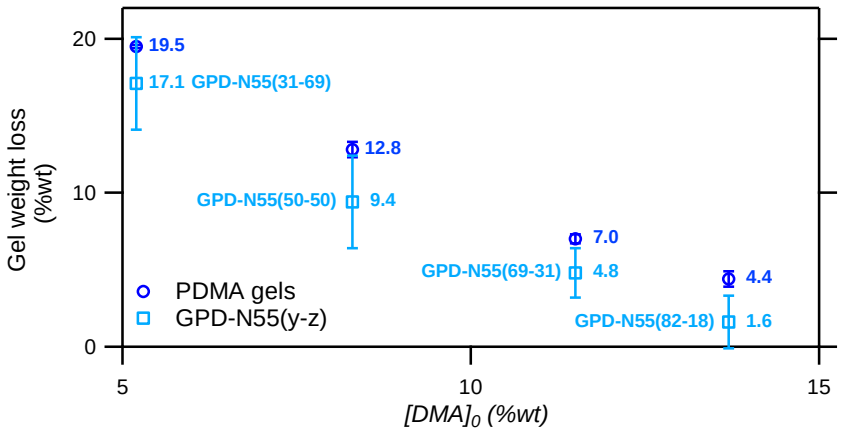

Figure 2.9 Comparative weight loss of the homo-PDMA and GPD-N55(y-z) hydrogels as a function of the initial DMA weight concentration

In **Figure 2.9**, which compares the weight loss of the GPD-N55(y-z) and homo-PDMA gels synthesized with the same amounts of DMA monomer and MBA cross-linker, one can observe very similar variations for the two series. Since the weight loss is always lower for the grafted hydrogels, we could conclude that the release of PNIPAm chains is lower than the release of PDMA derivatives.

In **Figure 2.10**, we reported the weight losses for the two series of grafted hydrogels. We can observe that in the GPD-Nx series the amount of extractable remains practically constant, around 10 %, when the molar mass of PNIPAm macromonomers is less than 60 kg/mol. On the other hand, the amount of extractable material decreases significantly, around 6 %, when the size of the grafts becomes larger: x = 90-120 kg/mol. As in this series all the parameters are fixed, with the exception of the molar mass of PNIPAm, one possibility would be that longer chains can remain physically entangled in networks and cannot escape from the gel during swelling experiments. It can also be assumed that the macromonomer PNIPAm can bind to the PDMA network by other reactions than the opening of the terminal double bond. Indeed, if we assume the possibility of transfer reactions to NIPAm units belonging to the macromonomer, these reactions will statistically favour the chemical attachment to the PDMA network of large chains compared to small ones.

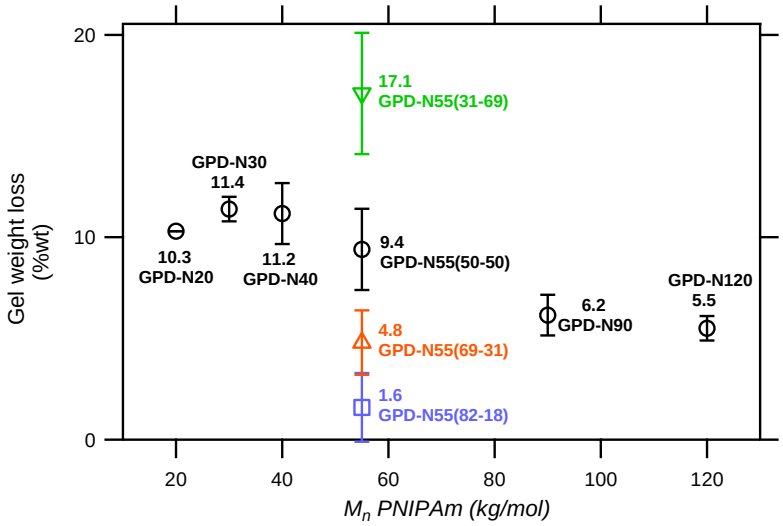

Figure 2.10 Representation of both the GPD-Nx and GPD-N55(y-z) hydrogels weight losses with M_n the average molar mass of PNIPAm grafts

VI. Conclusion

Two series of grafted hydrogels, characterized by a hydrophilic PDMA network bearing pendant chains of PNIPAm of defined length, were successfully synthesized. With the exception of the samples prepared at low monomer concentration (less than 8% by weight of DMA), most graft hydrogels are characterized by only a small fraction of extractables (10% or less) which highlights that most of the polymer material is attached to the network and that its composition is close to the initial feed weight ratio. These hydrogels, prepared either by changing the PNIPAm chain length or the PDMA/PNIPAm composition, make the platform of this comparative study. In the following, we will have to keep in mind that all the hydrogels will be studied in the state of preparation, which means that the small fraction of unbound polymer will remain present.

Chapter 3

Structure and thermodynamic properties of PDMA hydrogels grafted with PNIPAm side-chains

Chapter 3: Structure and thermodynamic properties of PDMA hydrogels grafted with PNIPAm side-chains

Chapter 3: Structure and thermodynamic properties of PDMA hydrogels grafted with PNIPAm side-chains

I. Introduction

In the preceding chapter we have described the multiple step synthesis of two homologous series of thermo-responsive brush-like hydrogels and characterized their composition. Before analysing their mechanical properties and modifications induced by changing the temperature, the aim of this intermediate chapter is to make a bridge between the molecular architecture and the macroscopic properties by describing the thermodynamic behaviour of the hydrogels and their self-assembling properties triggered by the phase transition of the PNIPAm side-chains.

II. Experimental section

II.1. Materials

Perfluorodecalin (Aldrich, ≥95 %) and deuterated water (D_2O, ≥99 %, Aldrich) were used as received. Water was purified with a Millipore system combining a reverse osmosis membrane (Milli RO) and ion exchange resins (Milli Q) for synthesis and purification.

II.2. Characterization

Differential Scanning Calorimetry (DSC). The phase transition of the hydrogels was investigated by differential scanning calorimetry using a DSC Q200 from TA Instruments. Hydrogels at preparation state (ca. 25 mg) were submitted to temperature cycles between 5 and 60 °C under nitrogen atmosphere. The heating and cooling rates were fixed at 10 °C/min.

Turbidimetry. Absorbance measurements were carried out at different temperatures with a UV–vis Hewlett-Packard 8453 spectrophotometer using a 0.2 cm path length quartz cell, in a wavelength range from 200 to 1100 nm, and equipped with a temperature controller (±0.1 °C). The hydrogel sample was directly synthesized in the UV-vis cell prior to the test. Turbidimetry curves were built by collecting the absorbance at 670 nm with a scanning rate of 0.25 °C/min.

Swelling measurements. Equilibrium swelling experiments were performed in pure water at designated temperatures. The samples at their preparation state were initially cut in the shape of discs (8 mm diameter, 5 mm thickness and about 0.3 g) then immersed in a large excess of water which was exchanged once a day. The swollen gels at equilibrium were weighed (m_{sw}) then dried and the swelling ratio at equilibrium (Q_{eq}) was calculated as $Q_{eq}=m_{sw}/m_d$, m_d being the dry weight. The equilibrium swelling is reached after maximum 3 weeks for all the studied formulations.

SANS experiments. SANS experiments were performed at Laboratoire Léon Brillouin (CEA-Saclay, France) on the PAXY spectrometer. The wavelength of the incident neutron beam was set at λ_θ = 15 Å and λ_θ = 6 Å with corresponding sample-to-detector distances of 3.0 m and 6.7 m, respectively. These configurations provide a scattering vector modulus [$q=4\pi sin(\theta/2)/\lambda_\theta$] ranging between 0.002 and 0.2 Å^{-1} (where θ is the scattering angle). For SANS experiments, gel plates of 2 mm thickness were specially synthesized in D_2O to intensify the scattering contrast between the polymer network and the solvent.

For isotropic analyses, the gel discs (diameter = 14 mm and thickness = 2 mm) punched from the samples in their preparation state were fitted inside a ring spacer hermetically sandwiched between two quartz slides. The gel samples were then placed in a temperature controlled auto-sampler and let to equilibrate at least during 1 hour at a given temperature (between 20 and 55 °C) prior to the scattering experiments.

For anisotropic measurements performed with hydrogels under uni-axial deformation, a special device was developed as described in a previous paper[1] (see **Figure 3.1**). With this setup, the hydrogel strip, immersed into the thermo-stated chamber filled with perfluorodecalin, can be studied for hours without any risk of drying. In the following, all the anisotropic scattering experiments have been carried out during at least 1 hour for each sample in a given deformation state. For all the analyses, the efficiency of the detector cell was normalized by the intensity delivered by a pure water cell of 1 mm thickness and absolute measurements of the scattering intensity I(q) (cm^{-1} or 10^{-8} Å^{-1}) were obtained from the direct determination of the incident neutron flux and the cell solid angle. Finally, the coherent scattering intensity of the gel was obtained after subtracting the contribution of the solvent used, as well as the perfluorodecalin for samples studied in the oil environment. For 2D

[1] S. Rose, A. Marcellan, T. Narita, F. Boué, F. Cousin and D. Hourdet, **Soft Matter**, *2015*, 11, 5905-5917

SANS experiments, the incident neutron flux recorded on a two dimensional detector built up with 15500 cells of 25 mm^2, is directly transformed into a 2D image with a colour code. After sector averaging, the data were quantitatively analysed in terms of diffusion pattern. In order to investigate the change of the intensity profiles as a function of the deformation rate, the corresponding intensities $I_{//}(q)$ and $I_{\perp}(q)$ were radially averaged along a given direction within a rectangular sector (masks) of axis parallel (//) and perpendicular ($\perp$), respectively, to the deformation axis.

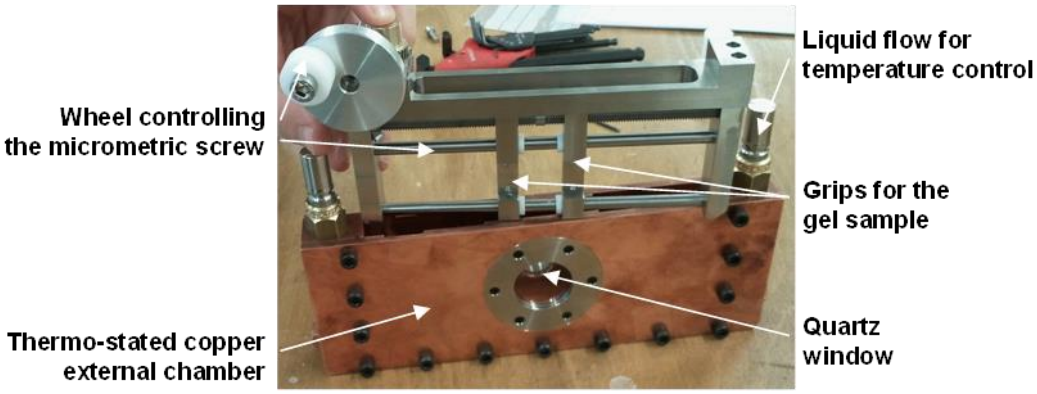

Figure 3.1 Experimental device developed for neutron scattering analysis of hydrogels under uni-axial deformation

III. Phase transition of grafted hydrogels.

III.1. Calorimetric experiments

The LCST-type phase transition of PNIPAm in aqueous solutions is a well-known phenomenon that has been widely reported in the literature.[2,3] At low temperature, PNIPAm chains are soluble in water and exhibit a coiled conformation in order to maximize their hydrogen bonds with water molecules. Above a critical temperature, the chains start to undergo a sharp coil-to-globule transition in water, changing from the hydrophilic state to the hydrophobic one. During demixing (see **Figure 3.2**), energy is required to disrupt the interactions between the water molecules and the amide groups, and therefore, the phase transition of PNIPAm is an endothermic process that can be easily followed by calorimetry. Indeed, DSC experiments have shown that the characteristic parameters of the transition, typically the temperature and the transition enthalpy, are strongly coupled to the structure of

[2] S. Afroze, E. Nies and H. J. Berghmans, **Mol struct**, *2000*, 554, 55-68
[3] H. G. Schild and D. A. Tirell, **J Phys Chem**, *1990*, 94, 4352-4356

the polymer chain (molar mass, chemical composition and topology) and to the environmental conditions (pH, ionic strength, co-solvent, etc.).2[3,4,5]

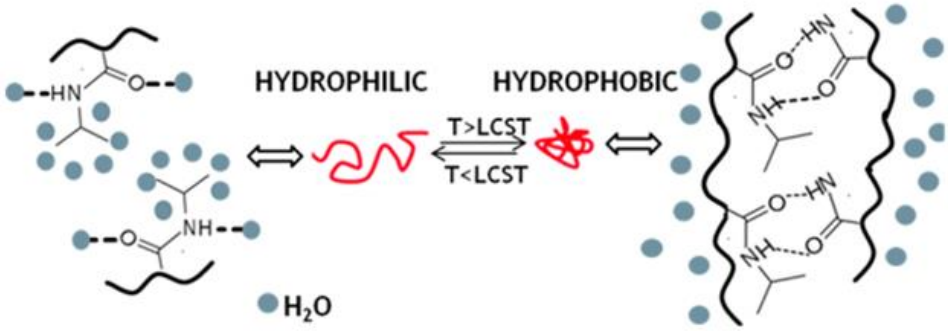

Figure 3.2 Schematic representation of the coil-to-globule transition of PNIPAm with the corresponding physical interactions.[6,7]

III.1.1. GPD-N55(y-z) hydrogels

As illustrated in **Figure 3.3**, all GPD-N55(y-z) hydrogels exhibit an endothermic peak between 30 and 40 °C which reveals the phase transition of the PNIPAm side-chains.

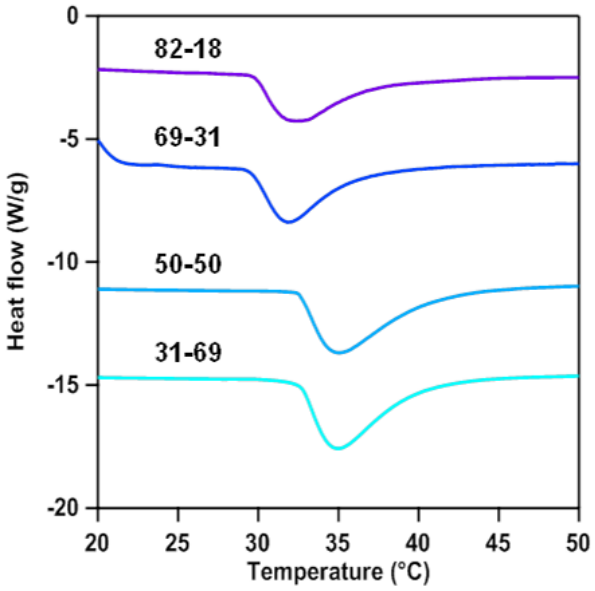

Figure 3.3 Differential Scanning Calorimetry analysis of GPD-N55(y-z) hydrogels between 20 and 50 °C at a scanning rate of 10 °C/min

From the extrapolated values reported in **Table 3.1**, it can be noticed that the transition temperatures do not really differ from one sample to another and that the transition enthalpy, expressed in kJ per mole of NIPAm units, remains also constant and close to 4 kJ/mol_{NIPAm} regardless of the weight ratio between PDMA and PNIPAm. This value, which is in good

[4] K. Otake, H. Inomata, M. Konno and S. Saito, **Macromolecules**, *1990*, 23, 283-289
[5] T. Patel, G. Ghosh, S.-I. Yusa and P. J. Bahadur, **Dispers Sci Technol**, *2011*, 32, 1111-1118
[6] I. Dimitrov, B. Trzebicka, A. H. E. Müller, A. Dworak and C. B. Tsvetanov, **Prog. Polym. Sci.**, *2007*, 32, 1275-1343
[7] M. Meewes, J. Ricka, M. de Silva, R. Nyffnegger and T. Binkert, **Macromolecules**, *1991*, 24, 5811-5816

agreement with the literature data concerning the dehydration process of the PNIPAm chains from aqueous solution (ΔH= 4-6 kJ/mol$_{NIPAm}$),2,3 emphasizes that the aggregation process of PNIPAm side-chains seems weakly influenced by their average composition and distribution.

Table 3.1. Transition temperatures and enthalpy of GPD-N55(y-z) hydrogels determined by DSC. T_{in} corresponds to the very beginning of the phase transition while T_{max} was determined from the maximum of the endotherm.

Sample	T_{in} (°C)	T_{max} (°C)	ΔH (kJ/mol$_{NIPAm}$)
GPD-N55 (82-18)	29.9	32.4	4.1
GPD-N55 (69-31)	29.6	31.8	4.2
GPD-N55 (50-50)	32.3	34.7	3.4
GPD-N55 (31-69)	32.6	35.0	3.9

III.1.2. GPD-Nx(50-50) hydrogels

Most of the previous comments also hold for the GPD-Nx series as reported in **Figure 3.4** and **Table 3.2**.

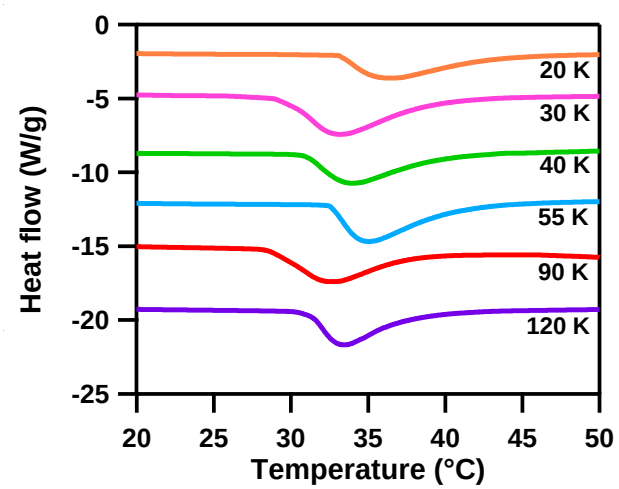

Figure 3.4 Differential Scanning Calorimetry analysis of GPD-Nx(50-50) hydrogels between 20 and 50 °C at a scanning rate of 10 °C/min

Indeed, the association temperature (T_{in} = 31 ± 2 °C) and the transition enthalpy (ΔH = 4.0 ± 0.7 kJ/mol$_{PNIPAm}$) are almost independent of the average molar mass of the PNIPAm grafts, and, therefore, of their number which varies in the opposite way as all the GPD-Nx hydrogels were prepared with a fixed PNIPAm concentration of 8.35 wt %.

For all these networks, it should be mentioned that if most of the PNIPAm chains are chemically anchored on the PDMA network, a small fraction of un-grafted PNIPAm macromonomers remains physically embedded into the polymer network which is studied in the preparation state. Nevertheless, the unique behaviour observed by DSC with all grafted

hydrogels suggests that all PNIPAm chains participate in the aggregation process and, consequently, in the formation of a microphase-separated network.

Table 3.2. Transition temperatures and enthalpy of GPD-Nx(50-50) hydrogels determined by DSC. T_{in} corresponds to the very beginning of the phase transition while T_{max} was determined from the maximum of the endotherm.

Sample	T_{in} (°C)	T_{max} (°C)	ΔH (kJ/mol$_{NIPAm}$)
GPD-N20	33.2	36.4	4.0
GPD-N30	28.9	31.7	4.7
GPD-N40	25.8	28.4	3.7
GPD-N55	32.3	34.7	3.4
GPD-N90	31.0	32.8	4.8
GPD-N120	31.2	33.5	3.8

III.2. Turbidimetry

Complementary experiments were carried out by turbidimetry with the two series of grafted hydrogels, GPD-N55(y-z) and GPD-Nx(50-50), by scanning the temperature between 15 and 50 °C at a rate of 0.25 °C/min (**Figure 3.5** and **Figure 3.6**). In the following discussion, we will only consider the absorbance values below 3 for qualitative comparison as it corresponds to the limit of the UV-visible spectrometer detection.

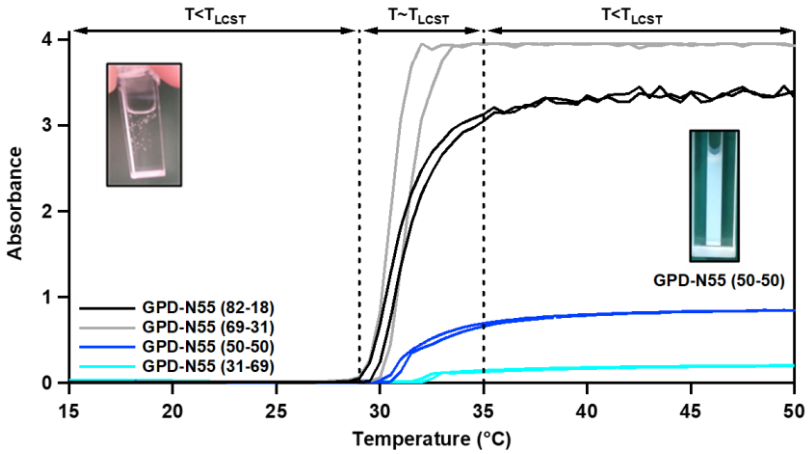

Figure 3.5 Evolution of the turbidity of the GPD-N55(x-y) hydrogels with temperature

For all hydrogels, except GPD-N120, the turbidity starts to increase above T = 30-32 °C, in good agreement with previous DSC experiments on similar PNIPAm-bearing systems. The aggregation process of PNIPAm grafts is fully reversible with a negligible hysteresis as shown on **Figure 3.5** and **Figure 3.6.**

Surprisingly, we can see in **Figure 3.5** that the turbidity at high temperature of the GPD-N55(y-z) hydrogels decreases with increasing PNIPAm content, implying differences in the size, shape, number, distribution or even the stability of the PNIPAm aggregates.

The same experiments performed with GPD-Nx hydrogels also emphasize in a non-intuitive way that the turbidity decreases with the increase of the average molar mass of the PNIPAm grafts. In this series, GPD-N120 designed with the longest PNIPAm side-chains remains almost transparent above the transition temperature even if the grafted chains undergo a phase transition in these conditions (see DSC experiment in **Figure 3.4**). With this series, the variation of absorbance with the average molar mass of PNIPAm side-chains (M_{sc}), and, consequently, with the average molar mass between consecutive grafts (M_g), clearly highlights the role of the network architecture which would imply the formation of smaller and/or more isolated aggregates by increasing the values of $M_g \cong M_{sc}$. We must also consider that the fraction of non-grafted "mobile" macromonomers, which increases when the number of PNIPAm macromonomers increases (i.e., when their molar mass decreases), can also interfere in these macroscopic turbidity experiments.

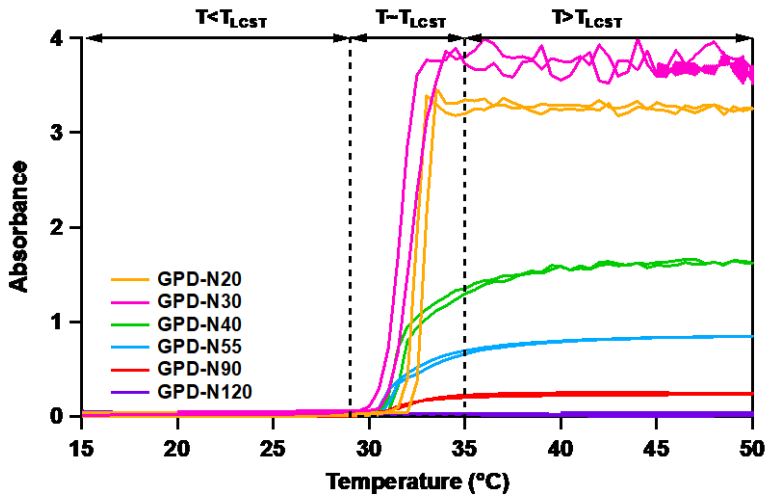

Figure 3.6 Evolution of the turbidity of the GPD-Nx(50-50) hydrogels with temperature

Now that we have shown that all grafted hydrogels undergo a phase transition at about 30 °C, we will investigate their thermodynamic properties (swelling behaviour) as well as the nano-/micro-structure of segregated hydrogels by small angle neutron scattering. In the following, T=20 °C and T ≥ 50 °C will be respectively used as the reference temperatures for the homogeneous regime and the segregated regime in order to be far from the transition temperature.

IV. Swelling properties

IV.1. Comb-like or bottlebrush architectures?

An important point to introduce before analysing the thermodynamic properties is the molecular structure of our grafted hydrogels. As described by S.S Sheiko[8] in the diagram of states given in **Figure 3.7**, brush-like polymers in solution can adopt various conformations depending on the degree of polymerization of the side-chains (n_{sc}) and the number (n_g) of monomers between two consecutive side-chains (or grafting density n_g^{-1}).

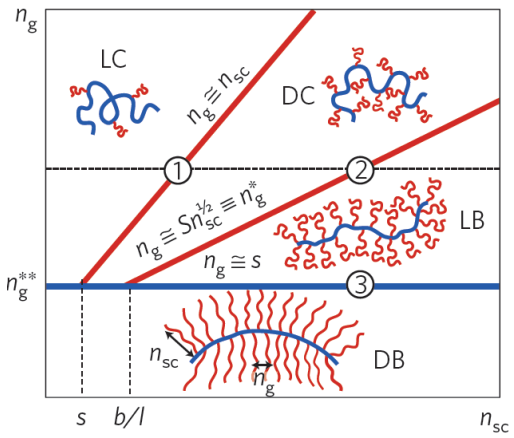

Figure 3.7 Diagram of states of brush-like polymers as determined by the degree of polymerisation (DP) of the side chains (n_{sc}) and the grafting density (n_g^{-1}) (logarithmic scales).
Comb regimes exhibit unperturbed Gaussian backbones and side chains:
LC: loosely grafted combs strongly interpenetrate,
DC: dense combs exhibiting weak interpenetration.
In bottlebrush regimes, the mesoscopic molecules are segregated:
LB: loosely grafted bottlebrushes show Gaussian side chains, but the backbone is stretched by side-chain crowding,
DB: dense bottlebrushes show extended side-chains and backbones.

The solid lines indicate crossovers between regimes that occur on changing n_{sc} and n_g^{-1} as **(1)** LC-DC at $n_g \cong n_{sc}$, **(2)** DC-LB at $n_g \cong Sn_{sc}^{1/2} \equiv n_g^*$ and **(3)** LB-DB at $n_g \cong n_g^{**} \cong s$, where $s = (v_m/(bl^2)$ and $S=v_m/(bl)^{3/2}$ are dimensionless parameters of the order of unity depending on v_m (monomer volume), l (monomer length), and b (Kuhn length of the linear polymer). (from S.S. Sheiko)8

Inspired by this diagram and considering the series GPD-Nx(50-50), prepared with the same weight fraction of PDMA and PNIPAm ($n_g \cong n_{sc}$), we can estimate from **Figure 3.7** that the molecular structure is right at the border between loosely graft combs (LC) and dense combs (DC). On the other hand, if we consider the GPD-N55(y-z) series, the *82-18*, *69-31* and *50-50* samples will follow a LC conformation while the *31-69* one will be in the DC state but far from the bottlebrush domain which would start in this series for a hypothetical *3-97* sample. As a first conclusion, we will consider in the following that our brush-like hydrogels behave as moderate grafted combs with a rather good interpenetration of the polymer chains, no segregation in the primary structure between PDMA and PNIPAm, and a Gaussian

[8] S.S. Sheiko, **Nature Materials**, *2016*, 15, 183-189

conformation of both side chains and backbone assuming a good compatibility between the two polymers.

IV.2. Swelling of polymer networks: theoretical considerations.

The swelling ability is a classical characteric of polymer networks, depending on temperature, chain length between cross-links, size of the solvent molecules and, of course, on the affinity of the polymer chains for the surrounding solvent molecules, with all these parameters being fixed by the experimental conditions.

The description of the swelling theory of Flory-Rehner is based on the hypothesis of separability of the free energy terms.[9] The swelling equilibrium is expressed by the variation of free energy, coming from the combination of a mixing term (ΔF_m) and an elastic one (ΔF_{el}) depending on the elastic deformation of the network:

$$\frac{\Delta F}{V} = \frac{\Delta F_m}{V} + \frac{\Delta F_{el}}{V} \qquad \textbf{Eq. 3.1}$$

with $\frac{\Delta F}{V}$ being the variation of energy density associated with the volume *V* of the studied system. The theory of Flory describes the mixing term as:

$$\frac{\Delta F_m}{V} = \frac{RT}{V_1}\left(\phi_1 . \ln \phi_1 + \chi_{12}\phi_1\phi_2\right) \qquad \textbf{Eq. 3.2}$$

where R is the universal gas constant, T is the absolute temperature, V_1 is the molar volume of the solvent, ϕ_1 and ϕ_2 are respectively the volume fractions of solvent and polymer in the gel sample, and χ_{12} is the Flory interaction parameter of the binary system.

The elastic term ΔF_{el} can be described by different models, making a link between the macroscopic deformation of the network (due to the swelling) and the local deformation of chains. The affine network model, developed by Flory, describes a local deformation of each elastic chain homothetic to the macroscopic deformation, as cross-linking points are supposed to be embedded in the network. In the phantom network model,[10,11] which is more relevant to describe a swollen network even under compression and at low extension, the junction points can freely move and fluctuate over time on a range which is not affected by the macroscopic

[9] P. J. Flory, and J. Rehner, **Journal of Chemical Physics**, *1943*, 11, 521-526
[10] E. Guth and H. M. James, **Ind. Eng. Chem.**, 1941, *33*, 624-629
[11] H. M. James and E. Guth, **J. Chem. Phys.**, *1943*, 11, 455-481

deformation.[12,13] In the case of an isotropic deformation, the phantom theory gives the following free energy density:

$$\frac{\Delta F_{el}}{V} = \left(1 - \frac{2}{f}\right)\frac{3kTn_e}{2V}\left(\frac{(\lambda R_0)^2}{R_\Theta^2} - 1\right) \quad \textbf{Eq. 3.3}$$

where $R^2 = (\lambda R_0)^2$ and R_Θ^2 are the mean-square end-to-end distance of network strands in their final state (R^2), preparation state (R_0^2) and unperturbed conditions (R_Θ^2), while λ is the isotropic linear deformation defined as $\lambda = (\phi_0 / \phi_2)^{1/3}$, with ϕ_0 the polymer volume fraction in the preparation state, n_e the number of elastically active chains and f the functionality of the junction points.

The concentration of elastically active chains (n_e / V) for an ideal network can be written as:

$$\frac{n_e}{V} = \frac{\phi_2 N_A}{v_{pol}^{spe} M_C} = \frac{N_A \phi_2}{N_x V_1} \quad \textbf{Eq. 3.4}$$

with N_A the Avogadro's number, v_{pol}^{spe} the specific volume of the dry polymer and N_x the mean number of "equivalent" units between junction points.

We can notice that N_x is proportional to the true average degree of polymerization of strands (N) through the following relation:

$$\frac{N_x V_1}{V_2} = N = \frac{2[M]_0}{f[X]_0} \quad \textbf{Eq. 3.5}$$

with V_2 the molar volume of the monomer unit, $[M]_0$ and $[X]_0$ being, respectively, the molar concentrations of monomer and cross-linker in the preparation state.

In the treatment of the Flory form equation **(Eq. 3.3)**, the preparation state is often considered equivalent to Θ-conditions and the ratio R_0/R_Θ=1 does not appear in the final equation. Modern developments of network swelling and elasticity use a more general form to describe the elastic contribution as:

$$\frac{\Delta F_{el}}{V} = \left(1 - \frac{2}{f}\right)\frac{3kTn_e}{2V}\left(\frac{(\lambda R_0)^2}{R_{ref}^2} - 1\right) \quad \textbf{Eq. 3.6}$$

[12] J. E. Mark, and B. Erman, **Rubberlike elasticity – A molecular primer, John Wiley and Sons**, *1988*, New-York

[13] M. Rubinstein and R. H. Colby, **Polymer Physics, Oxford.**, *2003*, New-York

with R_{ref}^2, the mean-square end-to-end distance of a free chain with the same number of monomers as the strand in the same solution.

We can notice from **Eq. 3.6**, that it will be only when preparing and swelling the network in Θ-conditions that effectively the equality $R_0=R_\Theta$ is verified.

Starting from the variation of the free energy, one can calculate the osmotic pressure inside the gel arising from mixing and network elasticity as follows:

$$\Pi_{gel} = \Pi_m + \Pi_{el} = \phi_2^2 \frac{\partial}{\partial \phi_2}\left(\frac{\Delta F_m + \Delta F_{el}}{V\phi_2}\right) \quad \textbf{Eq. 3.7}$$

where Π_m and Π_{el} are respectively, the mixing and the elastic contributions to the osmotic pressure, $|\Pi_{el}| = G$ being the shear modulus. Using **Equations 3.2, 3.3** and **3.6**, we finally obtain:

$$\Pi_{gel} = -\frac{RT}{V_1}\left(\ln(1-\phi_2) + \phi_2 + \chi_{12}\phi_2^2 + \left(1-\frac{2}{f}\right)\frac{\phi_0^{2/3}\phi_2^{1/3}}{N_x}\frac{R_0^2}{R_{ref}^2}\right) \quad \textbf{Eq. 3.8}$$

with

$$-\Pi_{el} = G = \frac{RT}{V_2}\left(1-\frac{2}{f}\right)\frac{\phi_0^{2/3}\phi_2^{1/3}}{N}\frac{R_0^2}{R_{ref}^2} \quad \textbf{Eq. 3.9}$$

When immersed in a solvent, the polymer network can swell but the elasticity of cross-linked chains resists to this swelling. The swelling equilibrium ($Q_{Veq} = 1/\phi_2$) is reached when the pressure inside the gel (Π_{gel}) is equal to the osmotic pressure of the surrounding medium (Π_{out}). In the case of neutral networks swollen in a pure solvent, like water, this situation is described by the following equation:

$$\Pi_{gel} = -\frac{RT}{V_1}\left(\ln(1-\phi_2) + \phi_2 + \chi_{12}\phi_2^2 + \left(1-\frac{2}{f}\right)\frac{\phi_0^{2/3}\phi_2^{1/3}}{N_x}\frac{R_0^2}{R_{ref}^2}\right) = 0 \quad \textbf{Eq. 3.10}$$

Based on these thermodynamic equations and using scaling arguments, S. P. Obukhov et al.[14] have derived the following scaling relations connecting the modulus or the swelling degree at equilibrium to *N*, ϕ_0 and ϕ_2 as a function of environmental conditions, in either good solvent (T >> Θ) or Θ-solvent :

$$G \approx N^{-1}\phi_0^{5/12}\phi_2^{7/12} \text{ for T >> } \Theta \text{ and } G \approx N^{-1}\phi_0^{2/3}\phi_2^{1/3} \text{ for T = } \Theta \qquad \textbf{Eq. 3.11}$$

[14] S. P. Obukhov, M. Rubinstein and R. H. Colby, Macromolecules 1994, 27, 3191-3198

$$Q_{Veq} \approx N^{3/5}\phi_0^{-1/4} \text{ for T >> } \Theta \text{ and } Q_{Veq} \approx N^{3/8}\phi_0^{-1/4} \text{ for T = } \Theta \qquad \textbf{Eq. 3.12}$$

These scaling predictions are valid for the so-called strongly cross-linked networks where (trapped) entanglements are not considered. This means that the size of the elastic strand between two consecutive chemical cross-links (N) is shorter than the length of an entanglement strand at the preparation concentration, $N_e(\phi_0)$ which scales with ϕ_0 as:

$$N_e(\phi_0) \approx \phi_0^{-5/4} \text{ for T >> } \Theta \text{ and } N_e(\phi_0) \approx \phi_0^{-4/3} \text{ for T = } \Theta \qquad \textbf{Eq. 3.13}$$

Then, for lightly cross-linked networks, with $N > N_e(\phi_0)$, the modulus and swelling at equilibrium can be obtained from **Eq. 11-12** by replacing N by $N_e(\phi_0)$:

$$G \approx \phi_0^{5/3}\phi_2^{7/12} \text{ for T >> } \Theta \text{ and } G \approx \phi_0^{2}\phi_2^{1/3} \text{ for T = } \Theta \qquad \textbf{Eq. 3.14}$$

$$Q_{Veq} \approx \phi_0^{-1} \text{ for T >> } \Theta \text{ and } Q_{Veq} \approx \phi_0^{-3/4} \text{ for T = } \Theta \qquad \textbf{Eq. 3.15}$$

From thermodynamic equations, the swelling, Q_V, is directly related to the volume fraction of polymer in the gel ($Q_V=1/\phi_2$) but experimentally it is more convenient to use the swelling "in weight", called Q in the following, which is directly calculated from experimental data as follows:

$$Q = \frac{m_{swollen}}{m_{dry}} = (Q_V - 1)\frac{v_{spe}^{p}}{v_{spe}^{w}} + 1 \cong Q_V \qquad \textbf{Eq. 3.16}$$

with v_{spe}^{w} the specific volume of water, v_{spe}^{p} the specific volume of the polymer, m_{dry} the mass of the dried polymer network and $m_{swollen}$ the total mass of the swollen gel. As the specific volumes of PDMA and PNIPAm are close to 0.9 mL/g, there is less than 10 % difference between Q_V and Q in water and there is almost $Q_V = Q$ in heavy water as it will be the case for SANS experiments. Q_V is then assimilated to Q in the following discussion.

IV.2.1. Swelling of homo-PDMA hydrogels

Four different samples of PDMA hydrogels (**Table 2.3** in chapter 2), initially prepared from various polymer concentrations but with the same molar amount of cross-linker, were submitted to swelling experiments at two different temperatures. As reported in **Figure 3.8**, the swelling at equilibrium (Q_{eq}) decreases sharply with the initial polymer concentration ($Q_{eq} \propto [DMA]_0^{-1}$) with a scaling relation which can be compared to the theoretical prediction for lightly cross-linked networks in good solvent (**Eq. 3.15**).

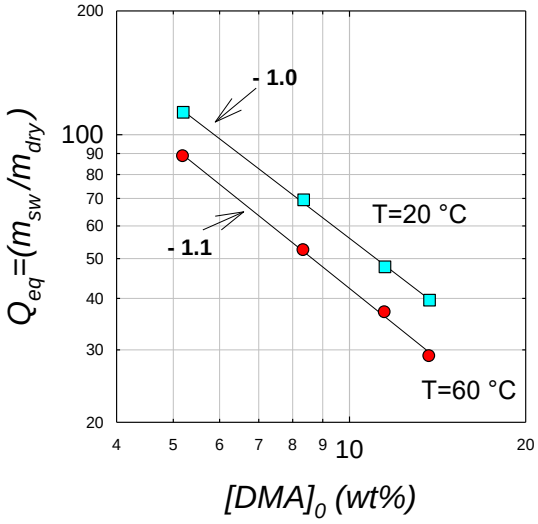

Figure 3.8 Swelling behaviour at thermodynamic equilibrium (Q_{eq}) of PDMA hydrogels as a function of temperature and DMA concentration in the preparation state : $[DMA]_0=100/Q_0$

This behaviour has already been reported by C. Wable[15] (based on a wide set of data related to the cross-linking polymerization of DMA with MBA). Indeed, by characterizing in the preparation state the shear modulus of various series of gels prepared with the same molar ratio of cross-linker and various monomer concentrations, she has been able to separate the contributions of entanglements and cross-links. The main conclusions were the following:

1) For all the networks prepared in the range $0.05 < \phi_0 < 0.12$, there was a non-negligible contribution of entanglements. For 1 mol % of cross-linker, the elasticity of the network was dominated by chemical cross-links, while it was the opposite for 0.1 mol % of MBA, as used in this work.

2) The efficiency of the cross-linking polymerization was much lower than theoretically predicted due to the increasing probability of cyclization when decreasing the initial monomer concentration. Working with a fixed molar ratio of cross-linker, she has shown that the efficiency of chemical cross-linking was increasing from 12, 21 and 31 to 44 % for PDMA gels prepared at ϕ_0 = 0.05, 0.07, 0.10 and 0.12, respectively. For $\phi_0 < 0.05$, no continuous network was formed. These results are in agreement with the work of N. Gundogan et al.[16] on PDMA hydrogels who explored the cross-linking efficiency on a much wider range of PDMA concentrations ($\phi_0 < 0.9$).

Of course, the efficiency of chemical cross-linking with polymer concentration can interfere in the plot of **Figure 3.8** by increasing the slope and therefore making the discussion

[15] Clemence Wable Thesis, **Synthèse, structure et propriétés d'hydrogels hybrides à base de polymères et de silicate**, University of Paris 6, *2013*
[16] N. Gundogan, O. Okay and W. Oppermann, **Macromol Chem Phys.**, *2004*, 205, 814-823

tricky about the quality of solvent. We will mainly keep in mind from this discussion that the properties of the gels we have designed are mainly controlled by trapped entanglements rather than by the contribution of chemical cross-links.

At 60 °C, all the PDMA gels deswell more or less in the same proportion, which means that the interactions between PDMA monomer units and water molecules become less favourable when increasing the temperature. This experimental result, which has often been reported in the literature, is related to the fact that PDMA would have LCST behaviour in water, with an estimated critical temperature of 216 °C.[17] Nevertheless, PDMA gels remain highly swollen at high temperature and this osmotic contribution is the driving force that will prevent the grafted copolymer hydrogels from collapsing dramatically.

IV.2.2. Swelling equilibrium of PDMA hydrogels grafted with PNIPAm side-chains

IV.2.2.1. Swelling equilibrium of GPD-N55(y-z)

If we analyse first the swelling behaviour of GPD-N55(y-z) hydrogels at low temperature, typically 20 °C, we can see in **Figure 3.9** that the swelling of grafted networks decreases when increasing the concentration of DMA monomers and then the density of elastically active chains as previously discussed with homo-PDMA gels. Nevertheless the grafted networks display a weaker swelling at equilibrium than the homo-PDMA gels prepared with similar amounts of monomer and cross-linker. In the case of grafted networks, where the overall polymer concentration is higher than the one of homo-PDMA gels due to the introduction of additional PNIPAm side-chains, the lower swelling at equilibrium could be attributed to the additional physical cross-links, arising either from a higher level of physical entanglements relative to the higher polymer concentration, and/or to transfer reactions involving PNIPAm macromonomer during the synthesis.

From the swelling equilibrium state at 60 °C, well above the transition temperature of PNIPAm, the grafted networks display a strong deswelling which increases with the fraction of PNIPAm incorporated within the gel. This behaviour is intermediate between homo-PDMA gels which show a weak deswelling upon heating, and the homo-PNIPAm ones which strongly collapse from $Q_{eq} \cong 80$ at 20 °C to $Q_{eq} = 2.3$ at 60 °C. As originally demonstrated by H. Guo et al,[18] the design of grafted networks allows keeping a relative "high" level of swelling above the transition temperature of PNIPAm. In the present case, all the grafted

[17] F. Fischer, D. Zuffereyb and R. Tahocesa, **Polym Int**, *2011*, 60, 1259–1262
[18] H. Guo, N. Sanson, D. Hourdet and A. Marcellan, **Adv. Mater.**, *2016*, 5857-5864

networks of this series will be able to keep their original dimensions (isochoric conditions), as defined by their preparation state (Q_0 = 6), between 20 and 60 °C provided that they remain isolated from the equilibrium environment.

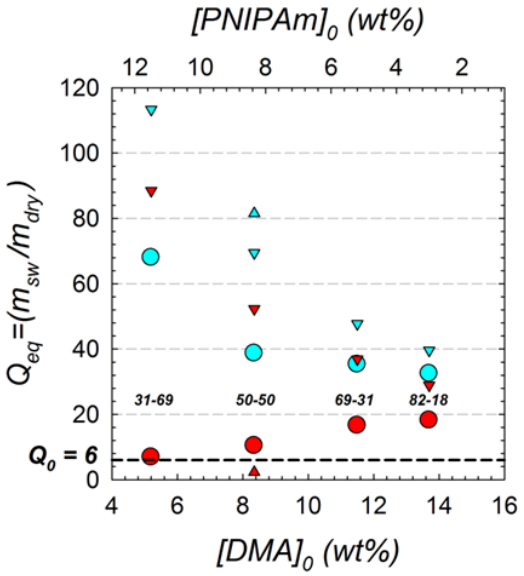

Figure 3.9 Swelling behaviour at equilibrium (Q_{eq}) at 20 (light blue) and 60 °C (red) of homo-PDMA (▼▼), homo-PNIPAm (▲▲) and GPD-N55(y-z) networks (●●) prepared with the same molar fraction of cross-linker (0.1 mol %) and various compositions of DMA monomer and PNIPAm macromonomer. Q_0 corresponds to the swelling at preparation state

GPD-N55(69-31)
20°C

GPD-N55(69-31)
60°C

IV.2.2.2. Swelling equilibrium of GPD-Nx(50-50)

For the GPD-Nx(50-50) series, prepared with equal amounts of DMA monomer and PNIPAm macromonomers and the same molar ratio of cross-linker, one can expect that the size of the PNIPAm side-chains could affect the swelling behaviour in a similar way to that the branching impacts the radius of gyration or the intrinsic viscosity of comb-like polymers. A simple way to discuss the effect of branching is to start from the C^* theorem proposed by P.-G. de Gennes for the swelling equilibrium of polymer networks[19] stating that in the swollen state, each elastic strand between cross-links will swell until full disinterpenetration and reaching the swelling equilibrium ($Q_{eq} \cong Q^*$) around the overlap concentration C^*:

$$Q^* \cong 1/C^* \cong 8N_A R_g^3 / M \qquad \textbf{Eq. 3.17}$$

with R_g being the radius of gyration of the polymer chain and M its average molar mass.
In the case of loosely grafted combs, the pervaded volume of the chain is known to decrease with the degree of branching of the polymer chain. The variation of its radius of gyration ($R_{g,b}$) is generally compared to the radius of gyration of a linear chain ($R_{g,l}$) of similar

[19] P-G. de Gennes, **Scaling Concepts in Polymer Physics: Cornell University Press: Ithaca**, *1979*, New-York

composition and average molar mass using the branching index *g* that has been theoretically defined by Y. Nakamura et al.[20] by:

$$g = \frac{R_{g,b}^2}{R_{g,l}^2} = \left\{ j(3j-2)r^3 + j(j+1)(j+2)r^2 + j(j+1)(2j+1)r + (j+1)^3 \right\} / (rj + j + 1)^3 \quad \textbf{Eq. 3.18}$$

with *j* the number of junction points per strand and $r = M_{sc}/M_g \cong n_{sc}/n_g$ (as defined in **Figure 3.7**), the molar mass of the side-chain (M_{sc}) over the molar mass of the connector (M_g), which is equal to 1 in the framework of this polymer series (y=z=50).

Assuming that the PNIPAm side-chains and the PDMA backbone are fully compatible ($\chi \cong 0$), and taking into account that the average molar mass (*M*) of elastic strands is constant for the whole polymer network series, the relative variation of *Q** is expected to scale as $g^{3/2}$ according to **Eq. 3.17-3.18**. For the purpose of comparison with experimental data, we have set $Q^* = Q_{eq}$ for the GPD-N55(50-50) sample referenced here as GPD-N55. The theoretical swelling of other gels was then calculated according to the C* theorem as:

$$Q^*_{GPD-Nx} = \frac{g^{3/2}_{GPD-Nx}}{g^{3/2}_{GPD-N55}} Q^*_{GPD-N55} \quad \textbf{Eq. 3.19}$$

As shown in **Figure 3.10**, the comparison at 20 °C between theoretical and experimental data is not fully consistent, even if we effectively observe a slight tendency for larger swelling as the molar mass of the PNIPAm side-chains increases.

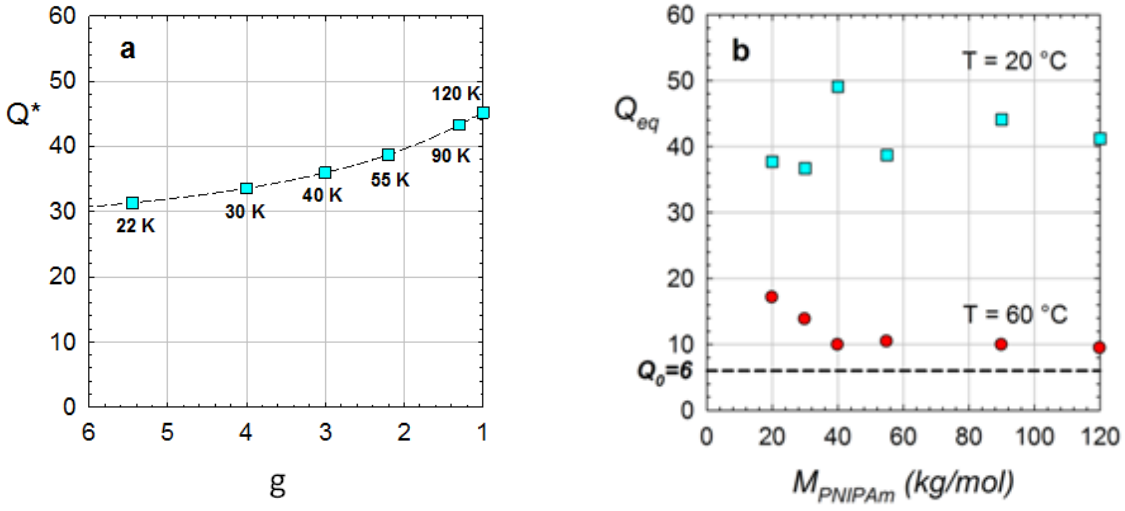

Figure 3.10 Swelling behaviour at equilibrium at 20 (■) and 60 °C (●) of GPD-Nx(50-50) networks prepared with PNIPAm macromonomers of different molar mass. **(a)** Theoretical variation according to the *C** theorem. **(b)** Experimental data. Q_0 corresponds to the swelling at the preparation state (error bars too small to be visible on the graph)

[20] Y. Nakamura, Y. Wan, J. W. Mays, H. Iatrou and N. Hadjichristidis, **Macromolecules**, *2000*, 33, 8323-8328

This lack of agreement can be attributed first to the low accuracy of swelling measurements, even if these experiments have been performed in triplicate. Indeed, a relative uncertainty of more or less 10 % can be estimated for the experimental values. Moreover, as the swelling also depends on the degree of entanglement of polymer chains, we can also assume that additional cross-links by side reactions will increase with the molar mass of PNIPAm grafts and will limit the swelling of the network.

At 60 °C, all the GPD-Nx(50-50) deswell compared to Q_{eq} at 20 °C as expected from the PNIPAm phase separation but they keep a relatively large amount of water ($Q_{eq} \cong 10 > Q_0$) which will allow us to work under isochoric conditions using hydrogels from their preparation state. We can also see that the swelling at 60 °C is almost independent of the PNIPAm side-chains except for the smaller ones (20 and 30 kg/mol). It is probably that a fraction of extractable materials containing un-grafted macromonomers is responsible for the lower efficiency to promote the hydrophobic deswelling.

V. Small Angle Neutron Scattering analyses

In order to investigate their nanostructure, Small Angle Neutron Scattering (SANS) experiments were performed on the synthesized hydrogels in their preparation state (in D_2O) as a function of temperature, both at rest and under deformation.

V.1. Structure of GPD-N hydrogels at room temperature

Conventional cross-linking radical polymerization of chemical hydrogels leads to the formation of non-relaxing frozen concentration fluctuations inducing "inhomogeneities" or "heterogeneities" in gels.[21] Knowing the heterogeneities in terms of both sizes and distribution within the gel is important as they impact their physicochemical properties such as the swelling/shrinking of gels or their turbidity. Scattering techniques are ideal to investigate the presence of inhomogeneities in swollen networks. To take into account spatial inhomogeneities in gels, the theoretical description of the scattering intensity *I(q)* for swollen polymer networks generally considers the addition of two main contributions arising from: [22,23,24]

[21] T.-P. Hsu, D. S. Ma and C. Cohen, **Polymer**, *1983*, 24, 1273-1278
[22] F. Horkay et al., **Polymer Gels and Networks**, *1996***,** 4, 451-465
[23] M. Shibayama, **Soft Matter**, *2008*, 2, 783-832
[24] M. Shibayama, **JAERI**, *Conf 1999*, 012

- thermal concentration fluctuations, as typically observed for dilute or semi-dilute polymer solutions. These thermodynamic fluctuations $I_{sol}(q)$ can be described and expressed, in the previously determined Θ-conditions, by a Lorentzian function of the correlation length (or blob size) ξ:

$$I_{sol}(q) = \frac{I_{sol}(0)}{1+q^2\xi^2} \qquad \textbf{Eq. 3.20}$$

with q the scattering vector,

- additional "frozen" fluctuations, i.e., solid-like heterogeneities which may originate from the polymerization process and prevent free motion of the polymer segments. Several relations have been proposed to describe the excess scattering observed in polymer gels ($I_{ex}(q)$) and more particularly the Debye-Bueche function:[25]

$$I_{ex}(q) = \frac{I_{ex}(0)}{\left(1+\Xi^2 q^2\right)^2} \qquad \textbf{Eq. 3.21}$$

where Ξ is a length scale characterizing the static inhomogeneities in the gel and q the scattering vector

By assuming simple additivity, the scattering intensity profile of polymer gels can be written as:

$$I(q) = I_{sol}(q) + I_{ex}(q) = \frac{I_{sol}(0)}{1+q^2\xi^2} + \frac{I_{ex}(0)}{(1+\Xi^2 q^2)^2} \qquad \textbf{Eq. 3.22}$$

In this expression, the last term, characteristic of covalent gels and coming from frozen heterogeneities can be enhanced by swelling or stretching: indeed, the more a region is cross-linked, the less it deforms, enhancing the density differences within the gel[26]. As previously shown by S. Rose et al.[27], these static heterogeneities are not a specific feature of chemical gels as it was also observed with linear PDMA chains in semi-dilute polymer solutions.

In **Figure 3.11**, the Zimm representation of scattering data obtained with the GPD-N120 hydrogel reveals a strong deviation from the Lorentzian function at the low q-range, indicating the presence of frozen heterogeneities. This behaviour is associated with large scale composition fluctuations formed during the cross-linking polymerization.

[25] W. Li Wu, M. Shibayama, S. Roy, H. Kurokawa, L. D. Coyen, S. Nomura and R. S. Stein, **Macromolecules**, *1990*, 23, 2245-2251
[26] J. Bastide and L. Leibler, **Macromolecules**, *1988*, 21, 2647-2649
[27] Severine Rose Thesis, **silica/polymer interactions: from the local structure to the mechanical reinforcement of hydbride hydrogels**, University of Paris 6, *2013*

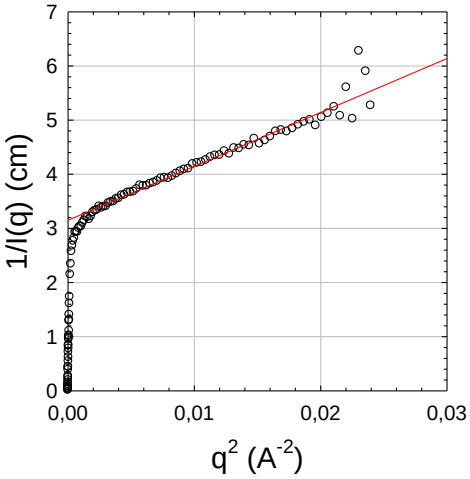

Figure 3.11 Characteristic Zimm representation of scattering data for the GPD-N120 hydrogel in D_2O (○) and linear fitting (—) of experimental data in the high *q*-range (ξ=5.6 Å) at T=20 °C

The correlation length ξ of thermal fluctuations can be obtained from the linear behaviour at the high *q*-range of the Zimm representation given in **Figure 3.11**. The characteristic length Ξ of static heterogeneities is then calculated from **Eq. 3.22** (see **Table 3.3**). An example of curve fitting is shown in **Figure 3.12** in the case of the GPDN-120 hydrogel.

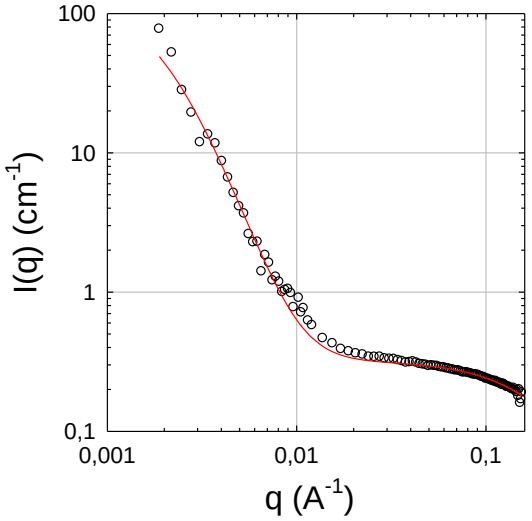

Figure 3.12 Double logarithmic representation of the scattered intensity profiles of GPD-N120 in D_2O (○). The fitting curve (—) was calculated from **Eq. 3.22** with ξ=5.6 Å and Ξ=450 Å. (T=20 °C)

The data, reported in **Table 3.3**, display a common value for the correlation length $\xi \cong 6$ Å which means that all GPD-Nx hydrogels prepared at the same overall polymer concentration (16.7 wt %) display similar thermal fluctuations whatever is the average molar mass of the PNIPAm grafts.

Table 3.3. Characteristic lengths of GPD-Nx hydrogels in the preparation state.

Sample	ξ (Å)	Ξ (Å)
GPD-N20	6.3	505
GPD-N40	5.7	566
GPD-N55	5.7	333
GPD-N90	5.5	372
GPD-N120	5.6	452

This correlation length, which scales with the blob size, is also in quantitative agreement with the concentration dependence reported by S. Rose[27] over a wide range of concentrations taking into account both semi-dilute solutions of linear PDMA chains and a series of PDMA hydrogels prepared with different polymer volume fractions and various degrees of cross-linking (see **Figure 3.13**).

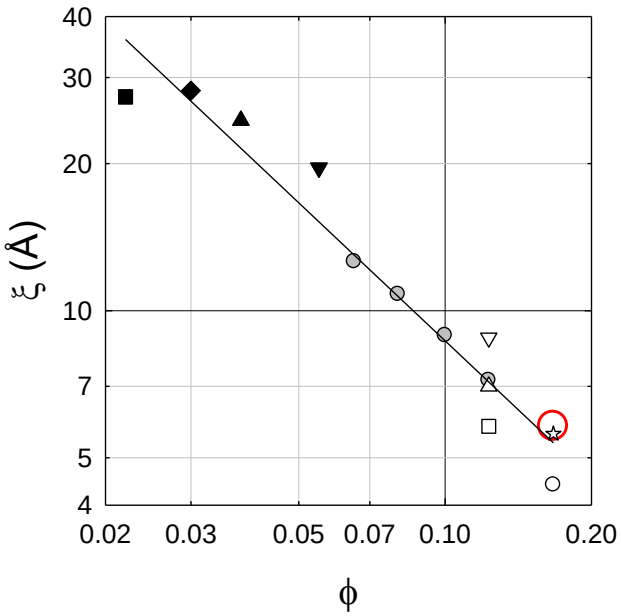

Figure 3.13 Concentration dependence of the correlation length calculated from PDMA/D_2O binary mixtures : Linear PDMA chains (●) and PDMA hydrogels in the preparation state (open symbols) or at equilibrium (filled symbols):
□ ($\phi_0^{PDMA} = 0.128$ / $r_{\%} = 0.1$) ; △ ($\phi_0^{PDMA} = 0.128$ / $r_{\%} = 0.5$) ; ▽ ($\phi_0^{PDMA} = 0.128$ / $r_{\%} = 1$) ; ◇ ($\phi_0^{PDMA} = 0.064$ / $r_{\%} = 1$) ; ○ ($\phi_0^{PDMA} = 0.167$ / $r_{\%} = 0.1$) ; ☆ ($\phi_0^{PDMA} = 0.167$ / $r_{\%} = 1$) ; and GPD-Nx hydrogels ○ ($\phi_0^{PDMA} + \phi_0^{PNIPAm} = 0.167$ / $r_{\%} = 0.1$).
ϕ_0 is the polymer volume fraction in the preparation state and $r_{\%}$ the molar percentage between MBA cross-linker and DMA monomers. Adapted from Rose et al[27]

These results mean that at the local level there is no major difference between pure PDMA samples and PDMA hydrogels grafted with PNIPAm side-chains as soon as they are compared at the same polymer concentration. As shown in **Figure 3.13**, the correlation length ξ follows a unique relation $\xi = \alpha\phi^{-0.94}$, with a scaling exponent close to -1 corresponding to

the unperturbed conditions, i.e., Θ-conditions, and a pre-factor α ≅ 1 Å. Quantitatively, these results are in good agreement with the correlation length obtained by T. Norisuye et al. for homo-PNIPAm hydrogels prepared and studied in similar conditions below their LCST (ξ = 15 Å for ϕ_0 = 0.078).[28] The extrapolation of experimental data to the melt state (ϕ_0=1) gives the corresponding correlation length ξ ≅ 1 Å. From this value, the corresponding blob size can be calculated as:[29]

$$\xi_b = 0.35/\xi \qquad \textbf{Eq. 3.23}$$

In this case, the blob size value is around 3 Å, close to the monomer size.

On the other hand, the characteristic length Ξ of static inhomogeneities appears to be much larger for the GPD-Nx series of grafted copolymer hydrogels compared to values obtained for homo-PDMA hydrogels.[27] This difference between semi-dilute polymer solutions, which only display dynamic fluctuations and gels is generally attributed to static heterogeneities which are frozen during their preparation. For instance, frozen heterogeneities can be introduced during the cross-linking reaction. This was shown by T. Norisuye et al.[28] by comparing gamma-ray cross-linked and chemically cross-linked PNIPAm gels; the latter being much more heterogeneous with frozen heterogeneities Ξ reaching 200 Å for high level of chemically cross-links (r_{MBA}=0.05). On their side, N. Orakdogen and O. Okay[30] have reported that the redox initiator system strongly impacts the formation of heterogeneities during the free radical cross-linking polymerization of acrylamide (AM) or DMA with MBA cross-linker. As a matter of fact, they clearly highlighted that the redox system potassium persulfate/*N*,*N*,*N'*,*N'*-tetramethylethylenediamine (KPS/TEMED) was inducing larger frozen heterogeneities in the network compared to KPS/Metabisulfite. Nonetheless, the impact is much lower with DMA/MBA compared to AM/MBA as the gelation threshold takes place above the overlap concentration of forming chains in the case of the latter system.[30]

In the present study, several hypotheses can be considered in order to explain these large frozen heterogeneities characterized by Ξ:

- In the preparation of grafted copolymer hydrogels, we have to take into account the difference between the reactivity ratios between the DMA monomer and the PNIPAm macromonomer, even if the chemical environments of the double bonds are roughly the same.

[28] T. Norisuye, N. Masui, Y. Kida, D. Ikuta, E. Kokufuta, S. Ito, S. Panyukov and M. Shibayama, **Polymer**, *2002*, 43, 5289-5297.
[29] D. Broseta, L. Ould Kaddour and J.-F. Joanny, **Europhys. Lett.**, *1986*, 2, 733-737
[30] N. Orakdogen and O. Okay, **J. Appl. Polym. Sci.**, *2007*, 103, 3228–3237

This was previously mentioned by H. Guo who reported similar reactivity ratios between DMA monomers and PNIPAm linear macromonomers of 36 kg/mol.[31] Nevertheless, we have to take into account that the reactivity ratios were determined during linear copolymerization and at low conversion (typically 5 %). In fact, the reactivity of the macromonomer within the cross-linked network being formed (at higher conversion) could be lower as it is the case for pendant vinyl compared to vinyl monomer.[32] If we assume a difference of reactivity ratio between the monomer and the macromonomer, we can speculate the formation of heterogeneous polymer sequences during the polymerization process in addition to heterogeneous distribution of chemical cross-linker.

- Moreover, we also have to consider the possibility of some local microphase-separation during the polymerization even if this phenomenon has not been optically observed during the copolymerization of DMA and PNIPAm macromonomer. Nonetheless, we can mention that in a preliminary study, dedicated to copolymer hydrogels based on acrylamide (AM), MBA and similar PNIPAm macromonomers, a macroscopic phase separation was rapidly observed during the polymerization which led us to replace afterwards AM by DMA. The characteristic size of heterogeneities (Ξ), given in **Table 3.3**, is ranging between 350 and 550 Å which is very large compared to chemically cross-linked homo-PDMA[27] or homo-PNIPAm[28] prepared in similar conditions of polymer concentration and low MBA molar ratio (Ξ ≅ 15 Å). Even if Ξ is larger for GPD-N20 and GPD-N40 compared to the 3 other samples with higher average molar mass of PNIPAm chains, it is difficult to really conclude quantitatively concerning the impact of the macromonomer size (and/or number) over the formation of frozen heterogeneities. We will mainly keep in mind that among the different hypotheses considered to explain the formation of static heterogeneities, a heterogeneous distribution of polymer sequences (PDMA and PNIPAm) within the network as well as the presence of non-grafted PNIPAm macromonomers seem quite reasonable.

V.2. Structure of GPD-N hydrogels with increasing temperature

V.2.1. General behaviour

Hydrogels were studied by small angle neutron scattering (SANS) as a function of the temperature in order to investigate the nanostructure formation of the polymer network in static conditions. We observe in **Figure 3.14** a sharp increase of the scattering intensity in the

[31] Hui Guo PhD, **Thermo-responsive toughening of hydrogels**, *2015*
[32] O. Okay, M. Kurz, K. Lutz and W. Funke, **Macromolecules**, *1995*, 28, 2728-2737

vicinity of the transition temperature, between 27 and 34 °C, for all GPD-Nx hydrogels. This behaviour is in good agreement with the DSC and turbidimetric measurements revealing the beginning of the phase transition between 29 and 32 °C for all GPD-Nx gels.

As all the GPD-Nx hydrogels exhibit a common behaviour with the temperature, we will mainly discuss in the following the data obtained with the GPD-N120 sample and conclusions will then be extended to other GPD-Nx hydrogels. As shown in **Figure 3.14**, a well-defined correlation peak appears at low q-values, between 0.005 and 0.015 Å^{-1}, when increasing the temperature from 20 to 55 °C. This behaviour underlines the aggregation process of the PNIPAm side-chains as the correlation peak arises from the formation of a two-phases structure with different contrasts (different concentrations) between rich and poor PNIPAm domains.

Unfortunately, we do not have a lot of data between 27 and 34 °C to follow the phase transition process but from initial experiments performed by H. Guo[33] on similar GPD-N systems, it was shown that the wavelength of the correlation peak gradually increases at the beginning of the phase separation, below 34 °C, and finally remains constant up to high temperature. This was attributed to a nucleation and growth mechanism with the formation, in a first step (between 29 and 34 °C), of an increasing number of nuclei (PNIPAm domains) and then, above 34 °C, to a growth of these domains, their number remaining constant as well as the characteristic distance between them (d_c) given by:

$$d_c = \frac{2\pi}{q_{peak}} \qquad \textbf{Eq. 3.24}$$

with q_{peak} the value of the scattering vector q at the maximum of the correlation peak.

In the case of GPD-N120, we only observe the second step of the phase transition, at T ≥ 34 °C (**Figure 3.14.f**), with the growth of a strong scattering peak which remains located at the same position (q_{peak}=0.0109 Å^{-1}) corresponding to d_c=580 Å. At high temperature, the scattered intensity decays in the high-q regime following the Porod law $I(q) \sim q^{-4}$, characteristic of a sharp interface between rich- and poor-PNIPAm domains.

[33] H. Guo, C. Mussault ; A. Brûlet, A. Marcellan, D. Hourdet and N. Sanson, **Macromolecules**, *2016*, 49, 4295-4306

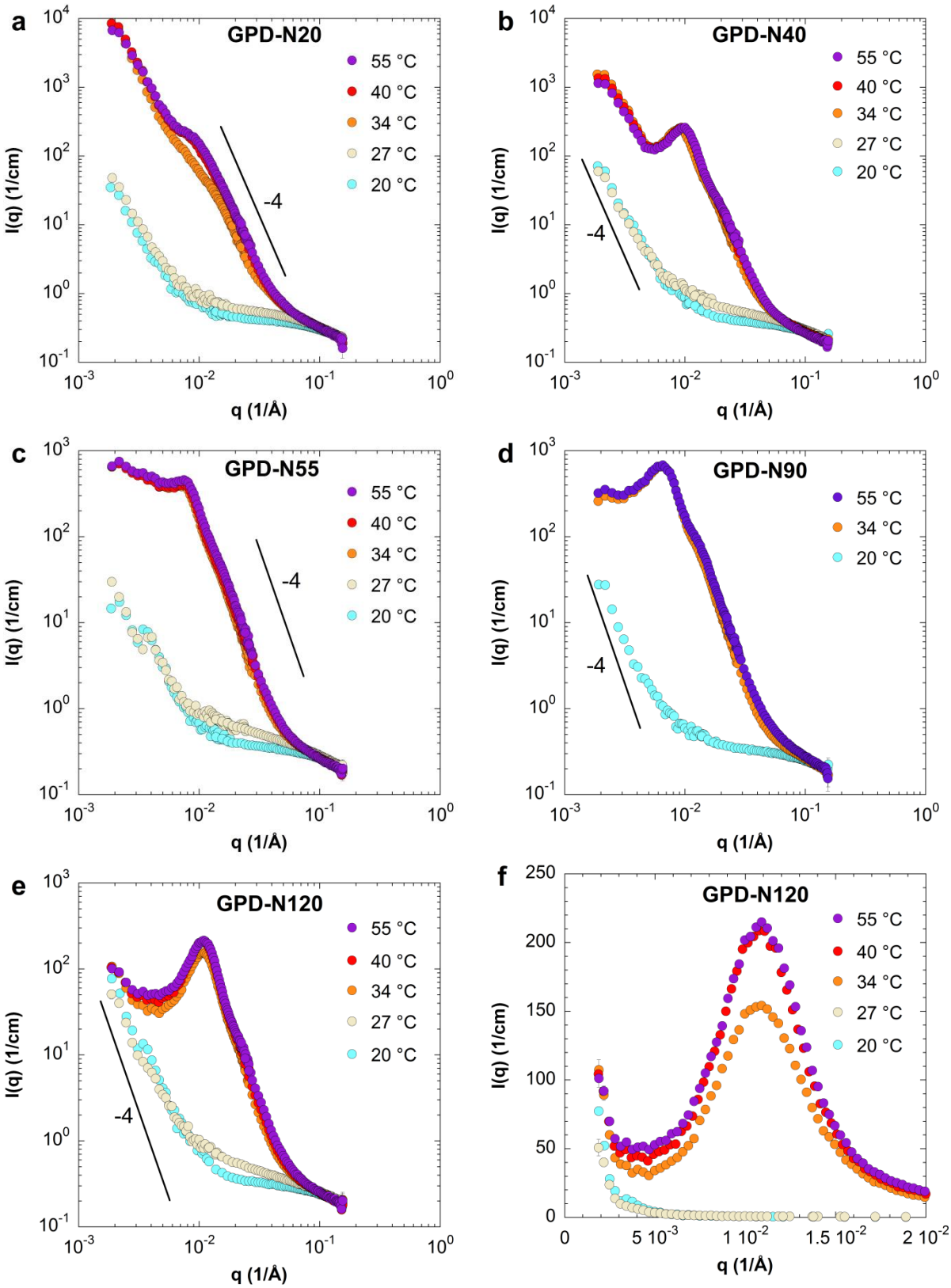

Figure 3.14 Temperature dependence of the scattering intensity of GPD-Nx hydrogels prepared in D_2O: **(a-e)** log-log plots and **(f)** lin-lin plot

The same holds for all the GPD-Nx hydrogels which exhibit a well-defined correlation peak above 34 °C (above 40 °C for GPD-N20) with the same intensity decay which follows the

Porod law in the high *q*-range. At this stage, it can then be qualitatively concluded that the PNIPAm side-chains self-assembled above a critical temperature into PNIPAm-rich domains with a sharp interface whatever is the GPD-Nx hydrogel. The values of characteristic distances determined by **Eq. 3.24** are gathered in **Table 3.4**.

Table 3.4. Structural parameters of phase separated hydrogels at T=55 °C, with q_{peak} the value of the scattering vector at the maximum of the correlation peak and d_c the correlation distance between aggregates.

Sample	q_{peak} (Å^{-1})	$d_c=2\pi/q_{peak}$ (Å)
GPD-N20	$9.0.10^{-3}$	700
GPD-N40	$10.0.10^{-3}$	630
GPD-N55	$7.5.10^{-3}$	840
GPD-N90	$6.4.10^{-3}$	980
GPD-N120	$10.9.10^{-3}$	580

A closer comparison between the scattering intensities of hydrogels can be done from the superposition of the SANS spectra plotted in **Figure 3.15**. As previously described, all GPD-Nx hydrogels exhibit rather similar patterns at 20 °C from which the characteristic lengths of the cross-linked networks have been calculated.

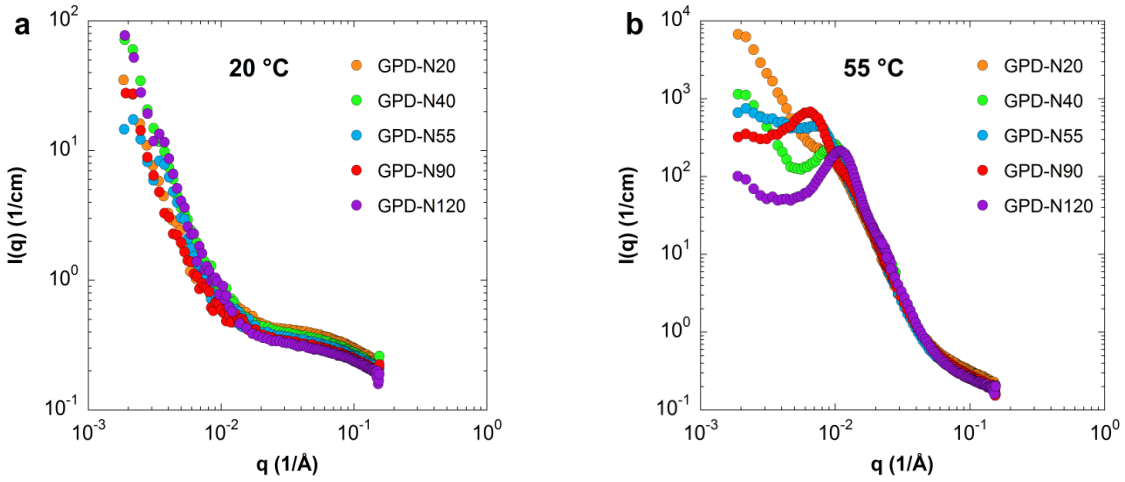

Figure 3.15 Superposition of scattering intensity profiles in log-log scale of GPD-Nx hydrogels in D_2O at **(a)** 20 °C and **(b)** 55 °C: ● GPD-N20; ● GPD-N40; ● GPD-N55; ● GPD-N90; ● GPD-N120

GPD-Nx hydrogels exhibit both similarities and differences in the phase-separated state at 55 °C. First, it is interesting to note that although the characteristic distance varies from one system to another, all scattering profiles superimpose in the high *q*-regime (see **Figure 3.15.b**). This means that, although the number of microdomains and their relative

distance vary from one hydrogel to another, traducing a clear inherent graft length effect, the segregated structures developed at high temperature are rather similar at the local scale, involving phase-separated PNIPAm domains of similar morphologies which exhibit a sharp interface with the swollen PDMA phase. On the other hand, there are large differences of scattering intensities at low q ($q \leq 4.10^{-3}$ Å^{-1}) between GPD-Nx hydrogels with an increase in scattering intensity with decreasing the average molar mass of PNIPAm grafts. This intensity upturn observed at low q is the signature of larger fluctuations revealing the presence of larger aggregates and/or attractive interactions between phase-separated domains. This result is in good agreement with the turbidity experiments plotted in **Figure 3.6** where it was shown that the absorbance at high temperature strongly increases when decreasing the molar mass of PNIPAm side-chains. This is especially the case for GPD-N20 and GPD-N40 which also exhibit a q^{-4} dependence at low q values evidencing the existence of larger aggregates with sharp interfaces. Taking into account the existence of un-grafted PNIPAm macromonomers previously discussed, this sharp upturn at low q could be the signature of the phase separation of free macromonomers able to diffuse through the network in order to form larger aggregates.

V.2.2. Invariant

In order to get more details on the formation of phase-separated PNIPAm domains, the experimental invariant (Inv_{exp}) was determined from the scattering curve:

$$Inv_{\exp} = \int_0^{\infty} q^2 I(q) dq \quad \textbf{Eq. 3.25}$$

For that purpose, we have extended the q^{-4} dependence to the very high q-range to remove the scattering background (see **Figure 3.16**). We have also to notice that, due to the high scattering dependence (q^{-4}) observed at low q for GPD-N20 and GPD-N40, the integration is not totally defined for these two samples and $Inv_{\exp}$ has to be considered as a default value.

In the case of incompressible biphasic systems, as it is for PNIPAm copolymer solutions above their transition temperature, the invariant is in theory a constant (Inv_{th}) that only depends on the volume fractions (ϕ_i) and the difference between the scattering length densities (ρ_i) of the two phases:

$$Inv_{th} = 2\pi^2 (\rho_1 - \rho_2)^2 \phi_1 \phi_2 \quad \textbf{Eq. 3.26}$$

In the following, index 2 will be used for the concentrated-PNIPAm phase and index 1 for the swollen PDMA phase with:

$$\rho_i = \sum \rho_{i,j} \phi_{i,j} \qquad \textbf{Eq. 3.27}$$

where $\rho_{i,j}$ is the scattering length density of the component j of the phase i and $\phi_{i,j}$ its volume fraction.

As the contrast $(\rho_1 - \rho_2)^2$ is a function of the scattering length density and volume fraction of the phase components, the very similar experimental values of the Invariant obtained for the 5 hydrogels (**Table 3**.5), highlight that the phase separation of PNIPAm proceeds in a similar way (similar composition of the two phases), independently of the molar mass of PNIPAm grafts.

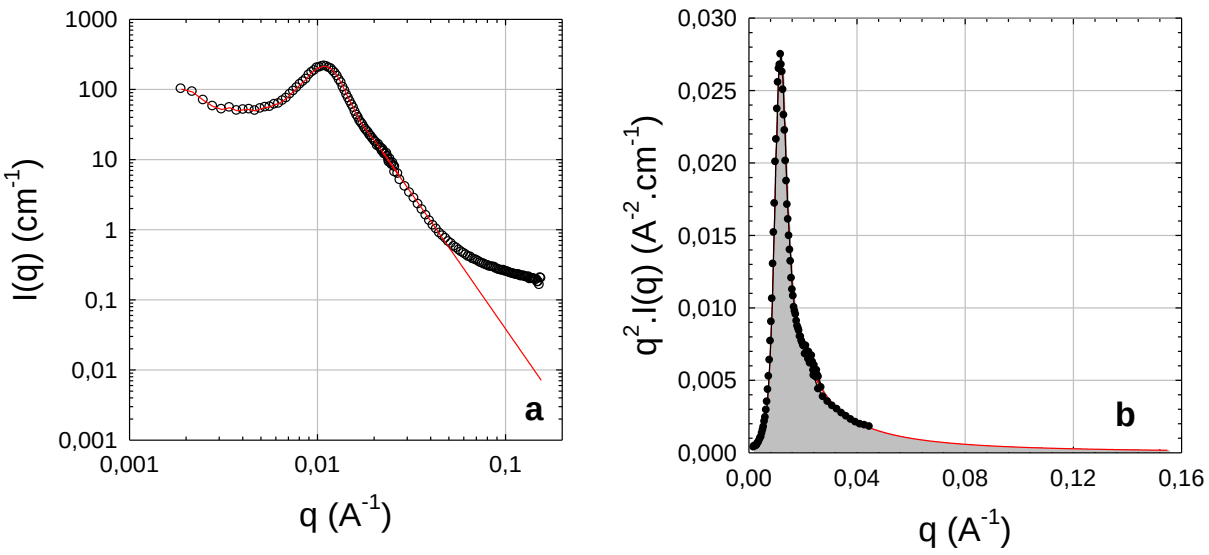

Figure 3.16 **(a)** Scattering data of GPD-N120 at 55 °C along with the fitting curve (—) used to calculate the invariant defined as the area under the curve $q^2I(q)$ versus q. **(b)** The corresponding integration with the corresponding fitting curve (—)

Then, using **Eq. 3.26-3.27**, it is possible to estimate the composition of the segregated phase. Here we assume that during the phase separation process, a fraction of PNIPAm side-chains (f_{PNIPAm}) self-assemble into concentrated domains of volume fraction ϕ_{PNIPAm}. As shown in a previously published work on the self-assembly of linear graft copolymers

PDMA-*g*-PNIPAm,[34] we will also assume that PDMA segments do not mix with PNIPAm in the concentrated phase but that a fraction of PNIPAm grafts (1-f_{PNIPAm}) is allowed to remain with PDMA in the swollen phase. By fixing one parameter, like f_{PNIPAm}, the theoretical value of Inv_{th} can be calculated as a function of ϕ_{PNIPAm}.

An example is given in **Figure 3.17.a**, assuming that all PNIPAm grafts self-associate into concentrated domains (f_{PNIPAm} = 1). Taking the average value Inv_{exp}=3.7.10^{-4} Å^{-3}.cm^{-1}, obtained with GPD-Nx hydrogels (**Table 3**.5), this gives a PNIPAm volume fraction of 0.32 in the concentrated phase 2. By changing the fraction of self-associating PNIPAm, different concentrations can be obtained for the concentrated phase as shown in **Figure 3.17.b**.

Assuming that the transition enthalpy determined by DSC is related to the fraction of PNIPAm that self-associate above the transition temperature, we will postulate that the ratio between the enthalpy measured for GPD-Nx hydrogels over the enthalpy of PNIPAm grafts solution gives a rough estimation of f_{PNIPAM} (**Table 3.5**). Under this assumption, and taking into account ΔH=4.5-5 kJ/mol$_{NIPAm}$ for the average transition enthalpy of PNIPAm chains in water, a volume fraction of PNIPAm in the concentrated domains close to 0.32-0.4 is obtained from **Figure 3.17.b**.[34,35] This result is in good agreement with the value reported by M. Shibayama et al.[36] for the swelling behaviour of homo-PNIPAm gels above their transition.

Table 3.5. Structural parameters of microphase-separated hydrogels at T = 55 °C, with Inv_{exp} the experimental invariant; $limq^4.I(q)$ the Porod limit; S_2/V_2 the specific surface of PNIPAm-rich microdomains calculated using ϕ_1 = 0.8 as the average volume fraction of the swollen PDMA phase.

Sample	q_{peak} (Å^{-1})	d=2π/q_{peak} (Å)	Inv_{exp} (Å^{-3}cm^{-1})	limq^4*$I(q)$ (Å^{-4}cm^{-1})	S_2/V_2 (Å^{-1})
GPD-N20	9.0.10^{-3}	700	3.5.10^{-4}	2.26.10^{-6}	0.016
GPD-N40	10.0.10^{-3}	630	3.6.10^{-4}	2.95.10^{-6}	0.021
GPD-N55	7.5.10^{-3}	840	3.7.10^{-4}	2.56.10^{-6}	0.017
GPD-N90	6.4.10^{-3}	1000	3.8.10^{-4}	2.53.10^{-6}	0.017
GPD-N120	10.9.10^{-3}	580	3.6.10^{-4}	3.07.10^{-6}	0.021

[34] H. Guo, A. Brûlet, P.R. Rajamohanan, A. Marcellan, N. Sanson and D. Hourdet, **Polymer**, *2015*, 60, 164-175
[35] G.H. Schild and D.A. Tirrell, **Langmuir**, *1991*, 7, 665-671
[36] M. Shibayama, M. Morimoto and S. Nomura, **Macromolecules**, *1994*, 27, 5060−5066

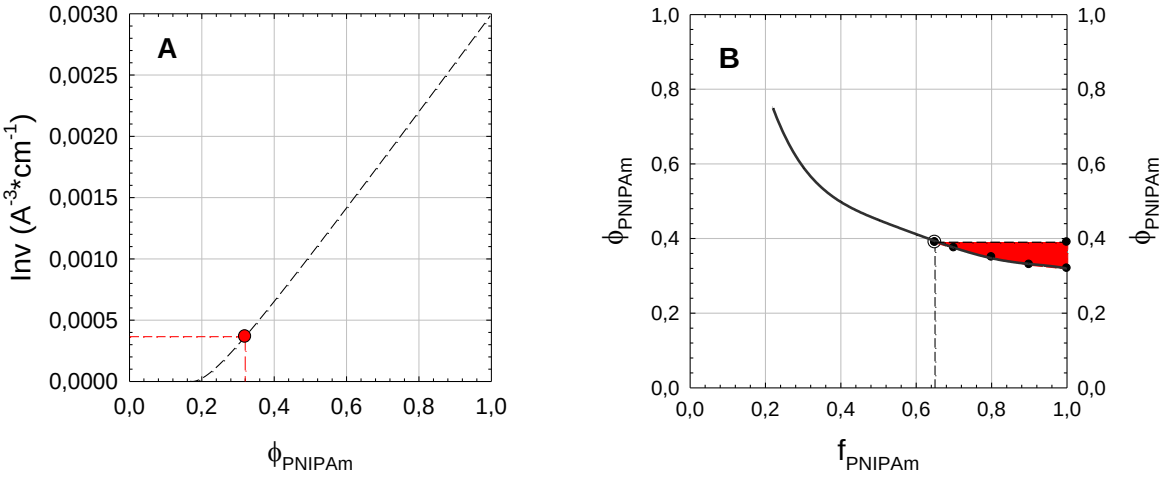

Figure 3.17 SANS data treatment of microphase-separated GPD-Nx gels (T=55 °C). **(A)** Variation of the theoretical Invariant (Inv_{th}) with the volume fraction of PNIPAm in the concentrated phase (ϕ_{PNIPAm}) assuming that all PNIPAm chains participate in this phase (f_{PNIPAm}=1). In this case, the average experimental value Inv_{exp}=3.7.10^{-4} Å^{-3}cm^{-1} gives: ϕ_{PNIPAM}=0.32. **(B)** Starting with Inv_{exp}=3.7.10^{-4} Å^{-3}cm^{-1}, the different couples (ϕ_{PNIPAm} ; f_{PNIPAm}) can be calculated for the microphase-separated domains. Assuming that $0.65 \leq f_{PNIPAm} \leq 1$, this plot allows to extrapolate the average composition of concentrated PNIPAm domains ($0.39 \geq \phi_{PNIPAm} \geq 0.32$) as well as their volume fraction: $0.14 \leq \phi_2 \leq 0.26$ ($0.86 \geq \phi_1 \geq 0.74$)

From the asymptotic behaviour obtained at high temperature ($I(q) \sim q^{-4}$), the total interface area of microdomains (S_2) in the whole scattering volume (V) can be calculated using the following relation:

$$\frac{S_2}{V} = \frac{\pi \phi_1 \phi_2}{Inv} \lim_{q \to \infty} q^4 I(q) \qquad \textbf{Eq. 3.28}$$

and the specific surface of PNIPAm concentrated domains ($S_{spe}=S_2/V_2$) can be deduced:

$$S_{spe} = \frac{S_2}{V_2} = \frac{S_2}{V\phi_2} = \frac{\pi \phi_1}{Inv} \lim_{q \to \infty} q^4 I(q) \qquad \textbf{Eq. 3.29}$$

Interestingly, at high temperature, the specific surfaces of microphase-separated PNIPAm domains are almost the same whatever the GPD-Nx hydrogel: $S_{spe} \cong 0.020$ Å^{-1}. While the specific surface can be easily calculated, the real size of the microphase-separated domains cannot be precisely determined as it is closely related to their morphology : S_2/V_2 being equal to $1/t$ for platelets of thickness t (t=50 Å), $2/R_0$ for cylinders of radius R_0 (R_0=100 Å), $3/R_0$ for spheres of radius R_0 (R_0=150 Å) and a/ξ, with a=4 to 7.16 for various random biphasic models with a correlation distance ξ (ξ = 200 or 360 Å, respectively).[37,38,39,40]

[37] T. Sottman, R. Strey and S-H. Chen, **J. Chem. Phys.**, *1997*, 106, 6483-6491

V.2.3. Looking for a model

During the previous work of H. Guo et al.[41] based on the comparison between linear and cross-linked polymers (G)PD-N and (G)PN-D of opposite topologies, one of the conclusions was that contrary to the (G)PN-D architecture which gives rise to a bicontinuous morphology above the critical temperature, the (G)PD-N hydrogels were assumed to adopt a micellar morphology. In this framework, the SANS data obtained with a single hydrogel sample were successfully adjusted using a spherical core-shell model interacting with hard sphere repulsions.

Based on this work, the same model has been used in a first attempt to fit the SANS data of our 5 hydrogel samples. Nevertheless, as this model converges with only some of the hydrogels, it generally leads to unrealistic parameters. Moreover, another difficulty with this series of homologous hydrogels is to combine the fact that, regardless of the GPD-Nx sample considered, the domains must have 1) a similar surface area and 2) a similar distribution and/or concentration of PNIPAm (same Inv_{exp}).

To tackle this problem, we have revisited the data treatment using a cylinder model with hard sphere structure (CHS model). From a general point of view this model provides the possibility to get domains of different sizes (different lengths) with almost the same specific surface if the radius of cylinders does not change so much. Furthermore, from a geometrical point of view it seems more realistic that the phase separation of PNIPAm side-chains proceeds mainly in "one" direction, instead of 3D for spheres, especially in the present case of covalent networks where the chemical cross-links bring supplementary topological constraints. For the fitting procedure, we have taken into account the two set of experimental data obtained in the low and intermediate q-range. The high q-range was not taken into account as it is not described by the model which ends up with a q^{-4} decrease. Then, for most hydrogels, we have ignored the low values of q (less than 0.005 $Å^{-1}$) because the model used cannot take into account the intensity upturn generally observed in this range. All the data treatments have been performed with the Sas View software.[42] A representative example is given in **Figure 3.18** with the GPD-N120 hydrogel where we have set 4 of the 9 variables that

[38] L. Auvray, J-P. Cotton, R. Ober and C. Taupin, **J Phys**, *1984*, 45, 913-928.
[39] I. S. Barnes, S. T. Hyde, B. W. Ninham, P.-J. Derian, M. Drifford and T. Zemb, **J Phys Chem**, *1988*, 92, 2286-2293.
[40] M. Teubner and R. Strey, **J. Chem Phys**, *1987*, 87, 3195-3200
[41] H. Guo, N. Sanson, A. Marcellan and D. Hourdet, **Macromolecules**, *2016*, 49, 9568–9577
[42] https://www.sasview.org/

define the model in order to maintain control over the modelling parameters and thus to avoid unrealistic adjustments.

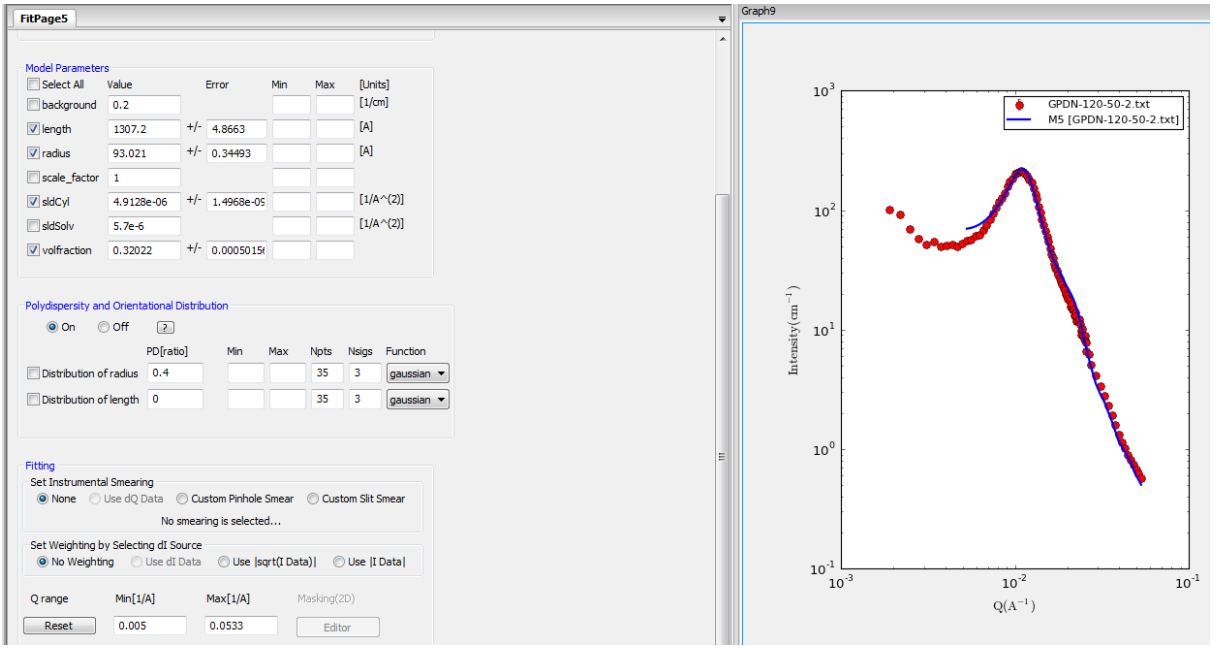

Figure 3.18 Data fitting and relative parameters based on the cylinder model with hard sphere structure using Sas view software for GPD-N120

In the panel of **Figure 3.18**, the fitting parameters are defined as follows:

- Background=0.2 (mainly incoherent contribution)

- Length of cylinder: free parameter

- Radius of cylinder: free parameter

- Scale factor=1 (absolute values)

- SldCyl=ρ_{cyl}= ρ_2: free parameter (scattering length density of the phase-separated phase)

- SldSolv=ρ_{sol}= ρ_1=5.7.10^{-6} Å^{-2} (scattering length density of the surrounding media). This value has been averaged from the two limits reported previously: (1) f_{PNIPAm}=1; ϕ_{PNIPAm} = 0.32 ⇨ ρ_1=5.75.10^{-6} Å^{-2} and (2) f_{PNIPAm}=0.65; ϕ_{PNIPAm} =0.39 ⇨ ρ_1=5.65.10^{-6} Å^{-2}.

- Volfraction=ϕ_{cyl}= ϕ_2: free parameter (volume fraction of cylinders)

- Distribution of radius=σ/R_0=0.4 (Polydispersity in order to reduce the oscillations of the form factor)

- Distribution of length=σ/L: not considered

The same procedure was applied to all the hydrogels and the summary of these fittings as well as the extrapolated parameters are gathered in **Figure 3.19** and **Table 3.6**.

As shown in **Figure 3.19**, the CHS model allows a rather good fitting of the experimental data in the range of the scattering vectors investigated. Moreover, we obtain a good agreement between the radius of the cylinders calculated from the specific surface and those extrapolated from the model. As previously discussed, only small variation of the specific surface is expected if the radii of the cylinders do not vary too much as it is the case. At high temperature, the main differences between the gels come from the length of the cylinders and their volume fraction that will define the position of the scattering peak. The volume fraction of the cylinders (ϕ_2) are in rather good agreement with previous values calculated from the Invariant: (f_{PNIPAm}=1; ϕ_{PNIPAm}=0.32 and ϕ_2=0.26). By comparison, the fitting of the GPD-N20 with ϕ_2=0.1 is much less reliable certainly due to the fraction of free PNIPAm macromonomers forming much larger aggregates which are not taken into account in this data treatment. Finally, taking into account the volume of the cylinders, the fraction of PNIPAm inside the domains (ϕ_{PNIPAm}) and the average molecular volume of the PNIPAm chains, it is also possible to calculate the average number of PNIPAm side-chains per cylinder, or the aggregation number (N_{ag}; see **Table 3.6**), whose main objective is to highlight the large number of chains involved in their formation.

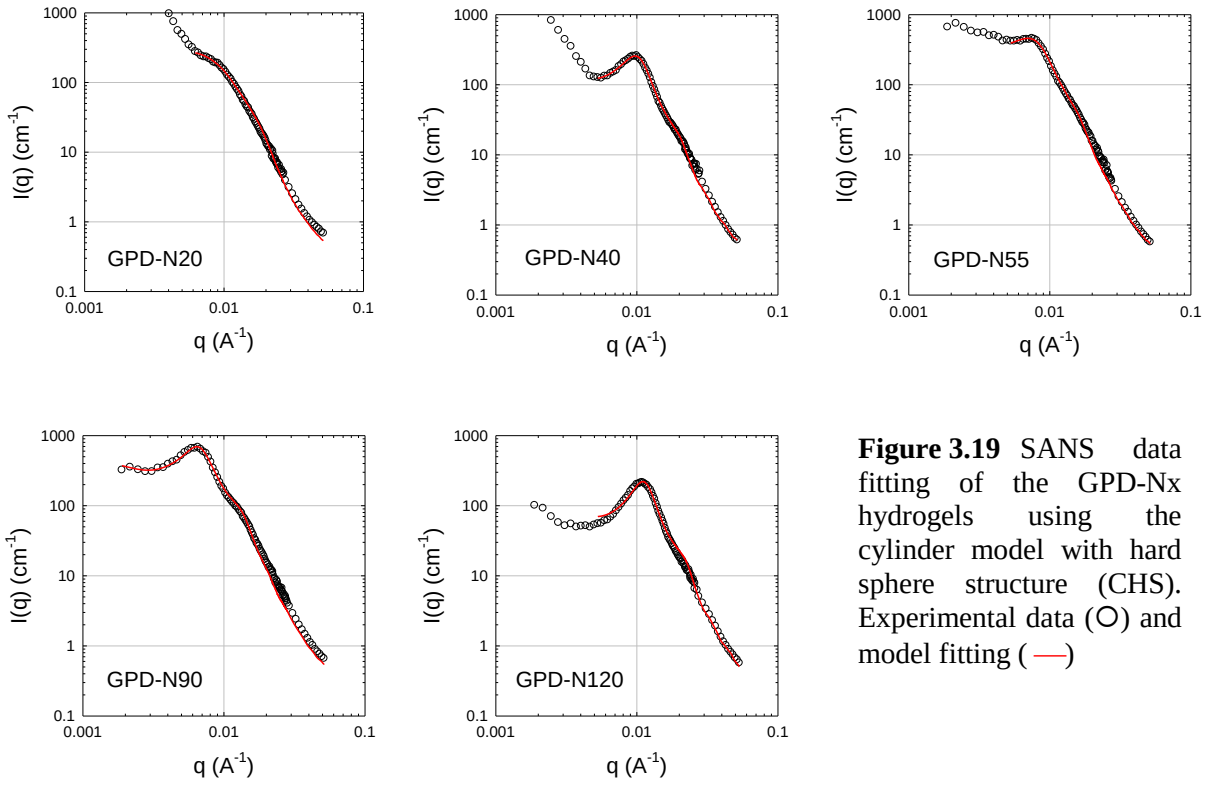

Figure 3.19 SANS data fitting of the GPD-Nx hydrogels using the cylinder model with hard sphere structure (CHS). Experimental data (○) and model fitting (—)

Table 3.6. Cylindrical parameters obtained from
1) the specific surface ($S_2/V_2=2/R_{cyl}$) assuming $\phi_1=0.8$ and
2) data fitting using the cylinder model with hard sphere structure (CHS)

Sample	Two phase system		Cylinder Model with Hard Sphere Structure			
	S_2/V_2 ($Å^{-1}$)	R_{cyl} (Å)	R_{cyl} (Å)	L_{cyl} (Å)	$\phi_{cyl}=\phi_2$	N_{ag}[a]
GPD-N20	0.016	125	100	1662	0.1	524
GPD-N40	0.021	95	97	1458	0.28	216
GPD-N55	0.018	111	115	1856	0.21	281
GPD-N90	0.017	118	116	2611	0.26	246
GPD-N120	0.022	90	93	1307	0.32	60

[a] Aggregation number, i.e., the average number of PNIPAm chains per scattering domain

In the literature, relative to the micelle formation of diblock, triblock and graft copolymers in selective solvents, the morphology of micellar aggregates is the result of the inherent molecular curvature arising from the relative sizes of the soluble and insoluble domains. The packing parameter (*p*), originally defined by J. N. Israelachvili et al.[43] for surfactant micelles, has then been extended to copolymers by S. Jain and F. S. Bates[44] and used to define the relative size of the insoluble region of a copolymer. As shown in **Figure 3.20**, the packing parameter takes into account the volume *v* of the insoluble block, its length (l_c) and the equilibrium area per molecule at the aggregate interface (a_0) as follows:

$$p = v/a_0 l_c \quad \textbf{Eq. 3.30}$$

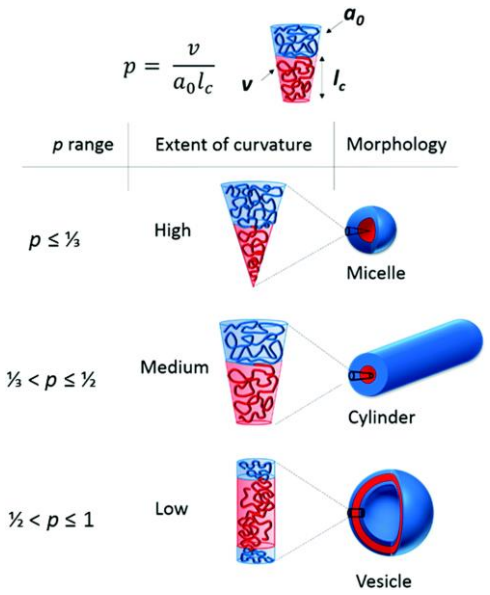

Figure 3.20 The different morphologies obtained as a function of the packing parameter, *p* (from E. B. K. Doncom et al.)[45]

[43] J. N. Israelachvili, D. J. Mitchell and B. W. Ninham, **Biochim. Biophys. Acta**, *1977*, 470, 185-201
[44] S. Jain and F. S. Bates, **Science**, *2003*, 300, 460–464
[45] E. B. K. Doncom, L. D. Blackman, D. B. Wright, M. I. Gibson and R. K. O'Reilly, **Chem.Soc.Rev.**, *2017*, 46, 4119-4134

As a general rule, spherical micelles are formed when $p \leq 1/3$, cylindrical micelles are formed when $1/3 < p \leq 1/2$, and enclosed membrane structures (vesicles or polymersomes) arise when $1/2 \leq p \leq 1$ (see **Figure 3.20**).

As the cylindrical morphology corresponds to the smallest range of packing parameter values ($1/3 < p \leq 1/2$), these worm-like aggregates are less frequently observed, compared to spherical micelles or polymersomes.[46]

In the case of diblock copolymers of symmetric composition, like PEP-PEO (poly(ethylene-*alt*-propylene)-*b*-poly(ethylene oxide)),[47] a transition from cylinder to sphere is expected in water when increasing the size of both blocks (see **Figure 3.21**).

By comparison, our system which is symmetrical, in the sense that the average molar mass of PDMA between two consecutive side-chains is similar to the molar mass of the side chains, does not follow this behaviour and no transition of morphology has been observed by increasing the molar mass of both components. Contrary to dilute or semi dilute solutions of isolated micelles, GPD-Nx hydrogels undergo strong additional constraints during the phase transition due to the presence of chemical cross-links and trapped entanglements which are not taken into account in classical theories of micellization based on mean-field or scaling approaches. In the case of the homologous series of GPD-Nx prepared with 0.1 mol % of cross-linker, the average distance between cross-links in the preparation state is theoretically d=100 Å, assuming a simple cubic distribution. We can notice that this distance is a little bit larger, d=150 Å, if we take into account the number of effective cross-links calculated from the elastic modulus characterized in the next chapter. If we assume schematically a squared network defined by the position of the cross-links every 100-150 Å, the phase transition can be understood through a cooperative self-assembling along one direction with a segregation between PNIPAm-rich and PDMA swollen domains.

[46] M. Karayianni and S. Pispas, **Springer International Publishing Switzerland, K. Prochazka (ed.), Fluorescence Studies of Polymer Containing Systems, Springer Series on Fluorescence 16**, *2016*

[47] H. Kaya, L. Willner, J. Allgaier, J. Stellbrink and D. Richter, **Appl Phys A Mater Sci Process**, *2002*, 74, s499-501

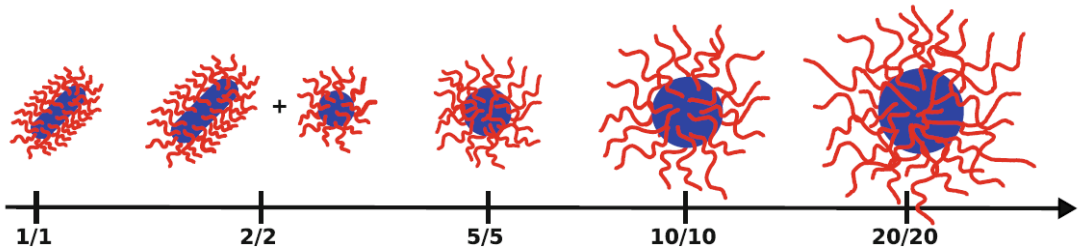

Figure 3.21 Illustration of the morphological behaviour of PEP-PEO micelles in aqueous solution: Transition from cylindrical to compact spherical micelles with increasing overall molar mass at equal composition: the numbers denote the approximate molar mass in kg/mol (from R. Lund et al.)[48]

The main conclusion that arises from this SANS study is that the aggregation process of grafted hydrogels with symmetrical composition is mainly controlled by the density of cross-linking rather than by the size of the side chains and inter-graft spacing. Due to the strong steric constraints introduced by the covalent cross-links, the thermo-responsive side chains self-assemble into cylindrical aggregates whose radius and composition are independent of the molar mass of the grafts. Since the phase separation occurs through a nucleation and growth mechanism, it can be assumed that the number of microdomains formed during the transition will depend on the nucleation process itself and so will the length of the cylinders. This hypothesis could explain the variability of the cylinder length which has been observed with the gel composition. Finally, a schematic representation of GPD-Nx hydrogels, below and above the transition temperature, is illustrated in **Figure 3.22**.

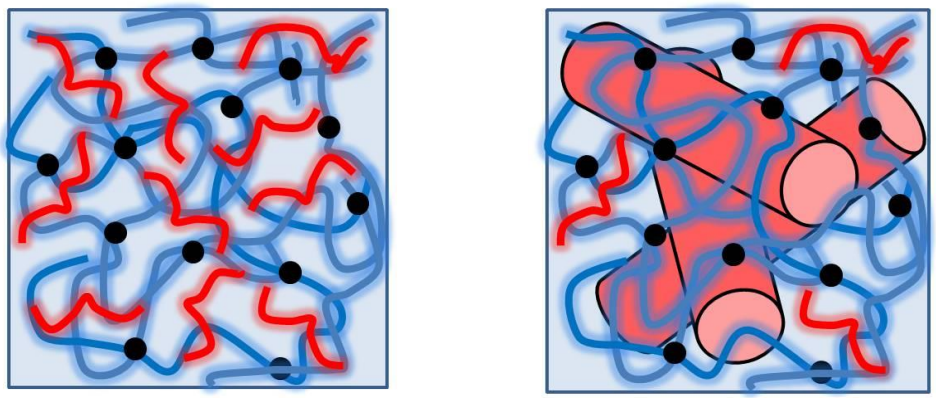

Figure 3.22 Schematic representation of the morphology of the GPD-Nx hydrogels at room temperature (**left**) and above the transition temperature (**right**). The colour code is blue for PDMA, red for PNIPAm, and black for the MBA cross-linker

[48] R. Lund, L. Willner and D. Richter, **Adv. Polym. Sci.**, *2013*, 259, 51-158

V.3. Structure of GPD-N hydrogels at high temperature under deformation

In order to get additional information of the microphase-separated structure that could be correlated with macroscopic mechanical tests, GPD-N40 and GPD-N120 were studied under deformation at 55 °C (**Figure 3.23**). First of all, the unstrained samples ($\lambda = 1$ with λ being the elongation) display an isotropic pattern with a circular diffraction ring corresponding to the correlation peak of the structure factor discussed previously. When the sample is stretched, the ring pattern is compressed in the parallel direction and elongated in the perpendicular one. Qualitatively, this highlights that phase-separated PNIPAm microdomains, which behave as neutron scatterers, move apart in the stretching direction (x or //) while they get closer perpendicularly (y or ⊥) due to the transverse compression. Similarly, the outer elliptic pattern underlines that cylindrical PNIPAm domains orient preferentially in the parallel direction. Moreover, at high level of stretching ($\lambda > 2$), the GPD-N40 hydrogel displays a spotted-like pattern with regular azimuthal angles that highlight an increase of the spatial order of the rod like domains under deformation. In order to obtain additional information in the low intensity region, and more especially in the high *q*-range, the SANS data obtained with the two neutron configurations were radially averaged along a given direction within a rectangular sector of axis parallel (//) or perpendicular (⊥), respectively, to the deformation axis. The corresponding intensities $I_{//}(q)$ and $I_{\perp}(q)$ are plotted in **Figure 3.24**. The anisotropic displacement of scatterers is especially emphasized with the sample GPD-N40 which can be stretched up to $\lambda=3$, contrary to GPD-N120 which breaks in the vicinity of $\lambda=2$.

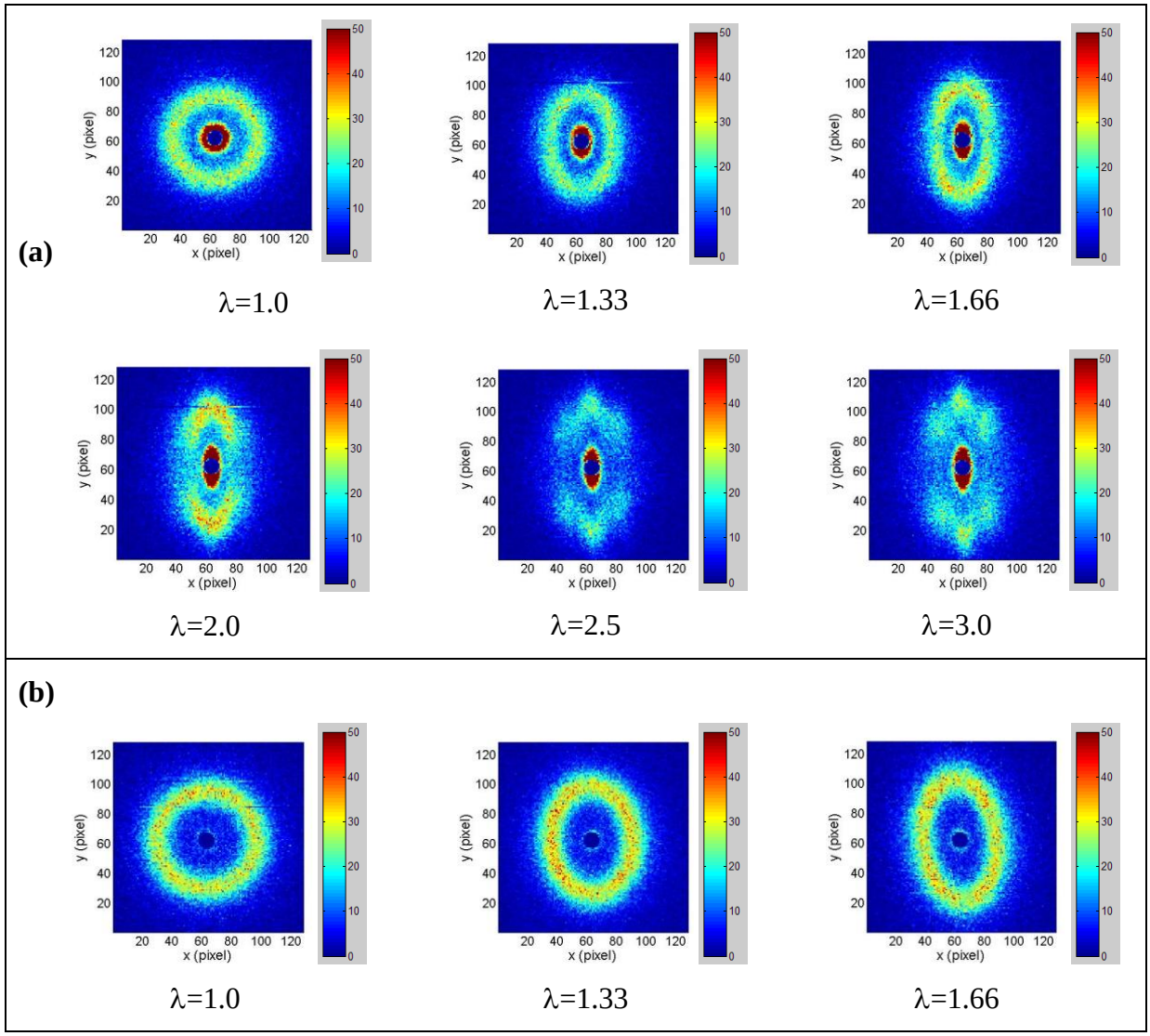

Figure 3.23 Variation of the SANS patterns with the deformation induced by a step-by-step loading at 55 °C. The direction of the uni-axial deformation is along the horizontal axis x. **(a)** GPD-N40 and **(b)** GPD-N120

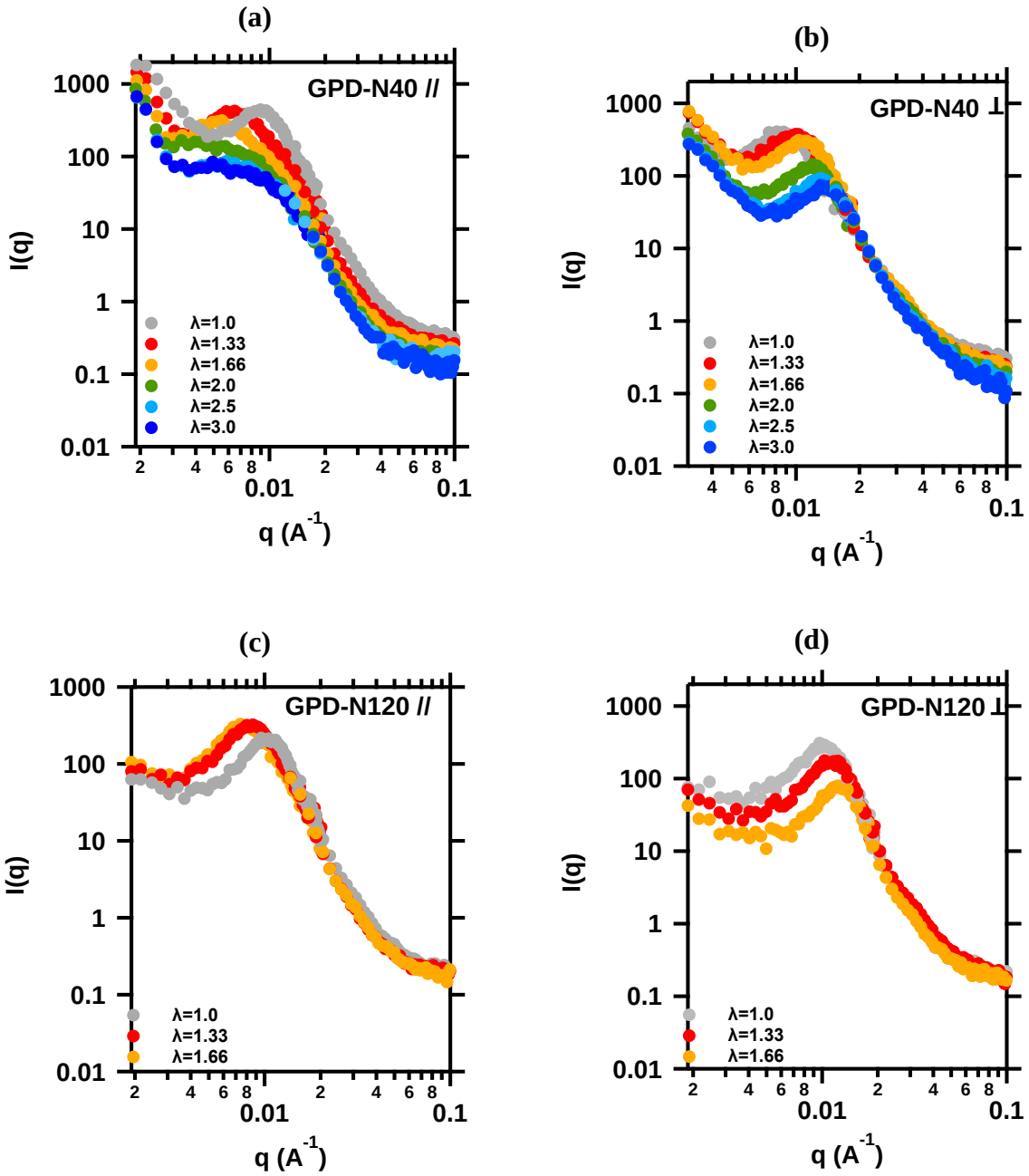

Figure 3.24 Scattering intensity profiles of GPD-N40 (respectively GPD-N120) under uni-axial deformation after sector averaging in the parallel, **(a)** (respectively **(c)**), and perpendicular direction of the deformation axis, **(b)** (respectively **(d)**): ○ λ=1.0; ○ λ=1.33; ○ λ=1.66; ○ λ=2.0; ○ λ=2.5; ○ λ=3.0

Moreover, as q_{peak} is inversely proportional to the average distance between PNIPAm domains (d_c), the ratios $R=q_{peak(\lambda=1)}/\ q_{peak(\lambda)}$ (proportional to $d_{c(\lambda)}/d_{c(\lambda=1)}$), determined in both parallel and perpendicular directions, provide useful information on the local deformation within the hydrogel. Indeed, as shown in **Figure 3.25**, it seems that the "local deformation", reported by the ratio R, is affine with the macroscopic deformation ($\lambda=L/L_0$) which is in agreement with previous work.[33] This is finally an additional proof that PNIPAm side-chains

self-aggregate into microdomains of reduced mobility and dynamics, which can keep their integrity under extension, at least up to some critical deformation.

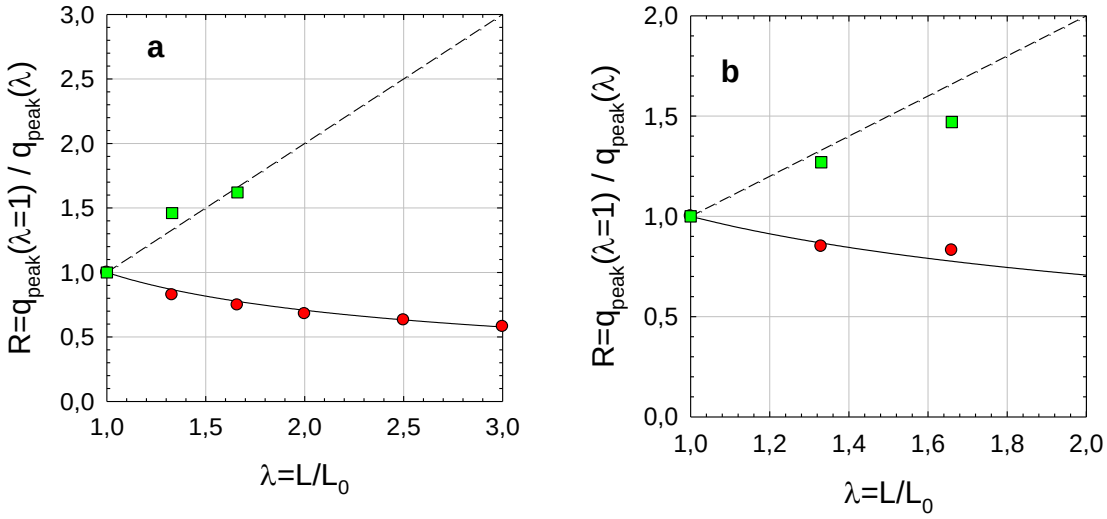

Figure 3.25 Comparison between the macroscopic affine deformation of hydrogel samples **(a)** GPD-N40 and **(b)** GPD-N120, along the parallel (dotted line) and the perpendicular-axes (solid line) with respect to the stretching direction, and the local deformation (symbols) probed through the scattering peak ratio: $R = q_{peak}(\lambda=1) / q_{peak}(\lambda)$

VI. Conclusion

By coupling different techniques we have investigated in this chapter the thermodynamic properties, as well as the self-assembling process of PNIPAm above its transition temperature. Based on calorimetric experiments, it was shown that the design parameters of the gels, either the DMA/NIPAm ratio or the PNIPAm average molar mass, have a very weak impact over the phase transition process as similar transition enthalpies and transition temperatures were obtained for both series of grafted hydrogels, GPD-Nx and GPD-N(y-z).

Complementary studies of the swelling behaviour have highlighted that the elasticity of hydrogels mainly originates from trapped entanglements rather than from chemical cross-links given the low level of MBA used in their synthesis. Although there is a strong impact of the monomer concentration over the swelling at equilibrium, there is no clear conclusion about the size of the pendant chains over the swelling ability as all the GPD-Nx networks swell and deswell in a very similar manner. Interestingly, above the transition temperature, all the gels deswell, as expected, but keep a high level of swelling which allows us to study them under isochoric conditions as soon as they are isolated in the preparation state.

Complementary studies by SANS allowed us to investigate in more detail the network structure of GPD-Nx hydrogels and their self-organization above the critical temperature. At

room temperature, we have shown the existence of large static heterogeneities that were introduced during the cross-linking copolymerisation. Upon heating, the PNIPAm side-chains self-associate into concentrated rod-like domains ($0.3<\phi_{PNIPAM}<0.4$). The very similar radii, obtained independently of the average molar mass of the PNIPAm side chains, suggest that the morphology of these phase segregated domains is controlled by the mesh size of the PDMA network. Under stretching, these domains follow the macroscopic affine deformation while retaining their integrity, at least up to a certain limit where they can undergo a disruption process.

Chapter 4

Mechanical reinforcement of PDMA hydrogels grafted with PNIPAm side-chains

Chapter 4: Mechanical reinforcement of PDMA hydrogels grafted with PNIPAm side-chains

Chapter 4: Mechanical reinforcement of PDMA hydrogels grafted with PNIPAm side-chains

I. Introduction

The volume-phase transition in swollen polymer networks has been extensively studied both theoretically and experimentally.[1,2,3,4,5,6,7] The low affinity of the polymer network for a poor solvent is responsible for a phase transition marked by a sudden change in the degree of swelling at macroscopic scale. The cooperative feature of the polymer network itself, combined with the possible control of polymer/water interactions via environmental *stimuli* such as ionic strength, pH, light, etc., allows for triggering extremely large volume changes in a relatively narrow range of environmental variables.

The gel volume-phase transition has opened a world of possible functionalities as a new route to design smart materials. The thermo-responsiveness of poly(*N*-isopropylacrylamide) (PNIPAm) in water has been extensively studied to design not only soft actuators[8] for fluidics[9] or optics[10] but also biomedical applications for drug delivery[11] or tissue engineering.[12,13] The thermal responsiveness of PNIPAm is related to a sharp miscibility gap observed in aqueous solutions above the lower critical solution temperature (LCST), i.e., above the transition temperature ($T>T_c$) where PNIPAm chains become hydrophobic and demix.[2,7,14] The intense interest in PNIPAm/water system arises also because its LCST occurs near physiological conditions, with T_c being close to 31-32 °C,[2,15] which is particularly suitable for biotechnological applications.

Recently, phase-separation has been explored as a new route for hydrogel toughening by investigating the mechanical response in the large strain regime[16,17,18,19,20,21,22] handling

[1] K. Dušek and D. Patterson, **J. Polym. Sci. Polym. Chem.**, *1968*, 6, 1209-1216.
[2] M. Heskins and J. E. Guillet, **J Macromol Sci A**, *1968*, 2, 1441-1455
[3] T. Tanaka, **Phys. Rev. Lett.**, *1978*, 40, 820-823
[4] P.-G. De Gennes, **Scaling Concepts in Polymer Physics**, **Cornell University Press**, *1979*, Ithaca
[5] A. Onuki, **Adv. Polym. Sci.**, *1993*, 109, 63-121
[6] M. Shibayama and T. Tanaka, **Adv. Polym. Sci.**, *1993*, 109, 1-62
[7] A. Halperin, M. Kroger and F. M. Winnik, **Angew. Chem. Int. Ed.**, *2015*, 54, 15342-15367
[8] P. Calvert, **Adv. Mater.**, *2009*, 21, 743-756
[9] D. J. Beebe, J. S. Moore, J. M. Bauer, Q. Yu, R. H. Liu, C. Devadoss and B. H. Jo, **Nature**, *2000*, 404, 588-590
[10] L. Dong, A.K. Agarwal, D.J. Beebe and H. Jiang, **Nature**, *2006*, 442, 551-554
[11] D. C. Coughlan, F. P. Quilty and O. I. Corrigan, **J. Controlled Release**, *2004*, 98, 97-114
[12] L. Klouda and A.G. Mikos, **Eur J Pharm Biopharm.**, *2008*, 68, 34-45
[13] T. Dvir, B. P. Timko, D. S. Kohane and R. Langer, **Nat. Nanotech.**, *2011*, 6, 13-22
[14] X. H. Wang, X. P. Qiu and C. Wu, **Macromolecules**, *1998*, 31, 2972-2976
[15] M. P. Algi and O. Okay, **Eur. Polym. J**, *2014, 59*, 113-121
[16] L.-W. Xia, R. Xie, X.-J. Ju, W. Wang, Q. Chen and L.-Y. Chu, **Nat. Commun**, *2013*, 4, 2226-2236

with the inherent practical difficulty to separate the intricate contributions of the microphase-separation by itself, as a reinforcing mechanism, and the change of the polymer concentration induced by the volume transition. As already described in chapter 3, our group has developed network topologies that allow enhancing significantly on-demand and reversibly the mechanical response in covalently cross-linked gels using nano/micro phase-separation at fixed overall volume.[20] As illustrated in **Figure 4.1** and **Figure 4.2**, the gel design relies on a hydrophilic covalently cross-linked poly(*N*,*N*-dimethylacrylamide) (PDMA) network combined with responsive poly(*N*-isopropylacrylamide) (PNIPAm) grafted side-chains acting as the thermo-sensitive reinforcing agent, i.e., effective above T_c. As demonstrated in chapter 3, the fine adjustment of the grafting of PNIPAm side-chains to the PDMA network, i.e., the balance between hydrophobic/hydrophilic moieties, allows to maintain the overall level of hydration from the preparation state at room temperature and beyond the phase-transition temperature, i.e., $T>T_c$. As revealed by neutron scattering experiments, the biphasic morphology of the grafted gels that develops above T_c implies the coexistence of swollen and collapsed domains, each domain differing in the chain conformation, hydrophilicity/hydrophobicity and dynamics, but belonging to the same percolating network. We anticipate that the introduction of contrasting mechanical properties within the gel would produce mechanical reinforcement as in common nanocomposite (NC) materials. In this way, by embedding inorganic nanofillers as clay or silica in a hydrophilic network, NC gels have demonstrated dramatic improvements of fracture toughness.[23,24,25,26] The concept here consists in triggering reversibly organic fillers in the gel that could impart both for the mechanical stiffening and toughening, using PNIPAm/PNIPAm hydrophobic interactions as reversible sacrificial bonds.[27,28] In contrast to NC gels where dissipative processes take place at the NP/matrix interface, here dissipation is expected to originate from the disruption of the filler

[17] H. Kamata, Y. Akagi, Y. Kayasuga-Kariya, U.-i. Chung and T. Sakai, **Science**, *2014*, 343, 873-875
[18] S. Kondo, T. Hiroi, Y. Han, T.-H. Kim, M. Shibayama, U. Chung and T. Sakai, **Adv. Mater.**, 2015, 27, 7407-7411
[19] S. Koshiro, N. Tasuku, H. Toshiyuki, N. Takayuki, K. Takayuki and J. P. Gong, **Adv. Mater.**, *2015*, 27, 6990-6998
[20] H. Guo, N. Sanson, D. Hourdet and A. Marcellan, **Adv. Mater.**,*2016*, 28, 5857-5864
[21] S. Nakagawa, W. Li and M. Shibayama, **Macromolecules**, *2018*, 51, 6645-6652
[22] F. Wang and R. A. Weiss, **Macromolecules**, *2018*, **DOI: 10.1021/acs.macromol.8b00490 ASAP**
[23] K. Haraguchi, T. Takehisa and S. Fan, **Macromolecules**, *2002*, 35, 10162-10171
[24] S. Rose, A. Dizeux, T. Narita, D. Hourdet and A. Marcellan, **Macromolecules**, *2013*, 46, 4095-4104
[25] C. J. Wu, J. J. Wilker and G. Schmidt, **Macromol. Biosci.**, *2013*, 13, 59-66
[26] S. Rose, A. Prevoteau, P. Elziere, D. Hourdet, A. Marcellan and L. Leibler, **Nature**, *2014*, 505, 382-385
[27] J. P. Gong, Y. Katsuyama, T. Kurokawa and Y. Osada, **Adv. Mater.**, *2003*, 15, 1155-1158
[28] T. L. Sun, T. Kurokawa, S. Kuroda, A. Bin Ihsan, T. Akasaki, K. Sato, M. A. Haque, T. Nakajima and J. P. Gong, **Nat. Mater**, 2013, 12, 932-937

itself, i.e., the phase-separated PNIPAm domain, and its final unravelling. Such a purely organic NC gel should expect to feature also self-healing capabilities.

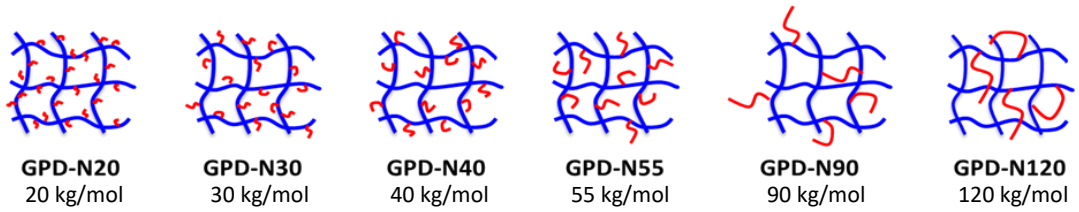

Figure 4.1 Schematic representation of **GPD-Nx** hydrogels prepared by varying the average molar mass (x) of PNIPAm side chains.

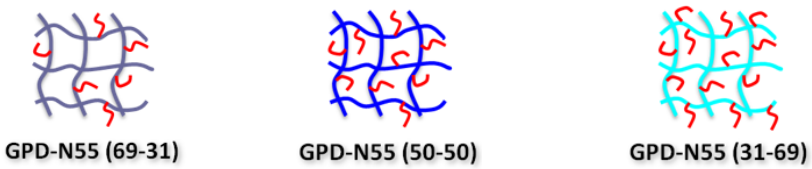

PDMA/PNIPAm w/w	69/31	50/50	31/69
PDMA in gel (wt %)	11.5	8.35	5.2
PNIPAm in gel (wt %)	5.2	8.35	11.5

Figure 4.2 Schematic representation of GPD-N55(y-z) networks prepared with various weight ratios between the PDMA network (y) and the PNIPAm grafts (z). The PNIPAm macromonomers are drawn in red, and the PDMA networks in dark blue, blue and light blue for 69, 50 and 31 wt % of the total polymer weight, respectively.

The purpose of this Chapter is to explore in a systematic way, and under isochoric conditions, the mechanical responses at small and large strains of polymer networks capable of developing a variety of heterogeneous structures at $T>T_c$ as a function of the density, the average molar mass or the content of the thermo-responsive PNIPAm side-chains (see **Figure 4.1** and **Figure 4.2**). In the model systems developed, the load-bearing phase consists of the non-responsive PDMA network carrying pendant chains of PNIPAm which are expected to contribute weakly to the network elasticity under the coil state but, above T_c, will act as reversible organic fillers (by analogy to composite fillers). As in classical composite engineering, still general and fundamental issues on the reinforcement mechanisms arise. Achieving stiffening together with fracture toughening is always challenging and it is well

known that the relative amount of filler/matrix unsatisfactorily models the stiffening by itself. Parameters as the filler size, its size distribution, its concentration into the network, the dispersion state of the filler, the control of the filler/matrix interfaces as the magnitude of the interactions and their dynamics also account for the optimization of the reinforcement.

This chapter seeks to identify the relevant parameters that allow an effective mechanical reinforcement, both in terms of stiffness and fracture resistance. We anticipate that both the length of the grafts, as the interval between successive grafts, together with the number of grafts should be key-parameters to better understand the mechanisms of reinforcement. This is invaluable in guiding the macromolecular design of gels with advanced mechanical responses.

II. Experimental part

II.1. Materials

The synthesis and characteristics of GPD-Nx(y-z) hydrogels have been previously described in chapters 2 and 3. All the experiments were performed with gels in the preparation state, either freshly prepared or stored in parafin oil in order to avoid their drying.

II.2. Characterization

II.2.1. Rheological measurements

The viscoelastic properties of hydrogel discs (20 mm diameter, 2 mm thickness) were studied at the preparation state using a stress-controlled rheometer (DHR3 from TA Instruments) equipped with roughened plate/plate geometry (diameter 20 mm). Particular care was taken to avoid the drying of the samples by immersing them into paraffin oil during the experiment. Both temperature and frequency sweep measurements were performed.

Temperature sweep. The temperature experiments were performed in the linear regime, which was established for each sample by a stress sweep at 1 Hz. The temperature was controlled by a high power Peltier system that provides fast and precise adjustment of the temperature during heating and cooling cycles. The experimental conditions were fixed at constant frequency of 1 Hz and 0.1% strain amplitude.

In these conditions, the dynamic moduli (*G'* and *G"*) and *tan δ* were recorded between 10 and 60 °C by applying heating and cooling scans at 0.1 °C/min as follows: (1) heating from 25 to 60 °C, (2) cooling until 10 °C, (3) heating up to 60 °C, (4) cooling back to 10 °C and (5) heating up to 25 °C. As the thickness of the sample is quite large (2 mm), a low temperature scanning rate allows a better control of the thermal homogeneity within the gel and, consequently, reduces the hysteresis associated with the heat transfer and the kinetics of PNIPAm phase-separation.

Frequency sweep. Frequency sweep tests were performed at 20 and 60 °C. Within these frequency tests, the angular frequency ω was varied from 1 to 100 rad/s (i.e., f_1 = 0.159 to 15.9 Hz), whereas the strain amplitude was held at 0.1%. The storage modulus $G'(\omega)$ and loss modulus $G"(\omega)$ were measured and drawn against angular frequency ω in a double logarithmic reference frame, as all these parameters varied over several orders of magnitude.

II.2.2. Mechanical tensile tests

Tensile tests were performed on a standard tensile Instron machine, model 5565, equipped with a 10 N load cell (with a relative uncertainty of 0.16 % in the range from 0 to 0.1 N). The gel samples used for tensile tests were cut with a punch and their final dimensions are: L_i = 25 mm (initial length), w = 5.0 mm (width) and h = 2.0 mm (thickness). The gauge length was kept constant at L_0 ~15 mm for all tests except for adhesion ones (see adhesion tests in the following experimental part). Moreover, all the tests were carried out at the same strain rate: 0.06 s^{-1}.

In order to prevent water evaporation from the gel samples, especially at high temperature, these ones were immersed in a specific chamber filled with paraffin oil.

For all the tensile tests, time (t), force (F) and displacement (ΔL) were recorded while the nominal stress (σ_{nom}) and strain (ε) were calculated as follows:

$$\sigma_{nom} = \frac{F}{w*h} \quad \textbf{Eq. 4.1}$$

$$\varepsilon = \frac{\Delta L}{L_0} \quad \textbf{Eq. 4.2}$$

Four different types of mechanical tests were carried out at both 20 and 60 °C in the previously described experimental conditions: monotonic uni-axial tensile tests, loading/unloading uni-axial cycles, fracture tests and adhesion tests. For the tests at 60 °C, the gels stayed immersed in paraffin oil for 10 min, before to launch the test, in order that the whole sample was well thermostated at 60 °C and that the PNIPAm phase-separation has reached equilibrium.

Uni-axial tensile tests. For all uni-axial tensile tests (see **Figure 4.3.a**), the work at break was calculated as the area under the σ vs ε curves and associated Mooney plots were drawn by plotting the reduced stress σ_R vs $1/\lambda$ with $\sigma_R = \frac{\sigma}{\lambda - \frac{1}{\lambda^2}}$ and $\lambda = \varepsilon + 1$ the elongation.

Loading/unloading uni-axial tensile tests. Loading-unloading experiments were performed at 50, 100 and 200 % of strain in the same conditions as the uni-axial tensile tests in order to characterize the dissipated strain energy (hysteresis) with recovery times of 3 and 5 min in between. Fatigue experiments were carried out between 0 and 300 % for one hundred cycles.

Fracture tests. Fracture tests (see **Figure 4.3.b**) were performed in the same conditions as tensile tests with the exception that the sample was notched in the middle. The notch was around 2 mm length for a sample total width of 4.9 mm. Fracture energy data were obtained using the single edge notch geometry and the fracture energy (G_C) has been calculated using the following expression:[29]

$$G_C = \frac{6Wc}{\sqrt{\lambda_c}} \qquad \textbf{Eq. 4.3}$$

with c the length of the notch, λ_c the strain at break in single edge notch experiment, and W the strain energy density calculated by the integration of the nominal stress versus strain until ε_c, ($\varepsilon_c = \lambda_c - 1$) the strain at break.

Adhesion tests. We used single lap-shear geometry (**Figure 4.3.c**). The total length of assembled ribbons was 40 mm. The contact pressure was made at room temperature at 1 kPa and during 1 min. The assembled ribbons were then immersed in oil during 10 min either at 20 or 60 °C before to launch the test. The overlap length and width were l_{over} = 5 mm and w =

[29] H. Greensmith, **J. Appl. Polym. Sci.**, *1963*, 7, 993−1002

5 mm, respectively, and the ribbon thickness is h = 2 mm. For the lap-shear test, when failure occurred by interfacial peeling, we evaluated the adhesion energy from the measured adhesive failure force F_{max} using the expression for short lap-joints:[30]

$$G_{adh} = 3\frac{F_{max}^2}{2w^2Eh} \qquad \textbf{Eq. 4.4}$$

where w and h denote, respectively, the width and thickness of the ribbon, and E is the tensile modulus.

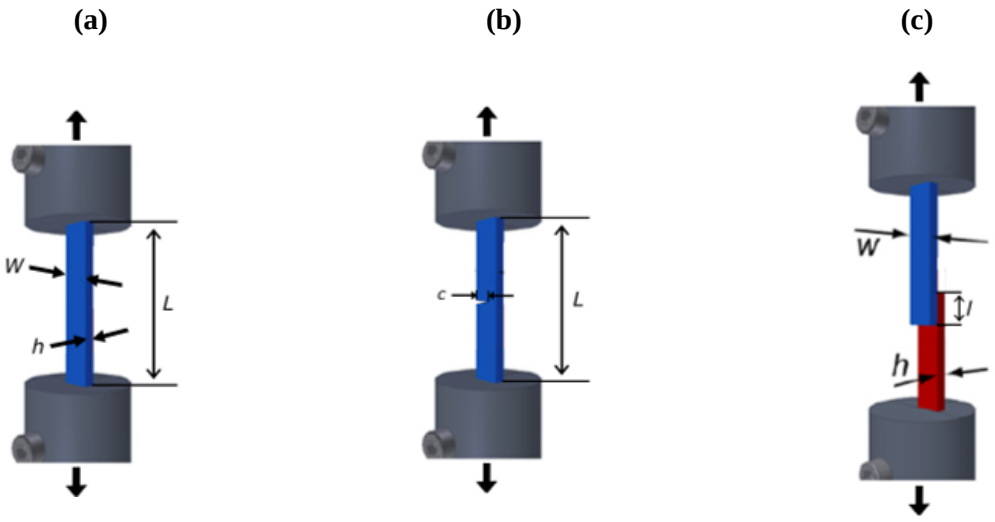

Figure 4.3 **(a)** Uni-axial tensile test geometry **(b)** Fracture test geometry **(c)** Lap-joint geometry

II.2.3. Shape memory

The shape-memory properties were investigated by first stretching the gel to a certain nominal stretch ratio at 20 °C, and then immersing it at 60 °C during 3 min (**Figure 4.4.a**). The gel was then unloaded (i.e., at zero external force) by removing one clamp (**Figure 4.4.b**). The gels were kept unloaded at 60 °C for 2 min, 48 h or 72 h respectively. Strain recovery was followed by cooling down the gel at 20 °C for another 2 min. The gel length was measured over time.

[30] A. Johner and J-F. Joanny, **J. Chem. Phys.**, *1992*, 96, 6257-6273

(a) **(b)**

Figure 4.4 Photos of hydrogels **(a)** maintained under specified deformation at 60 °C **(b)** unloaded (i.e., at zero external force) at 60°C

III. Results and discussion

III.1. Study of the thermo-responsiveness of GPD-Nx networks by Linear Rheology

The mechanical properties of the thermo-responsive grafted networks were first studied at small deformations, within the viscoelastic linear regime, in order to specifically investigate the consequence of the self-assembly on the dynamic moduli, probing the mechanical response of the microstructure without strong perturbations from its conformation at rest.

As already pointed out in Chapter 3, from the point of view of the structure, the phase-separation process also triggers dramatic changes of viscoelastic properties near T_c. Such temperature dependence is illustrated in **Figure 4.5** with the GPD-N55 gel studied at constant frequency (1 Hz). By heating the sample from its preparation state above T_c, the emergence of collapsed domains within the gel gives rise to an increase of the elastic modulus, *G',* by one order of magnitude. This reflects the composite structure of the gel which can be pictured as stiff collapsed PNIPAm domains embedded within a soft and highly hydrated PDMA matrix.

As expected, both elastic and loss moduli, *G'* and *G"* demonstrate steep upturns beginning around the phase separation temperature.[20,31,32] The enhancemement of moduli originates from the collapse of the PNIPAm side-chains into concentrated domains exhibiting reduced dynamics.[33] Note that, for the GPD-N55 gel, the contribution of dissipative losses

[31] M. Shibayama, M. Morimoto and S. Nomura, **Macromolecules**, *1994*, 27, 5060-5066
[32] T. Takigawa, T. Ikeda, Y. Takakura and T. Masuda, **J. Chem. Phys.**, *2002*, 117, 7306-7312
[33] H. Guo, A. Brulet, P. R. Rajamohanan, A. Marcellan, N. Sanson and D. Hourdet, **Polymer**, *2015*, 60, 164-175

remains quite low, since *G''/G'* is around 0.1, and almost the same at 25 and 60 °C, respectively for the gel in the coil and phase-separated state.

As observed in **Figure 4.5**, the pristine properties are fully recovered when the temperature is lowered below T_c, with almost no hysteresis when the heating/cooling rate is low enough, typically 0.1 °C/min. Different cycles of heating/cooling showed perfectly superimposable behaviours, demonstrating the stability of the hydrogel heterogeneous nanostructure. Water is not irreversibly expelled from the sample upon heating and during the timescale of the experiment, i.e., about tens of hours.

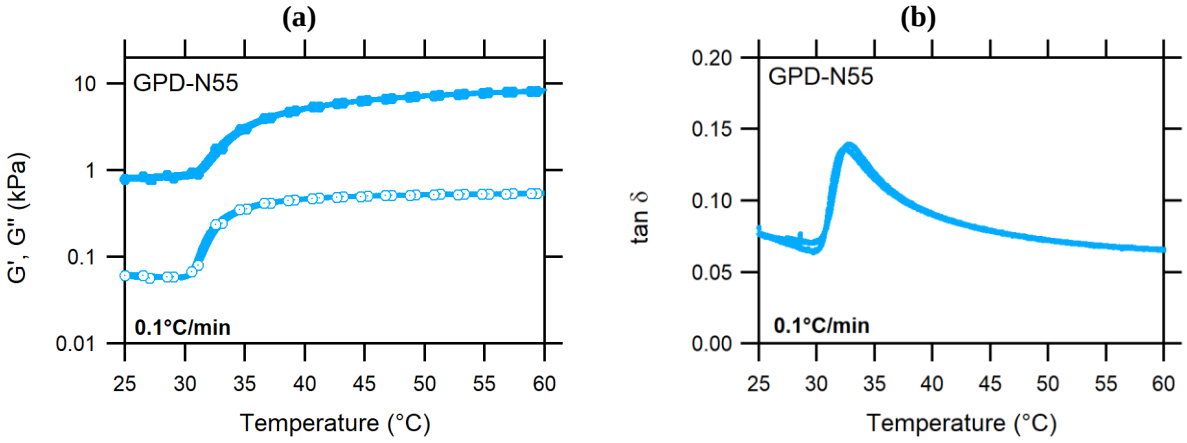

Figure 4.5 Temperature dependencies of **(a)** the dynamic shear storage modulus, *G'* (filled symbols) and loss modulus, *G''* (open symbols), and **(b)** the loss tangent, *tan δ*, as a function of temperature for GPD-N55. (Cooling and heating rates = 0.1 °C/min, f_1 = 1 Hz, strain amplitude = 0.1%)

The viscoelastic properties, i.e., the elastic and loss shear moduli as well as *tan δ*, for the GPD-Nx hydrogel series, where the average molar mass of the NIPAm side-grafts is varied, are reported in **Figure 4.6**. A similar trend is observed for the different lengths and densities of grafted side-chains as for GPD-N55 described above. As shown in **Figure 4.6.a-b**, a rather sharp increase of both *G'* and *G''* around the temperature of phase-separation is noticed. This general feature, already reported in literature for homo-PNIPAm networks[31,34,35,36] is assigned to the formation of strong interactions between the NIPAm units in the aggregated domains. This implies the rise of the elastic modulus due to the formation of physical fillers together with higher dissipative properties induced by the emergence of heterogeneities in gel dynamics. We can also point out that the temperature dependence of the

[34] S. Hirotsu, **Macromolecules**, *1990*, 23, 903-905
[35] A. Y. Grosberg and S. K. Nechaev, **Macromolecules**, *1991*, 24, 2789-2793
[36] S. Hirotsu, **Macromolecules**, *2004*, 37, 3415-3424

dynamic moduli is in very good agreement with the variation of the SANS spectra presented in chapter 3. Indeed, we observed that the structure of hydrogels changed dramatically between 27 and 34 °C and evolved very little beyond 40 °C. This behaviour can indeed be easily compared to the drastic increase of the elastic modulus between 30 and 35 °C followed by a very small variation beyond 40 °C. Similarly, the shift of about 5 °C towards higher temperatures observed for the GPD-N20 sample is also in adequacy with the structural and calorimetric observations observed in chapter 3. Moreover, *tan δ* depicted in **Figure 4.6.c** exhibits a maximum at a temperature around T_c which is well correlated with the transition temperature obtained by thermal analysis and turbidimetry (see **Figure 4.6.d**).

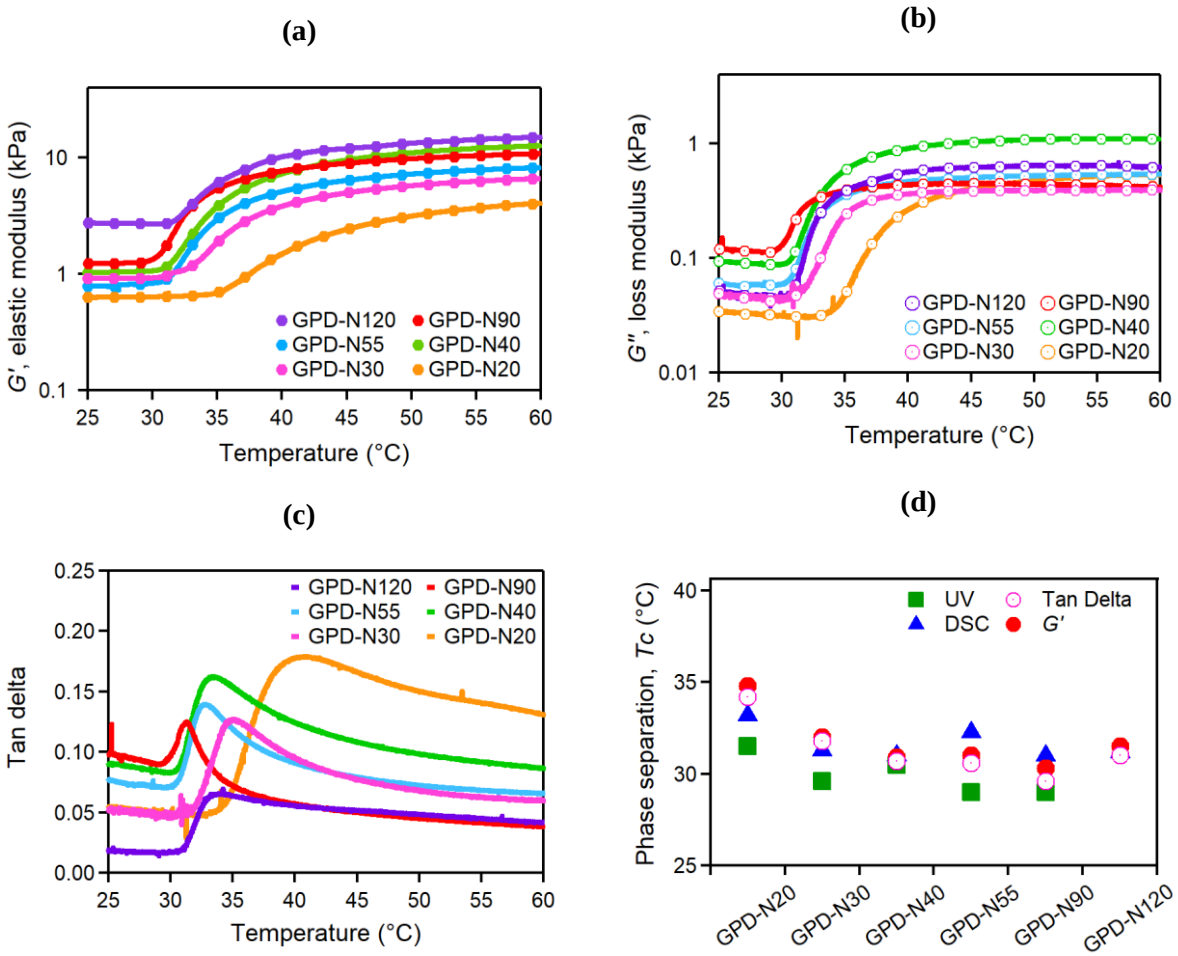

Figure 4.6 Viscoelastic properties versus Temperature and transition temperatures of GPD-Nx series. **(a)** Dynamic shear elastic (or storage) modulus *G'*, **(b)** loss modulus *G''* and **(c)** *tan δ*. (Heating rate = 0.1 °C/min, f_1 = 1 Hz, strain amplitude = 0.1%). **(d)** Comparison between the phase-separation transitions, T_c, as determined by turbidimetry (UV-vis), Differential Scanning Calorimetry (DSC) and linear rheology (*G'* and *tan δ*)

As summarized in **Figure 4.7.a**, all the gels exhibit a significant enhancement of their stiffness in the micro-phase separation regime, i.e., largely above the phase transition at 60 °C, with respect to the coil state. Nevertheless, while the overall polymer concentration and composition of the gels are fixed, i.e., same PNIPAm/PDMA ratio, the efficiency of the mechanical reinforcement varies significantly with the graft layout. At 20 °C, at the coil state, the elastic shear modulus reflects the topology of the grafted PDMA networks. In fact, as shown in **Figure 4.7.a**, except for GPD-N120, *G'* values measured at 20 °C are rather similar for the GPD-Nx series, around 0.9 ± 0.3 kPa. Such a value is in line with the response of homo-PDMA gel at 8.3 wt % (*G'* ≅ 1.0 kPa), designed as control experiment to address the non-thermo-responsiveness of the network backbone (see **Figure 4.7b**). This suggests that all GPD-Nx hydrogels (except GPD-N120) have an equivalent PDMA cross-linked network. On the basis of the entropy-driven elasticity theory in phantom network,[37,38] each elastically active chain of the network is supposed to contribute equally for *kT* to the modulus. The mean molar mass between effective cross-links can be calculated for the GPD-Nx series and gives an average value of about 120 kg/mol. Taking into account measurement uncertainties, the elastic modulus *G'* of the GPD-N120 gel appears slightly higher than that of the others. This increase in the effective density of elastic chains can be attributed to the contribution of the high length PNIPAm side chains to entanglements and/or to side reactions such as transfer reactions that could occur during the polymerization.[39]

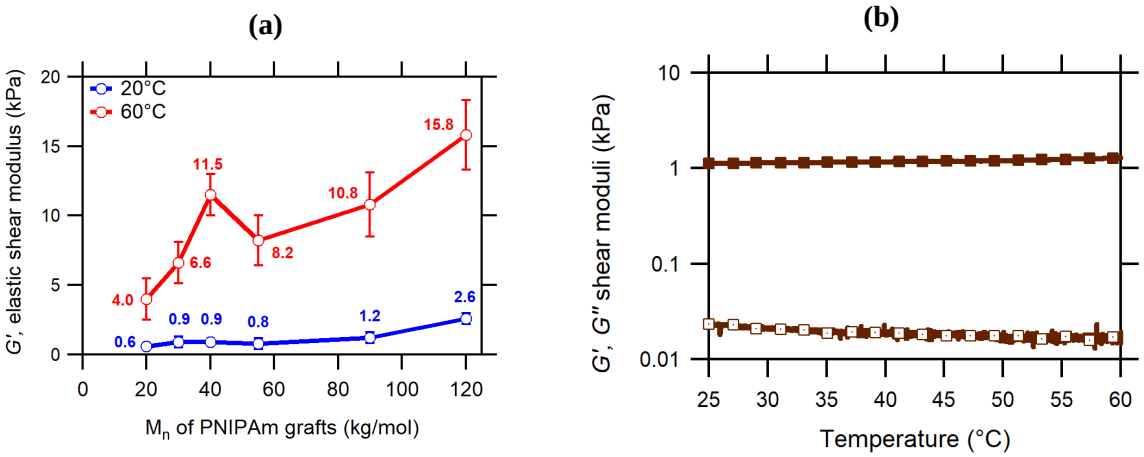

Figure 4.7 **(a)** Variation of the elastic (or storage) shear modulus *G'* of GPD-Nx hydrogels at 20 (blue) and 60 °C (red) of with the average molar mass of PNIPAm grafts at 1 Hz and 0.1 % oscillation strain. **(b)** Dynamic shear elastic (or storage) modulus *G'* (filled symbols) and loss modulus *G''* (open symbols) for a homo-PDMA gel. (Heating rate = 0.1°C/min, f_1 = 1 Hz, strain amplitude = 0.1%)

[37] L. R. G Treloar, **Transactions of the Faraday Society**, *1942*, 38, 0293-0298
[38] P. J. Flory and J. Rehner, **J. Chem. Phys.**, *1943*, 11, 512-520
[39] H. L. Needles and R. E. Whitfield, **J. Org. Chem.**, *1964*, 29, 3632-3634

III.2. GPD-Nx gel dynamics by Linear Rheology

The signature of topological defects of the network, as dangling chains of the PDMA network or the contribution of PNIPAm grafted side chains, has been analyzed in light of the relaxation processes by scanning the shear frequency by two orders of magnitude, from 1 to 100 rad/s, as shown in **Figure 4.8**. The amplitude of the loss modulus, *G''* is directly related to the amount of dangling chains,[40] with one free end and the other one belonging to the network, and to their relative length with respect to the mesh size of the network. In the case of homo-PDMA gels at 20 °C, the frequency-dependence, $G'' \sim \omega^{\alpha}$ with $\alpha = 0.5$, highlights the presence of defects in the network that have been formed during the polymerization process. At a molecular level, the power-law relaxation process reveals the slow relaxation dynamics of dangling chains in the presence of topological constraints, i.e. entanglements within the network.[40,41] The value of the exponent α which varies with the rate of the relaxation process of the dangling ends, is expected to decrease with l_g, the average length of the grafts, with respect to ξ_n, the mesh size l_g/ξ_n, i.e., α scales with the reciprocal of the number of constraints per dangling chains. Here, no significant effect of chain length is observed for the GPD-N40 and GPD-N120, since α=0.4 in both cases which reflects the random feature of the polymerization (and cross-linking), involving a broad distribution of ξ.4,[42,43]

At 60 °C, in contrast to the results reported on homo-PNIPAm gels,[31] the relaxation processes of GPD-Nx gels seem to be suppressed in the frequency range investigated since *G'* and *G''* remain almost constant. This highlights the stability of PNIPAm aggregates and the fact that they dominate the viscoelastic behaviour of the gels, at least in the small range of strain perturbations investigated (ω = 1.0-100 rad/s).

[40] J. G. Curro and P. Pincus, **Macromolecules**, *1983*, 16, 559-562
[41] L. H. Cai, T. E. Kodger, R. E. Guerra, A. F. Pegoraro, M. Rubinstein and D. A. Weitz, **Adv. Mater.**, *2015*, 27, 5132-5140
[42] J. Bastide and L. Leibler, **Macromolecules**, *1988*, 21, 2647-2649
[43] M. Shibayama, **Polym. J**, *2011*, 43, 18-34

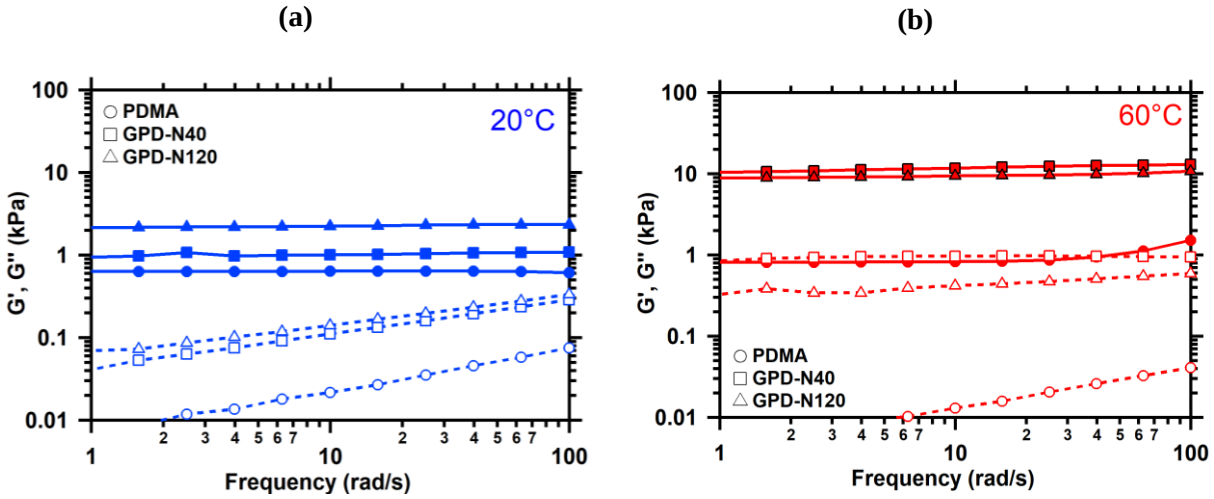

Figure 4.8 Frequency dependence of the storage (filled symbols, *G'*) and loss (open symbols, *G''*) moduli of representative GPD-Nx hydrogels (with x=0, 40 and 120) measured at **(a)** 20 and **(b)** 60 °C (oscillation strain = 0.1%)

III.3. Large strain behaviour and recovery

Figure 4.10 shows the large strain behaviour of the GPD-N55 sample in tensile mode that has been investigated at 20 and 60°C, sufficiently far from the critical temperature of the phase transition. While linear rheology does not involve large structural perturbations, large strain experiments allow exploring the capabilities of the organic NC gel to self-reorganize under stress. PDMA network is supposed to feature entropy-driven elasticity on either side of the phase-separation temperature and to transmit stresses to the phase-separated domains since the PDMA network is topologically defined as the load-bearing phase and is not thermo-responsive within the experimental range of temperature investigated.

In order to graphically enhance the deviation from entropy-driven elasticity, stress-strain behaviours have been plotted as reduced stress,[44] σ_R, versus reciprocal elongation, $1/\lambda$, to focus on the early stages of deformation as follows:

$$\sigma_R = \frac{\sigma}{(\lambda - \lambda^{-2})} = 2C_1 + \frac{2C_2}{\lambda} \qquad \textbf{Eq. 4.5}$$

with σ, the nominal stress (force divided by the initial section) and λ, the elongation defined as: $\lambda = 1 + \varepsilon$

[44] M. Mooney, **J. Appl. Phys.**, *1940*, 11, 582-592

The two semi-empirical constants, C_1 and C_2 are commonly used in rubbers for the early stages of deformation to separate the entropic signature of the cross-links from the one of the entanglements, respectively. The stretching of an ideal network, made of ideal Gaussian chains between cross-links should correspond to a horizontal line (C_2=0). As illustrated in **Figure 4.9**, C_2 refers to the deviation from the theoretical change of entropy of the ideal Gaussian chain, i.e., softening usually assigned to entanglements, while C_1, being extrapolated to large strains ($1/\lambda \rightarrow 0$), gives the density of covalently cross-linked chains.

In our case, C_2 could be hardening ascribed to conformational changes harder to proceed in phase-separated domains or softening due to the disruption of collapsed domains. Note that the reduced stress could also be plotted versus elongation.

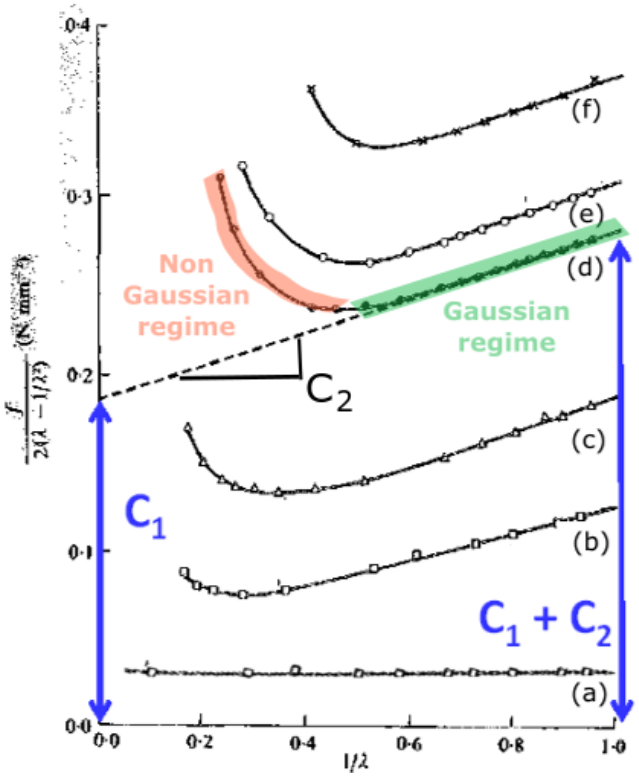

Figure 4.9 'Mooney' plot of experimental force-extension data for peroxide cross-linked rubbers containing respectively (b) 1, (c) 2, (d) 3, (e) 4 and (f) 5 mol % peroxide. Line (a) is representative of the purely entropic elasticity (C_2=0) i.e., for rubbers without entanglements.
Curve (c) denotes two regime under extension: the first one is a Gaussian regime taking place before strain-hardening (green) and the second one, revealing strain-hardening, is non Gaussian i.e., there is an energetic contribution coming from the finite extensibility of the network (adapted from L. Mullins)[45]

As shown in **Figure 4.10.a-b**, below *Tc*, gel demonstrates the classical response of a polymer network that is dominated by entropic elasticity, since the reduced stress vs. 1/λ gives almost flat variation upon stretching. $C_2 \rightarrow 0$ and the value of the reduced stress corresponds to the shear modulus, *G*. In other words, in contrast with what was observed in Chapter 3, there is no clear signature of entanglements in the tensile response (within the frequency investigated). The tensile modulus can be estimated from small strains and is quite

[45] L. Mullins, **J. Appl. Polym. Sci.**, *1959*, 2, 257-263

in line with the *G'* values obtained by linear rheology. Assuming that the volume change upon stretching is negligible, as expected from rubber elasticity, the relation between the tensile modulus, *E* and the shear modulus, *G* is given by:

$$E = 2(1 + \nu)G \cong 3G$$

with ν, the Poisson's ratio which tends to 0.5 for pure incompressible behaviour.

Conversely, at 60 °C, the general shape of the tensile curve shown in **Figure 4.10.a**, especially at the early stages of deformation, exhibits a linear stress-strain relation that significantly overestimates the purely entropic contribution of the network at 20 °C and underlines the additional energetic contribution that arises from the phase-separation into hydrophobic concentrated PNIPAm domains. This effect is clearly emphasized in **Figure 4.10.b**, by an initial hardening. The microphase-separated GPD-N55 gel at 60 °C demonstrates a remarkable combination of properties, as illustrated **Figure 4.10.c-d**. The formation of PNIPAm-rich domains not only increases the stiffness but also leads to an enhancement of the dissipative strain energy by the increase of the hysteresis of the cyclic mechanical response. The dissipative mechanisms are observed to be controlled by the stretching level and result in a residual strain just after unloading for applied strain levels beyond 50%. The strain energy dissipation originates from the local rearrangements at stake in the phase-separated micro-domains, involving intra-chain and inter-chain disruption of interacting NIPAm/NIPAm segments upon stretching. This mechanism enables the stress release[32] and the energy dissipation, as sacrificial bonds. In contrast to covalent bond breaking, which is permanent, the phase-separation process involves reversible interactions such as H-bonding and hydrophobic interactions that potentially may be reformed. Furthermore, the energetic component of the free energy will favor the bridging of PNIPAm segments above T_c and promote the replacement of the lost-links. Thus, as illustrated in **Figure 4.10.c**, perfect recovery of the strain and the mechanical behaviour were noticed after a few minutes of rest, suggesting that the dual-phase structure of the gel is perfectly reformed and the gel is capable of self-healing in bulk after a relatively short period of rest. As expected from previous results obtained by rheology, the dissipative processes in GPD-N55 gel are weakly time-dependent. This feature allows for GPD-N55 gels to exhibit remarkable fatigue resistance, as illustrated in **Figure 4.10.d**. Except for the first cycle demonstrating hysteresis, the following one hundred of consecutive cycles present almost closed-loops and a

mechanical response well-overlapped, including for relatively high strain amplitudes (here for 300 % of strain) with no lost in stiffness or creeping phenomena over time.

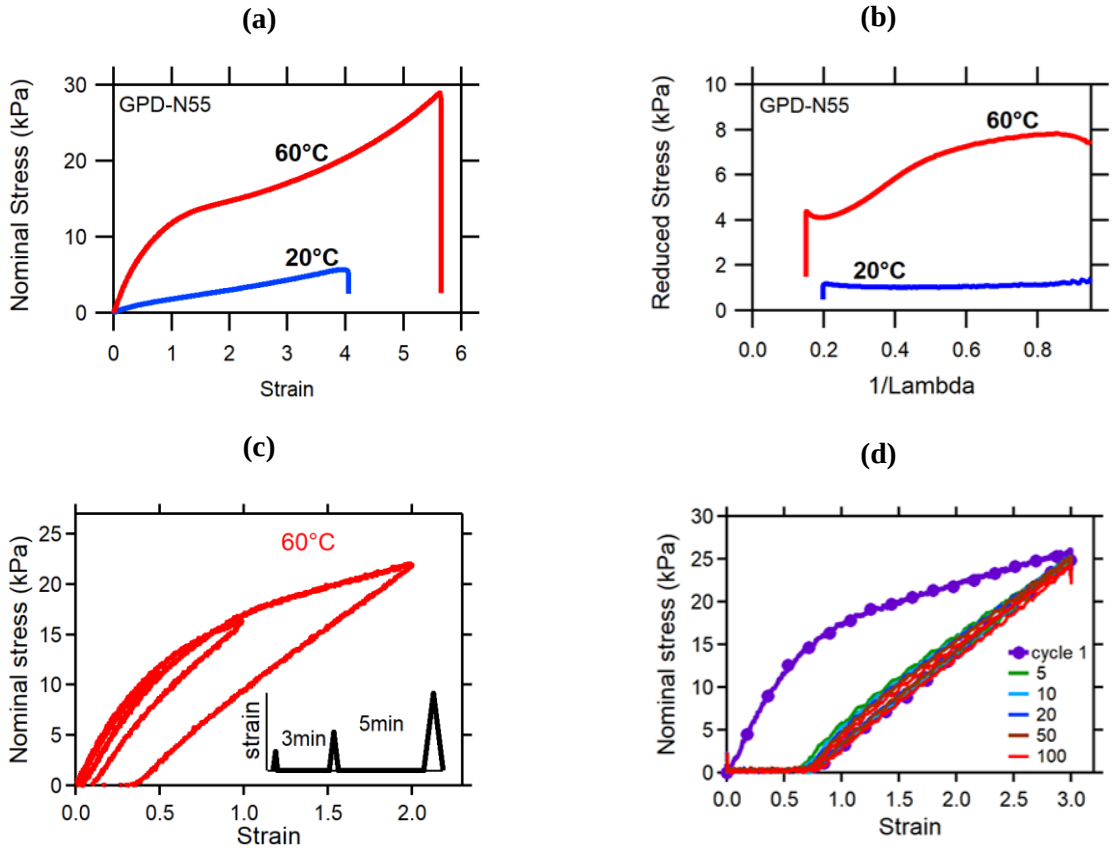

Figure 4.10 Large strain behaviour of GPD-N55 gels at a strain rate of 0.06 s^{-1}. (**a)** Tensile stress-strain curves of GPD-N55 at 20°C and 60°C and **(b)** Corresponding stress-strain curves plotted as the reduced stress versus 1/λ. λ is defined as the ratio of the deformed length divided by the initial length, and the reduced stress as the nominal stress divided by (λ-1/λ^2). This representation clarifies the deviations from classical rubber elasticity model displayed by the gel at 60 °C: softening is observed above 26% of strain. The GPD-N55 behaviour at 20 °C is given as a guideline and follows the theoretical rubberlike behaviour. **(c)** GPD-N55 strain and recoveries behaviour were investigated by performing a series of loading/unloading cycles under different tensile stretches (50%, 100% and 200% of strain) with resting periods in between 3 minutes and 5 minutes, see insert. **(d)** GPD-N55 fatigue test in tensile mode. 100 consecutive cycles were applied at 60 °C. All the tensile tests were performed at a 0.06 s^{-1} strain rate

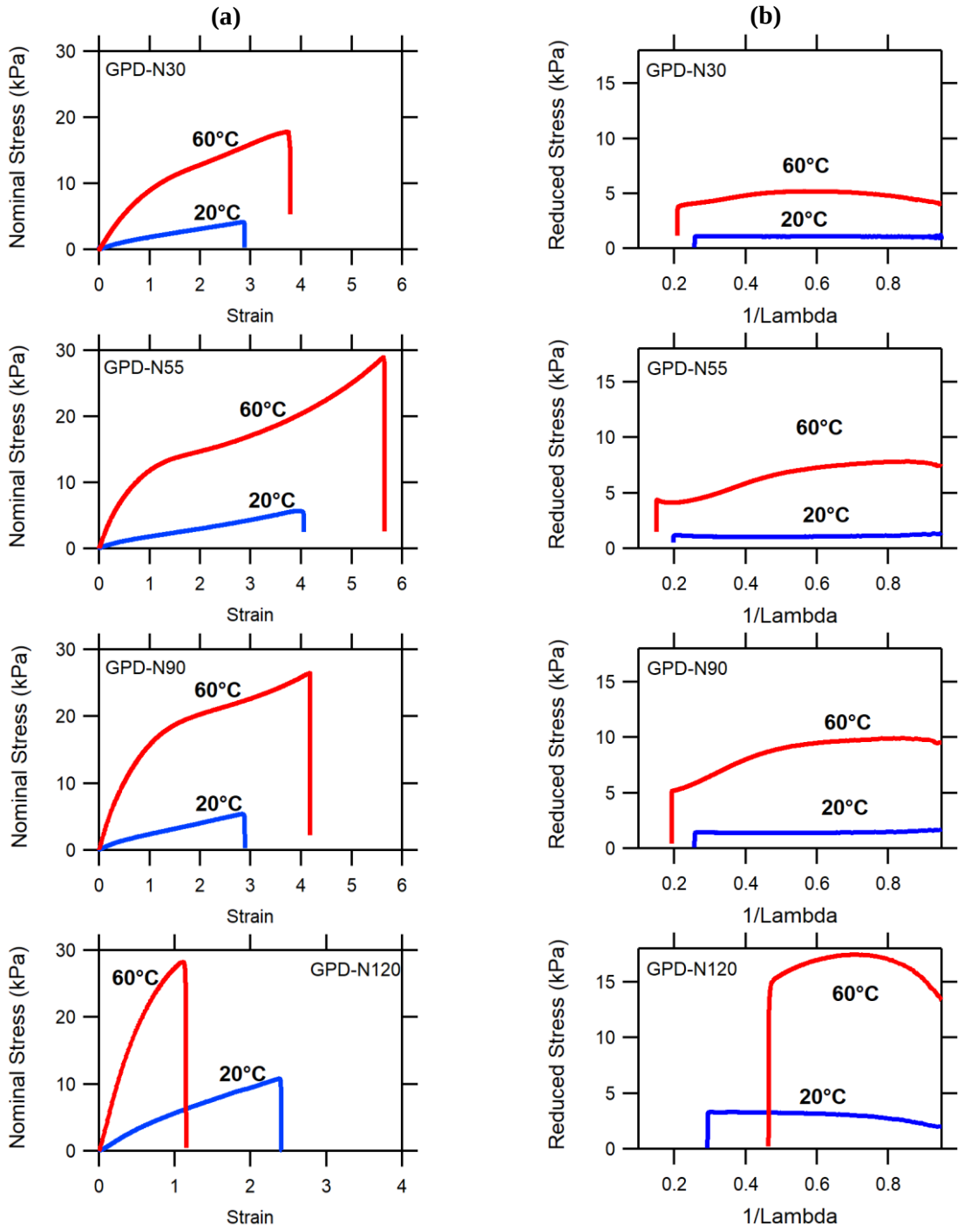

Figure 4.11 Large strain behaviour of GPD-Nx gels at a strain rate of 0.06 s^{-1}. **(a)** Tensile stress-strain curves of GPD-Nx gels at 20 and 60°C and **(b)** Corresponding stress-strain curves plotted as reduced stress as a function of 1/λ. This representation enhances the deviations from the classical rubber elasticity model displayed by the gel at 60 °C: a strong hardening is observed at the early stages of deformation followed by softening above 50% of strain. The GPD-Nx behaviour at 20 °C is given as a guideline and follows the theoretical rubberlike behaviour. All the tensile tests were performed at a 0.06 s^{-1} strain rate

III.4. Role of network topology on the mechanical reinforcement (stiffening)

As already noticed for GPD-N55, the initial stiffness is significantly increased at 60 °C compared to 20 °C for all the grafted hydrogels of the GPD-Nx series, as depicted in **Figure 4.11**. The tensile moduli obtained from the initial slope of the stress-strain curves are consistent with the results obtained by linear rheology. The elongation at break seems also to be strongly enhanced, except for the longest grafted side-chains (GPD-N120 gels), but this result has to be taken with caution as failure systematically occurred in the clamps for all the samples, suggesting that they initially experience damage prior to the test during tightening inside the jaws. Specific focus on fracture properties will be given later in a dedicated section. As plotted in **Figure 4.11.b**, comparatively, GPD-N120 exhibits the strongest initial hardening. Beyond a critical strain value, a large strain softening is observed and reflects the disruption of the physical fillers by the unravelling of collapsed PNIPAm chains upon stretching.[46] GPD-N120 also exhibits the strongest softening, suggesting that long grafts allow to form well-defined stiff collapsed domains but failed for a quite narrow level of elongation. This could explain the sharpness of both hardening and stiffening for GPD-N120.

As shown in **Figure 4.12.a-b**, all the curves seem to extrapolate for large elongation (λ=5) to a similar reduced stress of about 4 kPa, regardless of the average molar mass of the grafts. This is much higher than the response of the network at 20 °C (~1 kPa). Therefore, collapsed domains are presumably able to dissociate and partially reform upon stretching, especially for grafts from 30 to 90 kg/mol. As the stiffening seems to be closely related to the additional energetic contribution of PNIPAm phase-separated domains, the results obtained for the GPD-Nx gels tend to demonstrate that, despite the same PNIPAm concentration in the gel, the PNIPAm grafts length is a crucial parameter to efficiently stiffen the gel. Notwithstanding the increase of molar mass between consecutive grafts unfavouring the aggregation of collapsed domains, the GPD-N120 gels exhibit the highest elastic moduli. **Figure 4.12.c-d** shows the large strain behaviour for the GPD-N55(y-z) series. The idea was to keep the graft length constant (N55, 55 kg/mol) as well as the overall polymer concentration, in order to explore the effect of the relative amount of the mass between two consecutive grafts on the mechanical reinforcement. Usually, in composite materials, the mechanical reinforcement is related to the fraction of hard domains but here, surprisingly, as shown in **Figure 4.12.c**, the initial moduli are almost the same for the GPD-N55(x-y) series,

[46] A. Halperin and E. B. Zhulina, **Europhys. Lett.**, *1991*, 15, 417-421

independently of the number of PNIPAm grafts and of the average distance between them. Conversely, the strain at break is significantly increased with the PNIPAm/PDMA ratio. Focusing on the maximum of the reduced stress in **Figure 4.12.d** which is supposed to be related to the beginning of the disruption of the collapsed domains, it is noticeable that it occurs at almost the same critical stress, suggesting that the failure of collapsed domains is highly controlled by the length of the grafts.

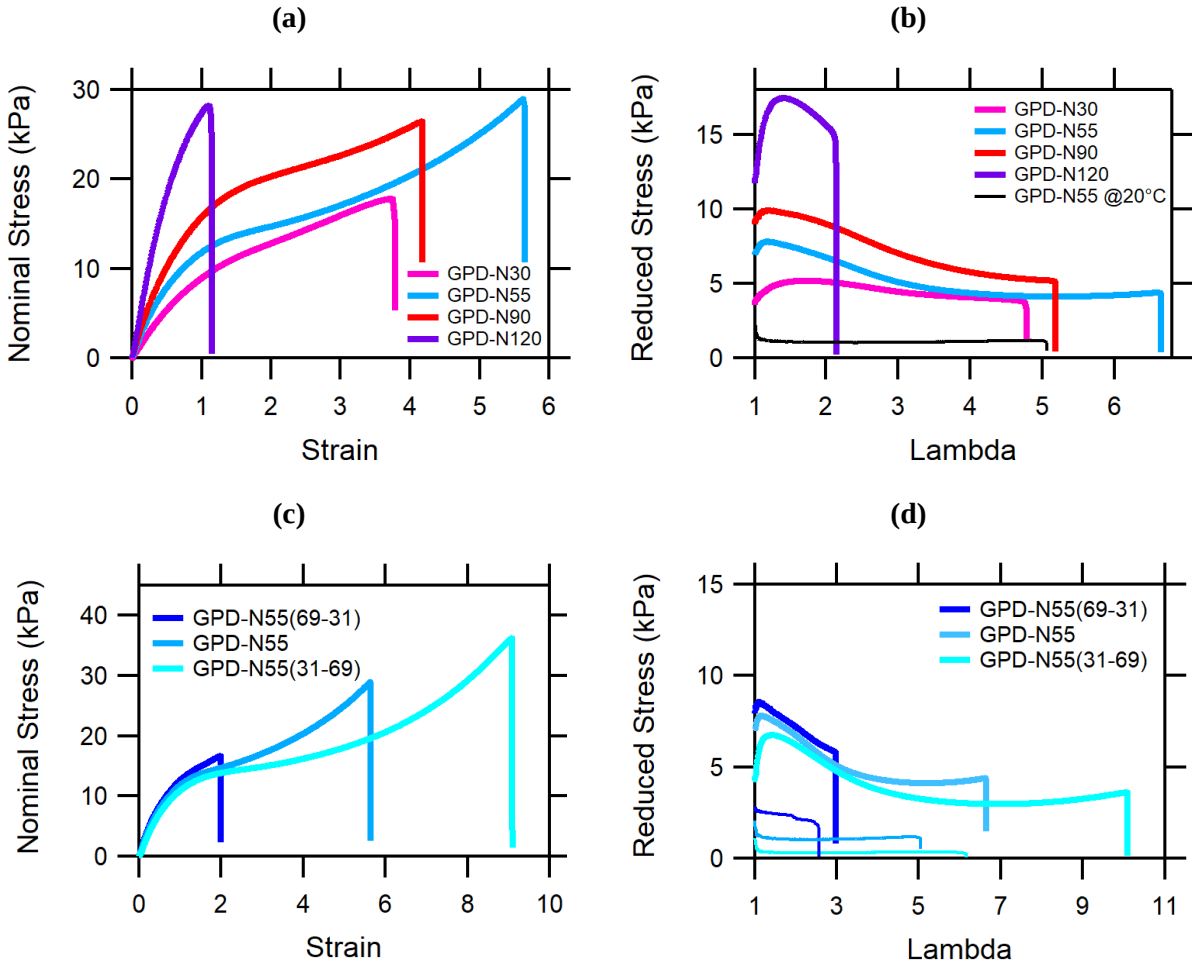

Figure 4.12 Large strain behaviour of GPD-Nx and GPD-N55(y-z) hydrogels at a strain rate of 0.06 s^{-1}. **(a)** (respectively **(c)**)Tensile stress-strain curves of GPD-Nx (respectively GPD-N55(y-z)) gels at 20°C and 60°C **(b)** (respectively **(d)**) Corresponding stress-strain curves plotted as reduced stress as a function of Lambda. This representation enhances the deviations from the classical rubber elasticity model displayed by the gel at 60 °C: a strong hardening is observed at the early stages of deformation followed by softening. The GPD-Nx and GPD-N55(y-z) behaviours at 20 °C (thin lines) are given as a guideline and follow the theoretical rubberlike behaviour

Figure 4.13.a gathers the results obtained at 20 and 60°C for all the topologies investigated, i.e., the two hydrogel series. It appears that the GPD-N120 gel is characterized by the highest modulus at 60 °C. By analogy to composite materials, we propose in **Figure**

4.13.b an estimate of the ratio of the moduli at 60 and 20 °C, as a stiffening ratio. Indeed, in filled rubbers, engineering the efficiency of stiffening is commonly addressed in terms of the ratio between the composite versus the unfilled matrix.[47,48] As expected, this parameter enlightens the remarkable thermo-reinforcement obtained for the GPD-N55(31-69) gel by considering the extremely weak signature of the PDMA network at the coil state. By heating above T_c, the modulus is increased by about 35 times together with an enhancement of the strain at break by 2 times. This is a quite remarkable result in the field of nanocomposite engineering. Conversely, the stiffening ratio attenuates the reinforcement effect for GPD-N120 gels because the modulus at 20 °C is slightly higher for this specific formulation certainly due to entanglements or transfer reactions during the polymerization.

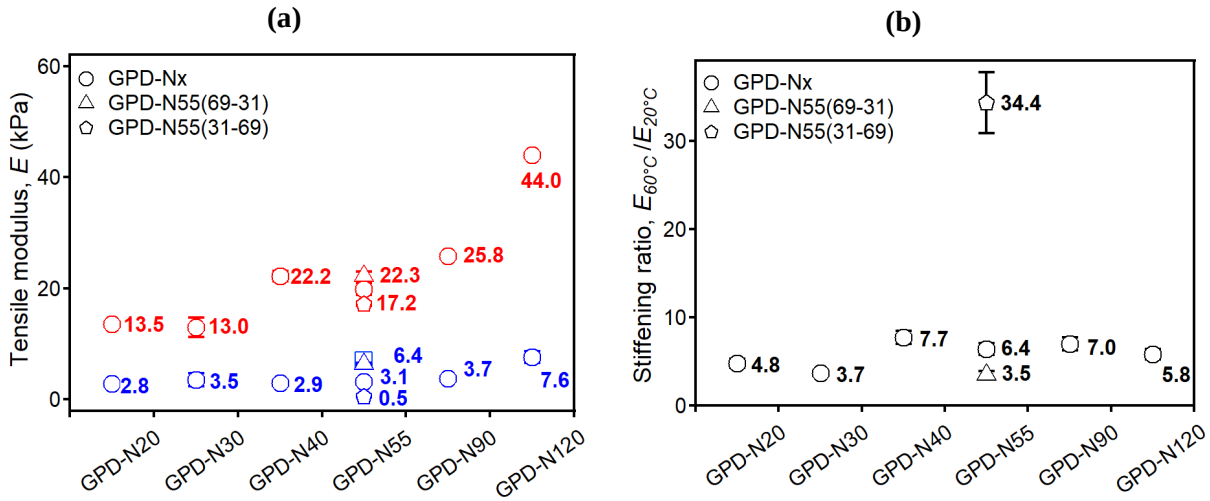

Figure 4.13 Summary of **(a)** the tensile modulus E and **(b)** the stiffening ratio $E_{60°C}/E_{20°C}$ depending on both the PNIPAm side-chains average molar mass (GPD-Nx series) and the PDMA/PNIPAm composition of the network at both 20 and 60 °C. All the tensile tests were performed at a 0.06 s^{-1} strain rate

III.5. Mechanisms of Fracture Toughening and shape-memory properties

Fracture derives from the location of a critical defect and its propagation across the sample. As already discussed, it is rather difficult to get rid of defects and to have a perfect control on the architecture at a molecular level. To overcome the inherent difficulty to design fracture, the gel edge is notched prior to the experiment. As shown in **Figure 4.14** the fracture energy, $\mathcal{G}c$, traducing the strain energy required to propagate the crack across the entire width of the gels, is notably enhanced at T=60 °C compared to the one at T=20 °C, i.e., when

[47] E. Guth and R. Simha, **Kolloid-Zeitschrift**, *1936*, 74, 266-275
[48] E. Guth, **J. Appl. Phys.**, *1945*, 16, 20-25

PNIPAm grafts are in the coil state. Interestingly, the GPD-N120 gel exhibits the highest fracture energy, around 190 J/m^2, but neither the linear viscoelastic behaviour, i.e., the intensity of the dissipative component, *G''*, nor the work of extension W_{ext}, given by the area under the tensile curve could anticipate this feature. Indeed, the estimate of W_{ext} gives a maximum value around 147 kJ/m^3 for GPD-N55(31-69) and minimal value of 27 kJ/m^3 for GPD-N120. In contrast, the GPD-N55(x-y) series seems to be more in line with our expectations as fracture resistance is increased by the introduction of thermo-responsive moieties. This result suggests that specific dissipative mechanisms take place at the vicinity of the advancing crack, where polymer chains are highly stretched and undergo high strain rates.

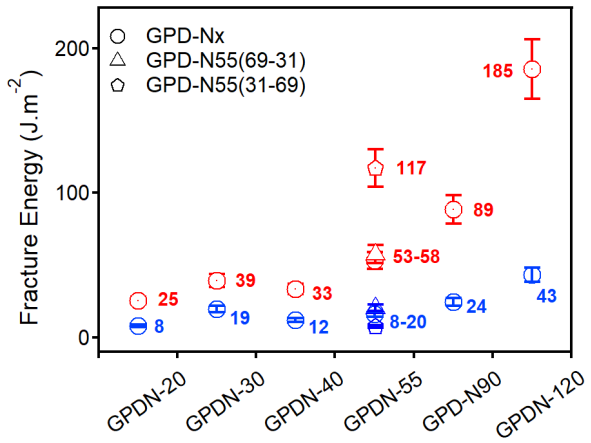

Figure 4.14 Summary of fracture energies depending on both the PNIPAm side-chains molar mass (GPD-Nx series) and the PDMA/PNIPAm composition of the network at both 20 and 60 °C. All the tensile tests were performed at a 0.06 s^{-1} strain rate

The length of the graft and its full stretching from its globular conformation seems to be a key parameter for fracture toughening. As expected from theory,[46] we anticipate that the PNIPAm fillers could act as a reservoir for stretch-induced dissipation. As a matter of fact, the higher the length of the graft, the more the unravelling of the polymer at high values of strain. It seems clear that the efficiency of the mechanical reinforcement should perform differently by considering isolated phase-separated PNIPAm grafts (involving exclusively intra-chain interactions) or phase-separated domains, originating from the aggregation of several collapsed grafts. The characteristic length scales involved in the phase-separated domains obtained by SANS do not allow having a clear picture of the gel structure that is required for such a mechanical reinforcement, since phase-separated domains do not differ deeply by varying the grafting density or graft lengths. Seeking to tackle this important issue, we designed shape-memory and self-adhesion experiments to respectively probe the inter-chain bridging efficiency and the dissipative capabilities to generate a robust adhesive layer.

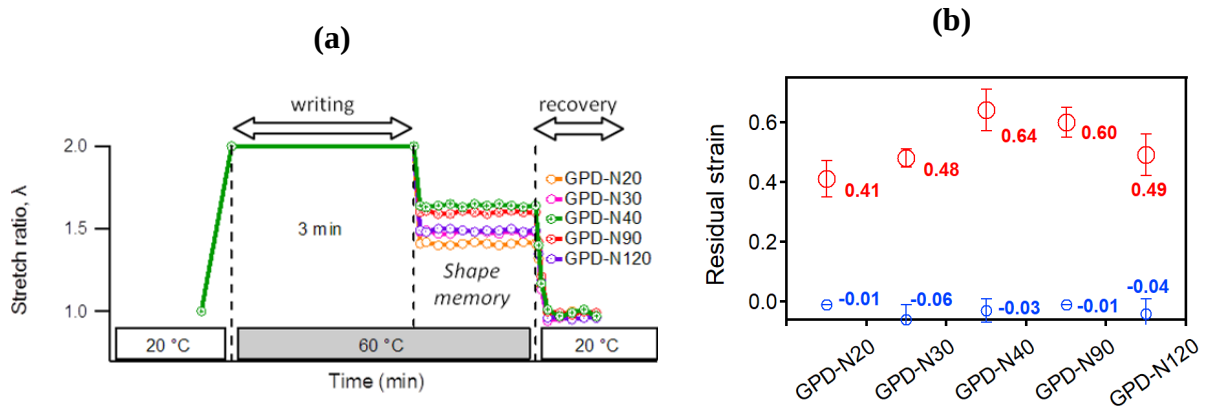

Figure 4.15 **(a)** Shape recovery curves of GPD-Nx gels with time. First, the gels were stretched to λ=2 at 20 °C prior to be heated in oil at 60 °C to perform the "writing" procedure. After keeping λ=2 for 3 min at 60 °C, stress was released, and the residual stretched ratio was measured over time. Finally, the gels were cooled down to 20 °C to fulfil the "recovery" process. **(b)** Summary of the residual strain at 60 and 20 °C after the "writing" and the "recovery" processes, respectively

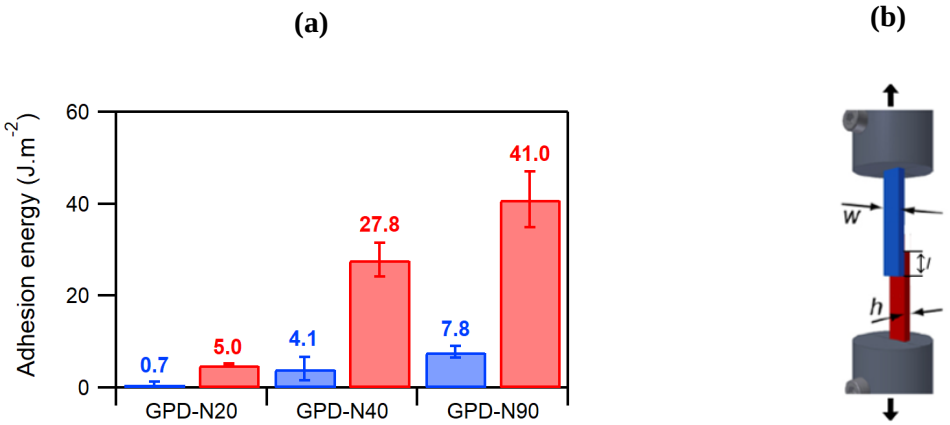

Figure 4.16 **(a)** Adhesion energies depending on the PNIPAm side-chains molar mass (GPD-Nx series). All the tensile tests were performed at a 0.06s^{-1} strain rate. **(b)** lap-shear test geometry

Of course, shape-memory properties are desirable for many applications,[49] but they also provide insights into the inter-chain bridging efficiency. As illustrated in **Figure 4.15**, the formation of phase-separated domains, exhibiting slow dynamics as described previously, is also responsible for the shape memory effect. After "writing" a stretch level of λ=2 at 60 °C during 3 min, the stress was removed. Only a partial retraction of the gel is observed, suggesting that internal stresses due to the extension of the PDMA network are compensated by the formation of inter-chain microdomains acting as physical cross-links. Note that the residual strain at 60 °C remains almost constant over time, even for days, after 72 h. When the

[49] X. Hu, D. Zhang and S.S. Sheiko, **Adv. Mater.**, *2018*, 30, article 1707461

temperature is lowered at 20°C, the initial shape is quickly recovered since physical associations are suppressed. As shown in **Figure 4.15**, no significant effect of chain length is observed even for short grafts as GPD-N20 gels are able to generate inter-chain aggregates to stabilize the PDMA network under a macroscopic strain of about 40 %. These results are consistent with the SANS analysis reported in Chapter 3 as PNIPAm collapsed domains give rise to large heterogeneities that gather together large numbers of chains.

In contrast, self-adhesive properties strongly depend on the length of the grafts, as shown in **Figure 4.16**. Self-adhesion properties enable to probe the capability of PNIPAm grafts to bridge the interface between two grafted hydrogels of the same nature and most importantly to dissipate strain energy under stress. Close contact was first established at 20 °C, and then the lap-joint assembly was heated at 60 °C during 10 min and under a constant pressure of 1 kPa. As shown in **Figure 4.16**, adhesion energy increases significantly with graft length for both temperatures. At 20 °C, the adhesion increases with the length of the dangling chain due to the combined effect of the efficiency to connect the two surfaces (by interdiffusion) and the increase of dissipative processes, as G'' is supposed to increase with the number of entanglements per dangling chain. At 60 °C, a net increase of adhesiveness is observed. Results are qualitatively in line with fracture energy and confirm the crucial role of chain length for achieving efficient mechanical toughening in terms of stiffening and fracture (as adhesion) toughening. These results open interesting perspectives in the field of responsive underwater adhesion.

IV. Conclusion

By investigating hydrogels at both low and large deformations, we have investigated the influence of the PNIPAm graft average molar mass and the PDMA/PNIPAm composition within the gels on their mechanical properties. First of all, it was demonstrated that homo-PDMA gels, GPD-N40 and GPD-N120 possess defects in their network with a broad distribution of the mesh size coming from the random feature of the polymerization process. As $G'' \sim \omega^{\alpha}$ with α=0.5 for homo-PDMA gels and $G'' \sim \omega^{\alpha}$ with α=0.4 for both GPD-N40 and GPD-N120, the contribution of the length of the grafts to the frequency-dependence seems to be weak.

Moreover, linear rheological experiments and fatigue tests on GPD-N55 highlight that both the dissipative processes reinforcing the gel and the capacity of its dual-phase structure

to perfectly reform under thermal cycling, are weakly time-dependent. In fact, perfect recovery of strain and mechanical behaviour are observed after few minutes of rest which traduces good self-healing properties. Then, as the hydrogel stiffening seems to be closely related to the additional energetic contribution from PNIPAm phase-separated domains, as expected, increasing the PNIPAm/PDMA ratio enhances the reinforcement. It is especially observed with GPD-N(31-69) with an elastic modulus and strain at break strikingly increased respectively by 35 times and 2 times by heating above the critical temperature T_c. This is a quite remarkable result in the field of nanocomposite engineering.

Furthermore, the GPD-Nx series brings to light that despite the same PNIPAm concentration in the gel, the molar mass of the PNIPAm grafts is a crucial parameter to efficiently stiffen the gel. It is even independent of the increasing interval between the adjacent grafts, unfavouring the aggregation of collapsed domains, as demonstrated for GPD-N120 exhibiting the highest elastic modulus. The fracture energy is notably enhanced by the length of the grafts. For GPD-N120, fracture energy reaches about 200 J/m^2 above phase separation in contrast to 40 J/m^2 at 20 °C. On the other hand, the stiffening ratio attenuates the reinforcement effect for GPD-N120 as its elastic modulus is slightly higher at 20 °C, certainly due to entanglements or transfer reactions during the polymerization. Interestingly, gels exhibit responsive adhesion properties. Indeed, adhesion efficiency is the combination of the ability to connect the two gel surfaces and the increase of dissipative processes involved upon stretching. The adhesive and fracture energies are qualitatively in line, both increasing with the average molar mass of PNIPAm side-chains. As a matter of fact, in both cases, the propagation of a crack (at the interface or in bulk) is at stake. Our results demonstrate that the length of PNIPAm grafts is crucial for fracture toughening and adhesion properties.

Chapter 5

Hydrogels with dual thermo-responsive mechanical performance

Chapter 5: Hydrogels with Dual Thermo-Responsive Mechanical Performance

Chapter 5: Hydrogels with Dual Thermo-Responsive Mechanical Performance

Abstract

Original chemical hydrogels combining antagonistic upper critical solution temperature (UCST) and lower critical solution temperature (LCST) polymers were elaborated via free radical polymerization. These dual thermo-responsive chemical hydrogels, combining poly(*N*-isopropylacrylamide) (PNIPAm) side-chains within a poly(*N*-acryloylglycinamide) (PNAGA) network, were designed following a simple and versatile procedure. These hydrogels exhibit two phase transitions both at low (upper critical solution temperature, UCST) and high (lower critical solution temperature, LCST) temperatures, thereby modifying their swelling, rheological and mechanical properties. Rheological and mechanical experiments performed under isochoric conditions show a thermo-induced reinforcement both at low and high temperature, induced by the formation of phase-separated polymer domains acting as organic reinforcing fillers.

Hydrogels with Dual Thermo-Responsive Mechanical Performance

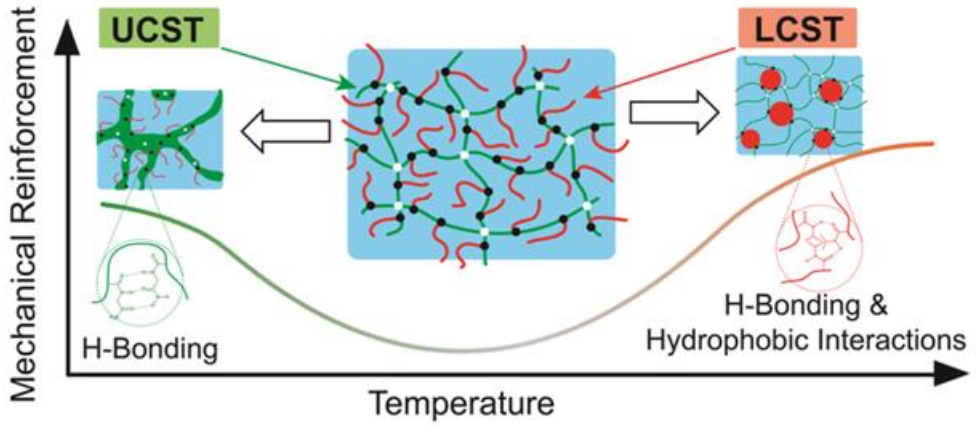

It is noteworthy to precise that this chapter is adaptated from the paper "**Hydrogels with Dual Thermo-responsive Mechanical Performance**" referenced as following: H. Guo, C. Mussault, A. Marcellan, D. Hourdet and N. Sanson, **Macromolecular Rapid Communications**, *2017*, 38, (17), 1700287

I. Introduction

As demonstrated in Chapters 3 and 4, a successful mode of hydrogel reinforcement based on the universal concept of polymer phase separation has been developed. This concept is interesting as phase separation can be controlled by applying external *stimuli*, such as pH or temperature[1,2,3,4] thereby making it possible to modify in a controlled manner the properties of hydrogels. Such behavior can be achieved by using thermo-responsive polymers and this was clearly demonstrated in both Chapters 3 and 4 with the increase of the mechanical properties. These ones are driven by the formation of phase-separated polymer domains, induced by intra-/inter- hydrogen bonds between the nitrogen atoms of the acrylamide groups and the acid hydrogens of poly(N-isopropylacrylamide) but also by hydrophobic interactions between the isopropyl groups. These physical interactions play the role of a highly dissipative viscoelastic network as they can break during mechanical loading. Such hydrogels can retain a high level of water (more than 80 wt %) on both sides of the transition temperature.[5,6] To achieve this, lower critical solution temperature (LCST) polymer chains such as PNIPAm and hydrophilic poly(*N*,*N*-dimethylacrylamide) (PDMA) were combined into the same cross-linked architecture. Within this network, the hydrophilic counterpart allows to maintain a high level of hydration, even above the phase transition temperature of the PNIPAm. Using these hydrogels in the preparation state, it was possible to keep their volume constant, with a relatively high swelling state both well above and below the critical temperature and to clearly identify the role of the PNIPAm phase separation in the mechanical reinforcement. The designed hydrogels exhibit strong thermo-toughening with excellent fatigue resistance, full recovery and remarkable fracture properties. So far, only LCST-type polymers have been investigated, restricting both the nature and the range of applications.

[1] S. Ashraf, H. K. Park, H. Park, S. H. Lee, ***Macromol. Res.***, *2016*, 24, 297-304
[2] L. Klouda, **Eur. J. Pharm. Biopharm.**, *2015*, 97, 338-349
[3] M. C. Koetting, J. T. Peters, S. D. Steichen, N. A. Peppas, **Mater. Sci. Eng. R**, *2015*, 93, 1-49
[4] S. R. Van Tomme, G. Storm, W. E. Hennink, **Int. J. Pharm.**, *2008*, 355, 1-18
[5] H. Guo, N. Sanson, D. Hourdet, A. Marcellan, **Adv. Mater.**, *2016*, 28, 5857-5864
[6] H. Guo, C. Mussault, A. Brûlet, A. Marcellan, D. Hourdet, N. Sanson, **Macromolecules**, *2016*, 49, 4295-4306

(a)

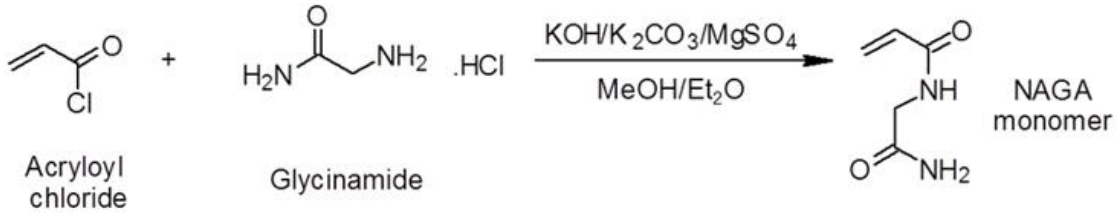

(b)

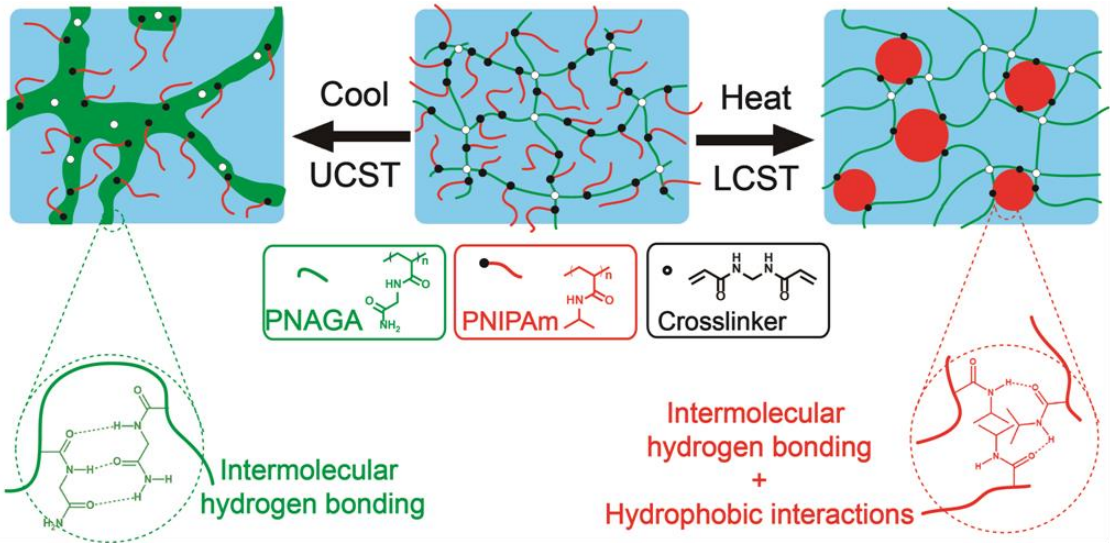

Figure 5.1 **(a)** Synthesis procedure of NAGA monomer. **(b)** Schematic representation of thermo-responsive self-assembling of GPA-N36 hydrogels at low and high temperatures

As mentioned previously, the development of thermo-responsive hydrogels working in a broad range of temperatures, with control of their properties induced either by heating and/or cooling, is an important requirement in order to extend the spectrum of applications. Recently, neutral polymers exhibiting an upper critical solution temperature (UCST) in water,[7,8,9,10] especially poly(*N*-acryloylglycinamide) (PNAGA), have been receiving increasing attention.[11,12,13] The phase transition process of PNAGA in water is driven at low temperature by intra- and intermolecular hydrogen bonding between repeat units located on either the same or different polymer chains. In the present work, we developed an original dual thermo-responsive hydrogel, combining LCST- and UCST-type polymers that will be

[7] S. Glatzel, A. Laschewsky, J. F. Lutz, **Macromolecules**, *2011*, 44, 413-415
[8] J. Seuring, S. Agarwal, **Macromol. Rapid Comm.**, *2012*, 33, 1898-1920
[9] J. Seuring, S. Agarwal, **ACS Macro Lett.**, *2013*, 2, 597-600
[10] A. Fujihara, N. Shimada, A. Maruyama, K. Ishihara, K. Nakai, S. I. Yusa, **Soft Matter**, *2015*, 11, 5204-5213
[11] S. Glatzel, N. Badi, M. Pach, A. Laschewsky, J. F. Lutz, **Chem. Comm.**, *2010*, 46, 4517-4519
[12] J. Seuring and S. Agarwal, **Macromol. Chem. Phys.**, *2010*, 211, 2109-2117
[13] M. Boustta, P. E. Colombo, S. Lenglet, S. Poujol, M. Vert, **J. Controlled Release**, *2014*, 174, 1-6

able to thermally respond in isochoric conditions and to tune its mechanical properties over a broad range of temperature (see **Figure 5.1**). Indeed, uniting PNAGA and PNIPAm into the same network, gives us a unique opportunity to investigate and compare the role of antagonistic phase separation mechanisms, triggered at low and high temperatures, over the mechanical properties. Based on the polymer phase separation process, the versatility of the designed hydrogels will provide a promising method to test the universality of the phase-separation-induced reinforcement.

II. Experimental Section

II.1. Materials

N-isopropylacrylamide (NIPAm, Aldrich), *N*,*N*'-methylenebisacrylamide (MBA, Aldrich), potassium peroxodisulfate (KPS, Aldrich), *N*,*N*,*N*',*N*'-tetramethylethylenediamine (TEMED, Aldrich), acryloyl chloride (97%, Aldrich) and glycinamide hydrochloride (98%, Aldrich) were used as received. All organic solvents were of analytical grade and water was purified with a Millipore system combining a reverse osmosis membrane (Milli RO) and ion exchange resins (Milli Q) for synthesis and purification.

II.2. Characterization.

Differential Scanning Calorimetry (DSC). The phase transition of hydrogels was investigated by differential scanning calorimetry using a DSC Q200 from TA Instruments. Hydrogels at preparation state (ca. 80 mg), equilibrated with a reference filled with the same quantity of pure water, were submitted to temperature cycles between 10 and 70 °C under nitrogen atmosphere. The heating and cooling rates were fixed at 2 °C min^{-1}.

Nuclear magnetic resonance (NMR) spectroscopy. For the characterization of monomer, the measurements were performed on a Bruker Avance III HD spectrometer operating at 400 MHz for ^{1}H, using a standard 5 mm broadband Smart probe at 25 °C.

The measurements at different temperatures were carried out on a Bruker Avance III HD spectrometer operating at 600 MHz for ^{1}H, with 32 transients, 45 degree flip angle, 2.5 sec acquisition time, 2 sec relaxation delay. The temperature control was achieved by a Bruker BCU II unit and a built in temperature control unit. The sample was allowed to equilibrate for 10 minutes at each temperature prior to the test. The ^{1}H chemical shifts were referred to the residual HOD peak at each temperature.

Capillary electrophoresis (CE). The experiments were performed with a Beckmann P/ACE MDQ system equipped with a diode-array spectrophotometer (detection at wavelength 200 nm +/- 10 nm). The bare silica capillary (J & W Scientific) was 75 i.d. x 31 cm. The run buffer was 25 mM, NaH_2PO_4/Na_2HPO_4 at pH=7.1. Prior to the measurements, the capillary was flushed with 0.1 M NaOH aqueous solution, rinsed 1 min with water, and equilibrated with the run buffer. Between runs, the capillary was rinsed for 1 min with the run buffer, then a short zone of sample diluted in the run buffer was hydrodynamically injected at the inlet (pressure of 0.2 psi, 4 s), possibly followed by similar injection of a 0.1 v% of DMSO (used as neutral marker) in the run buffer. Separation proceeded with a 9 kV voltage and 0.1 psi pressure applied at the inlet to mobilize analytes toward the detection window.

Inductively coupled plasma atomic emission spectroscopy. ICP-AES were performed on iCAP 6200 from Thermo Scientific.

Turbidimetry. Absorbance measurements were carried out at different temperatures with a UV–vis Hewlett-Packard 8453 spectrophotometer using a 0.2 cm path length quartz cell, in a wavelength range from 200 to 1100 nm and equipped with a temperature controller (±0.1 °C). The hydrogel sample was directly synthesized in the UV-vis cell prior to the test. Turbidimetry curves were built by collecting the absorbance at 670 nm with a scanning rate of 0.5 °C min^{-1}. The UCST- and LCST-type cloud points were defined as the temperature where the transmitted intensity reaches 50 % of the incident intensity. In the case of the PNAGA phase transition temperature, the heating curve was chosen according to the work reported by Seuring.[12]

Swelling measurements. Equilibrium swelling experiments were performed in pure water at designated temperatures. The samples at their preparation state were initially cut and placed in a large excess of water which was exchanged twice a day. The swollen gels were weighed (m_{sw}) and the swelling ratio at equilibrium (Q_e) was calculated as $Q=m_{sw}/m_d$, m_{dry} being the dry weight.

Rheology. The viscoelastic properties of hydrogels were studied in their preparation state, using a stress-controlled rheometer (AR 1000 from TA Instruments) equipped with a roughened plate/plate geometry (diameter 40 mm, angle 2, truncature 1500 μm). The experiments were performed in the linear viscoelastic regime, which was established for each sample by a stress sweep at 1 Hz. The temperature was controlled by a high power Peltier system that provides fast and precise adjustment of the temperature during heating and

cooling stages. Typically, the experimental conditions were fixed at constant frequency (1 Hz) and shear stress (2 Pa). Particular care was taken to avoid the drying of the sample by using a homemade cover, which prevents water evaporation during the experiment. In these conditions, dynamic moduli (*G'* and *G''*) were recorded between 2 and 70 °C by applying heating and cooling scans at 2 °C min^{-1}.

Large strain behavior in tension mode. Tensile tests were performed on a standard tensile Instron machine, model 5565, equipped with an environmental chamber allowing a precise control of the temperature. The device used a 10 N load cell (with a relative uncertainty of 0.16 % in the range from 0 to 0.1 N) and a video extensometer which follows the local displacement up to 120 mm (with a relative uncertainty of 0.11 % at full scale).

The gel samples used for the mechanical tests were synthesized in home-made moulds consisting of two covered glass plates spaced by a stainless steel spacer of 2 mm thickness. The gels were then cut with a punch and their final dimensions, were 30 mm x 4.9 mm x 2 mm. The length was taken constant (L~20 mm) for all the tests and the gel strip was marked with two dots with a white marker, for their recognition by the video extensometer. For high temperatures or long-term experiments, tests were conducted in an immersion cell consisting of a paraffin oil bath surrounding the sample in order to isolate the samples from the environment (prevent evaporation or swelling). As a control experiment, we initially checked the total immiscibility of the paraffin oil with the gel within the temperature range investigated in this study. All the tests were carried out at the fixed strain rate of 0.06 s^{-1}.

III. Dual thermo-responsive hydrogels synthesis

III.1. Synthesis of NAGA monomer

A new procedure for NAGA monomer synthesis was adapted from Seuring et al.[12] but greatly improved with the sake of enhancing total yield, facilitating purification process and avoiding the presence of ionic groups (see **Figure 5.2**). The main change relates to the use of organic miscible cosolvent MeOH/Et_2O in place of H_2O/Et_2O from the previous studies. In this case, the reaction is easier to process and the purification steps can be largely simplified (see **Table 5.1**). For instance, time-consuming steps such as lyophilisation and column chromatography are no longer necessary. Moreover, in our case, even though acryloyl chloride can react with methanol, the corresponding product, methyl acrylate, could be simply

removed by rotary evaporation or extraction. Therefore, we can work with an excess of acryloyl chloride to ensure that glycinamide hydrochloride could be totally converted into NAGA monomer.

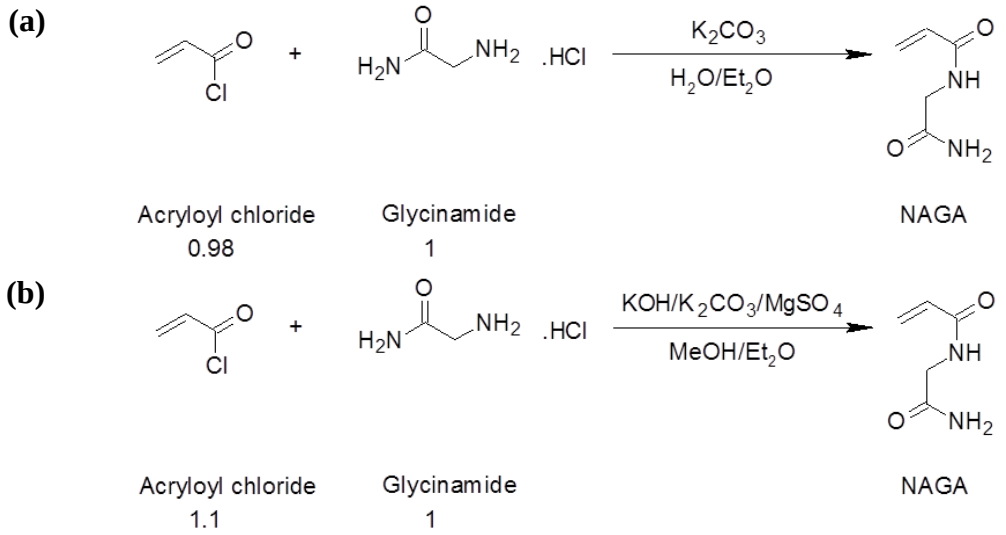

Figure 5.2 **(a)** Conventional synthesis procedure of NAGA monomer[12] **(b)** Modified synthesis procedure of NAGA monomer

Table 5.1. Comparison of work up steps between the conventional method and the revised method

Previous method	Our method
i. Removal of Et_2O by rotary evaporation	i. Removal of Et_2O by rotary evaporation
ii. Removal of water by lyophilization[a]	ii. Removal of methanol after filtration
iii. Extraction with acetone (6 times) and removal of volatile solvent[a]	iii. Extraction with acetone (twice) and removal of volatile solvent
iv. Column chromatography[a]	iv. Recrystallization
v. Recrystallization	

[a] these steps are time-demanding and labor-intensive

Typically, in a 500 mL three-necked round-bottom flask, glycinamide hydrochloride (5.53 g, 50 mmol), potassium hydroxide (5.61 g, 100 mmol), potassium carbonate (2.07 g, 15 mmol) and magnesium sulphate (12.60 g, 105 mmol) were well dispersed in 50 mL of dry methanol. The solution was cooled down in an ice bath and acryloyl chloride (4.98 g, 55 mmol) initially dissolved in 60 mL of diethyl ether was added dropwise over 2 h under vigorous stirring. The suspension was warmed up to room temperature and further stirred for 3 h to complete the reaction. Then, diethyl ether was removed by rotary evaporation and the

remaining suspension was gently warmed to 50 °C. After removing all the precipitate by filtration, the remaining volatile solvent was evaporated, and the residual solid was recovered with hot acetone to give rise to the crude product. NAGA monomer was finally recrystallized from isopropanol to yield pure product of 4.89 g, yield=76.4%. ^{1}H NMR (400 MHz, DMSO-d_6): δ=3.78 (d, J=6.0 Hz, 2H), 5.65 (dd, 1H, J_1=2.1 Hz, J_2=10.2 Hz), 6.13 (dd, 1H, J_1=2.1Hz, J_2=17.1 Hz), 6.36 (dd, 1H, J_1=10.2 Hz, J_2=17.1 Hz), 7.07 (s, 1H), 7.40 (s, 1H), 8.31 (s, 1H) (see **Figure 5.3**). Capillary Electrophoresis: Acrylic acid impurities <0.01%wt (see **Figure 5.4**), Potassium content: 0.7 ppm (ICP-AES).

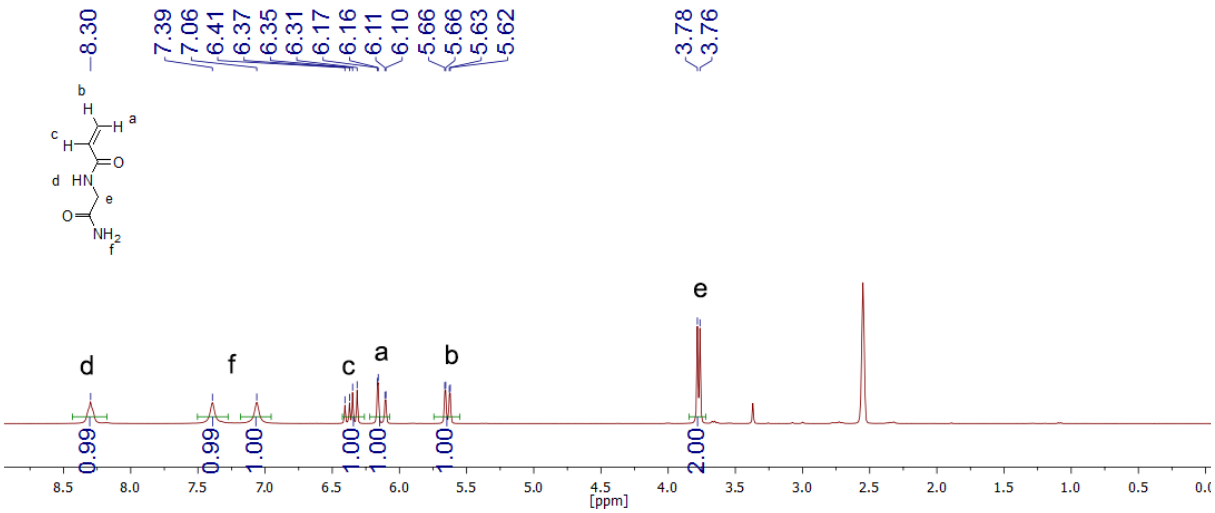

Figure 5.3 ^{1}H NMR spectra of NAGA monomer in DMSO-d_6. The NMR signals located at 2.55 and 3.4 ppm correspond to DMSO and water respectively

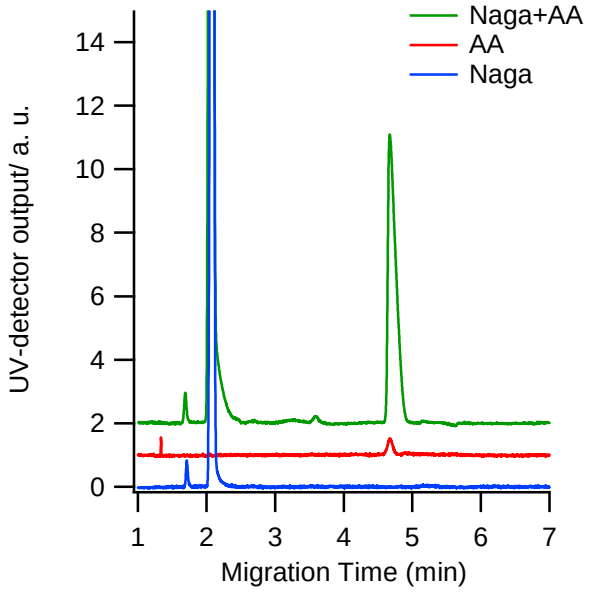

Figure 5.4 Capillary electrophoresis spectra of NAGA monomer (blue line), Acrylic acid (red line) and a mixture of both (green line), all in 25 mM NaH_2PO_4/Na_2HPO_4 buffer at pH=7.1. The CE signals located at 2.06 and 4.67 min correspond to NAGA and Acrylic Acid respectively

III.2. Hydrogel preparation

III.2.1. Synthesis of pure PNIPAm and PNAGA gels

Monomer and chemical cross-linker (stock solution of MBA) were initially dissolved in a given amount of water under nitrogen bubbling at 30 °C. Stock solutions of KPS and TEMED were separately prepared under nitrogen atmosphere and after 30 min, aliquots were added into the reaction medium. After fast mixing (2 min), the final formulation was rapidly transferred between glass plates of 2 mm width under nitrogen atmosphere and the reaction was left to proceed overnight at 30 °C. The resulting hydrogels were then cut with a die-cutter of rectangular or round shape and directly used for DSC and swelling experiments or stored into paraffin oil before mechanical testing in order to avoid any change in hydrogel composition induced by swelling or drying. For both gels, the weight ratio of "monomer/water" was constant, equal to 1/5 (Q_0=6), and the molar ratio of "monomer:MBA:KPS:TEMED" was set equal to 100:0.1:1:1.

III.2.2. Synthesis of PNAGA chemically cross-linked network with PNIPAm grafts (GPA-N36)

First, the synthesis of the PNIPAm macromonomer was achieved as previously described using a telomerization process with cysteamine hydrochloride followed by modification of the amino end-group with acrylic acid in order to get the vinyl function.[3] The absolute characterization of the macromonomer by size exclusion chromatography gave an average molar mass of M_n=36 kg mol^{-1} ($Đ$=1.4).

Due to the transition temperatures of PNIPAm and PNAGA, the hydrogel synthesis was carried out under a N_2 atmosphere at 30 °C, where both polymers are in coil conformations. Typically, NAGA monomer (1 g, 7.8 mmol), PNIPAm macromonomer (1 g) and chemical cross-linker MBA (1.20 mg, 0.1 mol % to monomer) were dissolved in a corresponding amount of water. After 30 min of deoxygenation with nitrogen bubbling at 30 °C, KPS (21.1 mg, 1 mol % to monomer) and TEMED (9.1 mg, 1 mol % to monomer) were dissolved separately in water, deoxygenated, and transferred subsequently into the aforementioned medium. The weight ratio "monomer/macromonomer/water" of gel was kept constant, equal to 1/1/10 (Q_0=6). After fast mixing (2 min), the final solution was rapidly transferred into different moulds under nitrogen atmosphere, either plates of 2 mm width or syringes of 5 mL. The reaction was left to proceed at 30 °C overnight.

IV. Results and Discussion

NAGA monomer was synthesized following a new procedure based on the synthesis of Seuring et al. but modified in order to both facilitate the synthesis process and avoid the presence of ionic groups, detrimental for the UCST behavior of PNAGA in water as shown in **Figure 5.1.a**.[12] Indeed, by using only miscible organic solvents, this new synthesis procedure is less time-consuming by reducing the number of purification steps and avoiding the presence of ionic group (see **Figure 5.2 to Figure 5.4** and **Table 5.1**). Dual thermo-responsive hydrogels were designed by copolymerizing equal amounts of NAGA monomer and PNIPAm macromonomer with additional chemical cross-linker. The resulting gel was named GPA-N where A and N36 stand for NAGA monomer and PNIPAm macromonomer of average molar mass M_n = 36 kg/mol, respectively. The dual thermo-responsive behavior of GPA-N36 hydrogel was finely investigated by turbidity experiments, swelling measurements, differential scanning calorimetry (DSC) and ^{1}H NMR spectroscopy as shown in **Figure 5.6** and **Figure 5.5**. Owing to the combination of PNAGA and PNIPAm in the same network, turbidity experiments clearly highlight the dual thermo-response of GPA-N36 hydrogel in water with both UCST- and LCST-type behaviors (see **Figure 5.6.a**). Indeed, on both sides of ambient temperature, GPA-N36 hydrogel becomes increasingly turbid when the gel is either heated up or cooled down, indicating the phase separation process of PNIPAm and PNAGA, respectively (see inset of **Figure 5.6.a**). While no notable hysteresis was observed for the PNIPAm phase separation, the phase separation of PNAGA clearly exhibits a hysteresis of 10 °C, even at low heating/cooling rates of 0.5 °C min^{-1}, demonstrating a very slow kinetic process as already reported in the literature.[14] According to the turbidity experiments, UCST- and LCST-type cloud points of GPA-N36 hydrogel were found to be 14 and 36 °C respectively in agreement with DSC experiments (see **Figure 5.5.b**).

[14] J. Seuring, F. M. Bayer, K. Huber, S. Agarwal, **Macromolecules**, *2012*, *45*, 374-384

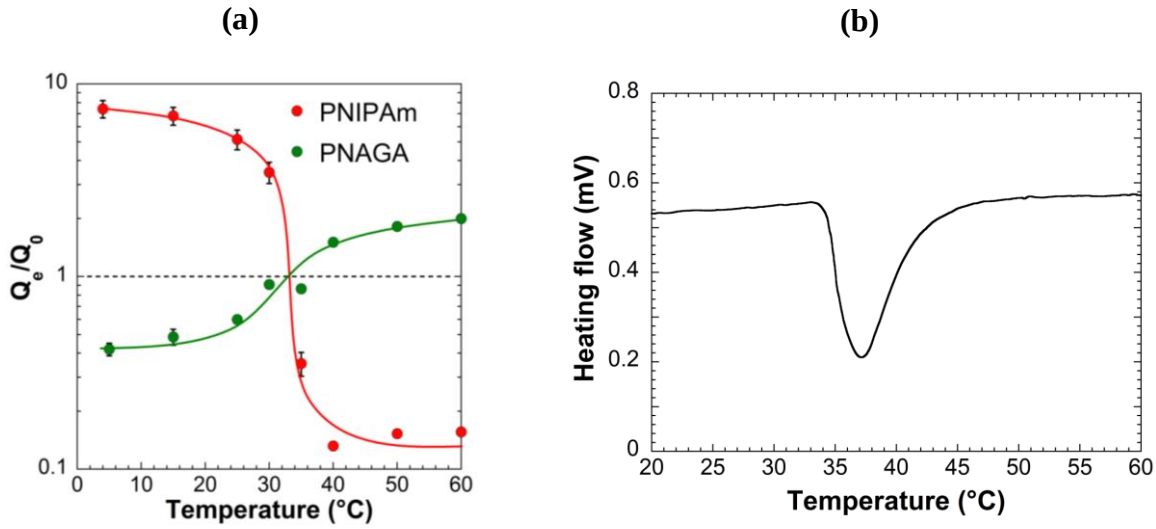

Figure 5.5 **(a)** Swelling behaviour of pure PNIPAm (red) and PNAGA (green) gels in water as a function of the temperature. Solid lines are used as guides to the eye. The dotted line corresponds to Q_e/Q_0=1. Both pure PNIPAm and PNAGA gels exhibit a volume change due to their phase transition. **(b)** Thermogram of GPA-N36 hydrogels obtained by differential scanning calorimetry at 2 °C min^{-1}. The PNAGA phase separation cannot be determined with conventional DSC, due to the very low value of enthalpy of the transition[14]

Taking into account the phase transition temperatures of the two polymers, the swelling ratio at equilibrium in pure water, Q_e, was investigated as a function of temperature (see **Figure 5.6.b**). From 30 to 35 °C, GPA-N36 hydrogel swells (Q_e>10) as PNIPAm and PNAGA chains exhibit a coil conformation, thereby fostering their hydrogen bonds with water molecules, which is in agreement with the transparency of GPA-N36 hydrogel (see **Figure 5.6.a**). By contrast, due to the UCST and LCST behaviors of the designed GPA-N36 hydrogel, NAGA (respectively NIPAm) polymer chains undergo a conformational transition at low (respectively high) temperature generating different polymer phase-separated domains depending on the gel topology (see **Figure 5.1.b**).[5,6] Despite the phase separation process, the GPA-N36 hydrogel retains almost the same swelling ratio as in the preparation state both at high (T≥40 °C, $Q_e \cong Q_0$=6) and low (T=5 °C, $Q_e \cong$7) temperatures. This is mainly due to the osmotic contribution of hydrophilic polymer chains, namely PNIPAm at low temperature and PNAGA at high temperature, promoting the gel swelling or at least compensate the large collapse of the antagonistic polymer phase beyond the critical temperature (see **Figure 5.5.a**). Note that the phase transition of PNAGA in both pure PNAGA and GPA-N36 gels takes place in a broad range of temperatures as reported in the literature[16] whereas a sharp transition is observed for PNIPAm-based gels. As the equilibrium swelling ratios of GPA-N36 gels (Q_e) are always equal to or higher than Q_0 in the whole range of temperatures, mechanical experiments can be carried out under isochoric conditions (without any risk of volume

change) by simply working with gel samples maintained in their preparation state by immersion into immiscible solvent like paraffin oil for instance. Finally, the phase transition of both polymers was also evidenced from ^{1}H NMR measurements performed at different temperatures as shown in **Figure 5.6.c**. Upon heating the NMR signals corresponding to the methyl and methine groups of PNIPAm, respectively observed at 1.1 and 3.9 ppm (zoom in **Figure 5.6.c**), progressively decrease, whereas the NMR signals of NAGA (3.5-4 ppm) exhibit a better resolution at 50 °C. This set of experimental techniques clearly demonstrates the dual thermo-responsive behavior of the GPA-N36 hydrogels in water.

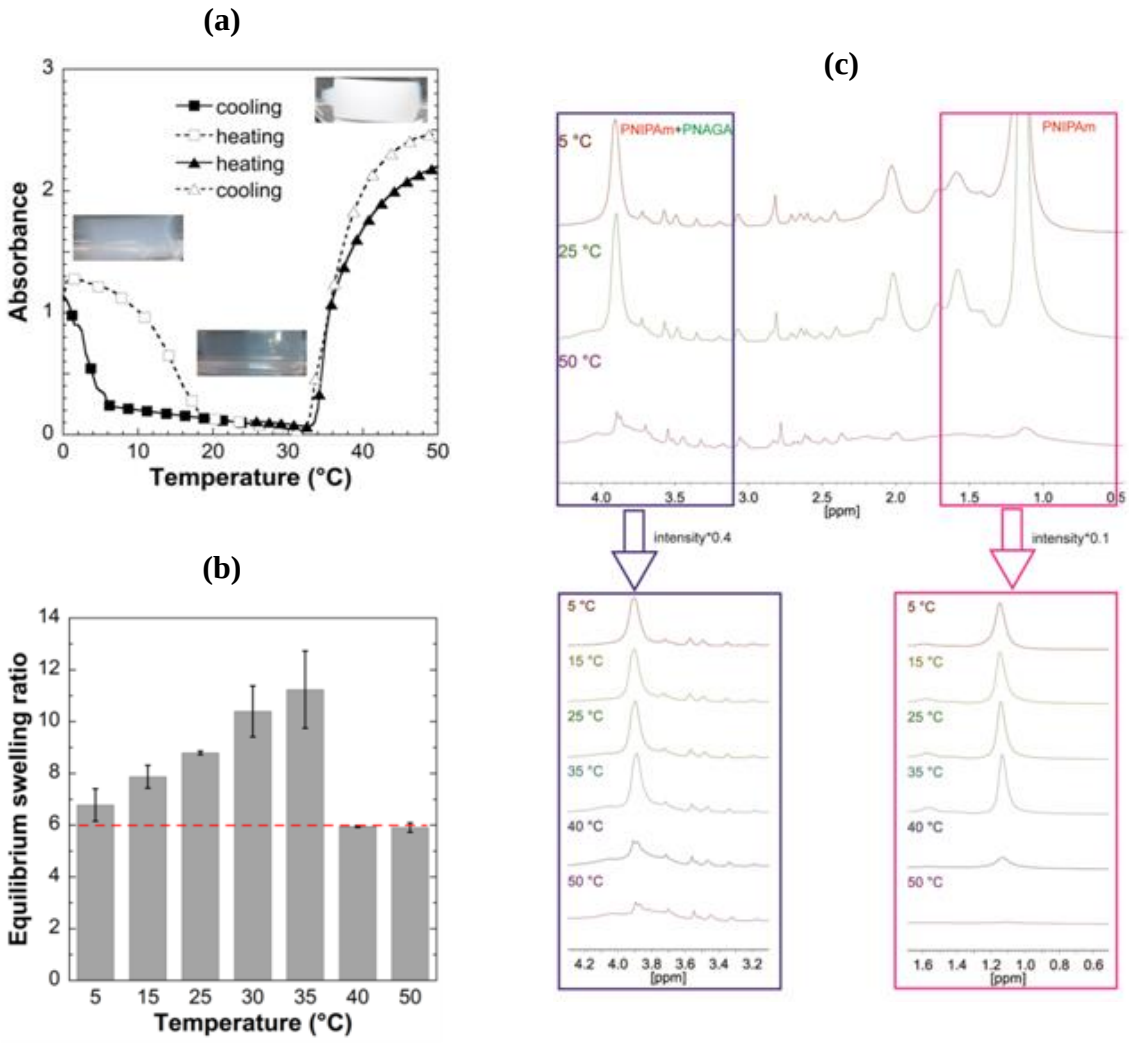

Figure 5.6 Dual thermo-responsive behaviour of GPA-N36 hydrogel. **(a)** Turbidity curves as a function of the temperature with a heating/cooling rate of 0.5 °C min^{-1}. The GPA-N36 hydrogel was both cooled and heated from 25 to 0 °C and from 25 to 50 °C. The insets correspond to their macroscopic appearance at 5, 25 and 50 °C. **(b)** Equilibrium swelling ratio, Q_e, in pure water at different temperatures. The swelling ratio of the hydrogel at preparation state Q_0=6 was indicated by the red dotted line. **(c)** Temperature variation of ^{1}H NMR spectra of GPA-N36 hydrogel in D_2O and zooms corresponding respectively to the NIPAm and NAGA NMR signals

In order to investigate the impact of the PNAGA phase separation on the rheological properties, a comparison between dual thermo-responsive GPA-N36 gels (present work) and a single thermo-responsive gel, GPD-N36,5,6 was carried out as a function of temperature (see **Figure 5.7.a**). GPD-N36 is a hydrophilic poly(*N*,*N*-dimethylacrylamide), PDMA, network (referred as GPD) grafted with thermo-responsive PNIPAm side-chains (denoted as-N36) having both the same average molar mass as the present PNIPAm macromonomers, the same cross-linker amount and the same weight ratio as used in this study (M_n = 36 kg/mol). As shown in **Figure 5.7.a**, both GPA-N36 and GPD-N36 display very similar viscoelastic behavior at high temperature with a value of elastic modulus around 10 kPa, demonstrating the impact of the PNIPAm phase separation on the elastic properties. Note that the temperature at which the thermo-reinforcement starts as well as the observed hysteresis during the heating/cooling cycle (2 °C min^{-1}) were very close, highlighting the similar topology. However, at low temperature, the elastic modulus of GPD-N36 remains very low (1 kPa) as both polymers PDMA and PNIPAm are in coil state. On the other hand, a higher value of *G'* was observed for GPA-N36 (7 kPa) which clearly demonstrates the thermo-reinforcement of GPA-N36 gels at low temperature.

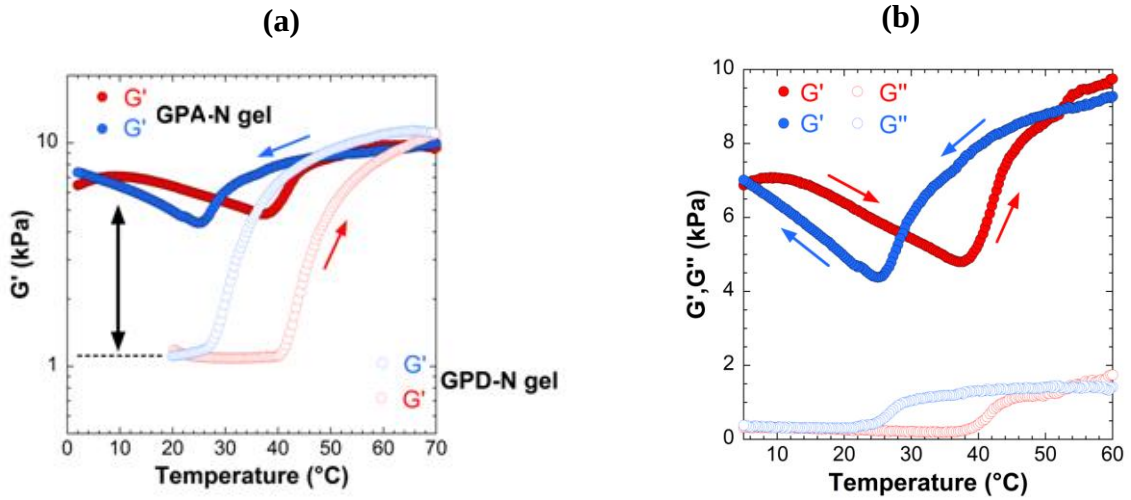

Figure 5.7 **(a)** Comparison of elastic moduli, *G'*, at 1 Hz at preparation state with a heating/cooling rate of 2 °C min^{-1} (red, upon heating; blue, upon cooling) of dual thermo-responsive GPA-N36 gel (filled symbols) and singular thermo-responsive gel, GPD-N36 (empty symbols). **(b)** Temperature dependence of viscoelastic properties: elastic modulus, G', (filled symbols) and loss modulus, G'', (empty symbols) at 1 Hz of GPA-N36 hydrogel at preparation state with a heating/cooling rate of 2 °C min^{-1} (red, upon heating; blue, upon cooling)

As illustrated in **Figure 5.7.b**, the temperature phase separation of each thermo-responsive polymers, PNAGA and PNIPAm, strongly influences the viscoelastic properties of GPA-N36 hydrogel at low and high temperature respectively. Upon heating from 5 to 36 °C,

the elastic modulus, *G'*, first decreases continuously, from 7 to 5 kPa and subsequently increases sharply until a value of 10 kPa with increasing the temperature from 36 to 60 °C. The increase of the elastic modulus on both sides of the minimum observed at 36 °C (*G'*=5 kPa) is in good agreement with the phase separation process of the two thermo-responsive components of GPA-N36 gel and mirrors the previous turbidity and swelling experiments. Below the UCST-, and above the LCST-type cloud points, PNAGA and PNIPAm chains self-associate respectively into collapsed domains forming additional interactions and physical cross-links into the polymer network. This dual thermo-reinforcement constitutes a major step compared to existing single thermo-reinforcement system in which thermo-responsive polymers were embedded into a hydrophilic matrix (**Figure 5.7.a**). Compared to the UCST phase transition of PNAGA, the thermo-reinforcement induced by the LCST phase transition of PNIPAm appears more effective in terms of elastic contribution and sharpness of the transition, which can be related either to different self-association mechanisms and/or kinetics effects. From these results, it appears obvious that mechanical properties can be effectively increased with temperature by modulating the chains solubility (from coil to globule conformation) and inducing collapsed domains into the grafted hydrogel.[5,6] When the same experiment is carried out by cooling, from 50 to 5 °C, a similar behavior can be observed with a shift of the transition temperature from 10 to 15 °C towards low temperatures mainly due to kinetic effects related to the thickness of the gel sample and to the relative high rate of cooling (2 °C min^{-1}) compared to the slow kinetics of PNAGA phase separation.[15]

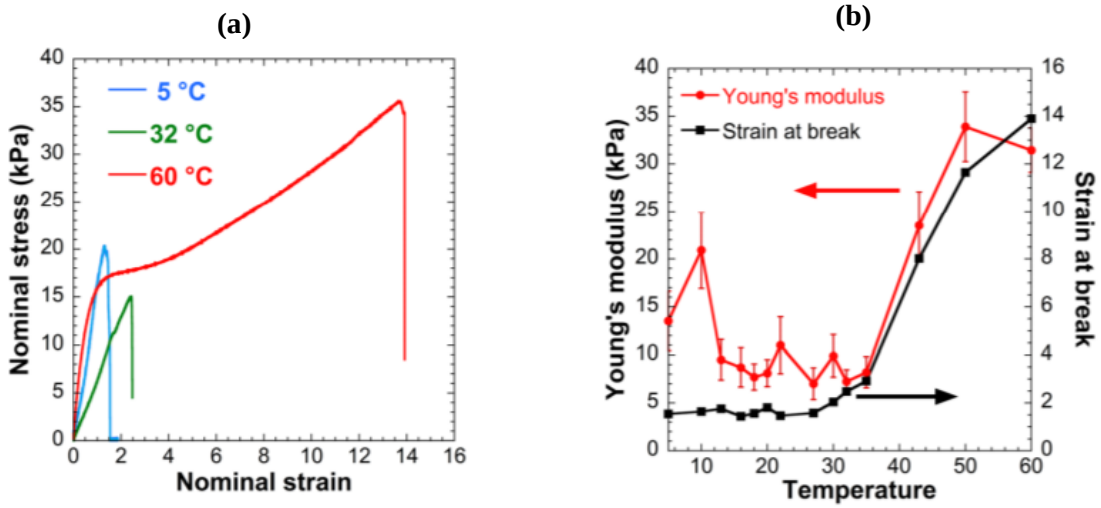

Figure 5.8 **(a)** Large strain mechanical behavior of GPA-N36 hydrogel (a) Uniaxial tensile stress-strain force curves of GPA-N36 gel at 5, 32 and 60 °C. **(b)** Tensile modulus (red, left axis) and strain at break (black, right axis) of GPA-N36 gel at different temperatures (strain rate=0.06 s^{-1})

With the aim of getting a better overview of the impact of the dual temperature phase separation process on the mechanical performances, large strain behavior in tension mode was also investigated on GPA-N36 gel at various temperatures. As illustrated in **Figure 8**, GPA-N36 gel demonstrates very clear temperature dependence under stretching. At 32 °C, the initial tensile modulus, E, reaches a value of about 8 kPa with a strain at break of 300% (**Figure 5.8.a**). In this condition, both UCST- and LCST-type associative interactions are expected to be ineffective and the gel response should mainly originate from entropic elasticity of the covalent network. At lower temperature (T=5 °C), the PNAGA phase separation improves the gel stiffness as shown by the value of the initial modulus around E~14 kPa but slightly decreases at the same time its extensibility (150-180%). Interestingly, above the phase separation of PNIPAm (T=60 °C), the self-association of PNIPAm side-chains simultaneously enhance both stiffness (E~32 kPa) and elongation at break (more than 1000%). A simple estimate of the work of extension, given by the area under the tensile curve, yields $W \cong 270$ kJ.m^{-3} (compared to $W \cong 19$ kJ.m^{-3} at 32 °C) revealing that physical interactions efficiently delay fracture. It is worth mentioning that the elastic moduli determined by mechanical testing are in agreement with those obtained from dynamic experiments, assuming pure incompressibility with $E=3G$. The temperature dependence of the phase separation-induced thermo-toughness of GPA-N36 gel is explicitly shown in **Figure 8.b** where the variation of the initial tensile modulus is in good agreement with the expected phase transition temperatures of PNAGA (T<10 °C, E~15-20 kPa) and PNIPAm (T>35 °C, E~30-35 kPa) discussed previously.

From these studies, by covalently introducing PNIPAm side-chains into a PNAGA network, we demonstrate that LCST- and UCST-type phase transitions can be effectively coupled to reinforce the gel both at high and low temperatures. Meanwhile, significant differences can be observed from the association of PNAGA and PNIPAm. Especially, the extensibility of hydrogels strongly increases above the LCST of PNIPAm while it decreases below the UCST of PNAGA. Distinct mechanisms for conformational transition of the two polymers can be taken into account to explain these opposite performances. In the case of PNIPAm, the polymer chains collapse above the LCST through hydrophobic interactions coupled with intra and intermolecular hydrogen bonds. By comparison, the phase separation of PNAGA involves only hydrogen bonds between hydrophilic repeat units. Referring to previous research, it is reported that hydrogen bonds in hydrogels have relatively lower

association strength due to the competition of water for binding sites.[15] Consequently, we postulate that in aqueous environment, the hydrogen bonded complexes formed by PNAGA chains can be more easily broken under applied stress. By comparison, the hydrophobic interactions formed within PNIPAm are much more difficult to release in aqueous environment.

In order to emphasize the versatility of our approach, the temperature-responsiveness of hydrogels and consequently their mechanical properties can be modulated by exploiting the phase separation process of thermo-responsive polymers. For instance, it is well known that salt addition can modify the hydration level of polymers and then their phase transition temperature.[15,16,17] Here, turbidity experiments were carried out on GPA-N36 gels swollen in Na_2SO_4 aqueous solution of different concentrations (0, 0.25 and 0.5 M) (**Figure 5.9**). The temperature range in which both PNAGA and PNIPAm chains take a coil conformation was reduced from 15 °C in pure water to 8 °C in Na_2SO_4 at 0.25 M. Finally, at 0.5 M, the temperature range was shifted to very low temperature and only LCST phase separation of GPA-N36 gel was observed.

Turbidity experiments were carried out on GPA-N36 hydrogels swollen in Na_2SO_4 aqueous solution of different concentrations. The results were reported in **Figure 5.9**.

[15] E. A. Appel, J. del Barrio, X. J. Loh, O. A. Scherman, **Chem. Soc. Rev.**, *2012*, 41, 6195-6214
[16] F. Liu, J. Seuring, S. Agarwal, **J. Polym. Sci. Polym. Chem.**, *2012*, 50, 4920-4928
[17] Y. Zhang, P. S. Cremer, **Ann. Rev. Phys. Chem.**, *2010*, 61, 63-83

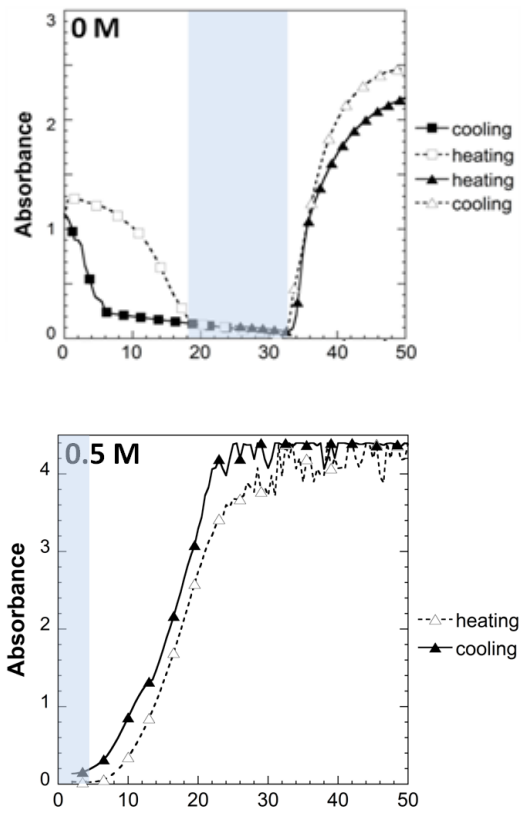

Figure 5.9 Turbidity curves of GPA-N36 gels swollen in Na_2SO_4 aqueous solution of different concentrations (0, 0.25 and 0.5 M) as a function of the temperature with a heating/cooling rate of 0.5 °C min^{-1}

V. Conclusion

In conclusion, both LCST and UCST thermo-responsive phase separation of designed antagonist gels were enabled to trigger large modifications of the mechanical properties and constitute an efficient route for gel toughening. Although the phase separated morphology induced by temperature has been shown to have a strong impact on the mechanical properties, the present study on GPA-N36 hydrogels demonstrates that the thermo-reinforcement efficiency also depends on the nature of the associations involved in the phase separation process and consequently on the choice of polymer precursors for the gel synthesis. This is clearly one of the key parameter for the design of mechanically reinforced hydrogels via the phase separation mechanism.

General Conclusion

General conclusion

Hydrogels are interesting materials for different industrial applications especially in the biomedical field. However, their intrinsic weak mechanical properties combined with the low responsivity to environmental conditions remain a major impediment when we want to extend the spectrum of applications. To tackle this problem, we designed in this work two series of thermo-responsive grafted hydrogels (GPD-N) made of a hydrophilic chemically cross-linked network of *N*,*N*-dimethylacrylamide (PDMA) with *N*-isopropylacrylamide (PNIPAm) thermo-responsive side-chains. The impact of the molar mass and the density of the thermo-responsive grafted polymer chains as well as the hydrophilic/thermo-responsive ratio on the hydrogels nanostructure, thermodynamic and mechanical properties were investigated.

The first challenging goal of this work was to clearly dissociate the contribution related to the formation of a phase separated morphology above the transition temperature from the one related to the increase of polymer concentration induced by the volume phase transition. To achieve this, we design hydrogels in such way that the hydrophilic part (PDMA network) prevents the volume transition of the thermo-responsive grafters (PNIPAm). The main consequence of this design was the thermo-responsive grafted hydrogels (GPD-N) not exhibiting a volume phase transition even above the LCST of the NIPAm grafters and consequently the possibility to work under isochoric conditions.

After the elaboration of two series of grafted hydrogels, we correlate the influence of the thermo-responsive PNIPAm side-chains on the thermodynamic properties of hydrogels with their self-assembling behaviour above the critical temperature, the resulting segregated morphology and their mechanical properties using a set of experimental techniques.

Interestingly, it has been demonstrated that the thermodynamic properties of hydrogels are weakly influenced by the molar mass of PNIPAm macromonomers. Indeed, all gels exhibit similar transition enthalpies and transition temperatures. Moreover, at nanoscale, small angle neutron scattering (SANS) experiments reveal that the self-assembling of PNIPAm side-chains above the critical temperature leads to similar rod-like phase-separated domains of

different length characterized by both similar radii and specific area. It thus highlights that at nanoscale, the mesh size of the PDMA network controls the morphology of the PNIPAm phase-separated domains whatever the average molar mass of PNIPAm side-chains. However, at a macroscopic scale, even if the hydrogels swelling is not really impacted by the molar mass of PNIPAm side-chains, their turbidity is highly influenced, emphasizing a difference in phase-separated domain number, distribution and organization at mesoscale. In fact, the hydrogel turbidity and the scattered intensities at low scattering vector demonstrated that the PNIPAm side-chains with higher average molar mass give rise to more isolated or repulsive phase-separated domains as well as a more organized structure at mesoscale. Nonetheless, the phase-separated domains forming inside a pre-stretched hydrogel at temperature above the critical one, lead to a similar behaviour in terms of shape-memory. It thus emphasizes that the PNIPAm graft inter-chain efficiency to balance the PDMA network entropic elasticity is independent of their molar mass. In contrast, the mechanical properties of the hydrogels are strongly impacted by the molar mass of the PNIPAm side-chains. It establishes that the architecture of the hydrogels is correlated with the impact of the PNIPAm average molar mass on phase-separated domains dissipative mechanisms by unravelling phenomenon. The architecture of hydrogels thus impacts their mechanical properties.

Indeed, their stiffness, extensibility and fracture toughness increase with the average molar mass of PNIPAm side-chains except for hydrogels having the highest PNIPAm grafters (GPD-N120). As a matter of fact, GPD-N120 exhibits the highest stiffness and fracture energy which is certainly due to entanglements and/or transfer reactions that reinforce it even under its critical temperature but it also induces a lower strain at break.

Parallel to this investigation, the composition ratio between the hydrophilic PDMA network and the thermo-responsive PNIPAm side chains was also investigated. As for the PNIPAm side-chains molar mass, the thermodynamic properties of the gels are independent of their composition ratio; they exhibit similar transition enthalpies and transition temperatures. In contrast, their average composition induces obvious macroscopic differences with a huge impact on the swelling, mainly due to the cross-linking polymerization efficiency depending on the initial DMA monomer concentration and the thermo-responsive content into the network. Furthermore, well-above the critical temperature, the higher the PNIPAm/PDMA ratio, the lower the gel swelling, demonstrating that the fraction of PNIPAm impacts on the PDMA network capacity to swell by balancing its hydrophilic nature by creating inter-chain

bonding. Moreover, the strain at break is strikingly reinforced with the increase of the PNIPAm/PDMA ratio but surprisingly the stiffness is not impacted. It is certainly due to the phase-separated domains breaking depending on the average molar mass of PNIPAm side-chains but not on their concentration within the network.

Then, we extend the mechanical reinforcement induced by the phase separation to others polymers. Replacing the hydrophilic PDMA network by poly(*N*-acryloyl glycinamide) (PNAGA) exhibiting a thermo-responsive behaviour (UCST) opposite to the one of PNIPAm side-chains (LCST), a schizophrenic hydrogel with dual thermo-responsiveness was obtained. However, the mechanical properties at low temperature were lower than at high temperature. This highlights therefore that the nature of the thermo-responsive polymers is crucial for the reinforcement. Actually, as the energy dissipating process inducing enhanced mechanical properties is strongly dependent on the phase-separated domain breaking and reforming, the nature of the physical interactions stabilizing the phase-separated domain is of first importance to reinforce hydrogels. Indeed, in the case of the phase-separated PNIPAm domains, hydrophobic and hydrogen bonds occur while only hydrogen bonds are present in the case of phase-separated PNAGA domains. Moreover, it was also demonstrated that the phase transition temperature and consequently certainly the mechanical properties can be modulated by the surrounding incorporating medium such as the nature and the concentration of salts in our case.

To conclude, in this work, we demonstrated that grafted hydrogels can be mechanically reinforced by thermo-responsive phase separation under isochoric conditions. It was also proved that the nature of thermo-responsive polymers, their molar mass and their fraction within the hydrogel can be correlated to the resultant macroscopic behaviour as well as their enhanced mechanical properties. Nonetheless, their thermodynamic properties are impacted only by the nature of the thermo-responsive polymers and the phase-separated domains morphology seems to be independent on the average molar mass of thermo-responsive side-chains at nanoscale.

Knowing that the phase separation process is the driving force to mechanical reinforcement, it is then interesting to return to fundamentals of the polymer phase separation by investigating the impact of the nature of the thermo-responsive polymers and especially the type of the physical interactions. Indeed, as demonstrated, PNIPAm phase-separation leads to

a combination of both hydrophobic interactions and H-bonds that highly reinforce the gel whereas only H-bonds drive the phase separation process of PNAGA leading to poor mechanical properties. Based on these two examples of thermo-responsive polymers we can consider future investigations with either (i) other polymers to deeply understand the interactions which drive the mechanical reinforcement or (ii) biocompatible polymers to be closer to practical applications. For example, the poly(*N*,*N*-diethylacrylamide) (PDEAm) exhibits a LCST behaviour in water as PNIPAm but its phase separation is only induced by hydrophobic interactions. Comparing poly(*N*,*N*-diethylacrylamide) (PDEAm) and poly(*N*-isopropylacrylamide) could help us to understand the supplementary role of intra hydrogen bonds in the mechanical reinforcement. Likewise, the impact of the steric hindrance on the phase separation process could be studied using poly(*N*-isopropylmethacrylamide) (PNIPMAm) which possesses an additional methyl group. On the other hand, poly(vinylcaprolactam) (PVCl) or poly(ethyleneglycol methacrylate) (PEGMA) which are both thermo-responsive and biocompatible could be used for biomedical applications.

The phenomenon of phase separation is not restricted to water as solvent, and as such, we could consider a similar mechanical reinforcement using hydrophobic polymers in organic solvent. In the same way, the use of organic solvent would reduce the force of the hydrophobic interactions but strengthen hydrogen bonds.

Moreover, it would be possible to use other stimuli or to generate heat by illumination or magnetic field. For instance, the incorporation of magnetic or plasmonic particles inside a thermo-responsive polymer network can induce phase-separation by applying a magnetic field or laser respectively which allows to locally exciting the particles so to generate heat.

By these future perspectives, we clearly see the possibilities and the versatility of our system based on the universal concept of phase separation.

Résumé

Afin d'étudier spécifiquement le rôle des processus de séparation de phase sur le renforcement des propriétés mécaniques des hydrogels, nous avons travaillé en conditions isochores en développant des architectures non seulement thermosensibles mais également capables de conserver un taux d'hydratation très élevé de part et d'autre de la température de transition de phase. Pour cela, des gels greffés ont été préparés à partir d'un réseau réticulé de polymère hydrophile en introduisant des chaînes latérales thermosensibles de type LCST (PNIPAm). A partir de cette structure primaire, et en maintenant fixe le rapport massique des précurseurs hydrophile/thermosensible, nous montrons que les caractéristiques thermodynamiques de la transition de phase (température et variation d'enthalpie) restent pratiquement indépendantes de la masse molaire des greffons de même que leur processus d'auto-assemblage qui conduit à la formation de domaines cylindriques concentrés en greffons PNIPAm. A l'instar des matériaux composites, la formation de ces domaines denses en polymère stabilisés par des interactions physiques vont ainsi largement augmenter la rigidité des gels à haute température ainsi que leur résistance à la fracture en jouant le rôle de dissipateur d'énergie. Nous montrons que ce renforcement thermo-contrôlé augmente avec la taille des chaînes à LCST. Dans le cas où l'on fait varier la composition massique hydrophile/thermosensible, tout en maintenant constante la masse molaire des greffons, on démontre des comportements opposés à basse et haute températures avec de bonnes propriétés à froid lorsque le réseau est riche en matrice hydrophile réticulée (élasticité d'origine entropique) et de très bonnes propriétés à chaud lorsque le comportement mécanique est contrôlé par les domaines concentrées en greffons à LCST (élasticité d'origine enthalpique). Le phénomène de séparation de phase des greffons PNIPAm étant thermo-réversible par nature, et les interactions entre ces mêmes chaînes peu dynamiques à haute température, nous montrons que ces hydrogels greffés cumulent, respectivement, des propriétés d'auto-adhésion et de mémoire de forme. Enfin, en généralisant le processus de séparation de phase, nous montrons que le remplacement du réseau hydrophile par un réseau thermosensible de type UCST, permet d'obtenir un double phénomène de séparation de phase, à basse et à haute température. Si les températures de transition sont parfaitement corrélées avec les caractéristiques thermodynamiques de chacun des polymères, le renforcement mécanique dépend plus quant à lui des énergies d'interaction qui se développent lors de la transition de phase au sein du réseau à UCST (liaisons-H) ou entre les greffons à LCST (interactions hydrophobes + liaisons-H).

Abstract

To specifically study the impact of phase-separation processes on hydrogels mechanical reinforcement, we worked under isochoric conditions developing architectures not only thermo-responsive but also able to keep a high level of hydration on both sides of the phase-separation temperature. For this purpose, grafted hydrogels have been formulated from a chemically cross-linked hydrophilic polymer network grafted with thermo-sensitive side-chains of LCST type (PNIPAm). From this primary structure and keeping constant the weight ratio between the hydrophilic and thermo-responsive parts, we demonstrate that the thermodynamic characteristics of the phase transition (enthalpy and temperature transitions) are only very weakly dependent on the molar mass of PNIPAm grafts as well as their self-assembly process which leads to cylindrical domains concentrated in PNIPAm grafts. Like the nanocomposite materials, the formation of these dense polymer domains stabilized by physical interactions highly enhances both the gels stiffness and fracture resistance at high temperature by dissipating energy. We show that this temperature-controlled reinforcement increases with the molar mass of the PNIPAm grafts. Varying the hydrophilic/thermo-responsive parts weight ratio while keeping constant the molar mass of the grafts, opposite behaviours at low and high temperatures were established. When the hydrophilic cross-linked network weight is high compared to the one of thermo-responsive grafts, the hydrogels exhibit good properties at low temperature (entropic elasticity) whereas at high temperature, their mechanical behaviour is controlled by the phase-separated domains concentrated in PNIPAm grafts (energetic elasticity). The phase-separation phenomenon of PNIPAm grafts being thermo-reversible by nature and the interactions between these chains being weakly dynamic at high temperature, we demonstrate that these grafted hydrogels exhibit both adhesive and shape-memory properties. Finally, expanding the phase-separation concept, we show that replacing the hydrophilic network by a UCST type thermo-responsive one allows getting a dual thermo-response with phase-separation occurring at both low and high temperatures. While these transition temperatures are perfectly correlated to the thermodynamic characteristics of each polymer, the mechanical reinforcement is more dependent on the energy due to the nature of interactions developing inside the UCST network (H-bonds) or between the LCST grafts (H-bonds and hydrophobic interactions) during the phase-separation process.